

Copyright Warning & Restrictions

The copyright law of the United States (Title 17, United States Code) governs the making of photocopies or other reproductions of copyrighted material.

Under certain conditions specified in the law, libraries and archives are authorized to furnish a photocopy or other reproduction. One of these specified conditions is that the photocopy or reproduction is not to be “used for any purpose other than private study, scholarship, or research.” If a user makes a request for, or later uses, a photocopy or reproduction for purposes in excess of “fair use” that user may be liable for copyright infringement,

This institution reserves the right to refuse to accept a copying order if, in its judgment, fulfillment of the order would involve violation of copyright law.

Please Note: The author retains the copyright while the New Jersey Institute of Technology reserves the right to distribute this thesis or dissertation

Printing note: If you do not wish to print this page, then select “Pages from: first page # to: last page #” on the print dialog screen

The Van Houten library has removed some of the personal information and all signatures from the approval page and biographical sketches of theses and dissertations in order to protect the identity of NJIT graduates and faculty.

ABSTRACT

TIME-FREQUENCY INVESTIGATION OF HEART RATE VARIABILITY AND CARDIOVASCULAR SYSTEM MODELING OF NORMAL AND CHRONIC OBSTRUCTIVE PULMONARY DISEASE (COPD) SUBJECTS

**by
Douglas A. Newandee**

A study has been designed to add insight to some questions that have not been fully investigated in the heart rate variability field and the cardiovascular regulation system in normal and Chronic Obstructive Pulmonary Disease (COPD) subjects. It explores the correlations between heart rate variability and cardiovascular regulation, which interact through complex multiple feedback and control loops. This work examines the coupling between heart rate (HR), respiration (RESP), and blood pressure (BP) via closed-loop system identification techniques in order to noninvasively assess the underlying physiology.

In the first part of the study, the applications of five different bilinear time-frequency representations are evaluated on modeled HRV test signals, actual electrocardiograms (ECG), BP and RESP signals. Each distribution: the short time Fourier transform (STFT), the smoothed pseudo Wigner-Ville (SPWVD), the Choi-Williams (CWD), the Born-Jordan-Cohen (BJC) and wavelet distribution (WL), has unique characteristics which is shown to affect the amount of smoothing and the generation of cross-terms. The CWD and the WL are chosen for further application because of overcoming the drawbacks of other distributions by providing higher resolution in time and frequency while suppressing interferences between the signal components.

In the second part of the study, the Morlet, Meyer, Daubechies 4, Mexican Hat and Haar wavelets are used to investigate the heart rate and blood pressure variability from both COPD and normal subjects. The results of wavelet analysis give much more useful information than the Cohen's class representations. Here we are able to quantitatively assess the parasympathetic (HF) and sympatho-vagal balance (LF:HF) changes as a function of time. As a result, COPD subjects breathe faster, have higher blood pressure variability and lower HRV.

In the third part of the study, a special class of the exogenous autoregressive (ARX) model is developed as an analytical tool for uncovering the hidden autonomic control processes. Non-parametric relationships between the input and outputs of the ARX model resulting in transfer function estimations of the noise filters and the input filter were used as mechanistic cardiovascular models that have shown to have predictive capabilities for the underlying autonomic nervous system activity of COPD patients. Transfer functions of COPD cardiovascular models have similar DC gains but show a larger lag in phase as compared to the models of normal subjects.

Finally, a method of severity classification is presented. This method combines the techniques of principal component analysis (PCA) and cluster analysis (CA) and has been shown to separate the COPD from the normal population with 100% accuracy. It can also classify the COPD population into "at risk", "mild", "moderate" and "severe" stages with 100%, 90%, 88% and 100% accuracy respectively. As a result, cluster and principal component analysis can be used to separate COPD and normal subjects and can be used successfully in COPD severity classification.

**TIME-FREQUENCY INVESTIGATION OF HEART RATE VARIABILITY AND
CARDIOVASCULAR SYSTEM MODELING OF NORMAL AND CHRONIC
OBSTRUCTIVE PULMONARY DISEASE (COPD) SUBJECTS**

**By
Douglas Alan Newandee**

**A Dissertation
Submitted to the Faculty of
New Jersey Institute of Technology
In Partial Fulfillment of the Requirements for the Degree of
Doctor of Philosophy in Electrical Engineering
Department of Electrical and Computer Engineering**

May 2003

Copyright © 2003 by Douglas Alan Newandee

ALL RIGHTS RESERVED

APPROVAL PAGE

TIME-FREQUENCY INVESTIGATION OF HEART RATE VARIABILITY AND CARDIOVASCULAR SYSTEM MODELING OF NORMAL AND CHRONIC OBSTRUCTIVE PULMONARY DISEASE (COPD) SUBJECTS

Douglas Alan Newandee

Dr. Stanley S. Reisman, Dissertation Advisor Professor of Biomedical Engineering, NJIT Professor of Electrical and Computer Engineering, NJIT	Date
---	------

Dr. Richard A. Haddad, Committee Member Professor of Electrical and Computer Engineering, NJIT	Date
---	------

Dr. Timothy N. Chang, Committee Member Associate Professor of Electrical and Computer Engineering, NJIT	Date
--	------

Dr. Ronald E. De Meersman, Committee Member Professor, Columbia University, College of Physicians and Surgeons	Date
---	------

Dr. Matthew N. Bartels, Committee Member Assistant Professor, Columbia University, College of Physicians and Surgeons	Date
--	------

BIOGRAPHICAL SKETCH

Author: Douglas Alan Newandee

Degree: Doctor of Philosophy

Date: January 2003

Undergraduate and Graduate Education:

- Doctor of Philosophy in Electrical Engineering
New Jersey Institute of Technology, Newark, NJ, 2003.
- Master of Science in Biomedical Engineering
New Jersey Institute of Technology, Newark, NJ, 1996.
- Bachelor of Science in Biology/Premedical Studies
Bloomfield College, Bloomfield, NJ, 1994.
- Master of Science in Electrical Engineering
Stevens Institute of Technology, Hoboken, NJ, 1987
- Bachelor of Science in Electrical Engineering
Rochester Institute of Technology, Rochester, NY, 1981

Major: Electrical Engineering

Presentations and Publications:

D.A. Newandee and S.S. Reisman,
“Investigation of EEG Coherence in Group Meditation,” *Proceedings of the 22nd IEEE Annual Northeast Bioengineering Conference*, 1996, Rutgers University, New Brunswick, New Jersey.

D.A. Newandee and S.S. Reisman,
“Application of Wavelet Transform to Heart Rate Variability”, *Proceedings of the 28th IEEE Annual Northeast Bioengineering Conference*, 2002, Drexel University, Philadelphia, Pennsylvania.

BIOGRAPHICAL SKETCH (Continued)

- D.A. Newandee, S.S. Reisman, R.E. De Meersman, and M.N. Bartels,
“The Effects of Respiration on Heart Rate and Blood Pressure Spectra During Exercise below Ventilatory Threshold”, *Proceedings of the 28th IEEE Annual Northeast Bioengineering Conference*, 2002, Drexel University, Philadelphia, Pennsylvania.
- D.A. Newandee and S.S. Reisman,
“Wavelet Transform Representation Comparison for Heart Rate Variability Analysis”, *Proceedings of the 29th IEEE Annual Northeast Bioengineering Conference*, 2003, New Jersey Institute of Technology, Newark, New Jersey.
- D.A. Newandee, S.S. Reisman, R.E. De Meersman, and M.N. Bartels,
“COPD Severity Classification Using Principal Component and Cluster Analysis on HRV Parameters”, *Proceedings of the 29th IEEE Annual Northeast Bioengineering Conference*, 2003, New Jersey Institute of Technology, Newark, New Jersey.
- B.A. Davis, L.S. Krivickas, R. Maniar, D.A. Newandee, and J.H. Feinberg,
“The reliability of monopolar and bipolar fine-wire electromyographic measurement of muscle fatigue”, *Medicine & Science in Sports & Exercise* 30(8):1328-1335, 1998.
- R.E. De Meersman, M.N. Bartels, D.A. Newandee, and S.S. Reisman,
“The Effects of Respiration on RR Interval Spectra During Exercise”, *12th International Symposium on the Autonomic Nervous System*, 2001, Palm Springs, California.

This dissertation is dedicated
to the memory of my Grandparents

ACKNOWLEDGMENT

The author wishes to express his most sincere gratitude to his advisor, Dr. Stanley S. Reisman, for his unsurpassed patience, mentorship, friendship, and moral support throughout this research. He has, by setting examples, instilled a great appreciation of good work ethic, curiosity, creativity and honesty that are so essential for success and enjoyment for a career in academics.

Special thanks are extended to Dr. Richard A. Haddad, Dr. Timothy N. Chang, Dr. Ronald E. De Meersman and Dr. Matthew N. Bartels for serving as members of the dissertation committee. Dr. Haddad and Dr. Chang have constantly kept me well grounded with Adaptive Control, Digital Signal Processing and Systems Identification theories. Dr. De Meersman and Dr. Bartels of Columbia University (College of Physicians and Surgeons, NY) have provided the idea, much valuable information on COPD, and the use of data from both COPD and normal subjects. These data were collected at the Atchley Human Pulmonary Performance laboratory and the Black building at the Columbia Presbyterian Hospital, NY and used as the main resource for this dissertation. Special gratitude and appreciation are extended to John Gonzalez of the Columbia Presbyterian Hospital, who performed the tedious task of data collection for this research.

Many thanks should go to Dr. Michael Lacker and Dr. Tara Alvarez for many of the Friday mini seminars on Linear Algebra, Principal/Independent Component Analysis and Modeling of Physiological Systems.

The author also appreciates the former and present NJIT doctoral students: Dr. Rindala Saliba, Dr. Xiaorui Tang, Anne Marie Petrock, Jason Steffener, Sachin

Patwardhan, Shuang Shuang Dai and many others for their support and friendship. They have also been constant sources of ideas, suggestions and discussions for this research. Their immense enthusiasm has helped me getting over many ups and downs of doctoral research.

Deepest gratitude and respect should go to my parents for all their support, love and encouragement throughout my education; to my brothers, Dr. Stephen and Dr. James Newandee for their concern, constant encouragement, and many discussions on COPD, time-frequency distributions and wavelet applications; to my sisters, Kimberly and Carrie, for always being ready to lend a helping hand.

This dissertation simply could never have been completed without the love, understanding and support of my wife, Hoa, and my two young children: Helena and Daniel. Thank you for all the time you really needed my presence but I could not be there because of my devotion to this research. For all your patience and sacrifice, I am forever grateful.

And finally, much appreciation should go to Dr. Ronald S. Kane and Ms. Clarisa González-Lenahan for reviewing, making correction recommendation and approving the final version of this dissertation.

TABLE OF CONTENTS

Chapter	Page
1 INTRODUCTION.....	1
1.1 Scope of research.....	1
1.2 Goals and Contributions.....	8
1.3 Outline of the dissertation	12
2 PHYSIOLOGY BACKGROUND.....	14
2.1 Cardiovascular Systems and the Heart	14
2.2 Blood Pressure.....	20
2.3 Metabolic Function/Respiration.....	21
2.4 The Nervous System	22
2.4.1 The Autonomic Nervous System.....	23
2.4.2 The Baroreflex Mechanism.....	27
2.5 Heart Rate and Heart Rate Variability	29
2.5.1 Physiology of changes in heart rate	29
2.5.2 Heart rate variability as a measure of Autonomic Function	31
2.5.3 Baroreflex Response	32
2.6 The Electrocardiogram (ECG).....	34
2.7 Chronic Obstructive Pulmonary Disease (COPD)	37
2.7.1 Classification of COPD by severity.....	39
3 ENGINEERING BACKGROUND.....	42
3.1 Time-Frequency Distributions	43

TABLE OF CONTENTS (Continued)

Chapter	Page
3.2 The Uncertainty Principle	47
3.3 The Analytic Signal and Instantaneous Frequency	48
3.4 Properties of Time-Frequency Distributions	50
3.5 Covariance and Invariance	52
3.6 Comparison of Time-Frequency Distributions	53
3.6.1 Short Time Fourier Transform.....	53
3.6.2 Wigner Distribution.....	56
3.6.3 The Choi-William (Exponential Distribution)	62
3.7 The Wavelet Transform.....	65
3.7.1 Continuous Wavelet Transform.....	67
3.7.2 Parseval Relation of Wavelet Transform.....	73
3.7.3 Discrete Wavelet Transform	74
3.8 Power Spectral Analysis of HRV.....	77
3.9 Power Spectral Analysis of Blood Pressure	85
3.10 Coherence Analysis.....	87
3.11 Weighted-coherence	91
3.12 Partial Coherence Analysis	92
3.12.1 Multivariate Analysis	92
3.12.2 Partial Spectral	92
3.13 System Identification.....	95

TABLE OF CONTENTS (Continued)

Chapter	Page
3.13.1 Estimating Transfer Functions of Non-linear Systems	96
3.13.2 The ARX Models	101
3.14 Principal Component Analysis.....	107
3.14.1 Basic Concepts of PCA.....	109
3.15 Cluster Analysis.....	112
3.15.1 Joining (Tree Clustering)	113
3.15.2 Hierarchical Tree.....	113
3.15.3 Distance Measures.....	114
3.15.4 Euclidian Distance.....	115
3.15.5 Squared Euclidian Distance	116
3.15.6 City Block (Manhattan) Distance	116
3.15.7 Chebychev Distance.....	116
3.15.8 Power Distance.....	116
3.15.9 Percent Disagreement.....	117
3.15.10 Amalgamation or Linkage Rules	117
3.15.11 Single Linkage (Nearest Neighbor).....	118
3.15.12 Complete Linkage (Furthest Neighbor).....	118
3.15.13 Unweighted Pair-Group Average	118
3.15.14 Weighted Pair-Group Average	119
3.15.15 Unweighted Pair-Group Centroid.....	119

TABLE OF CONTENTS (Continued)

Chapter	Page
3.15.16 Weighted Pair-Group Centroid	119
3.15.17 Ward's Method.....	120
3.15.18 Two-way Joining	120
3.15.19 K-means Clustering.....	122
3.15.20 Computations.....	123
3.15.21 Interpretation of Results	123
4 METHODS	124
4.1 Experiment Protocol	124
4.1.1 Study Procedure	124
4.1.2 Data Acquisition Procedure	125
4.2 Data Analysis.....	131
4.2.1 Wigner Time Frequency Analysis	131
4.2.2 Power Spectrum Analysis of Heart Rate Variability.....	132
4.2.3 Power Spectrum Analysis of Blood Pressure Variability	134
4.2.4 Coherence and Weighted-coherence of HR and Respiration.....	135
4.2.5 Coherence and Weighted-coherence of HR and Blood Pressure....	136
4.2.6 Partial Coherence	136
4.2.7 Time-Frequency Analysis	137
4.2.8 System Identification Analysis	142
4.2.9 Analysis of Generation of broadband Respiration Signal.....	142

TABLE OF CONTENTS (Continued)

Chapter	Page
4.2.10 Principal Component Analysis	145
4.2.11 Cluster Analysis	148
5 RESULTS	149
5.1 Spectral Analysis	149
5.2 Time Frequency Analysis.....	158
5.2.1 Time Frequency Analysis Applied to Sine Waves.....	158
5.2.2 Time Frequency Analysis of Heart Rate Variability.....	165
5.2.3 Time Frequency Analysis (WL) of COPD HRV data.....	171
5.2.4 Best Distribution of TF Representation for HRV Study	175
5.2.5 Best Wavelet Selection for HRV TFR	176
5.2.6 Vagal Tone and Sympathovagal balance of COPD subjects	180
5.2.7 Time Frequency Analysis (Wavelet) of BPV.....	188
5.3 Coherence/Partial Coherence of Heart Rate Variability	199
5.4 Cardiovascular System Models for Normal Subjects.....	215
5.5 Cardiovascular System Models for COPD Subjects	225
5.6 PCA.....	227
5.7 Cluster Analysis.....	234
6 CONCLUSIONS	237
6.1 Future Work.....	241
APPENDIX A EXERCISE PHYSIOLOGY	242

TABLE OF CONTENTS (Continued)

Chapter	Page
A.1 Borg Perceived Exertion Scale.....	242
A.2 The Karvonen Formula	242
A.3 Figure Out Your Target Heart Rate!	244
A.3.1 Taking Your Pulse.....	244
A.3.2 Maximum Heart Rate	244
A.3.3 Resting Heart Rate	245
A.3.4 Target Heart Rate Range.....	245
A.3.5 Calculate	245
APPENDIX B ANALYSIS PROGRAM LISTINGS	246
B.1 Cross-Spectral Analysis Steps.....	246
B.1.1 4dsp	249
B.2 MATLAB Programs.....	259
B.2.1 Test Signal of Three Sinusoids at 0.3, 0.1 and 0.5 Hz	259
B.2.2 Time-frequency Analysis and Activity Plot Program	260
B.2.3 Program to Generate Sympatho Vagal Activity Plots Using Wigner Distribution	269
B.2.4 Wavelet Analysis and Activity Plot Program.....	275
B.2.5 System Identification Procedure	283
B.2.6 Principal Component Analysis	288
B.2.7 Cluster Analysis Program	296

TABLE OF CONTENTS (Continued)

Chapter	Page
B.2.8 Cross-correlation Program	300
APPENDIX C CROSS-SPECTRAL ANALYSIS.....	301
C.1 General Partial Coherence Equation.....	301
C.2 Partial Coherence of HR and BP (Extract Resp).....	301
C.3 Partial Coherence of HR and Resp (Extract BP).....	302
C.4 Partial Coherence of BP and Resp (Extract HR).....	302
REFERENCES	303

LIST OF TABLES

Table	Page
2.1 The Nervous System.....	22
2.2 Autonomic Effects on Selected Organs of the Body.....	27
2.3 GOLD Severity Classification of COPD	41
3.1 Some Desirable Properties of Time-Frequency Distributions	51
4.1 Wavelet Names available for Analysis (94+)	141
4.2 Data Set Parameters used for PCA and Cluster Analysis.....	146
4.3 Principal Components from Normal and COPD Data Set	147
5.1 Correlation Indices of Wavelet Representations	178
5.2 Cross-spectral Analysis of all 8 Normal Subjects	205
5.3 Cross-spectral Analysis of all 47 COPD Subjects.....	207
5.3.1 Statistical Analysis of Coherence and Partial Coherence for Normal and COPD Group	213
5.4 Gain and Phase Data of Normal Subjects	223
5.5 Gain and Phase Data of COPD Subjects.....	226
5.6 Principal Components from Normal and COPD Data I	228
5.7 Principal Components from Normal and COPD Data II.....	230
5.8 Principal Components from Normal Exercise Data	232
5.9 Principal Components of Different Population Group.....	233
5.10 Summary of Normal-COPD Severity Classification.....	236

LIST OF FIGURES

Figure	Page
2.1 The heart	15
2.2 The systemic and pulmonary circulations.....	16
2.3 The intrinsic conduction system of the heart	17
2.4 The sequence of cardiac excitation	19
2.5 The sympathetic nervous system and parasympathetic nervous system.....	26
2.6 Autonomic innervation of the heart	30
2.7 Effect of autonomic stimulation on the slope of the pacemaker potential	31
2.8 An electrocardiogram tracing (lead I)	34
2.9 The ECG placement of the positive and negative electrodes	36
3.1 Classes of time-frequency distributions.....	46
3.2 The Wigner distribution of the sum of two finite duration sine waves.....	60
3.3 The Performance of the Choi-William distribution.....	64
3.4 Division of the frequency domain for the STFT and the Wavelet Transform.....	70
3.5 The time-frequency plane resolution cells of the STFT vs. WT	72
3.6 Figure depicting the construction of the IBI signal	78
3.7 IBI and IIBI signals of heart rate.....	79
3.8 Power spectrum of the heart rate IIBI signal	81
3.9 Plot of the split cosine bell taper used as a window in the FFT calculation	82
3.10 Example of power spectral density of HRV	83
3.11 One minute plot of raw blood pressure and its IIBI signal.....	85

LIST OF FIGURES (Continued)

Figure	Page
3.12 Power spectrum of BP IIBI	86
3.13 Examples of typical plant	95
3.14 Optimal data acquisition measurement system.....	98
3.15 Open-loop input driven ARX model.....	103
3.16 Feedback closed-loop ARX model	105
3.17 Principal component analysis illustration	110
3.18 Horizontal hierarchical tree plot.....	114
3.19 Contour graph of a two-way joining clustering	121
4.1 Theoretical power spectrum of band-limited Gaussian white noise	143
5.1 HRV analysis of a COPD subject	151
5.2 BPV analysis of a COPD subject	152
5.3 HRV analysis of a normal subject.....	154
5.4 BPV analysis of a normal subject	155
5.4.1 Comparison of the HRV frequency spectra of COPD and normal subjects	156
5.4.2 Comparison of the BPV frequency spectra of COPD and normal subjects	157
5.5 Test signal with 3 sine waves and its power spectrum	160
5.6a STFT of a signal with 3 sine waves at 0.3, 0.1 and 0.5 Hz	161
5.6b SWVD of a signal with 3 sine waves at 0.3, 0.1 and 0.5 Hz	161
5.6c CWD of a signal with 3 sine waves at 0.3, 0.1 and 0.5 Hz	162
5.6d BJCD of a signal with 3 sine waves at 0.3, 0.1 and 0.5 Hz	162

LIST OF FIGURES (Continued)

Figure	Page
5.7a Morlet WT of a signal with 3 sine waves at 0.3, 0.1 and 0.5 Hz	163
5.7b Meyer WT of a signal with 3 sine waves at 0.3, 0.1 and 0.5 Hz	163
5.7c dB4 WT of a signal with 3 sine waves at 0.3, 0.1 and 0.5 Hz	164
5.7d Mexican Hat WT of a signal with 3 sine waves at 0.3, 0.1 and 0.5 Hz	164
5.7e Haar WT of a signal with 3 sine waves at 0.3, 0.1 and 0.5 Hz	165
5.8 HR IIBI and power spectrum plots of a normal subject at 3 min rest paced breathing at 8 bpm	166
5.9a STFT plots of a normal subject at 3 min rest, paced breathing at 8 bpm.....	167
5.9b SWVD plots of a normal subject at 3 min rest, paced breathing at 8 bpm.....	167
5.9c CWD plots of a normal subject at 3 min rest, paced breathing at 8 bpm.....	168
5.9d BJCD plots of a normal subject at 3 min rest, paced breathing at 8 bpm.....	168
5.10 Morlet WT HRV plots of a normal subject at 3 min rest, paced breathing at 8 bpm	170
5.11 HR IIBI and power spectrum of a COPD subject at rest breathing at 16 bpm .	171
5.12 Morlet WT of a COPD subject at 5 min rest paced breathing at 16 bpm	172
5.13 Meyer WT of a COPD subject at 5 min rest paced breathing at 16 bpm.....	173
5.14 CWT (dB4) HRV plot of a COPD subject at 5 min rest paced breathing at 16 bpm	173
5.15 CWT (Mexican Hat) HRV plot of a COPD subject at 5 min rest paced breathing at 16 bpm.....	174
5.16 CWT (Haar) HRV plot of a COPD subject at 5 min rest paced breathing at 16 bpm	174

LIST OF FIGURES (Continued)

Figure	Page
5.17 Graph of correlation indices for wavelet representations.....	179
5.18 Sympathetic and parasympathetic mixture Plots of HR using Morlet wavelet (COPD subject in 5 min rest, breathing at 16bpm)	183
5.19 Normalized sympathetic and parasympathetic mixture plots of HR using Morlet wavelet (COPD subject in 5 min rest, breathing at 16bpm).....	183
5.20 Sympathetic and parasympathetic mixture plots of HR using Meyer wavelet (COPD subject in 5 min rest, breathing at 16bpm)	184
5.21 Normalized sympathetic and parasympathetic mixture plots of HR using Meyer wavelet (COPD subject in 5 min rest, breathing at 16bpm)	184
5.22 Sympathetic and parasympathetic mixture plots of HR using Daubechies 4 wavelet (COPD subject in 5 min rest, breathing at 16bpm).....	185
5.23 Normalized sympathetic and parasympathetic mixture plots of HR using Daubechies 4 wavelet (COPD subject in 5 min rest, breathing at 16bpm).....	185
5.24 Sympathetic and parasympathetic mixture plots of HR using Mexican Hat wavelet (COPD subject in 5 min rest, breathing at 16bpm).....	186
5.25 Normalized sympathetic and parasympathetic mixture plots of HR using Mexican Hat wavelet (COPD subject in 5 min rest, breathing at 16bpm).....	186
5.26 Sympathetic and parasympathetic mixture plots of HR using Haar wavelet (COPD subject in 5 min rest, breathing at 16bpm)	187
5.27 Normalized sympathetic and parasympathetic mixture plots of HR using Haar wavelet (COPD subject in 5 min rest, breathing at 16bpm).....	187
5.28 Plot of BP IIBI and power spectrum using FT	188
5.29 3D and contour plot of blood pressure spectrum using Morlet wavelet	190
5.30 3D and contour plot of blood pressure spectrum using Meyer wavelet.....	190
5.31 3D and contour plot of blood pressure spectrum using DB4 wavelet.....	191

LIST OF FIGURES (Continued)

Figure	Page
5.32 3D and contour plot of blood pressure spectrum using Mexican Hat wavelet .	191
5.33 3D and contour plot of blood pressure spectrum using Haar Wavelet.....	192
5.34 Sympathetic and parasympathetic mixture plots of BP using Morlet WT	194
5.35 Normalized sympathetic and parasympathetic mixture plots of BP using Morlet wavelet	194
5.36 Sympathetic and parasympathetic mixture plots of BP using Meyer WT	195
5.37 Normalized sympathetic and parasympathetic mixture plots of BP using Meyer wavelet	195
5.38 Sympathetic and parasympathetic mixture plots of BP using dB4 WT	196
5.39 Normalized sympathetic and parasympathetic mixture plots of BP using dB4 wavelet	196
5.40 Sympathetic and parasympathetic mixture plots of BP using Mex Hat WT ...	197
5.41 Normalized sympathetic and parasympathetic mixture plots of BP using Mexican Hat WT	197
5.42 Sympathetic and parasympathetic mixture plots of BP using Haar WT	198
5.43 Normalized sympathetic and parasympathetic mixture plots of BP using Haar wavelet	198
5.44 Plot of raw respiration, ECG, BP, HR IIBI, BP IIBI, HR & BP spectra of a COPD subject	200
5.45 The LF coherence plots of a subject (COPD).....	201
5.46 The LF partial coherence plots of a subject (COPD)	202
5.47 The HF coherence plots of a subject (COPD)	203
5.48 The HF partial coherence plots of a subject (COPD)	204

LIST OF FIGURES (Continued)

Figure	Page
5.49 LF coherence plots of COPD subjects (1-47) and normal (48-55) subjects	210
5.50 HF coherence plots of COPD subjects (1-47) and normal (48-55) subjects.....	210
5.51 LF partial coherence plots of COPD subjects (1-47) and normal (48-55) subjects.....	211
5.52 HF partial coherence plots of COPD subjects (1-47) and normal (48-55) subjects.....	211
5.53 Coherence and partial coherence comparison between normal and COPD.....	214
5.54 Simple feedback and control model of ABP and HR regulation. Respiration enters both sides of the loop as an external noise source	215
5.55 Plot of output HR IIBI (Top) and input RSP (Bottom) signals	218
5.56 ARX model of HRV using RSP as input and IIBI as output	221
5.57 Poles and zeros graph of the HRV model using rsp as input and IIBI as output	221
5.58 Bode plot of the HRV model using RSP as input and IIBI as output	222
5.59 Compare the estimate of the transfer function by spectral analysis	223
5.59.1 An adaptive COPD cardiovascular system model.....	225
5.60 Normal and COPD classification using PCA	228
5.61 Normal and COPD classification using PCA	230
5.62 Normal classification using Principal Component Analysis (PCA)	232
5.63 Separation of Normal (Red) from COPD subjects	235
5.64 Severity classification of normal and COPD subjects.....	236
A.1 The Borg scale of perceived exertion	243

ABBREVIATIONS

A

ABP	Arterial Blood Pressure
ANS	Autonomic Nervous System
ARMA	AutoRegressive Moving Average
ARX	AutoRegressive with eXoneous input
AV	Atrial Venous Node

B

BJ	Box Jenkins
BJD	Born Jordan Distribution
BP	Blood Pressure
BPV	Blood Pressure Variability
BRSI	Baroreflex Sensitivity Index

C

CHF	Congestive Heart Failure
CNS	Central Nervous System
CO	Cardiac Output
COPD	Chronic Obstructive Pulmonary Disease
CWD	Choi-William Distribution

E

ECG	Electrocardiogram
ED	Exponential Distribution (see CWD)

F

FEV1	Forced Expiration Volume in the 1 st second
FFT	Fast Fourier Transform
FIR	Finite Impulse Response
FT	Fourier Transform
FVC	Forced Vital Capacity

ABBREVIATIONS (Continued)

G

GUI	Graphical User Interface
GWN	Gaussian White Noise

H

HF	High Frequency Activity (0.15-0.4 Hz)
HR	Heart Rate
HRV	Heart Rate Variability

I

IBI	Interbeat Interval
IIBI	Interpolated Interbeat Interval

L

LED	Light Emitting Diode
LF	Low Frequency Activity (0.04-0.15 Hz)
LF: HF	Sympatho-vagal Balance
LLTI	Lumped-Linear Time Invariant
LVRS	Lung Volume Reduction Surgery

M

MA	Moving Average
MAP	Mean Arterial Pressure
MLE	Maximum Likelihood Estimation
MSC	Mean-squared coherence

N

NETT	National Emphysema Treatment Trial
------	------------------------------------

O

O ₂	30 % Oxygen supplementation
OE	Output Error Model

ABBREVIATIONS (Continued)

P

PID	Proportional-integral-derivative
PNS	Peripheral Nervous System

R

RA	Room Air
RESP	Respiration Signal
RID	Born-Jordan-Cohen Distribution
RR	R-to-R peak interval of ECG
RSA	Respiratory Sinus Arrhythmia

S

SA	Sino-Atrial Node
SID	System Identification
SPWD	Smooth Pseudo Wigner Ville Distribution
STFT	Short Time Fourier Transform
SV	Stroke Volume
S/V	Sympatho-vagal Balance
SWVD	Smooth Wigner Ville Distribution

T

TFA	Time-Frequency Analysis
TFR	Time-Frequency Representation
TPR	Overall Arteriole Resistance

V

VE	Ventilation
VLf	Very Low Frequency (<0.04 Hz)
VO ₂	Volume of Oxygen per unit time

W

WD	Wavelet Distribution
WT	Wavelet Transform
WVD	Wigner-Ville Distribution

CHAPTER 1

INTRODUCTION

1.1 Scope of Research

It is of interest to use noninvasive autonomic techniques to learn more about differences in the physiology of diseased patients. The development of improved treatments for these patients is important, and the development of improved monitoring techniques to assess risk of morbidity and mortality, as well as to assess response to treatment is needed. One particular population of patients, which is used in this study, is those with chronic obstructive pulmonary disease (COPD).

The monitoring of the progression of pulmonary disease and the prediction of mortality and morbidity in these conditions is usually performed through the measurement of static and dynamic lung volumes, and through tests which measure the physiologic efficiency of gas exchange in the lungs. However, the effects of severe pulmonary disease are not limited to the lungs. Often there are serious accompanying cardiac problems and severe alterations to the normal state of autonomic regulation. Patients with pulmonary disease are subject to a hyperadrenergic state and have many alterations in their autonomic physiology that can be documented. [1] There are three non-invasive measures of autonomic function, which can be performed in a simple fashion and can offer a clear window into the state of the subject. These include the heart rate variability (HRV), beat-to-beat blood pressure variability (BPV), and baroreceptor sensitivity. In subject populations with cardiac disease, the abnormalities found in these measures were found to have very strong correlations with subsequent

mortality and sudden death. [2] Because of some of the similarities between patients with severe pulmonary disease and patients with severe heart disease, the systematic study of the autonomic disturbances in these individuals, along with an analysis of the survival of the patients with and without treatment should be undertaken.

Respiratory sinus arrhythmia (RSA) is a phenomenon that has been recognized and studied for years, and it has been described as a rhythmical fluctuation in R-R intervals that is characterized by a decrease in the RR interval length during inspiration, and an increase in the R-R interval length during expiration [2]. Spectral analysis techniques have allowed researchers to conclude that RSA can primarily be attributed to vagal activity and can be used as an index of vagal control of the heart. It has been shown that the variation of blood pressure seen with respiration is also associated with the heart rate variability. The physiologic mechanism of heart rate variability is mediated through respiratory afferents synapsing in the medulla oblongata and entraining the central regulatory oscillator. Similarly, the mechanism of blood pressure variability (BPV) is entrained to respiration, and is a combination of the effects of the changes of stroke volume and the increase in vagal tone with inspiration. With the use of spectral analysis, the raw data obtained by blood pressure and heart rate monitoring can be broken down into useful observations. The interpretation of the significance of the data are still being refined, but for several cardiac disease states there have been clear indications that the loss of RSA is associated with increased morbidity, and increased sudden death.

Since the relationship of altered heart rate variability and increased mortality have been documented in cardiac populations, the population of patients with severe

pulmonary disease (COPD) is an excellent candidate to now be studied. Patients with pulmonary disease also have significant alterations of their autonomic regulation. In COPD patients breathing patterns are altered, causing abnormalities in the entrainment of the normal central oscillators.

A recent study by Pagani, et al [3] demonstrated that there is a decrease in the high frequency (parasympathetic) activity detected in patients with COPD compared to age matched controls, and a decrease in low frequency (sympathetic) activity. This work also demonstrated that the RSA vagal index, which provides an assessment of the gain of respiratory modulation of RR variability, is altered in patients with COPD. Unfortunately, there has not been much focused work studying the relationship of the pulmonary functions and alterations in autonomic regulation as monitored by HRV, BPV, or BRS and linking these parameters to morbidity and mortality. Since there are several physiological correlations between the populations of patients with COPD and congestive heart failure (CHF), there is a good reason to believe that some of the findings in the CHF population may also extend to patients with COPD.

With the correlations that are possible to see from the previous work that has been done in cardiac disease and heart failure, it should be possible to demonstrate that these autonomic tests are clear predictors of morbidity and mortality, and that improvements in the parameters that one measures, correlate with improved outcomes.

The first part of this study has been designed to answer questions about interactions between the nervous system, the cardiac and the pulmonary system; and issues concerning heart rate variability activity. The study consists of several sections that were performed on different days on the population of:

- 1) Patients with severe pulmonary disease that are being enrolled into the National Emphysema Treatment Trial (NETT) to study lung volume reduction surgery (LVRS) as well as to the elective population undergoing lung volume reduction surgery.
- 2) Normal individuals with no known cardiac or pulmonary disease.

Our hypotheses are as follows:

In COPD patients:

- 1) The most severely diseased patients will have the lowest HRV, BPV and decreased BRS, corresponding to decreased survival and higher morbidity.
- 2) The results of the autonomic testing of the patients will improve after pulmonary rehabilitation.
- 3) Regardless of the treatment arm of the study, the patients that improve the results of their autonomic testing will have better survival and decreased morbidity.

In normal individuals:

- 1) HRV, BPV and BRS are higher in normal individuals than in COPD patients.
- 2) The results of the autonomic testing are better for normal individuals than COPD patients.

The application of the data analysis in the time and frequency domain is continued in studying a regulatory feedback loop, called the baroreflex mechanism, which exists in the cardiovascular system in which autonomic nervous system activity is altered in response to changes in blood pressure. The results from this part of the research will allow one to discuss the influence of respiration on heart rate variability in response to different means of paced-breathing maneuvers (by COPD patients) such as

breathing room air (RA) or with oxygen supplement (O₂) during rest and exercise, that alter baroreflex activity, in order to assess COPD related changes in baroreflex response.

When HRV is analyzed in the frequency domain, the power spectrum of HRV does not show its temporal changes. There are many physiological situations of interest where heart rate changes rapidly over time and the monitoring of these temporal changes may be very important. Time frequency representations are perfect candidates to monitor these temporal-spectral changes. Time frequency analysis is performed on the HRV data to show vagal tone and the sympatho-vagal balance as a function of time. In this part of the study, several time frequency representations such as the short time Fourier transform, the smoothed pseudo Wigner-Ville, the Choi-William, the Born-Jordan-Cohen are used in comparison with wavelet distributions (Morlet, Meyer, Daubechies, Mexican Hat and Haar) for analyzing HRV and physiological signals.

Coherence spectral plots are graphical representations of the coherence between two signals. Coherence can be viewed as correlation coefficients in the frequency domain [5]. It is a measure of the linear dependence between two signals, normalized to values between zero and one. The applications of coherence in past studies have been directed toward the analysis of the electroencephalogram or EEG signals. In this study, however, coherence is used not for EEG signals but for the combinations between heart rate, blood pressure and respiration signals. The coherence spectral plots in the whole HRV frequency range (0.04 to 0.7 Hz) are presented and the average weighted sum, the weighted coherence values, in the low frequency band (LF: 0.04 to 0.15 Hz) and in the high frequency band (HF: 0.15 to 0.4 Hz) are obtained for further statistical analyses (i.e. principal component analysis, PCA and cluster analysis, CA). These values are

examined for determining the inter-relationship between heart rate, blood pressure and respiration of the cardiovascular system.

Once the study of the relationships between heart rate, blood pressure and respiration are established, the influence of one component was removed while the coherence between the two residual (signal) components were examined. It is here the technique of partial coherence is introduced as another novel technique in investigating HRV. Again the weighted partial coherence values in the LF and HF bands are obtained for further analysis.

Beside the traditional data analysis in the time domain and frequency domain the last part of this study also used other control system techniques of system identification to examine stationary and non-stationary conditions of heart rate variability. To further investigate the role of the autonomic nervous system and to understand the complex links between respiratory activity and arterial pressure, the transfer functions between respiration, heart rate (HR), and arterial systolic blood pressure in COPD and healthy subjects were determined during 5-min periods in which the respiratory rate was controlled in a predetermined but pseudo-random fashion.

Linear analyses of fluctuations in heart rate and other hemodynamic variables have been used to elucidate cardiovascular regulatory mechanisms. Since the role of nonlinear contributions to fluctuations in hemodynamic variables has not been fully explored, this study also presents a nonlinear system analysis of the effect of fluctuations in respiration and arterial blood pressure (ABP) on heart rate (HR) fluctuations.

A time domain technique is presented to estimate transfer characteristics from fluctuations of respiration to heart rate (HR). Pure moving average (MA) and

autoregressive (ARX) system identification techniques [6] are introduced to characterize the system. Pre-processing (pre-filtering of the HR fluctuations and pre-enhancement of the high frequency contents of respiration) was proven to be effective in obtaining stable estimates of MA coefficients. Model order selection of the ARX system based on a priori knowledge of the system characteristics is proposed. Data analysis using the time domain techniques may reveal some temporal transfer characteristics which are poorly resolved using frequency domain analysis.

This study also employs a new approach to Exogenous Input AutoRegressive (ARX) modeling [7], which automatically seeks the best model order to represent, investigated linear, time invariant systems using their input/output data. The algorithm seeks the ARX parameterization, which accounts for variability in the output of the system due to input activity and contains the fewest number of parameters required to do so. The unique characteristics of the proposed system identification algorithm are its simplicity and efficiency in handling systems with delays and multiple inputs. Results of applying the algorithm to simulated data and experimental biological data are presented. In addition, a technique for assessing the error associated with the impulse responses, calculated from estimated ARX parameterizations, is presented. This technique is one example of a variety of techniques of system identification. It was shown that system identification techniques could yields new insight into the sequence of changes that occurs with COPD autonomic neuropathy and provided an accurate easily comprehensible measurement of respiratory induced HR variability.

The last task of this study is normal-COPD separation and COPD severity classification. Major contributing components of the cardiovascular system are

identified using principal component analysis. Cluster analysis is used to separate the normal subjects from the COPD subjects in a mixed population. Once the separation is completed, cluster analysis is again used to assign the COPD subjects according to their severity group. The severe COPD subjects are identified and recommended for lung reduction surgery if necessary.

1.2 Goals and Contributions

The goals of this research are:

1. To apply time-frequency analysis to heart rate variability in order to investigate the difference in HRV during rest and exercise between normal subjects and COPD subjects.
2. To use time-frequency analysis to understand and to develop tools that can describe rapid changes in the time varying spectrum due to exercise. Expansion of the concept of spectral analysis of heart rate variability to time-frequency analysis gives one the ability to quantitatively assess the parasympathetic and sympatho-vagal balance changes as a function of time for normal and COPD subjects.
3. To use four different kernels of the general class of time-frequency distributions (linear: the short time Fourier transform, and bilinear: the smoothed pseudo Wigner-Ville, the Choi-William, the Born-Jordan-Cohen) and wavelet distribution (linear) to investigate the transitions between rest, exercise and recovery.
4. To evaluate and assess which distribution among the bilinear time-frequency distributions and wavelet distribution give the most physiologically significant information from the data of COPD subjects.

5. To use the best choice of the time-frequency distribution and wavelet distribution performed on the heart rate variability signal to quantify the area under the low frequency and high frequency ranges during different breathing conditions (room air, 30 % oxygen supplement) at rest and exercise as reflected in the heart rate variability signal of COPD subjects.
6. To use coherence and partial coherence in learning the relationships between heart rate variability, blood pressure variability and respiration as well as the sympatho-vagal balance of the autonomic nervous system.
7. To develop a general class of Exogenous Input AutoRegressive (ARX) models for the cardiovascular system from experimental data using system identification techniques. Once the model is obtained it can be used for COPD parameter testing (since the values of some of these parameters may not be attainable for COPD patients). This may provide COPD cardiovascular models for further study of the disease noninvasively.
8. To use principal component analysis and cluster analysis as tools that allow diagnosing the COPD severity noninvasively and accurately. This may help physicians further in deciding who may be best suited for lung reduction surgery.

This work clarifies some of the questions about heart rate variability on COPD subjects which are of fundamental importance in diagnosing the severity of the disease, in assessing the benefit of the rehabilitation procedure and ultimately in determining who may benefit the most from lung reduction surgery. The major contributions of this work can be summarized as follows:

1. Present the application of time-frequency analysis as an innovative approach to better represent the biological signals, namely HRV, BP and respiration on normal and COPD subjects. Four different time-frequency representations (Short-time Fourier Transform, the smoothed-pseudo Wigner, the Choi-William and the Born-Jordan-Cohen) and wavelet distribution are applied on modeled HRV test and experimental signals taken from COPD and normal subjects.
2. Compare the best Cohen class time-frequency representation to the wavelet distribution to see which representation overcomes the drawbacks of others by providing higher resolution in time and frequency while suppressing interferences between the signal components. Use these 2 distributions (one from the Cohen class and the wavelet distribution) to investigate the degradation of health from a change in activity of the autonomic nervous system (ANS) due to the COPD condition as reflected in the HRV signal. By expanding the concept of spectral analysis of HRV into time-frequency analysis, it is possible to quantitatively assess the parasympathetic (HF) and sympatho-vagal balance (LF:HF) changes as a function of time. As a result, the assessment of the ANS during rapid changes is made.
3. Analyze HRV and physiological signals using coherence and partial coherence to look at their inter-relationship as a whole or just residual components with the effect of the third component removed. This combination of techniques allows researchers to have unique opportunities to examine the vagal and sympatho-vagal systems.
4. A general class of Exogenous Input AutoRegressive (ARX) model is developed for the cardiovascular system using system identification techniques as an analytical tool for uncovering the hidden autonomic control processes in order to explain the physiological

mechanism behind HRV in both normal and COPD. The ARX model for each subject consists of filtered inputs plus additive noise and the output is the heart rate variability signal under investigation. Non-parametric relationships between the inputs (respiration and BP signals) and output (HRV) of the model will result in transfer function estimation of the noise filters and the input filters of these highly non-linear models.

Through a series of model transformations, the cardiovascular control mechanism can be expressed as a multiple-input single output linear system. The estimation of parameters for this class of ARX models is then defined as a maximum likelihood estimation (MLE) problem through state-space representations of input filters and noise filters. MLE techniques available in the MatLab System Identification toolbox then provide the means by which these ARX models can be parameterized to describe the observed HRV.

5. A severity-classification technique of the COPD disease states is developed using principal component analysis and cluster analysis on HRV parameters to identify and classify different subjects into proper disease states. In COPD, this helps identify severe patients who may be best candidates for surgery while in other diseases it may provide more accuracy and information in diagnosing a particular disease.

1.3 Outline of the Dissertation

The dissertation covers three topics in heart rate variability study of normal and COPD subjects. They are:

1. Time frequency representation and comparison of Cohen class and wavelet distribution;
2. Heart rate variability and cardiovascular modeling using non-parametric ARX model;
3. Normal, COPD separation and COPD severity classification.

Chapter 1 summarizes the scope of research involving both the normal and the Chronic Obstructive Pulmonary Disease population. The list of goals and contributions and a short outline of the dissertation are described.

Chapter 2 summarizes the physiology background for studying the human cardiovascular system. The description and operating mechanism of the heart, lung, the electrocardiogram (ECG), the blood pressure and the respiration are presented.

Chapter 3 presents the engineering tools to analyze the biological signals of ECG, BP and respiration. The basic signal representation used in this dissertation is the time – frequency representation. It includes both the linear (STFT and wavelet distributions) and the quadratic time – frequency distributions (Cohen’s class: Wigner-Ville, Choi-Williams, and Born-Jordan-Cohen distributions).

Chapter 4 presents the experimental protocols and data analysis methods used in the study of this dissertation. The data analysis methods included spectral analysis, time-frequency analysis (linear: STFT, WL and bilinear: WVD, CWD, BJC), cross-

spectral analysis, system identification, principal component and cluster analyses on HRV, BPV of normal and COPD subjects.

Chapter 5 presents the results and discussion of the study. First, the spectral analysis results as a method for describing periodic processes are presented. Second, the results of the time-frequency analysis for Cohen's class distributions and wavelet distributions applied to sine waves, HRV and BPV of both normal and COPD subjects are discussed. Third, the criteria are determined and the selection of the best wavelet is performed. Fourth, the activity plots of both normal and COPD subjects that represented the vagal tone and sympathovagal balance are also presented and discussed. Fifth, the cross-spectral analysis of the weighted coherence and partial coherence of the HRV of normal and COPD are presented. Sixth, the open loop and closed loop cardiovascular models for normal and COPD are discussed. Seventh, the principal components of the normal and COPD HRV study are found. Finally, the results of the normal, COPD blind separation and COPD severity classification are shown and discussed.

Chapter 6 concludes the work and suggests topics for future study. Hopefully, these topics, in addition to this research work, will motivate the prospective researcher to explore further unresolved issues in the field of heart rate variability, biological modeling and disease severity classification in the direction of signal processing application to signal analysis using time-frequency representation techniques such as wavelet distributions, adaptive signal decomposition or reconstruction and beyond.

CHAPTER 2

PHYSIOLOGY BACKGROUND

Biomedical engineering is the application of the principles of engineering, science, and mathematics to biology and medicine. In this dissertation the electrical signals or waveforms are examined because they can yield information of clinical significance about the biological systems. Therefore, in order to conduct biomedical research, the relevant physiological systems must be understood. The purpose of this section is to provide a general, but concise, background to the physiological systems that are relevant to the work in this research.

2.1 Cardiovascular Systems and The Heart

The cardiovascular system or simply, the circulatory system [5] consists of the heart, which is a muscular pumping device, and a closed system of blood vessels called arteries, veins, and capillaries. Blood contained in the circulatory system is pumped by the heart around a closed circle or circuit of vessels as it repeatedly passes through the various “circulations” of the body. The vital role of the cardiovascular system in maintaining homeostasis is dependent upon the continuous and controlled movement of blood to reach every cell in the body. Regulation of blood pressure and flow must change in response to cellular activity. Consequently, numerous control mechanisms help to regulate and integrate the diverse functions and component parts of the cardiovascular system to supply blood to specific body areas according to need.

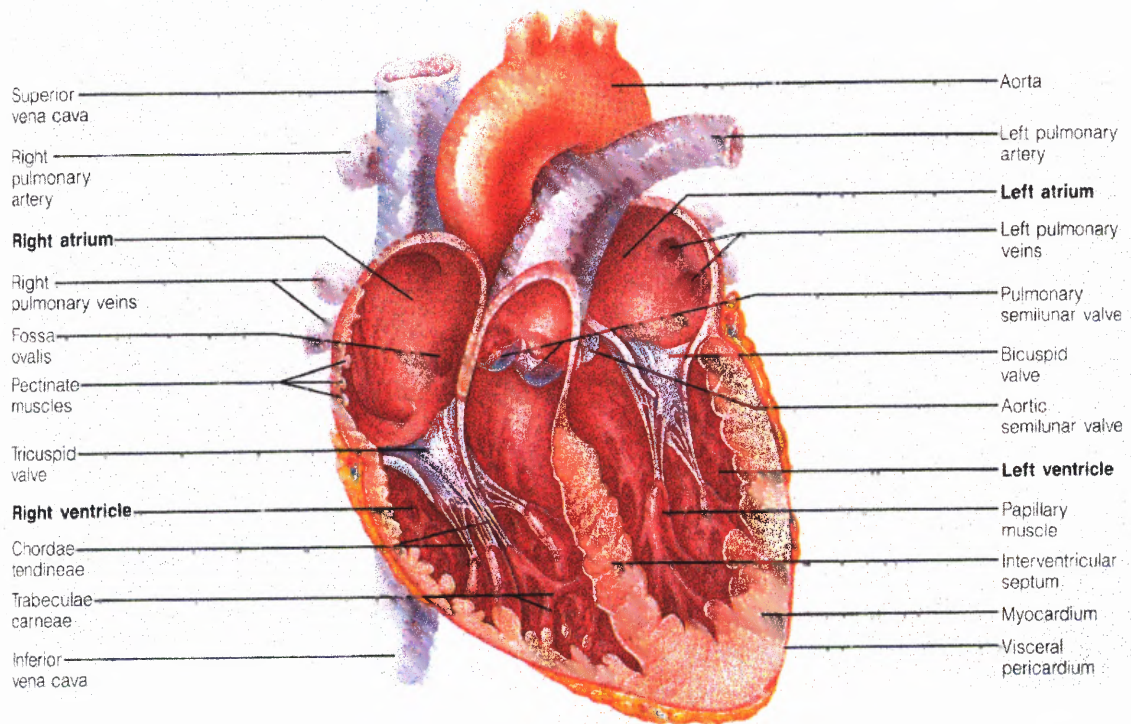


Figure 2.1 The heart. (From E. N. Marieb, *Human Anatomy and Physiology*, 3rd ed. New York: The Benjamin/Cummings Publishing Company, Inc., 1995.)

The heart, illustrated in Figure 2.1, is divided into two functional halves, each half containing two chambers: an atrium and a ventricle. The atrium of each side empties into the ventricle on that side. There is no direct flow between the two atria or the two ventricles in a healthy individual. Blood is pumped by the pulmonary circuit from the right ventricle through the lungs and then into the left atrium. The blood is then pumped by the systemic circuit, from the left ventricle, through all the tissues of the body except the lungs, and then to the right atrium.

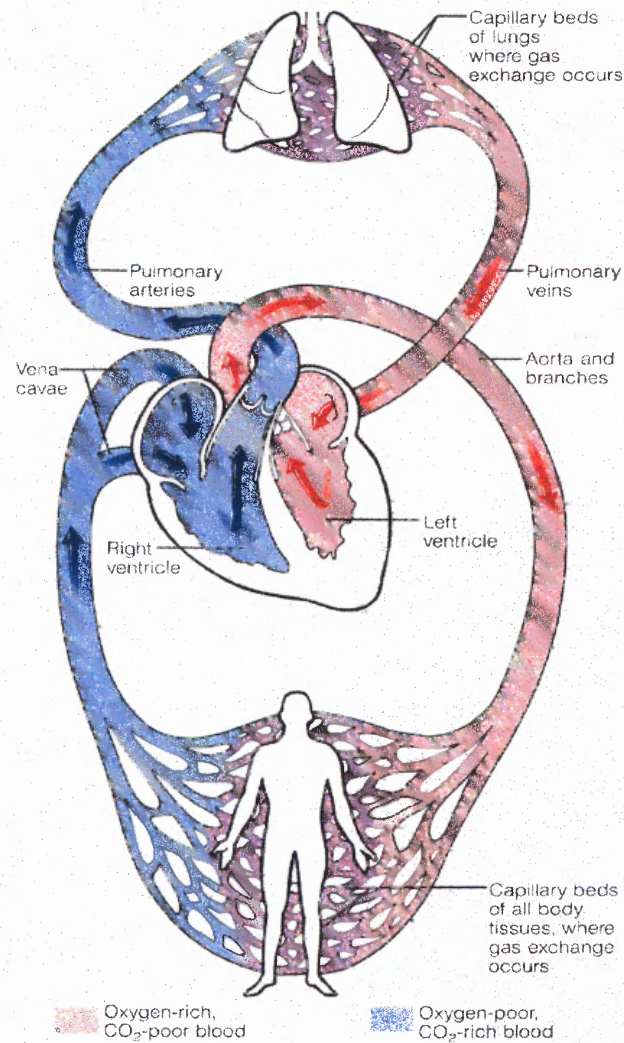


Figure 2.2 The systemic and pulmonary circulations. (From E. N. Marieb, *Human Anatomy and Physiology*, 3rd ed. New York: The Benjamin/Cummings Publishing Company, Inc., 1995.)

In both circuits, the vessels carrying blood away from the heart are called arteries and those carrying blood from either the lung or all other parts of the body back to the heart are called veins. Figure 2.2 illustrates the heart with the systemic and pulmonary circulations.

The heart, located in the chest, is a muscular organ, which is enclosing in a fibrous sac called the pericardium [5]. The walls of the heart are primarily composed of cardiac-muscle cells called the myocardium. Cardiac-muscle cells combine properties of both skeletal muscle and smooth muscle. However, even more important, approximately one percent of the cardiac-muscle fibers has specialized features that are essential for normal heart excitation [6]. They constitute a network known as the conducting system of the heart and are connected to other cardiac-muscle fibers by gap junctions. The gap junctions allow action potentials to spread from one cardiac-muscle cell to another.

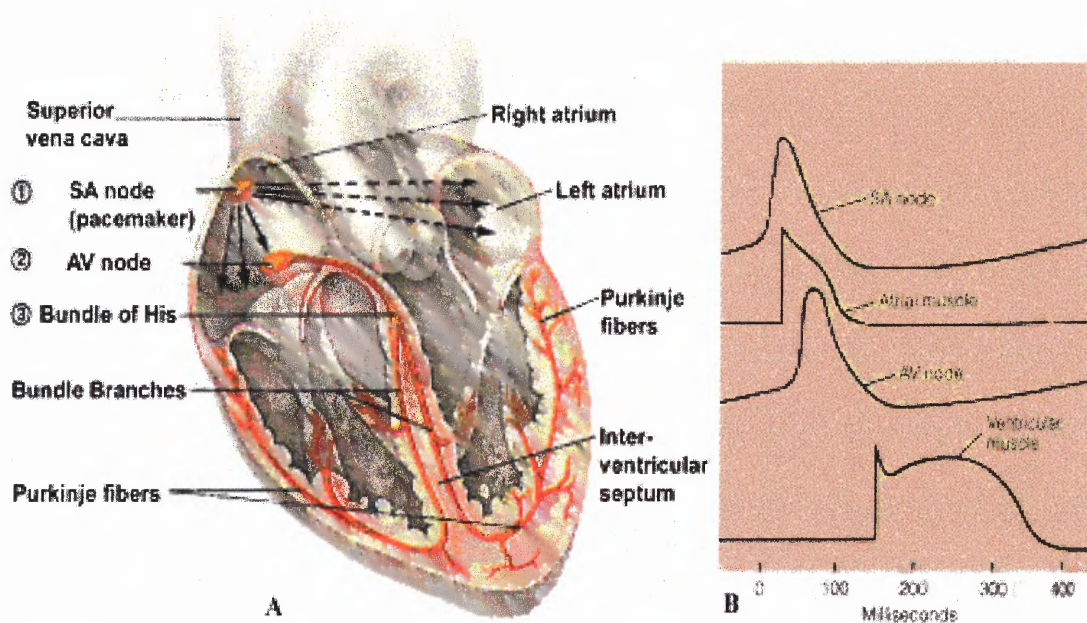


Figure 2.3 The intrinsic conduction system of the heart and succession of the action potential through selected areas of the heart during one heart beat. **B.** The sequence of potentials generated across the heart is shown from top to bottom beginning with the pacemaker potential generated by the SA node and ending with an action potential. (From E. N. Marieb, *Human Anatomy and Physiology*, 3rd ed. New York: The Benjamin/Cummings Publishing Company, Inc., 1995.)

Thus, the initial excitation of one myocardial cell results in excitation of all cells, and as a result, the pumping action of the heart. The conducting system of the heart is

illustrated in Figure 2.3. The initial depolarization normally arises in a small group of conducting-system cells called the sinoatrial (SA) node. The SA node is located in the right atrium near the entrance of the superior vena cava (the vein returning from the body tissues that are above the heart). The SA node has the fastest inherent discharge rate of any of the myocardial cells with pacemaker activity. Therefore, the SA node is the normal pacemaker for the entire heart [4]. The action potential initiated in the SA node spreads throughout the myocardium, passing from cell to cell by way of gap junctions. The spread throughout the right atrium and the left atrium does not depend on fibers of the conducting system. The spread is rapid enough that the two atria are depolarized and contract at essentially the same time.

The spread of the action potential from the atria to the ventricles involves a portion of the conducting system called the atrioventricular (AV) node. The AV node is located at the base of the right atrium. The AV node has an important characteristic that makes the cardiac cycle more efficient. For several reasons related to the electrical properties of the cells that make up the AV node, the propagation of action potentials through the AV node results in a delay of approximately 0.1 seconds [4]. This delay allows the atria to finish contracting and, therefore, completely emptying their contents of blood into their respective ventricles before ventricular excitation occurs.

Upon leaving the AV node, the action potential then travels to the septum, the area between the two ventricles, by the conducting-system fibers called the bundle of His [6]. The bundle of His then divides into the left and right bundle branches which eventually leave the septum and enter the walls of their respective ventricles. These fibers then make contact with the Purkinje fibers, which are large conducting cells that

rapidly distribute the action potential throughout most of the ventricles. The rapid conduction along the Purkinje fibers and the distribution of these fibers cause the depolarization of the left and right ventricular cells approximately simultaneously, thus resulting in a single coordinated contraction. Figure 2.4 illustrates the sequence of cardiac excitation.

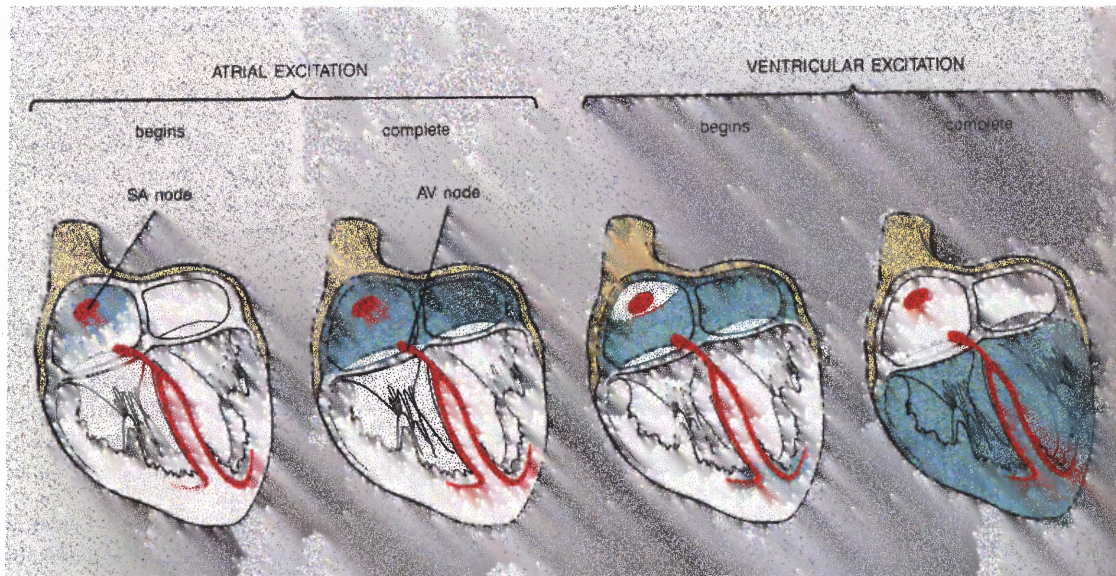


Figure 2.4 The sequence of cardiac excitation. (From A.J. Vander, J.H. Sherman, and D.S. Luciano, Human Physiology, 1994.)

2.2 Blood Pressure

The force that blood exerts against the walls of a vessel is called blood pressure. Normally, some amount of blood is present in every blood vessel of the body, including all arteries, arterioles, capillaries, venules and veins.

Blood volume is greatest in the veins. Venous blood pressure, however, is quite low because the vein walls are thin and compliant. Skeletal movement, mechanical movement from respiration and one-way valves, facilitates return of deoxygenated blood to the heart.

Less than fifteen percent of the blood volume is present in the arteries. Mean arterial pressure, however, is approximately 100 mm Hg. Mean arterial pressure (MAP) [6] depends upon total peripheral resistance (TPR) and cardiac output (CO). Specifically:

$$\text{MAP} = \text{TPR} * \text{CO} \text{ [mmHg]}. \quad (2.1)$$

The resistance of a particular arteriole depends upon the associated organ's requirements. Under different conditions, an arteriole radius will be varied by control mechanisms to accommodate the need of the associated organ. If the overall radius of all arterioles decreases, then the TPR is increased, which may cause arterial blood pressure to increase, depending upon the CO value.

When blood flows into arteries and arterioles, stretching occurs due to the pressure that blood exerts on the arterial walls. The maximum pressure, which is reached when the ventricles eject blood, is called the systolic pressure. The minimum arterial pressure occurs just before ventricular ejection begins and is called diastolic pressure [5].

2.3. Metabolic Function/Respiration

In the human, respiration serves to provide cells with oxygen, eliminate carbon dioxide and regulate the pH of the blood. In order to provide cells with oxygen, air from the environment enters the body during inhalation. Carbon dioxide and other unwanted substances are removed from the body during exhalation. Upon inhalation, air enters the body via the trachea, and then flows into the bronchi. The air then reaches the alveoli. The properties of the alveoli allow rapid and efficient exchange of gasses between the blood within the capillaries and the alveoli. The volume of oxygen per unit time (V_{O_2}) that is transported from the capillaries to the body cells is equal to the volume of the inspired oxygen that is diffused from the alveoli into the blood at any given instant. Analogously, the volume of CO_2 produced by the body cells per unit time (V_{CO_2}) is equal to the amount of CO_2 that diffuses from the blood to the alveoli. The total amount of air entering and leaving the body per unit time is the called ventilation (VE).

The Fick equation expresses the important relationship of tissue oxygen uptake (V_{O_2}) to cardiac output (CO) and the arterial-venous oxygen content difference ($CaO_2 - CvO_2$) [10] as shown below:

$$V_{O_2} (mL/min) = CO * (CaO_2 - CvO_2) \quad (2.2)$$

2.4 The Nervous System

Human behavior is controlled and regulated by two major communication systems, the endocrine system and the nervous system. The nervous system can be divided into two separate, but interconnected, parts. The first part consists of the brain and spinal cord and is called the central nervous system. The second part, which consists of nerves, which extend from the brain and the spinal cord out to all points of the body, is called the peripheral nervous system.

The peripheral nervous system consists of both an afferent division and efferent division. The afferent division conveys information from primary receptors to the central nervous system. The efferent division carries signals from the central nervous system out to effector cells such as muscles and organs. The efferent division is subdivided into a somatic nervous system and an autonomic nervous system. The somatic nervous system consists of all the nerve fibers going from the central nervous system to skeletal-muscle cells. The efferent innervation of all tissues other than skeletal muscle is done by the autonomic nervous system. Table 2.1 illustrates the organization of the human nervous system.

Table 2.1 The Nervous System

I. Central Nervous System	II. Peripheral Nervous System
A. Brain B. Spinal Cord	A. Afferent Division B. Efferent Division <ol style="list-style-type: none"> 1. Somatic Nervous System 2. Autonomic Nervous System <ol style="list-style-type: none"> a. Sympathetic Nervous System b. Parasympathetic Nervous System

2.4.1 The Autonomic Nervous System

Cardiac muscle cells, smooth muscle cells, and glands are innervated by the autonomic nervous system. Although it is not entirely true, the autonomic nervous system controls bodily functions that one often assumes to be automatically controlled. Such functions are heart rate, blood pressure, and body temperature. For example, when one is placed under a lot of physical stress such as climbing three flights of stairs, the person's heart rate and respiration rate automatically increase to supply the body with the energy needed on demand. Likewise, when a person is resting, the heart rate and respiration rate slow down due to the decrease in energy expenditure. Therefore, one can assume that the body automatically controls heart rate and respiration rate. However, it is possible to override the autonomic nervous system and consciously control some of its functions. A good example of this is that under certain meditation techniques, it has been shown that some people can actually lower their heart rate substantially below their resting rate, or even stop their heart from beating for a brief period of time. In addition, some people can slow their breathing rate to only one breath for every few minutes during deep meditation.

As shown in Table 2.1, the autonomic nervous system is divided into two anatomically and physiologically different systems [5][6]. These two systems are termed the sympathetic nervous system and the parasympathetic nervous system. Anatomically, the sympathetic and parasympathetic nervous systems differ for two reasons. One difference is that the nerve fibers of each system leave the central nervous system at different levels.

The sympathetic nerve fibers leave the central nervous system from the thoracic and lumbar sections of the spinal cord. The parasympathetic nerve fibers leave the central nervous system from the brain through cranial nerves III, V, VII, IX, and X and the second and third sacral spinal nerves. Cranial nerve X is also called the vagus nerve. The parasympathetic innervation of much of the thorax and abdomen, and especially the heart, is done by the nerve fibers, which leave from the brain through cranial nerve X. Therefore, parasympathetic activity related to the heart is often called vagal activity. Figure 2.5 illustrates the anatomic difference between the sympathetic nervous system and parasympathetic nervous system as well as some of their respective effector organs.

The second anatomical difference between the sympathetic and parasympathetic nervous systems has to do with the location of the ganglia. Each connection of the autonomic nervous system between the central nervous system and the effector cell consists of two-neuron chains connected by a synapse. Most, but not all, of the sympathetic ganglia are located close to the spinal cord and form two chains of ganglia, one on each side of the spinal cord, called the sympathetic trunk. Conversely, the parasympathetic ganglia lie within the organs innervated by the postganglionic neurons.

Physiologically, the sympathetic and parasympathetic nervous systems are also different [5]. One common physiological characteristic is that the major neurotransmitter released between the pre- and post-ganglionic fibers is acetylcholine. However, in the sympathetic division, the major neurotransmitter between the postganglionic fiber and the target cell is usually norepinephrine, a neurotransmitter that activates excitatory receptors, but in some cases can inhibit certain organs. In the parasympathetic division, the major neurotransmitter between the postganglionic fiber

and the target cell is the same as the pre- and post- ganglionic neurotransmitter, acetylcholine. Although acetylcholine generally has an excitatory effect, it is also known to have inhibitory effects as well, such as the slowing of the heart by the vagus nerve. In Figure 2.5, it is important to realize that some organs, such as the heart, eyes, and stomach, receive autonomic activity from both the sympathetic and parasympathetic nervous systems. This is often called "dual innervation". Usually, but not always, whatever affects the sympathetic nervous system has on the effector cells; the parasympathetic nervous system has the opposite effect [5]. In general, the sympathetic nervous system increases its response under conditions of stress. It is responsible for what is known as the fight-or-flight response. On the other hand, activity of the parasympathetic nervous system is associated with relaxing and the storing of energy. For example, heart rate increases with sympathetic activity and decreases with parasympathetic activity. Table 2.2 summarizes the effects of the autonomic nervous system on selected organs.

Dual innervation by nerve fibers that cause opposite responses provides a very fine degree of control over the effector organ- it is like equipping a car with both an accelerator and a brake [5]. One can slow the car simply by decreasing the pressure on the accelerator; however, the combined effects of releasing the accelerator and applying the brake provide faster and more accurate control. Analogously, the sympathetic and parasympathetic divisions are usually activated reciprocally; that is, as the activity of one division is increased, the activity of the other is decreased.

In addition to dual innervation, another important physiological characteristic is that the sympathetic and parasympathetic nervous systems are continually active.

Without these sympathetic and parasympathetic tones, each nervous system would only be able to produce one desired output, such as increasing heart rate. For instance, when sympathetic tone increases, heart rate increases. Conversely, when sympathetic tone decreases below its basal rate, the heart rate will decrease because of less sympathetic influence.

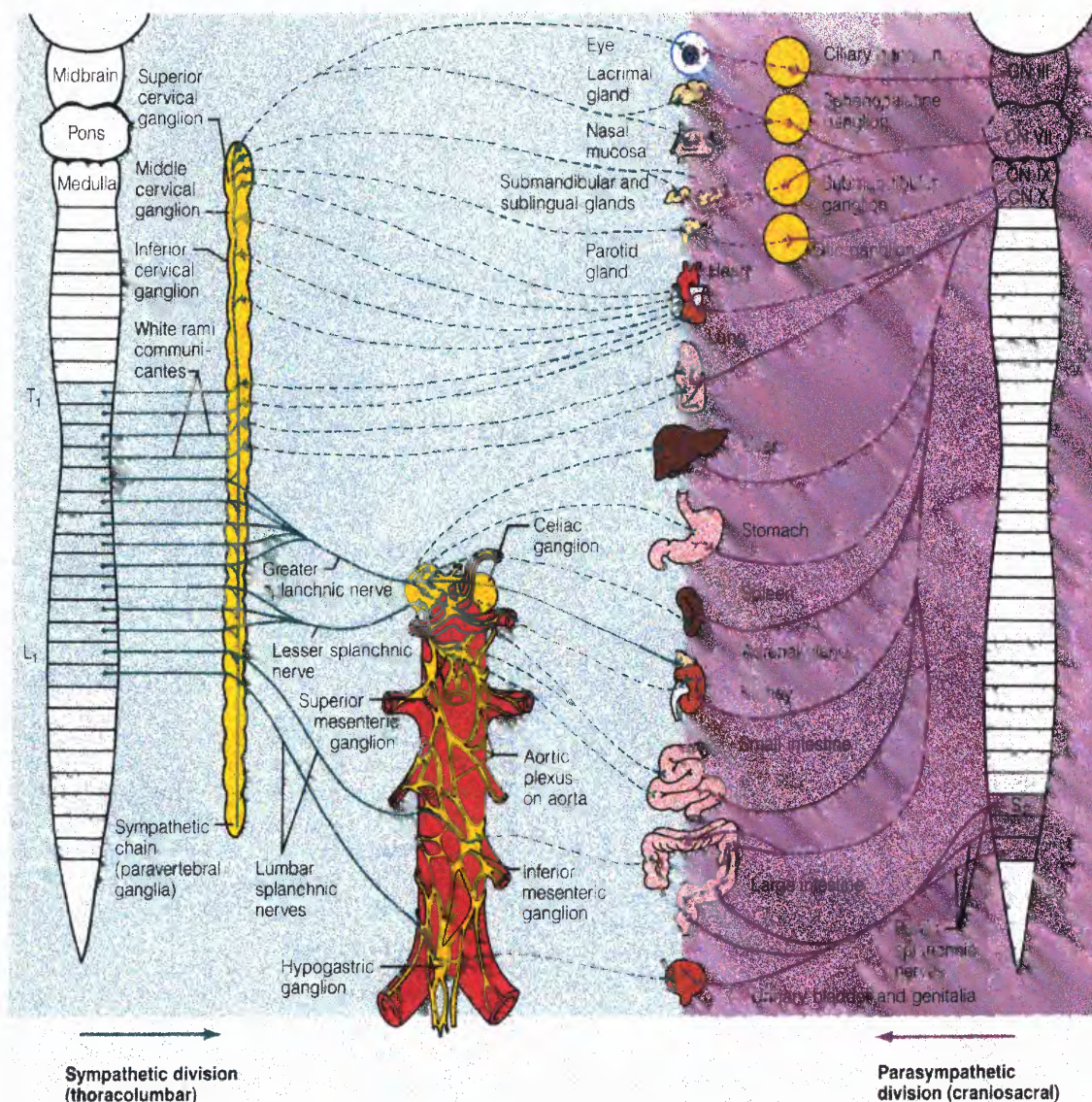


Figure 2.5 The sympathetic nervous system and parasympathetic nervous system. (From E. N. Marieb, *Human Anatomy and Physiology*, 3rd ed. New York: The Benjamin/Cummings Publishing Company, Inc., 1995.)

Table 2.2 Autonomic Effects on Selected Organs of The Body (From A.J. Vander, J.H. Sherman, and D.S. Luciano, Human Physiology, 1994)

Effector Organ	Effect of Sympathetic Stimulation	Effect of Parasympathetic Stimulation
Eyes Iris muscles Ciliary muscle	contracts (dilates pupil) Relaxes (flattens lens)	relaxes (constricts pupil) Contracts
Heart SA node Atria AV node Ventricles	Increases heart rate Increases contractility Increases conduction velocity Increases contractility	Decreases heart rate Decreases contractility Decreases conduction velocity Decreases contractility slightly
Arterioles Coronary Skin Skeletal muscle Abdominal viscera Salivary glands	Dilates (β_2); constricts (α) Constricts Dilates (β_2); constricts (α) Dilates (β_2); constricts (α) Constricts	Dilates None None None Dilates
Lungs Bronchial Muscle	Relaxes	Contracts
Stomach Motility, tone Sphincters Secretion	Decreases Contracts Inhibits (?)	Increases Relaxes Stimulates

2.4.2 The Baroreflex Mechanism

Of primary importance in circulation is the maintenance of the proper flow of oxygen-enriched blood to the brain and the rest of the body. Baroreceptors are stretch receptors located in the walls of the carotid sinus and the aortic arch [4], which are pressure sensors that monitor the arterial blood pressure. They are stimulated by distension of the structural tissue in which they are located, and exhibit an increased rate of discharge when the pressure in the structure increases. Afferent nerve fibers, specifically the ninth and tenth cranial nerves [4], communicate their activity directly to the cardio inhibitory

center in the medulla, which controls tonic vagal discharge at rest. A rise in systemic arterial pressure stimulates the cardio inhibitory center, which in turn increases vagal tone, resulting in decreased cardiac rate and vasodilation. A decrease in systemic arterial pressure decreases stimulation of the cardio-inhibitory center, producing a decrease in vagal tone and an increased discharge from the sympathetic cardiac nerves, resulting in an increased cardiac rate and vasoconstriction [4]. The result is a negative feedback mechanism that is vital in maintaining proper oxygen transport in the face of external perturbations.

2.5 Heart Rate and Heart Rate Variability

2.5.1 Physiology of Changes in Heart Rate

Change in heart rate is sensitive to changes in body temperature, plasma electrolyte concentrations and hormone concentrations [5]. However, the most important influence of beat-to-beat variations of heart rate comes from the autonomic nervous system. More specifically, sympathetic activity increases heart rate, whereas activity in the parasympathetic (vagus) nerves causes the heart rate to decrease. Due to considerably more parasympathetic activity to the heart than sympathetic activity in the resting state, the normal resting heart rate is below the inherent rate of 100 beats/minute.

The autonomic nervous system innervates the heart in a number of places. The sympathetic nervous system terminates at the SA node, the conduction system, atrial and ventricular myocardium, and coronary vessels. The parasympathetic fibers terminate in the SA and AV nodes, atrial and ventricular musculature, and coronary vessels. Interplay between the two systems will cause the heart to speed up or slow down, depending on which system is more active. Figure 2.6 illustrates the autonomic innervation of the heart [5].

Perhaps the most important site of innervation of the autonomic nervous system on the heart occurs at the SA node. As matter of fact, the SA node possesses an inherent discharge rate, often referred to as the pacemaker potential. The pacemaker potential is a slow depolarization of the cells of the SA node. The innervation of the sympathetic and parasympathetic nervous system on the SA node changes the characteristics of depolarization within the SA node cells, thus changing heart rate. Figure 2.7 illustrates these changes due to autonomic innervation.

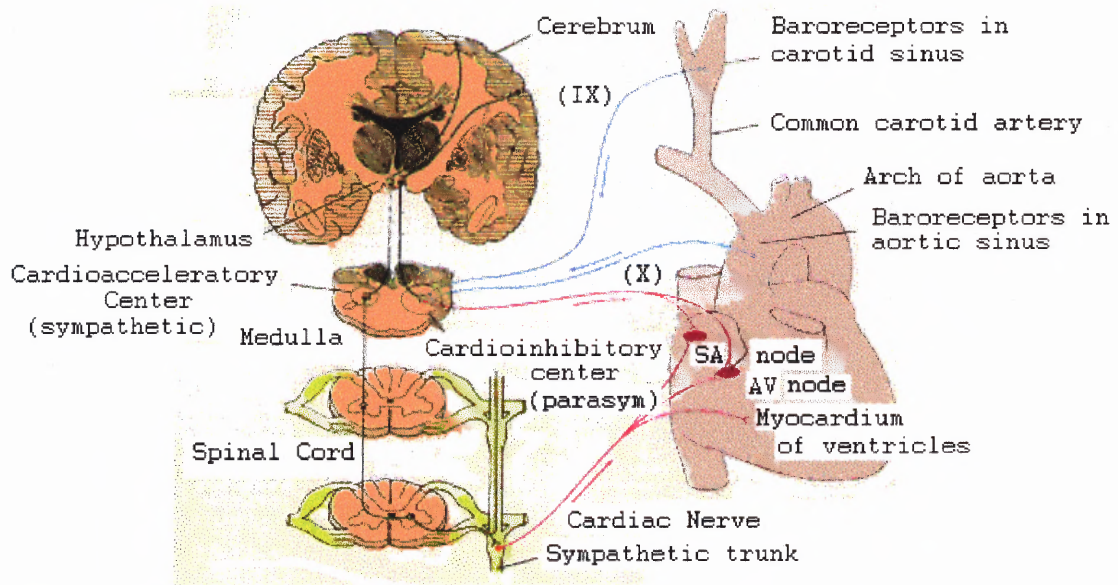


Figure 2.6 Autonomic innervation of the heart. (From G. J Tortora and N. P Anagnostakos, "Principles of Anatomy and Physiology," Harper and Row, Publishers, New York, 1990.)

For comparative purposes, the pacemaker potential labeled "Control" is the normal. From the figure, one can observe that sympathetic stimulation increases the slope of the pacemaker potential. As a result, the SA node cells reach the threshold more rapidly, thus increasing the heart rate. Conversely, parasympathetic stimulation decreases the slope of the pacemaker potential. Consequently, the SA node cells reach the threshold more slowly, and heart rate decreases. In addition to decreasing the slope of the pacemaker potential, parasympathetic stimulation also hyperpolarizes the plasma membrane of the SA node cells so that the pacemaker potential starts from a more negative membrane potential. As a result, the time it takes the SA node cells to reach the threshold increases, which decreases heart rate.

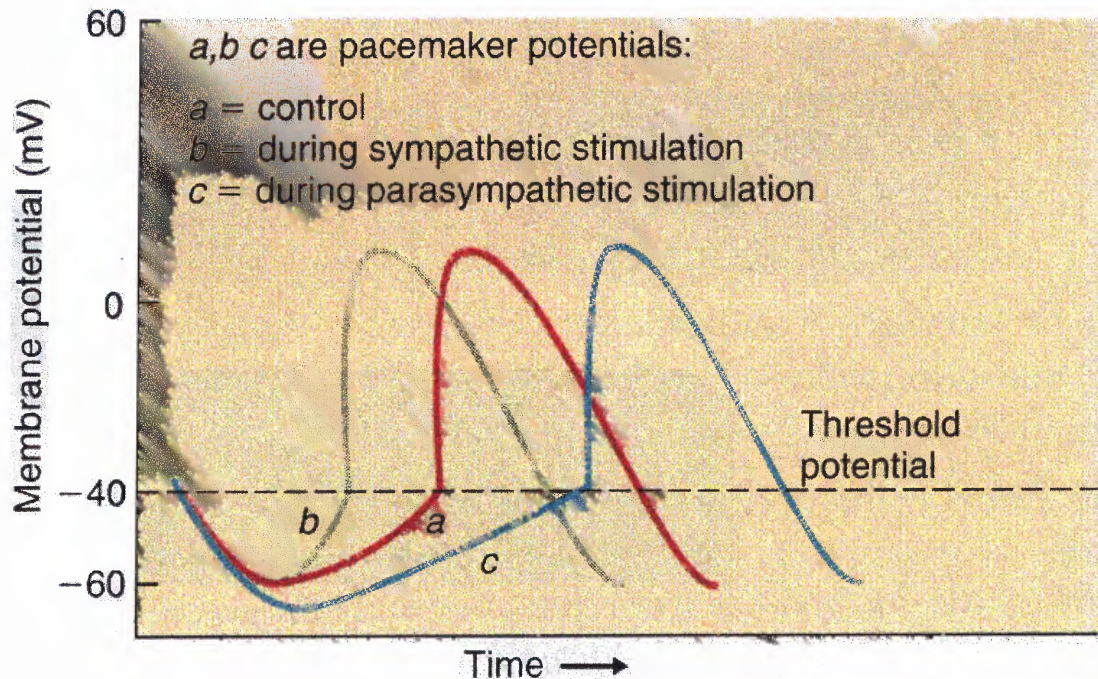


Figure 2.7 Effect of autonomic stimulation on the slope of the pacemaker potential. (From A.J. Vander, J.H. Sherman, and D.S. Luciano, Human Physiology, 1994.)

2.5.2 Heart Rate Variability as a Measure of Autonomic Function

Changes in heart rate usually involve the reciprocal action of the two divisions of the autonomic nervous system. An increased heart rate is the result of reduced parasympathetic tone and a concomitant increase in sympathetic activity. A decrease in heart rate is usually the result of increased parasympathetic tone and a simultaneous decrease in sympathetic tone. Therefore, changes in heart rate reflect the action of the sympathetic and parasympathetic nervous systems on the heart. However, under certain conditions, it is possible for heart rate to change by activity of only one division of the autonomic nervous system, independent of the other division, rather than reciprocal changes in both [8].

Initially, the effect of the autonomic nervous system on the heart was estimated by utilizing the traditional technique of average heart rate [8]. As a reference, the

average heart rate was measured under normal resting conditions. Then the average heart rate was measured under the administration of drugs. The drugs used were atropine, which blocks the effects of the parasympathetic nervous system, and propranolol, which masks the effects of the sympathetic nervous system. A qualitative assessment can then be made of the autonomic nervous system by comparing the reference heart rate to the heart rate while under the administration of the drugs. This method looks at the average over time of heart rate. However, when the ECG is looked at on a beat-to-beat basis, rather than over a period of time, fluctuations in the heart rate are observed [8]. Recent research indicates that fluctuations in heart rate are a healthy sign. In fact, one hypothesis is that the larger variations in the heart rate correlate to a healthier autonomic nervous system.

By contrast a number of physiologic and disease states produce alterations in autonomic function, which reduce the variability in heart rate [8].

2.5.3 Baroreflex Response

A decrease in blood pressure sensed by the baroreceptors produces an increase in sympathetic activity and a decrease in parasympathetic activity, resulting in an increase in heart rate and therefore an increase in blood pressure. An increase in blood pressure sensed by the baroreceptors produces an increase in parasympathetic activity and a decrease in sympathetic activity, resulting in a decrease in heart rate and therefore a decrease in blood pressure. The oscillations that result from this negative feedback loop have been shown to occur in the low frequency range (0.05-0.15Hz) [16].

In 1985, Akselrod et al. studied beat-to-beat variability of blood pressure, as well as heart rate, in response to respiration [11]. They concluded that blood pressure fluctuations at the respiratory frequency result almost entirely from the direct effect of centrally mediated heart rate fluctuations. Lower frequency fluctuations in blood pressure were associated with variability in vasomotor activity. Madwed et al. specifically investigated the low frequency oscillations in arterial blood pressure and heart rate using a simple computer model [12], but later applied their techniques to evaluate low frequency oscillations in arterial pressure during induced hemorrhage in dogs [13]. During hemorrhage, they found that the low frequency oscillations were dominant over the higher frequency respiratory related fluctuations, in contrast with the baseline condition. Lipsitz et al. studied the spectral characteristics of heart rate variability in response to postural tilt [14]. They found that total heart rate variability increases upon tilting in the young, while heart rate variability remained unchanged for older subjects during tilt. Malliani et al. studied cardiovascular neural regulation in the frequency domain, and found that the ratio of high frequency to low frequency power in heart rate variability is reflective of sympatho-vagal balance [15]. They concluded that functional states accompanied by an increased sympathetic activity are characterized by a shift in the balance of heart rate spectral power towards low frequency, and the opposite occurs during increased vagal activity, where the balance shifts towards high frequency spectral power in heart rate. Sleight et al. investigated the physiology and pathophysiology of heart rate and blood pressure variability in humans, finding that spectral analysis of cardiovascular variability is more a measure of baroreflex gain than of specific sympathetic or parasympathetic tone, or the balance between them [16].

However, they do note that there is often a correlation between gain of baroreflex activity and the autonomic balance of parasympathetic and sympathetic activity.

2.6 The Electrocardiogram

The electrocardiogram (ECG) is primarily a tool for evaluating the electrical events within the heart. The action potentials of cardiac muscles can be viewed as batteries that cause charge to move throughout the body fluids. These moving charges, or currents, represent the sum of the action potentials occurring simultaneously in many individual cells and can be detected by recording electrodes at the surface of the skin [6]. Figure 2.8 illustrates a typical normal ECG recorded between the right and left wrists for one heartbeat.

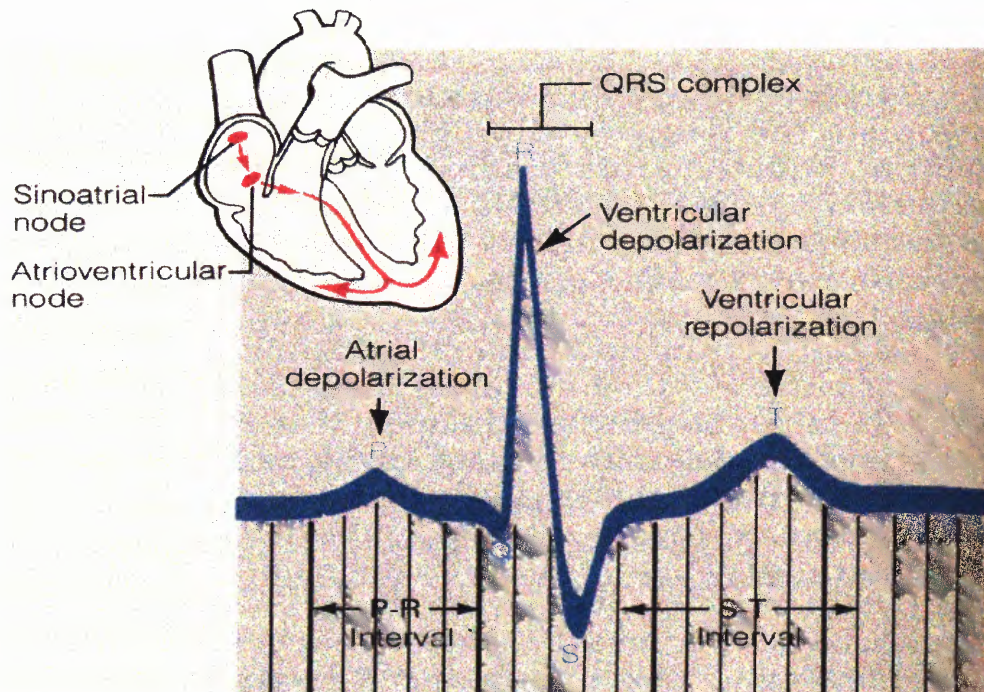


Figure 2.8 An electrocardiogram tracing (lead I) illustrating the three normally recognizable deflection waves and the important intervals. (From E. N. Marieb, Human Anatomy and Physiology, 3rd ed., 1995.)

The first deflection, the P wave, corresponds to the current flow during atrial depolarization (contraction). The second deflection, the QRS complex, is a result of ventricular depolarization. The third and final deflection is the T wave. The T wave is a result of ventricular repolarization (relaxation). It should be noted that atrial repolarization is usually not evident in the ECG because it occurs at the same time as the QRS complex.

As mentioned earlier, the ECG is a measure of the electrical activity of the heart measured on the skin. In order to measure the ECG, bipolar leads are required. The bipolar method of acquiring ECG detects electrical variations at two different locations on the skin and displays the difference to obtain one waveform. Figure 2.9 is an illustration of the standard limb lead connections that form the Einthoven's triangle. In addition, the diagram also shows the names of the respective leads. To record lead I, the negative terminal of the ECG monitor is connected to the right arm (RA) and the positive terminal is connected to the left arm (LA). To record lead II, the negative terminal of the ECG monitor is connected to the right arm and the positive terminal is connected to the left leg. To record lead III, the negative terminal of the ECG monitor is connected to the left arm and the positive terminal is connected to the left leg (LL). The reference point or ground is connected to the right leg (RL). It is important to realize that depending on where the electrodes are attached, a different waveshape will be obtained for the same electrical events occurring in the heart. In other words, leads I, II, and III all have a different waveform shape.

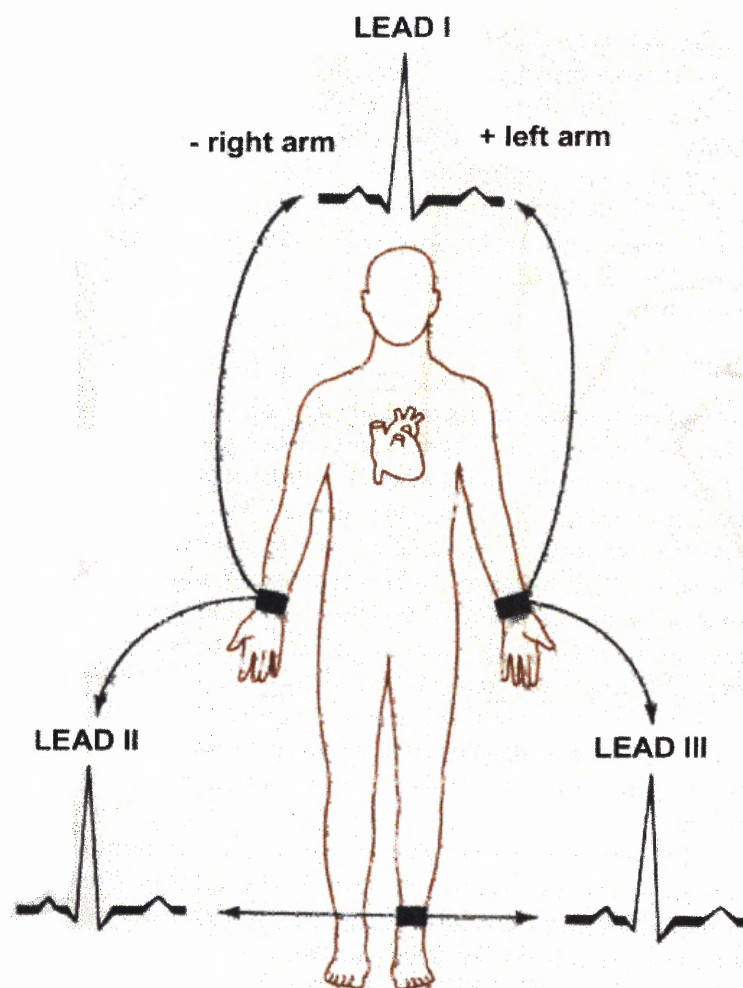


Figure 2.9 The placement of the positive and negative electrodes for three commonly used leads, as shown. (From J. G. Creager, *Human Anatomy and Physiology*. Belmont, CA: Wadsworth Inc., 1983.)

2.7 Chronic Obstructive Pulmonary Disease (COPD)

Chronic obstructive pulmonary disease (COPD) includes emphysema and chronic bronchitis--diseases that are characterized by obstruction to airflow. Emphysema and chronic bronchitis frequently coexist. Thus physicians prefer the term COPD. It does not include other obstructive diseases such as asthma. Nearly 16 million Americans suffer from COPD, which is the fourth leading cause of death, claiming the lives of almost 103,000 Americans annually. The annual cost to the nation for COPD is approximately \$31.9 billion, including healthcare expenditures of \$20.7 billion and indirect costs of \$11.2 billion. Smoking causes approximately 80 to 90 percent of COPD cases. A smoker is 10 times more likely than a nonsmoker to die of COPD. Other known causes are frequent lung infections and exposure to certain industrial pollutants. [9]

Chronic bronchitis is an inflammation and eventual scarring of the lining of the bronchial tubes. An estimated 14 million people suffer from chronic bronchitis, the seventh leading chronic condition in America. The rate of chronic bronchitis is 42 percent higher in females than in males. Symptoms of chronic bronchitis include chronic cough, increased mucus, frequent clearing of the throat and shortness of breath.

Emphysema causes irreversible lung damage. The walls between the air sacs within the lungs lose their ability to stretch and recoil. They become weakened and break. Elasticity of the lung tissue is lost, causing air to be trapped in the air sacs and impairing the exchange of oxygen and carbon dioxide. Also, the support of the airways is lost, allowing for obstruction of airflow. An estimated two million Americans have emphysema. Of the emphysema sufferers, 61 percent are male, and 39 percent are

female. While more men suffer from the disease than women do, the condition is increasing among women. Between 1982 and 1994 the emphysema prevalence rate in women increased 11 percent. Symptoms of emphysema include cough, shortness of breath and a limited exercise tolerance. Diagnosis is normally made by pulmonary function tests, along with the patient's history, examination and other tests.

As far as treatment for COPD is concerned, first the quality of life for a person suffering from COPD diminishes as the disease progresses. At the onset, there is minimal shortness of breath. People with COPD may eventually require supplemental oxygen and may have to rely on mechanical respiratory assistance. Depending on the severity of the disease, treatments may include bronchodilators, which open up air passages in the lungs; antibiotics; and exercise to strengthen muscles. To reduce and control symptoms of chronic bronchitis, sufferers should live a healthy lifestyle by exercising, avoiding cigarette smoke and other air pollutants, and eating well.

Pulmonary rehabilitation is a preventive health-care program provided by a team of health professionals to help people cope physically, psychologically, and socially with COPD. Lung transplantation is being performed in increasing numbers and may be an option for people who suffer from severe emphysema. Additionally, a new surgical procedure, lung volume reduction surgery, shows promise and is being performed with increasing frequency. Current research into COPD is focusing on gene therapy; it is hoped that clinical trials of this type of therapy will take place within the decade.

2.7.1 Classification of COPD by Severity

When classifying COPD severity in clinical settings, physicians rely on the results obtained from standardized spirometry. When performing spirometry, one measures:

1. Forced Vital Capacity (FVC) and
2. Forced Expiratory Volume in one second (FEV1).
3. The FEV1/FVC ratio is then calculated.

Spirometric results are expressed as % **predicted** using appropriate normal values for the person's sex, age, and height. Patients with COPD typically show a decrease in both FEV1 and FEV1/FVC. A postbronchodilator spirometric measurement of forced expiratory volume in one second (FEV1) less than 80% predicted and a ratio of FEV1 to forced vital capacity (FEV1/ FVC) below 70% suggest airflow limitation that is not fully reversible and according to Rennard: "A decreased ratio is considered an early sign of COPD, even if the FEV1 is normal." [7]

COPD is classified from stage 0 to stage III (Table 2.3) according to the guideline of the Global Initiative for Chronic Obstructive Lung Disease Committee (GOLD) as follow:

Stage 0: At Risk - Chronic cough and sputum production; lung function is still normal.

Stage I: Mild COPD - Mild airflow limitation ($FEV1/FVC < 70\%$ but $FEV1 > \text{or equal to } 80\% \text{ predicted}$) and usually, but not always, chronic cough and sputum production.

- At this stage, the individual may not be aware that his or her lung function is abnormal.

Stage II: Moderate COPD - Worsening airflow limitation ($30\% < \text{FEV}_1 < 80\%$ predicted), and usually the progression of symptoms, with shortness of breath typically developing on exertion.

- Acute exacerbations of symptoms, which have an impact on a patient's quality of life and prognosis, are especially seen in patients with $\text{FEV}_1 < 50\%$ predicted.

Stage III: Severe COPD - Severe airflow limitation ($\text{FEV}_1 < 30\%$ predicted) or the presence of respiratory failure or clinical signs of right heart failure. Patients may have severe (Stage III) COPD even if the FEV_1 is $> 30\%$ predicted, whenever these complications are present.

- At this stage, quality of life is very appreciably impaired and exacerbations may be life threatening.

TABLE 2.3 GOLD Severity Classification of COPD (From the Global Initiative for Chronic Obstructive Lung Disease GOLD Workshop, 1999)

GOLD CLASSIFICATION OF COPD	
Stage	Characteristics
0: At risk	Normal spirometry
	Chronic symptoms (cough, sputum production)
I: Mild COPD	FEV1/FVC < 70%
	FEV1 greater than or equal to 80% predicted
	With or without chronic symptoms (cough, sputum production)
II: Moderate COPD	FEV1/FVC < 70%
	FEV1 greater than or equal to 30% to < 80% predicted
	Ila: FEV1 greater than or equal to 50% to < 80% predicted
	Ilb: FEV1 greater than or equal to 30% to < 50% predicted
	With or without chronic symptoms (cough, sputum production, dyspnea)
III: Severe COPD	FEV1/FVC < 70%
	FEV1 < 30% predicted or FEV1 < 50% predicted plus respiratory failure or clinical signs of right heart failure
<p>GOLD, Global Initiative for Chronic Obstructive Lung Disease; COPD, chronic obstructive pulmonary disease; FEV1, forced expiratory volume in one second; FVC, forced vital capacity; respiratory failure, arterial partial pressure of oxygen < 60 mm Hg with or without arterial partial pressure of carbon dioxide greater than or equal to 50 mm Hg while breathing air at sea level.</p> <p>Data extracted from The GOLD Workshop Panel. [9]</p>	

CHAPTER 3

ENGINEERING BACKGROUND

The transformation of the electrocardiogram, blood pressure and respiration signals into heart rate variability, blood pressure variability and respiration spectra requires many intermediate steps such as peak detection, interpolation, resampling and spectral analysis. To date, there are no standardized ways to process this data to study heart rate variability, blood pressure variability, and respiration. This leads to varying experimental results and difficulties in the comparison of the experimental results from one research facility to another.

The purpose of this chapter is to introduce a brief background of various signal-processing methods used in this dissertation. First, a brief introduction to time-frequency distributions is presented. The uncertainty principle, the concepts of analytic signal, instantaneous frequency and the desired properties of the time-frequency distribution are discussed. The importance of covariance and invariance notion of the density function as an operator in the time-frequency distribution is mentioned. A brief theoretical background comparison of the short time Fourier transform, Wigner, windowed Wigner, Choi-Williams distributions and wavelets are discussed. Other methods of analysis including spectral analyses of HRV and BPV are also presented. The concepts of the cross-spectral analysis (coherence, weighted coherence, and partial coherence) and system identification are covered. Finally, the classification technique using principal component analysis and cluster analysis are also presented in detail.

3.1 Time-Frequency Distributions

From a given time series signal, $x(t)$, one can easily see how the "energy" of the signal is distributed in time. By performing a Fourier transform to obtain the spectrum, $X(\omega)$; one can readily see how the "energy" of the signal is distributed in the frequency domain. For a stationary signal, there is usually no need to go beyond the time or frequency domain. Unfortunately, most real world signals have characteristics that change over time, and the individual time domain or frequency domain does not provide means for extracting this information. There is obvious need for creating a function, $W(t, \omega)$, that represents the energy of the signal simultaneously in time and frequency. This function, $W(t, \omega)$, is commonly referred to as a time-frequency representation or time-frequency distribution. The most well-known time-frequency distribution is the spectrogram (squared magnitude of the short-time Fourier transform). However, there is a rich theory behind time-frequency analysis of which the spectrogram is just a small part. Two other well-known time-frequency distributions are the continuous wavelet transform and the Wigner (or Wigner-Ville) distribution.

The areas of time- frequency and time-scale analysis have seen many exciting developments in recent years [18-24]. The theory has been progressing rapidly and has been successfully applied to a wide variety of signals including the following: speech, biological, geophysical, machine monitoring, radar, and others. While there has been rapid progress in recent years, there are still many open questions regarding the construction of time-frequency distributions.

Since there are a wide variety of methods for constructing time-frequency distributions, it is useful to classify them according to their structure and properties.

Two common types of time-frequency distributions are those that are linear or quadratic functions of the signal. Examples of linear time-frequency distributions are the short-time Fourier transform and the wavelet transform. Examples of quadratic time-frequency distributions are the spectrogram, the scalogram (squared magnitude of the wavelet transform), and the Wigner distribution.

Time-frequency distributions are also often characterized by their behavior when an operator is applied to a signal. Three prominent examples of these operators are the time-shift operator, the frequency-shift operator (or frequency-modulation operator), and the scale operator. A time-frequency distribution is said to be covariant to an operator if the change in the signal is reflected in the time-frequency distribution. For example, if $y(t) = x(t - t_0)$ then a time-frequency distribution that is covariant to the time-shift operator should satisfy $W_y(t, \omega) = W_x(t - t_0, \omega)$. The class of all quadratic time-frequency distributions covariant to time-shifts and frequency-shifts is called Cohen's class. Similarly, the class of all quadratic time-frequency distributions covariant to time-shifts and scales is called the affine class. The intersection of these two classes contains time-frequency distributions, like the Wigner distribution, that are covariant to all three operators.

Spectrograms are quadratic functions of the signal and are also covariant to time shifts and frequency shifts, so spectrograms are also members of Cohen's class. Similarly, scalograms are quadratic functions of the signal and are covariant to time shifts and scales, so scalograms are members of the affine class. Recently, quadratic time-frequency distributions have been defined that are covariant to operators other than the three mentioned above. One example is the hyperbolic class of time-frequency

distributions [24]. Time-frequency distributions in the hyperbolic class are covariant to scales and hyperbolic time shifts. The hyperbolic class intersects with the affine class but not with Cohen's class. Baraniuk [30] has recently presented a fundamental result concerning the existence of quadratic time-frequency distributions covariant to arbitrary operators. One troublesome aspect of quadratic distributions is that they always contain "cross terms". The cross terms are undesirable for two reasons. First, a true distribution function should be non-negative and cross terms can have negative values. Second, the cross terms do not usually represent any energy present in the signal.

It is often desired that a time-frequency distribution be positive valued, and Cohen has created a general class of time-frequency distributions that are always positive valued [21]. Since this class is very general, it intersects with every class (quadratic and non-quadratic) of time-frequency distributions. The main difficulty with this class is that it is not clear how to construct time-frequency distributions in the class. Loughlin et. al. [32] and also Sang et. al. [33] have created positive time-frequency distributions by iterating quadratic time-frequency distributions. There has also been recent work in constructing distributions of quantities other than time and frequency [28-32]. The most common distributions outside of time and frequency are those of time and scale. The concept of scale is closely related to the concept of frequency and some time-frequency distributions have analogous time-scale distributions. A summary of the above methods for computing the distribution of a signal is presented in Figure 3.1

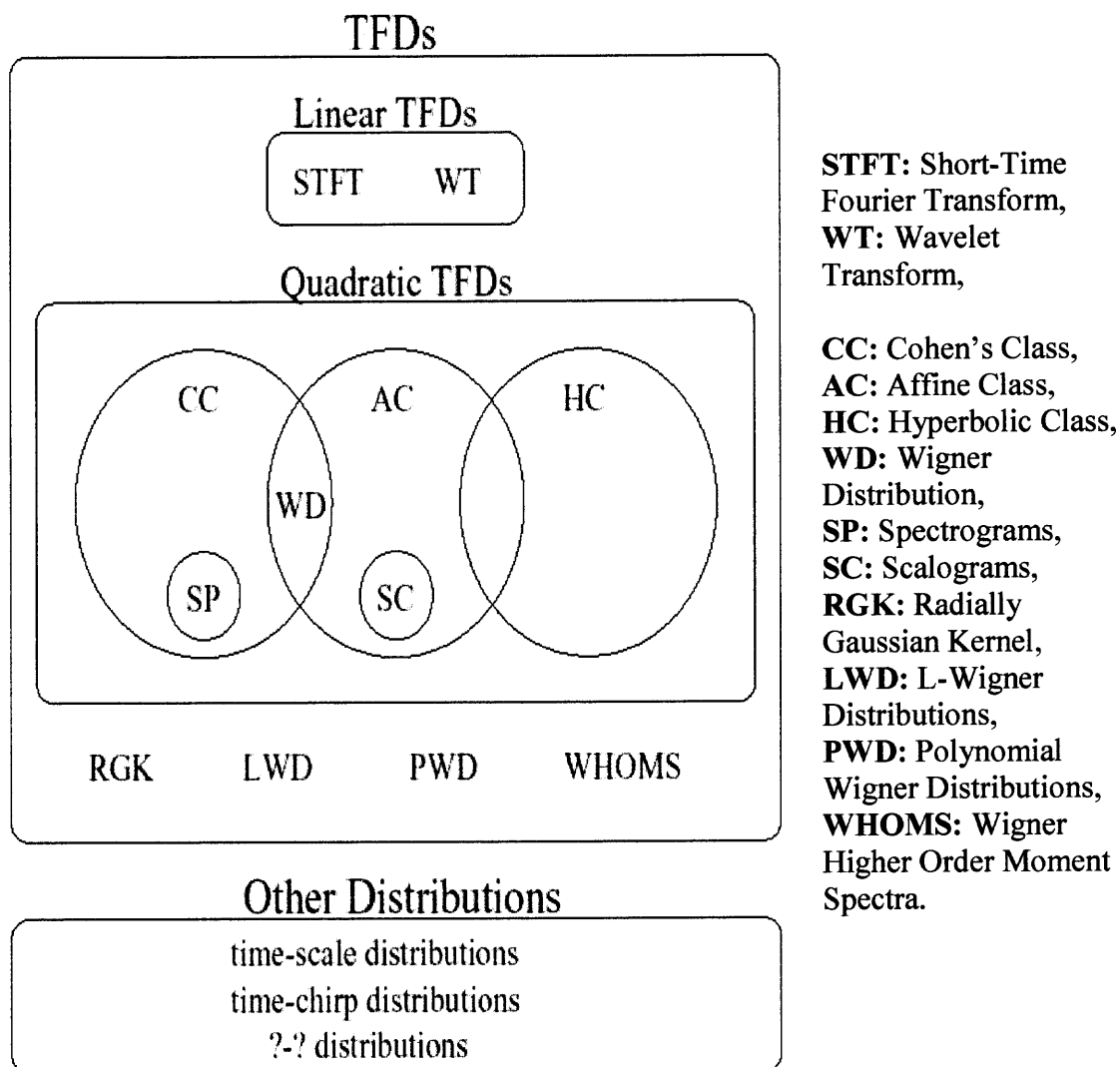


Figure 3.1 Classes of time-frequency distributions.

3.2 The Uncertainty Principle

The uncertainty principle in time-frequency analysis provides the lower limit on the spread of signal energy in time and frequency. To define the spread of a signal in time and frequency, one first need to define the average time and average frequency of a signal [38]:

$$\mu_t = \int t |x(t)|^2 dt \quad (3.1)$$

$$\mu_\omega = \int \omega |X(\omega)|^2 d\omega \quad (3.2)$$

The spread of the signal in time (duration) and frequency (bandwidth) are defined as:

$$\sigma_t^2 = \int (t - \mu_t)^2 |x(t)|^2 dt \quad (3.3)$$

$$\sigma_\omega^2 = \int (\omega - \mu_\omega)^2 |X(\omega)|^2 d\omega \quad (3.4)$$

The uncertainty principle states that:

$$\sigma_t \sigma_\omega \geq \frac{1}{2} \quad (3.5)$$

Therefore a signal cannot have an arbitrarily small duration and bandwidth. A Gaussian signal:

$$x(t) = \left(\frac{\alpha}{\pi}\right)^{1/4} e^{-\alpha t^2 / 2} \quad (3.6)$$

meets this bound with equality where α is an arbitrary constant.

3.3 The Analytic Signal and Instantaneous Frequency

Most signals are real valued functions of time. Since the Fourier transform of a real signal will be even, there is an unnecessary redundancy in a real signal. To eliminate the redundancy, one can compute what is called the "analytic signal" from the real valued signal. The analytic signal, $x_a(t)$, is of the form:

$$x_a(t) = x(t) + jH[x(t)] \quad (3.7)$$

where $H[\cdot]$ is the Hilbert transform operator.

There are three reasons for using the analytic signal in calculating a joint time-frequency distribution [68]:

1. The analytic signal only has positive frequencies; hence there are no interference terms between negative frequencies and positive frequencies. However, there is still interference between one positive frequency and another. This is an inherent property of bilinear distributions.

2. In computing examples of time-frequency distributions, one often uses signals of the form:

$$x(t) = A(t)e^{j\phi(t)} \quad (3.8)$$

The above is the analytic signal corresponding to $A(t)\cos(\phi(t))$. The frequency of a signal at a given time is denoted the instantaneous frequency, and for the signal in equation 3.8 it is defined as:

$$\omega_x(t) = \frac{d}{dt} \arg\{x(t)\} = \frac{d}{dt} \phi(t) \quad (3.9)$$

Thus for a signal of the form in equation 3.9, the "ideal" time-frequency distribution should be similar to:

$$W_x(t, \omega) = A(t)^2 \delta(\omega - \omega_x(t)) \quad (3.10)$$

where $\delta(\cdot)$ is a Dirac delta function. The above equation implies that the energy of the time-frequency distribution is concentrated along the instantaneous frequency of the signal. A dual quantity is the average time of a signal at a given frequency. This quantity is called the group delay. For a signal of the form:

$$X(\omega) = A(\omega) e^{j\phi(\omega)} \quad (3.11)$$

the group delay is defined as:

$$W_x(\omega) = \frac{d}{d\omega} \arg\{X(\omega)\} = \frac{d}{d\omega} \phi(\omega) \quad (3.12)$$

3. Dr. Leon Cohen has proposed a simple procedure to mathematically formulate the general class of time-frequency representations using bilinear distributions [69]:

$$\rho_z(t, f) = \iiint_{-\infty}^{\infty} e^{j2\pi\nu(u-t)} \cdot g(\nu, \tau) \cdot z(u + \frac{\tau}{2}) \cdot z^*(u - \frac{\tau}{2}) \cdot e^{-j2\pi f\tau} \cdot d\nu \cdot du \cdot d\tau \quad (3.13)$$

The $g(\nu, \tau)$ is an arbitrary function called the *kernel* and it determines the characteristics of the time-frequency distribution. Note that z is an analytic signal and z^* is the complex conjugate of z . Integrating equation (3.13) with respect to ν , one gets:

$$\rho_z(t, f) = \iint_{-\infty}^{\infty} G(t, \tau) \cdot z(u + \frac{\tau}{2}) \cdot z^*(u - \frac{\tau}{2}) \cdot e^{-j2\pi f\tau} \cdot du \cdot d\tau \quad (3.13a)$$

and the discrete time version is:

$$\rho_z(n, k) = \sum_{m=-M}^M \sum_{p=-M}^M G(p, m) \cdot z(n + p + m) \cdot z^*(n + p - m) \cdot e^{-j4\pi mk / N} \quad (3.13b)$$

The advantage of using equation 3.13b is that once the desired kernel is chosen, the distribution is fixed.

3.4 Properties of Time-Frequency Distributions

As indicated in the introduction, there are many methods for constructing time-frequency distributions. To provide guidelines for constructing time-frequency distributions, authors have proposed many "desirable" properties that time-frequency distributions should satisfy. For example, since time-frequency distributions are usually considered to be energy distributions, they should be real and positive functions. Also, the time marginal of a time-frequency distribution is the integral of the time-frequency distribution over frequency, and the time marginal should be identical to the distribution of signal energy over time. These properties and several others are listed in Table 3.1. For a more complete listing see [38].

Table 3.1 Some Desirable Properties of Time-Frequency Distributions

P1	Real valued:	$T_x^*(t, \omega) = T_x(t, \omega)$
P2	Time shift:	$T_{\tilde{x}}(t, \omega) = T_x(t - t_0, \omega) \quad \text{for} \quad \tilde{x}(t) = x(t - t_0)$
P3	Frequency shift:	$T_{\tilde{x}}(t, \omega) = T_x(t, \omega - \omega_0) \quad \text{for} \quad \tilde{x}(t) = x(t)e^{j2\pi\omega_0 t}$
P4	Time marginal:	$\int_{\omega} T_x(t, \omega) d\omega = x(t) ^2$
P5	Frequency marginal:	$\int_t T_x(t, \omega) dt = X(\omega) ^2$
P6	Time moments:	$\int_t \int_{\omega} t^n T_x(t, \omega) dt d\omega = \int_t t^n x(t) ^2 dt$
P7	Frequency moments:	$\int_t \int_{\omega} \omega^n T_x(t, \omega) dt d\omega = \int_t \omega^n X(\omega) ^2 d\omega$
P8	Time-frequency scaling:	$T_{\tilde{x}}(t, \omega) = T_x(at, \frac{\omega}{a}) \quad \text{for} \quad \tilde{x}(t) = \sqrt{ a }x(at) \quad \text{with} \quad a \neq 0$
P9	Instantaneous frequency:	$\frac{\int_{\omega} \omega T_x(t, \omega) d\omega}{\int_{\omega} T_x(t, \omega) d\omega} = W_x(t) = \frac{1}{2\pi} \frac{d}{dt} \arg x(t) $
P10	Group delay:	$\frac{\int_t t T_x(t, \omega) dt}{\int_t T_x(t, \omega) dt} = t_x(\omega) = -\frac{1}{2\pi} \frac{d}{d\omega} \arg X(\omega) $
P11	Finite time support:	$T_x(t, \omega) = 0$ for t outside $[t_1, t_2]$ if $x(t) = 0$ outside $[t_1, t_2]$
P12	Finite frequency support:	$T_x(t, \omega) = 0$ for f outside $[\omega_1, \omega_2]$ if $X(\omega) = 0$ outside $[\omega_1, \omega_2]$
P13	Moyal's formula (unitarity):	$(T_{x_1, y_1}, T_{x_2, y_2}) = (x_1, x_2)(y_1, y_2)^*$
P14	Convolution:	$T_{\tilde{x}}(t, \omega) = \int_{t'} T_h(t - t', \omega) T_x(t', \omega) dt' \quad \text{for} \quad \tilde{x}(t) = \int_{t'} h(t - t') x(t') dt'$
P15	Multiplication:	$T_{\tilde{x}}(t, \omega) = \int_{\omega'} T_h(t, \omega - \omega') T_x(t, \omega') d\omega' \quad \text{for} \quad \tilde{x}(t) = h(t)x(t)$
P16	Fourier transform:	$T_{\tilde{x}}(t, \omega) = T_x(-\frac{\omega}{c}, ct) \quad \text{for} \quad \tilde{x}(t) = \sqrt{ c }X(ct) \quad \text{with} \quad c \neq 0$
P17	Chirp convolution:	$T_{\tilde{x}}(t, \omega) = T_x(t - \frac{\omega}{c}, \omega) \quad \text{for} \quad \tilde{x}(t) = x(t) * \sqrt{ c }e^{j2\pi\frac{c}{2}t^2}$
P18	Chirp multiplication:	$T_{\tilde{x}}(t, \omega) = T_x(t, \omega - ct) \quad \text{for} \quad \tilde{x}(t) = x(t)e^{j2\pi\frac{c}{2}t^2}$

3.5 Covariance and Invariance

The notion of a density function being covariant or invariant to an operator plays an important role in time-frequency analysis. Three commonly used operators are the time-shift operator, the frequency-shift operator, and the scale operator defined, respectively as:

$$(T_{t_0} x)(t) = x(t - t_0) \quad \text{Time shift operator} \quad (3.14)$$

$$(F_{\omega_0} x)(t) = x(t) e^{j\omega_0 t} \quad \text{Frequency shift operator} \quad (3.15)$$

$$(D_a x)(t) = x(at) \quad \text{Scale operator} \quad (3.16)$$

Definition 1. A function of a signal is said to be covariant to an operator if the change in the signal is reflected in the function. A function of a signal is said to be invariant to an operator if the function remains the same despite the changes in the signal. For example, the time energy density, $|x(t)|^2$, is covariant to time shifts and invariant to frequency shifts. Similarly, the frequency energy density, $|X(\omega)|^2$, is covariant to frequency shifts and invariant to time shifts. In general, it is desirable for time-frequency distributions to be covariant to the above three operators. Let $y(t)$ be a shifted version of $x(t)$ in time and frequency:

$$y(t) = (F_{\omega_0} T_{t_0} x)(t) \quad (3.17)$$

A time-frequency distribution is covariant to time shifts and frequency shifts if it satisfies:

$$T_y(t - t_0, \omega - \omega_0) = T_x(t, \omega) \quad (3.18)$$

Similarly let $z(t)$ be a scaled version of $x(t)$:

$$z(t) = (D_a x)(t) \quad (3.19)$$

A time-frequency distribution is scale covariant if it satisfies:

$$aT_z(at, \omega/a) = T_x(t, \omega) \quad (3.20)$$

3.6 Comparison of Time-Frequency Distributions

3.6.1 Short Time Fourier Transform

The short time Fourier transform was the first tool devised for analyzing a signal in the time-frequency domain [20]. This is done by extracting a small piece of the signal and taking its Fourier transform, and by continuing this process, one can show the existing frequency components at each instant of time. This idea can mathematically be presented by first designing a window function, $h(\tau - t)$ which will emphasize the times around the fixed time of interest t . The signal is then multiplied with the window function and Fourier transform is taken:

$$S_t(f) = \int_{t-\Delta}^{t+\Delta} s(\tau)h(\tau - t)e^{-j2\pi f\tau} d\tau \quad (3.21)$$

As this process is continued for each particular time, one obtains a different spectrum. The totality of these spectra makes a time-frequency distribution. The energy density of the signal at the fixed time t is

$$\rho_{sp}(t, f) = \left| \int_{t-\Delta}^{t+\Delta} s(\tau)h(\tau - t)e^{-j2\pi f\tau} d\tau \right|^2 \quad (3.22)$$

where $\rho_{sp}(t, f)$ is called the spectrogram. The spectrogram can be also written in terms of the Fourier transforms of the signal and window function.

$$\rho_{sp}(t, f) = \left| \int_{f-\Delta}^{f+\Delta} S(f') H(f - f') e^{-j2\pi f' t} df' \right|^2 \quad (3.23)$$

where $H(f)$, $S(f)$ are Fourier transforms of the signal and window function respectively. Note that equation (3.23) can be used to study the behavior of the signal around the fixed frequency of interest f . The spectrogram should not be thought of as a different distribution because it is a member of a general class of distributions [22].

How large should the window be or how should one weigh each piece of the signal? To answer these questions one need to understand the time-bandwidth relation, or the uncertainty principle.

Now define the duration of a signal $s(t)$ by Δt :

$$(\Delta t)^2 = \int (t - \bar{t})^2 |s(t)|^2 dt \quad (3.24)$$

where \bar{t} is mean time and is defined as:

$$\bar{t} = \int t |s(t)|^2 dt \quad (3.25)$$

Now also define the bandwidth of the signal $S(f)$ in the frequency domain by Δf :

$$(\Delta f)^2 = \int (f - \bar{f})^2 |S(f)|^2 df \quad (3.26)$$

where \bar{f} is mean frequency and is defined as:

$$\bar{f} = \int f |S(f)|^2 df \quad (3.27)$$

The time bandwidth relation is:

$$\Delta t \cdot \Delta f \geq \frac{1}{4\pi} \quad (3.28)$$

The physical interpretation of time bandwidth is that the duration and bandwidth cannot be both made narrow because $|s(t)|^2$ and $|S(f)|^2$ cannot be changed independently [21]. The advantage of the short-time Fourier transform is that it has an easily understandable interpretation and is positive everywhere. This is a desirable property when one wants to interpret the spectrogram as the signal energy distribution in the time-frequency plane.

One of the shortcomings of the short-time Fourier transform is the trade off between time and frequency resolution. Consider two extreme choices of the analysis window $h(t)$. The first case is that of perfect time resolution, that is, if the analysis window $h(t)$ is a Dirac impulse.

$$h(t) = \delta(t) \Rightarrow \rho_{STFT}(t, f) = s(t)e^{-2j\pi ft} \quad (3.29)$$

where $s(t)$, $\rho_{STFT}(t, f)$ are the signal and short time Fourier transform of the signal respectively. In this case, the short time Fourier transform essentially reduces to the signal $s(t)$, preserving all time variations of the signal but not providing any frequency resolution. The second case is that of perfect frequency resolution obtained with the all-constant window $h(t) = 1$, then;

$$H(f) = \delta(f) \Rightarrow \rho_{STFT}(t, f) = S(f) \quad (3.30)$$

where $H(f)$, $S(f)$ are Fourier transform of window and signal respectively. Here the short time Fourier transform reduces to the Fourier transform and does not provide any time resolution. Therefore, because of the uncertainty principle, both $h(t)$ and $H(f)$ can not be made arbitrarily narrow.

Another shortcoming of the spectrogram is that it does not satisfy time and frequency marginal properties at the same instant. If one write the signal $s(t)$ and window $h(t)$ in terms of their amplitudes and their phase;

$$s(t) = A(t)e^{j\theta(t)} \quad \text{and} \quad h(t) = A_k(t)e^{j\theta_k(t)} \quad (3.31)$$

and similarly for their Fourier transforms:

$$S(f) = B(f)e^{j\theta(f)} \quad \text{and} \quad H(f) = B_k(f)e^{j\theta_k(f)} \quad (3.32)$$

Then the marginals are:

$$\int \rho_{STFT}(t, f) df = \int A^2(t') A_k^2(t' - t) dt' \quad (3.33)$$

$$\int \rho_{STFT}(t, f) dt = \int B^2(f') B_H^2(f - f') df' \quad (3.34)$$

These do not equal the instantaneous energy or energy density spectrum, namely $A^2(t)$ and $B^2(f)$ [38]. But they do approach them as one narrow the window in the respective domains. However window $h(t)$ and $H(f)$ cannot be narrowed concurrently.

The short time Fourier transform is a linear signal decomposition, and there are no cross-terms between signal components. However, the spectrogram is also a bilinear signal energy distribution due to the magnitude squaring operation. Thus, the spectrogram has cross terms that are not noticeable because they are inherently filtered out by a low-pass filter defined by the ambiguity function of the window [37].

3.6.2 Wigner Distribution

Among all the bilinear TFD, the Wigner distribution (WD) is the most studied and applied [40]. The Wigner distribution can be obtained from the Cohen general class equation:

$$\rho_z(t, f) = \iiint_{-\infty}^{\infty} e^{j2\pi v(u-t)} g(v, \tau) z\left(u + \frac{\tau}{2}\right) z^*\left(u - \frac{\tau}{2}\right) e^{-2j\pi f\tau} dv du d\tau \quad (3.35)$$

by taking $g(v, \tau) = 1$:

$$\rho_w(t, f) = \int z\left(t - \frac{\tau}{2}\right) z^*\left(t + \frac{\tau}{2}\right) e^{-2j\pi f\tau} d\tau \quad (3.36)$$

where $\rho_w(t, f)$, $z(t)$, and $z^*(t)$ are the Wigner distribution, an analytic signal and the complex conjugate of the analytic signal respectively. From equation (3.36) one see that for each particular time one are adding up pieces made from the product of the signal at a past time multiplied by the signal at an equal future time. The Wigner distribution satisfies many properties, which are described as follows:

The WD is a real valued function that is:

$$\rho_w(t, f) = \rho_w^*(t, f) \quad (3.37)$$

Since the kernel of the WD is one for any value of v and τ , then the complex conjugate of the kernel is always one. That is;

$$g(v, \tau) = g^*(-v, -\tau) = 1 \quad (3.38)$$

This is the constraint of the kernel for the distribution to be real.

The WD satisfies the time and frequency shift properties as long as the kernel of the WD is not a function of time and frequency that is;

$$s(t) = z(t - t_0) \Rightarrow \rho_s(t, f) = \rho_z(t - t_0, f) \quad (3.39)$$

$$s(t) = z(t) e^{j2\pi f_0 t} \Rightarrow \rho_s(t, f) = \rho_z(t, f - f_0) \quad (3.40)$$

where $z(t)$, $s(t)$, $\rho_z(t, f)$ and $\rho_s(t, f)$ are the signal, the shifted signal, the distribution of signal and the distribution of the shifted signal respectively. To prove this property, one

should take the kernel of the WD independent of time and frequency and set it equal to one, that is:

$$g(v, \tau) = 1 \quad \text{where } v \notin R_{time} \quad \text{and } \tau \notin R_{frequency} \quad (3.41)$$

Let $\rho_z(t, f), \rho_s(t, f)$ represent the WD of the signal $z(t)$ and the shifted signal $s(t)$, then:

$$\rho_s(t, f) = \int z(t - \frac{\tau}{2} - t_0) z^*(t + \frac{\tau}{2} - t_0) e^{-2j\pi f \tau} d\tau \quad (3.42)$$

and

$$\rho_s(t, f) = \int z(t - \frac{\tau}{2}) z^*(t + \frac{\tau}{2}) e^{-2j\pi f(t-t_0)} d\tau = \rho_z(t - t_0, f) \quad (3.43)$$

To prove the frequency shifting one can use a similar argument. The WD is uniquely related to the signal up to a constant phase factor [38]. To understand this idea, take the inverse Fourier transform of equation 3.36 with respect to f ,

$$z(t - \frac{\tau}{2}) z^*(t + \frac{\tau}{2}) = \int \rho_s(t, f) e^{2j\pi f \tau} df \quad (3.44)$$

Then, let:

$$t + \frac{\tau}{2} \rightarrow t'; t - \frac{\tau}{2} \rightarrow t \quad \text{and} \quad \tau \rightarrow t - t' \quad (3.45)$$

which gives:

$$z(t) z^*(t') = \int \rho_w(\frac{1}{2}(t' + t), f) e^{2j\pi(t-t')f} df \quad (3.46)$$

Taking a particular value for $t' = 0$ and dividing both sides by $z^*(t')$, one obtain;

$$z(t) = \frac{1}{z^*(0)} \int \rho_w(\frac{1}{2}t, f) e^{2j\pi f t} df \quad (3.47)$$

One can therefore recover the original signal from the Wigner distribution for a given resolution. The preceding relation can be used to determine whether a signal exists which will generate a given $\rho_w(t, f)$.

The Wigner distribution also satisfies the marginals properties. To prove these, one can use the constraint of the kernel for marginals properties, that is:

$$g(v, 0) = 1 \quad \text{and} \quad g(0, \tau) = 1 \quad (3.48)$$

By inspection, the kernel of the Wigner distribution $g(v, \tau) = 1$ satisfies both marginals. Thus, the Wigner distribution satisfies the total energy. Note the converse is not true [38]. For the first conditional moment at a fixed time, the Wigner distribution gives the instantaneous frequency and at a fixed frequency the first conditional moment would be the group delay.

For a finite duration signal, the Wigner distribution is zero before the signal starts and after the signal ends [38]. If one have a band limited signal, the Wigner distribution will be zero for all frequencies that are not included in that band. These properties are called the support properties of the Wigner distribution. In general the Wigner distribution is not zero when the signal is zero [40].

Consider the multicomponent signal $z(t)$:

$$z(t) = z_1(t) + z_2(t) \quad (3.49)$$

The Wigner distribution is:

$$\rho_w(t, f) = \rho_{w_{11}}(t, f) + \rho_{w_{22}}(t, f) + \rho_{w_{12}}(t, f) + \rho_{w_{21}}(t, f) \quad (3.50)$$

where $\rho_w(t, f)$, $\rho_{w_{11}}(t, f)$, and $\rho_{w_{22}}(t, f)$ are the auto Wigner distributions of $z(t)$, $z_1(t)$, and $z_2(t)$ respectively. The terms $\rho_{w_{12}}(t, f)$, and $\rho_{w_{21}}(t, f)$ are

called the cross Wigner distributions. Therefore the Wigner distribution of the sum of the two signals is not the sum of their respective Wigner distributions. In general the Wigner distribution puts cross terms in between any two frequencies and any two times [40].

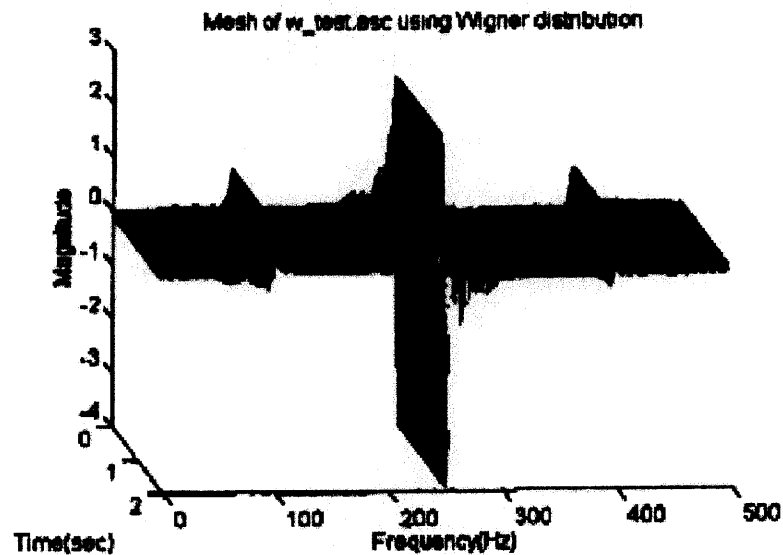


Figure 3.2 The Wigner distribution of the sum of two finite duration sine waves.

The figure above presents the Wigner distribution of a signal, which is the sum of two sine waves of one-second duration with frequencies of 100 and 400 hertz. Note the cross term in the middle of the two frequencies at 250 hertz. This is the most important draw back of the Wigner distribution (WD).

Another draw back of the Wigner distribution is that it always has negative regions throughout the time-frequency plane, except in the case of the Gaussian signal where the amplitude is modulated [40].

3.6.2.1 Windowed Wigner Distribution. In practice, one is forced to calculate the Wigner distribution using the equation:

$$\rho_W = \int h(\tau) z(t - \frac{\tau}{2}) z^*(t + \frac{\tau}{2}) e^{-2j\pi f\tau} d\tau \quad (3.51)$$

where $h(t)$ is a window function. This is due to the finite nature of the data. The resulting distribution has the effect of smoothing the Wigner distribution over frequency and is called the Pseudo Wigner distribution (PWD)[22]. The PWD sometimes results in a better-looking distribution in that certain cross terms are suppressed. One can clean the cross terms by smoothing the Pseudo Wigner distribution over time which is called the Smoothed Pseudo Wigner distribution (SPWD). Smoothing the Pseudo Wigner distribution is performed as follows:

$$\rho_{WS}(t, f) = \iint_{\text{window}(L)} L(t - t', f - f') \cdot \rho_W(t', f') dt' df' \quad (3.52)$$

where $L, \rho_{WS}(t, f)$ and $\rho_W(t, f)$ are smoothing function, the Smoothed Pseudo Wigner distribution and the Pseudo Wigner distribution respectively. The advantages of the Smoothed Pseudo Wigner distribution are that for certain types of smoothing, a positive distribution is obtained and the cross terms are suppressed. However smoothing destroys some of the desirable properties of the Wigner distribution: if L is taken to be independent of the signal, then the only way to obtain a positive distribution is by sacrificing the marginals properties [41].

3.6.3 The Choi-Williams (Exponential) Distribution

Choi and Williams presented a new approach where they address the main draw back of the Wigner distribution (cross terms)[40]. They used a generalized ambiguity function [40] and chose an exponential kernel, that is:

$$g(v, \tau) = e^{-v^2 \tau^2 / \sigma} \quad (3.53)$$

Substituting equation (3.53) in equation (3.36) and integrating with respect to v one obtains:

$$\rho_{CW}(t, f) = \iint \sqrt{\frac{\pi\sigma}{\tau^2}} e^{-\pi^2 \sigma (u-t)^2 / \tau^2 - j2\pi f} z^*(u - \frac{\tau}{2}) z(u + \frac{\tau}{2}) du d\tau \quad (3.54)$$

where $\rho_{CW}(t, f)$, $z(t)$, $z^*(t)$ are the Choi-Williams distribution, an analytical signal and complex conjugate of the analytical signal. The ability to suppress the cross terms comes by controlling σ .

In Figure 3.3, three cases were presented, where each contains two sine waves with frequencies of 100 and 400 hertz. The Choi Williams distribution was performed for the three cases but with different values for σ . Note, in case "a", σ is 10000, which makes the kernel equal to one, and the Wigner distribution is obtained. In case "b" and "c", σ is 50 and 1 respectively which produces a kernel, which is peaked, near the origin in the v, τ plane and hence offers better cross term suppression.

Hence one can control the relative suppression of the cross terms by reducing the value of σ . The Choi Williams distribution satisfies many of the desirable properties, as described below:

1. The Choi Williams distribution is real. To prove this, one can replace the v, τ with $-v, -\tau$ respectively in to the kernel function and perform the manipulation:

$$g^*(-v, -\tau) = e^{-(-v)^2(-\tau)^2/\sigma} = e^{-v^2\tau^2/\sigma} = g(v, \tau) \quad (3.55)$$

2. The Choi Williams distribution satisfies both the marginal properties, since:

$$g_{CW}(v, 0) = e^{-0^2\tau^2/\sigma} = 1 \quad (3.56)$$

and similarly for the other marginal. Since the marginal properties are satisfied, the total energy property will be satisfied.

3. The Choi Williams distribution does not satisfy the finite support properties. To show this, one introduces the following condition for determining whether a distribution is zero before a signal starts and after the signal ends. This work was done by Claasen and Mecklenbrauker [39] and is expressed as follows:

$$\int g(v, \tau) e^{-jv\tau} dv = 0 \quad \text{for} \quad |\tau| < 2|t| \quad (3.57)$$

Similarly, for the signal that is bandlimited in the region (f_1, f_2) the distribution should be zero for values of frequency less than f_1 , and greater than f_2 .

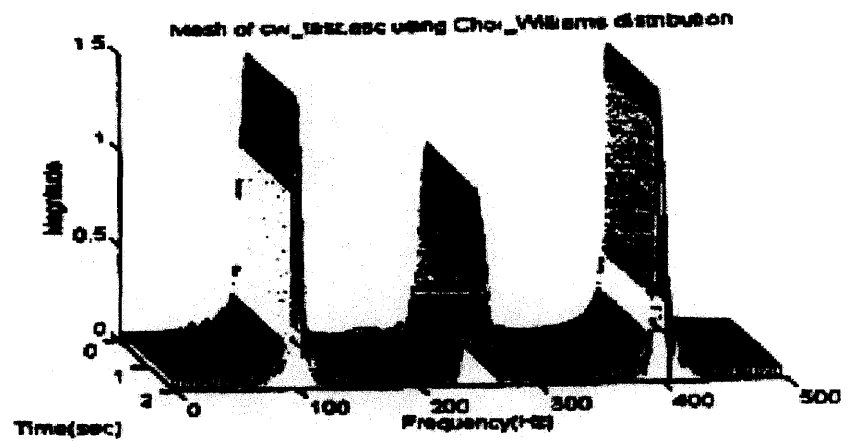
$$\int g(v, \tau) e^{-j2\pi f\tau} d\tau = 0 \quad \text{for} \quad |v| < 4\pi|f| \quad (3.58)$$

If one replace the kernel of the Choi Williams distribution in equation (3.52) and carry out the integration using a table of integrals [40], one obtain:

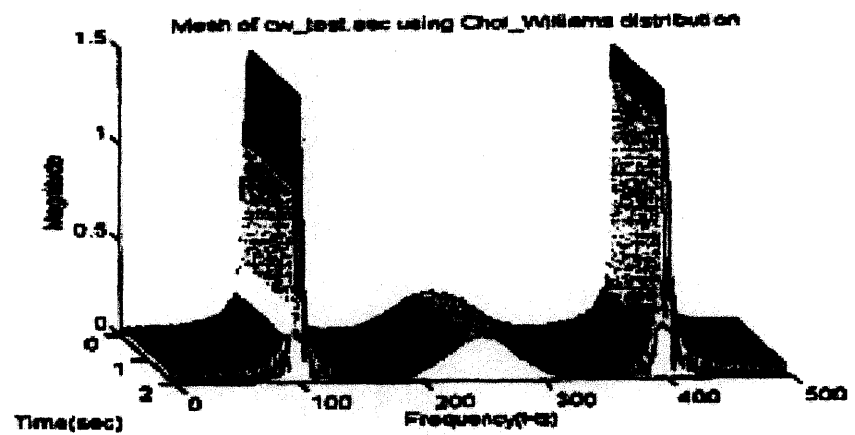
$$\int e^{-v^2\tau^2/\sigma} e^{-2jv\tau} dv = \frac{\sqrt{\pi}}{\sqrt{\tau^2/\sigma}} e^{\frac{t^2}{4\tau^2/\sigma}} \quad (3.59)$$

Note, the right hand side of equation (3.59) is not equal to zero; therefore, the Choi -Williams distribution does not satisfy the support properties.

(a)



(b)



(c)

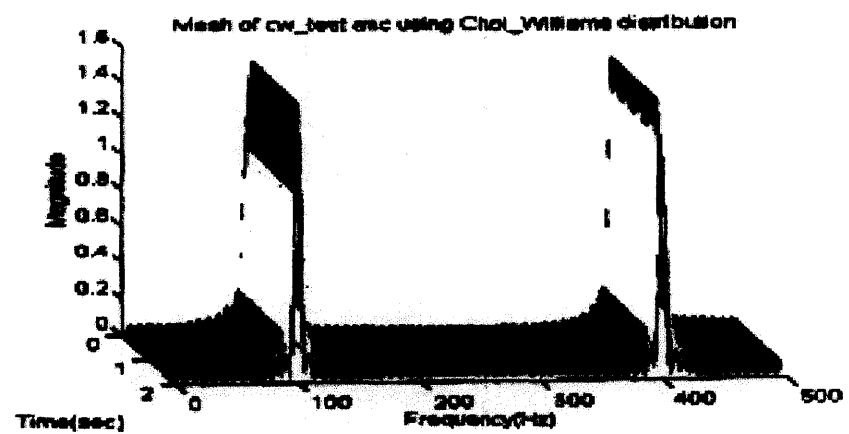


Figure 3.3 Performance of the Choi-William distribution upon three cases with
a) $\sigma = 1000$, b) $\sigma = 50$, c) $\sigma = 1$.

3.7 Wavelet Transforms

Analysis of signals using appropriate basis functions is one of the fundamental problems in the signal processing field. Fourier proposed the complex sinusoids as the basis functions for signal decomposition [41]. The Fourier transform of a finite energy continuous time signal $f(t)$, (i.e. $f(t) \in L^2$) is defined as:

$$F(\Omega) = \int_{-\infty}^{\infty} e^{-j\Omega t} f(t) dt \quad (3.60)$$

The strength of the standard Fourier analysis is that it allows the decomposition of a signal into its individual frequency components and establishes the relative intensity of each frequency component. Because of the infinite durations of these basis functions, any time-local information (e.g. an abrupt change in the signal) is spread over the whole frequency spectrum. Therefore, this transform cannot reflect any time-localized characteristic of $f(t)$ into the frequency domain. It only provides the frequency behavior of $f(t)$ in the interval $-\infty < t < \infty$. Gabor addressed this problem by introducing a window function to localize $f(t)$ and calculating the Fourier transform of the windowed signal as [42]

$$F_{SF}(\Omega, \tau) = \int_{-\infty}^{\infty} \omega(t - \tau) e^{-j\Omega t} f(t) dt \quad (3.61)$$

where $\omega(t - \tau)$ is the appropriate time-frequency localized window function. This transform is called the Windowed or Short-Time Fourier Transform (STFT) (also referred to as the Gabor transform when the window function used in the STFT is Gaussian).

The major advantage of the Short-Time Fourier Transform is that if a signal has most of its energy in the given time interval $[-T, T]$ and in the frequency interval

$[-\Omega, \Omega]$, then its STFT will be localized in the region $[-T, T] \times [-\Omega, \Omega]$ of the time-frequency plane. Of course, the uncertainty principle prevents the possibility of having arbitrary high resolution in both time and frequency domains, since it lower-bounds the time bandwidth product of any basis function by $\Delta T \Delta \Omega \geq \frac{1}{4\pi}$ where $(\Delta T)^2$ and $(\Delta \Omega)^2$ are the variances of the time function and its Fourier transform respectively [43][44].

An important parameter of a window function is its size (or scale). The selection of an appropriate window size poses a fundamental problem in signal analysis. Thus, by varying the window function used, one can trade the resolution in time for the resolution in frequency. An intuitive way to achieve this is to have short time duration high frequency basis functions, and long time duration low frequency ones. Fortunately, the wavelet transform provides for this desired feature and is defined as,

$$W_f(a, b) = \frac{1}{\sqrt{a}} \int \psi\left(\frac{t-b}{a}\right) f(t) dt \quad (3.62)$$

where $a \in R^+, b \in R$. Here a , and b are the scale and shift variables respectively, and they are continuous variables. Depending on the scaling parameter a , the wavelet function $\psi(t)$ dilates or contracts in time causing the corresponding contraction or dilation in the frequency domain. Therefore a flexible time-frequency resolution is achievable with the wavelet transform. Another significant difference of these transforms is that the STFT is never a real function on the time-frequency plane regardless of the choice of $\omega(t)$, but the wavelet transform is real if the basic wavelet $\psi(t)$ is chosen to be real.

3.7.1 Continuous Wavelet Transform

The continuous wavelet transform maps a function $f(t)$ onto time-scale space as

$$W_f(a, b) = \frac{1}{\sqrt{a}} \int \psi\left(\frac{t-b}{a}\right) f(t) dt \quad (3.63)$$

This operation can be expressed in a simpler inner product notation as

$$W_f(a, b) = \langle \psi_{ab}(t), f(t) \rangle \quad (3.64)$$

$\psi_{ab}(t)$ represents a family of functions obtained from a single wavelet function $\psi(t)$ and the dilation and translation parameters a and b as

$$\psi_{ab}(t) = \frac{1}{\sqrt{a}} \psi\left(\frac{t-b}{a}\right) \quad (3.65)$$

where a and b are continuous.

The wavelet function $\psi(t)$ is a band-pass function. It is desired that this function have a good time and frequency localization so that $f(t)$ is decomposed into elementary building blocks which are jointly well localized in time and frequency. The wavelet function has to satisfy the “admissibility” condition that makes it an isometry (up to a constant) of $L^2(R)$ onto $L^2(R \times R)$. This requirement limits the wavelet functions which must satisfy [45][46]

$$C_h = \int_{-\infty}^{\infty} \frac{|\Psi(\Omega)|^2}{|\Omega|} d\Omega < \infty \quad (3.66)$$

where $\Psi(\Omega)$ is the Fourier transform of the wavelet function $\psi(t)$. The admissibility condition is directly related to the decay of the wavelet function $\psi(t)$ which is required to have good localization. The admissibility condition for a continuous $\Psi(\Omega)$ is equivalent to a zero-mean wavelet function in time:

$$\Psi(0) = \int_{-\infty}^{\infty} \psi(t) dt = 0 \quad (3.67)$$

This condition forces that the wavelet function is a band pass function and decays at least as fast as $|t|^{1-\varepsilon}$ in time where ε is some decay constant. (In practice one needs to have much faster decay of $\psi(t)$, in order to have good time localization).

The admissibility condition assures that the “resolution of the identity” holds [45]. This guarantees that any function $f(t) \in L^2(R^n)$ can be reconstructed from the wavelet space as

$$f(t) = \frac{1}{C_h} \int_{-\infty}^{\infty} \frac{1}{a^2} da \int W_f(a,b) \psi_{a,b} db \quad (3.68)$$

where the wavelet coefficients were defined earlier in Eq. (3.63). Its mathematical proof is given in the references [45][46]. Whenever $\psi(t)$ is a real function, the integral limits of C_h in Eq. (3.68) are changed from 0 to ∞ .

Resolution of the identity ensures that the continuous wavelet transform (CWT) is complete if $W_f(a,b)$ are known for all a and b . A continuous signal $f(t)$ is represented by a pass band function $\psi(t)$ and its dilated and translated versions. The dilation in time leads to different resolutions in frequency. $\psi(t)$ is a prototype window and is normally referred to as the mother wavelet. The digital implementation of the CWT can be computed directly by convolving the signal with a scaled and dilated version of the mother wavelet. For a reasonably efficient implementation, an FFT may be applied to perform the convolution [46a].

In its discrete form, $a = a_0^j$ and $\tau = n \cdot a_0^{-j}$ where j and n are integers. This is referred to as the discrete wavelet transform (DWT), which is discussed in more detail in

section 3.7.3. If one chooses $a_0 \approx 1$ and $n \approx 0$, one is close to the continuous case. The choice of $a = 2^j$ and $\tau = n \cdot 2^{-j}$ is the most common choice; this is referred to as a dyadic wavelet basis. It allows much greater computational efficiency than the CWT; fast algorithms have been developed that are $O(n)$. The dyadic form also simplifies the constraints on the mother wavelet to achieve another desirable property: orthogonality of the analysis windows, which subtends an efficient representation. The dyadic DWT is almost always the chosen implementation because of its computational efficiency and the mutual orthogonality of its analysis windows (or subbands), and it will heretofore be referred to as simply the wavelet transform (WT) unless otherwise specified.

Because the mother wavelet may take many forms, the term scale is often preferred to frequency when using the WT. An analogy between scale and frequency is useful however, at this point, to illustrate the difference between the STFT and the WT. Consider a mother wavelet chosen to be

$$\psi(t) = g(t)e^{-2j\pi f_0 t} \quad (3.69a)$$

where $g(t)$ is the STFT analysis window, and f_0 is the fundamental frequency in the STFT analysis. This implies that the frequency analogous to the WT scale is $f = af_0 = 2^j f_0$. As the scale is increased, however, the frequency resolution (or equivalently, the bandwidth) of the orthogonal WT analysis window is proportional to its center frequency:

$$c = \frac{\Delta f}{f} = \frac{2^j}{2^j f_0} \quad (3.69b)$$

where c is a constant. Thus, the bandwidths of the analysis windows are spread logarithmically with respect to frequency, instead of linearly as with the STFT. This is illustrated in Figure 3.4.

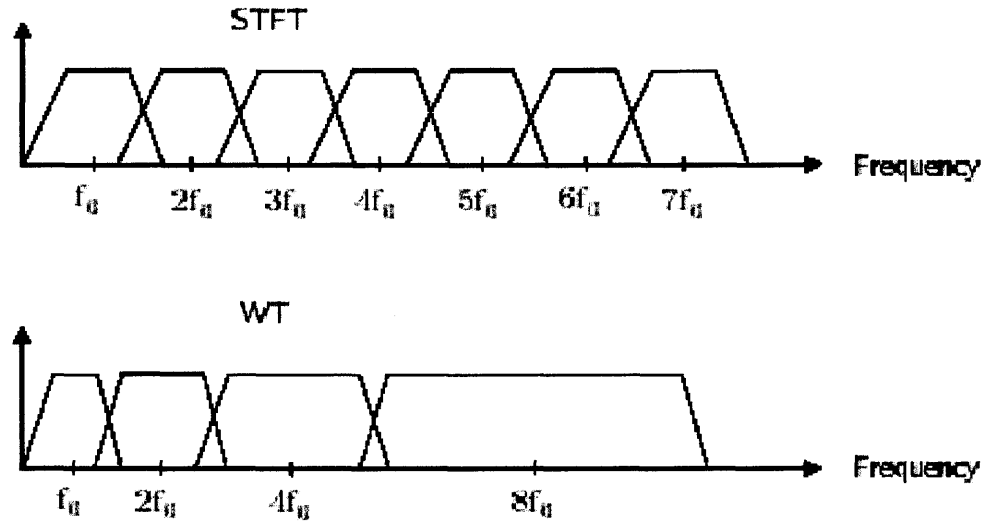


Figure 3.4 Division of the frequency domain for the STFT and the WT.

What ensures is that the time resolution Δt becomes arbitrarily good at high frequencies, and the frequency resolution Δf becomes arbitrarily good at low frequencies. For this reason, wavelet analysis is more effective than Fourier analysis when the signal of interest is dominated by transient behavior or discontinuities.

Figure 3.5 displays a wavelet function $\psi(t)$ and its dilations for different values of parameter “ a ” in the right column along with their short time Fourier transform equivalent counterpart in the left column. This figure helps to visualize the time-frequency plane and emphasizes the band pass nature of $\psi(t)$ and its dilations. The STFT gives fixed resolution (for a given window size), whereas the WT gives variable resolution, which results in higher frequencies better resolved in time and lower

frequencies better resolved in frequency. Furthermore, instead of keeping the size of the window constant and filling it with oscillations of different frequencies (like the FFT), the WT does the reverse. It keeps the number of oscillations constant and changes the width of the “window”. The STFT yields the decomposition of a signal into a set of equal bandwidth functions sweeping the entire frequency spectrum. On the other hand the wavelet transform provides the decomposition of a signal by a set of constant Q (or equal bandwidth on a logarithmic scale) band pass functions. The roles played by the transform parameters are different for the STFT and wavelet transforms. The time parameter τ in the STFT refers to an actual time instant, while the parameter b in the continuous wavelet transform refers to the time instant $\frac{1}{a}b$.

There is a time-frequency resolution trade-off in the wavelet transform. To quantify how the continuous wavelet transform spans the time-frequency plane, the measures of time and frequency resolutions are defined. Let σ_t and σ_Ω be the standard deviations of the mother wavelet function $\psi(t)$ in the time and frequency domains respectively and the corresponding variances are defined as [47]

$$\sigma_t^2 = \int (t - t_0)^2 |\psi(t)|^2 dt \quad (3.70)$$

and

$$\sigma_\Omega^2 = \int (\Omega - \Omega_0)^2 |\Psi(\Omega)|^2 d\Omega \quad (3.71)$$

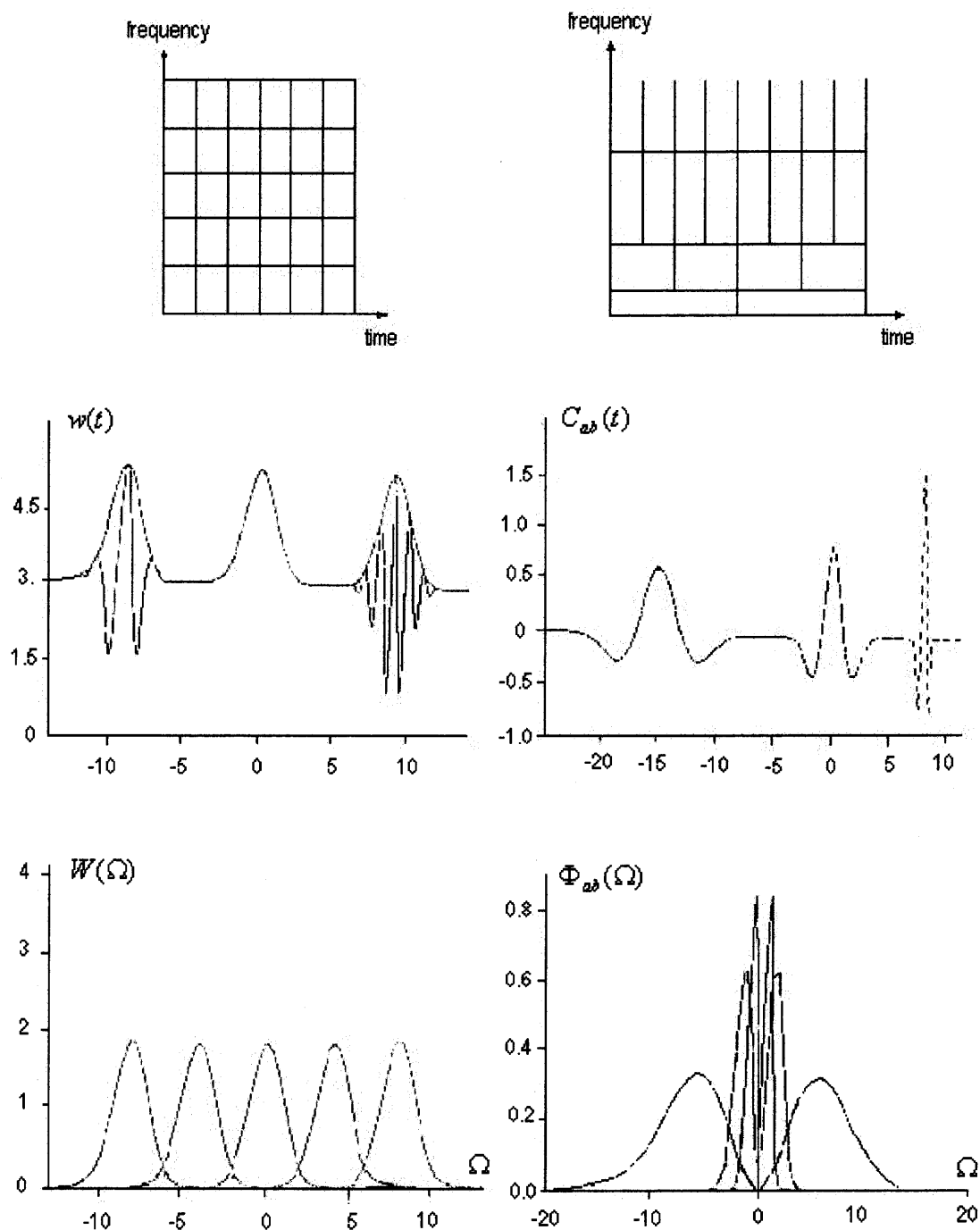


Figure 3.5 The time-frequency plane resolution cells of the STFT vs. Wavelet Transform (Mexican Hat).

Let the wavelet function $\psi(t)$ be centered at (t_0, Ω_0) in the time-frequency plane.

Hence $\psi(\frac{t-b}{a})$ is centered at $(t_0, \frac{\Omega_0}{a})$ with the variances

$$\sigma_{ab_t}^2 = \int_{-\infty}^{\infty} (t - t_0)^2 |\psi_{ab}(t)|^2 dt = a^2 \sigma_t^2 \quad (3.72)$$

and

$$\sigma_{ab_\Omega}^2 = \int_{-\infty}^{\infty} (\Omega - \frac{\Omega_0}{a})^2 |\psi_{ab}(\Omega)|^2 d\Omega = \frac{1}{a^2} \sigma_\Omega^2 \quad (3.73)$$

3.7.2 Parseval Relation of Wavelet Transforms (Energy Preservation Property)

The CWT has an energy conservation property that is similar to Parseval's formula of the Fourier transform. Now the Parseval relation in the wavelet transform can be shown as:

$$E = \int_{-\infty}^{\infty} \int_{-\infty}^{\infty} |W_f(a, b)|^2 \frac{dad b}{a^2} = C_h \int_{-\infty}^{\infty} |f(t)|^2 dt \quad (3.74)$$

holds for any signal $f(t)$ which is squared-integrable. Its proof requires the admissibility condition, which was defined in Eq. (3.66). By using the dual relation of the wavelet transform in the time-frequency domain

$$W_f(a, b) = f(t) * \psi_{ab}(-t) \Big|_{t=b} \Leftrightarrow F(\Omega) \frac{1}{\sqrt{a}} \overline{\Psi(a\Omega)} e^{j\Omega b} \quad (3.75)$$

one can get

$$\begin{aligned} \int_{-\infty}^{\infty} \int_{-\infty}^{\infty} |W_f(a, b)|^2 \frac{dad b}{a^2} &= \frac{1}{2\pi} \int_{-\infty}^{\infty} |F(\Omega)|^2 \int_{-\infty}^{\infty} \frac{|\Psi(a\Omega)|^2}{|a|} dad\Omega \\ &= C_h \int_{-\infty}^{\infty} |f(t)|^2 dt \end{aligned} \quad (3.76)$$

The measure $\frac{dad b}{a^2}$ used in the transform domain is consistent with the discussion of the scaling property. Scaling by s while conserving the energy will spread the wavelet transform by s in both the dimensions a and b , and thus a renormalization by $\frac{1}{a^2}$ is necessary. It is worth noting that the wavelet transform energy between the different scales is also preserves such that

$$\int_{-\infty}^{\infty} |\psi(t)|^2 dt = \int_{-\infty}^{\infty} \frac{1}{a} |\psi_{ab}(t)|^2 dt \quad (3.77)$$

3.7.3 Discrete Wavelet Transform

Although the admissibility condition assures the complete representation of $f(t)$ with its wavelet transform coefficients $W_f(a, b)$, it requires the wavelet transform operation to be performed for all values of a and b which are continuous parameters. This transform representation is not practical. One would prefer to perform the wavelet transform operation as few times as possible. Therefore these scaling or dilation, and translation or shift parameters, a and b respectively, are discretized. This discretization provides a transform grid or frame on the time-scale plane for the representation of signal $f(t)$. It is intuitive that this grid or frame should be defined properly such that the complete representation of $f(t)$ is still possible. This is called the Discrete Wavelet Transform (DWT). This version of the wavelet transform reduces the redundancies of the wavelet space $W_f(a, b)$ significantly. The mathematical reasoning on the choice of frames or grids is perfectly treated in the literature.

Now one can define the basis functions of a Discrete Wavelet Transform as the subset of continuous wavelet function [45 - 48]

$$\psi_{ab}(t) = \frac{1}{\sqrt{a}} \psi\left(\frac{t-b}{a}\right) \quad (3.78)$$

with the corresponding discrete transform lattices or grids

$$a = a_0^m \quad b = nb_0 a_0^m \quad (3.79)$$

Hence, the discrete wavelet transform basis functions can be expressed as

$$\psi_{mn}(t) = a_0^{-\frac{m}{2}} \psi(a_0^{-m} t - nb_0) \quad (3.80)$$

Here m and n are integers. It is intuitively seen that this discrete wavelet family approaches a continuous wavelet family when $a_0 \rightarrow 1$ and $b_0 \rightarrow 0$

It can be shown that the functions of a discrete wavelet transform basis $\psi_{mn}(t)$ can form a frame or the sets of m and n parameters are proper for the completeness if the wavelet function $\psi(t)$ satisfies the admissibility condition. Then the frame bounds are constrained by the inequalities [45] $0 < A < B < \infty$

$$A \leq \frac{\pi}{b_0 \log a_0} \int \frac{|\Psi(\Omega)|^2}{|\Omega|} d\Omega \leq B \quad (3.81)$$

These inequalities hold for any choice of a_0 and b_0 . These bounds diverge for non-admissible wavelet functions.

The discrete wavelet transform is defined on the grid points or in the frame of time-scale plane as

$$W_f(m, n) = \langle \psi_{m, n}, f \rangle = a_0^{-\frac{m}{2}} \int \psi(a_0^{-m}t - nb_0) f(t) dt \quad (3.82)$$

and the wavelet transform representation of the signal

$$f(t) = \sum_m \sum_n W_f(m, n) \psi_{mn}(t) \quad (3.83)$$

There is a particular interest on a binary or dyadic grid where $a_0 = 2$ and $b_0 = 1$, which leads to the conventional multiresolution concept and the orthogonal discrete wavelet transforms.

3.8 Power Spectral Analysis of Heart Rate Variability

Power spectral analysis of heart rate variability is a potentially powerful tool for evaluating the activity of the autonomic nervous system noninvasively. Power spectral analysis is a technique which transforms a signal from the time domain to the frequency domain. The time domain signal used for computing the heart rate variability power spectrum is known as the interbeat interval (IBI). The following is a brief description of how to obtain the IBI signal.

To begin the analysis, the ECG is converted from analog to digital form and stored in ASCII format on the data acquisition computer running in LabVIEW. The data is then transferred over to a signal-processing computer. Another LabVIEW program is used to obtain the HRV power spectrum. The following is a description of the necessary steps to obtain the power spectrum of HRV.

The first step to obtain the power spectrum of HRV is to detect every R-wave in the ECG. Because the R-wave complex is pronounced in the ECG, the LabVIEW detection program can easily detect these R-waves.

Before trying to detect the R-waves, the ECG signals are detrended using a locally weighted robust regression algorithm built in LabVIEW. To help detect each R-wave, a vertical threshold (which the R-wave must exceed) and a horizontal threshold (to prevent detecting an R-wave for a period of time after one was detected) can be varied. If an error occurs during the R-wave detection, the analyst can use existing software to manually detect or undetect the incorrectly detected R-waves.

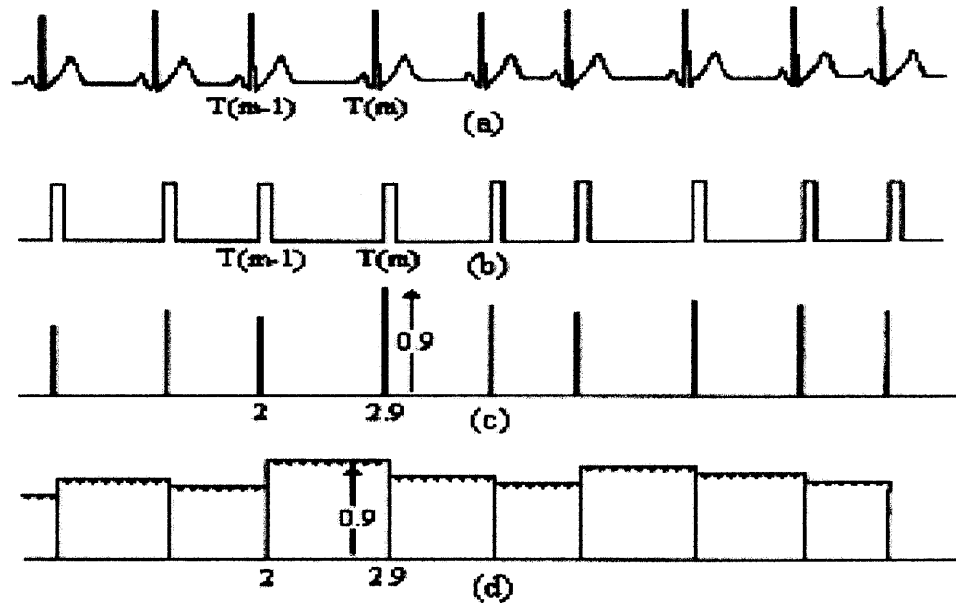


Figure 3.6 Figure depicting the construction of the IBI signal. (From S.J. Shin, W.N. Tapp, S.S. Reisman, and B.H. Natelson, "Assessment of autonomic regulation of heart rate variability by the method of complex demodulation," 1989.)

Once the R-waves are properly detected, an interbeat interval (IBI) signal can be constructed. To obtain the IBI signal, the distance in time between a specific beat (T_m) and the beat previous in time (T_{m-1}) is calculated. This value of time difference then becomes the amplitude of the IBI signal at that specific beat. Mathematically, the IBI signal is computed by the formula $IBI_m = T_m - T_{m-1}$. See Figure 3.6 for a graphical representation.

Although the IBI represents the heart period at discrete points, the IBI signal is not suitable for FFT analysis because the discrete points, located at each R-wave, are not evenly spaced. In order to produce equidistant IBI samples suitable for analysis, the IBI signal must be interpolated. The interpolation method used was that of a backward step function. This method assumes no new information about the direction of the time

series is available until the next heartbeat occurs. Therefore, the amplitude of all of the interpolated values between a beat at time T_{m-1} , and the beat at T_m , were set equal to the time difference between T_m and T_{m-1} . The interpolated interbeat interval (IIBI) is then sampled to produce an IIBI with evenly spaced samples. For example, in Figure 3.6(c) if a beat occurs at a time equal to 2 seconds and the next beat occurs at a time equal to 2.9 seconds, then the interpolated values between time 2 seconds and 2.9 seconds are all 0.9 as shown in Figure 3.6(d). After the IIBI signal is obtained, it is detrended using a locally weighted robust regression algorithm (available in LabVIEW), which acts like a filter. Essentially, this removes low frequency components below .05 Hz. If these low frequency components are not removed, they can dominate the power spectrum and decrease the detail of the components in the frequencies above 0.05 Hz. Another example of an IBI signal and an IIBI signal is shown in Figure 3.7.

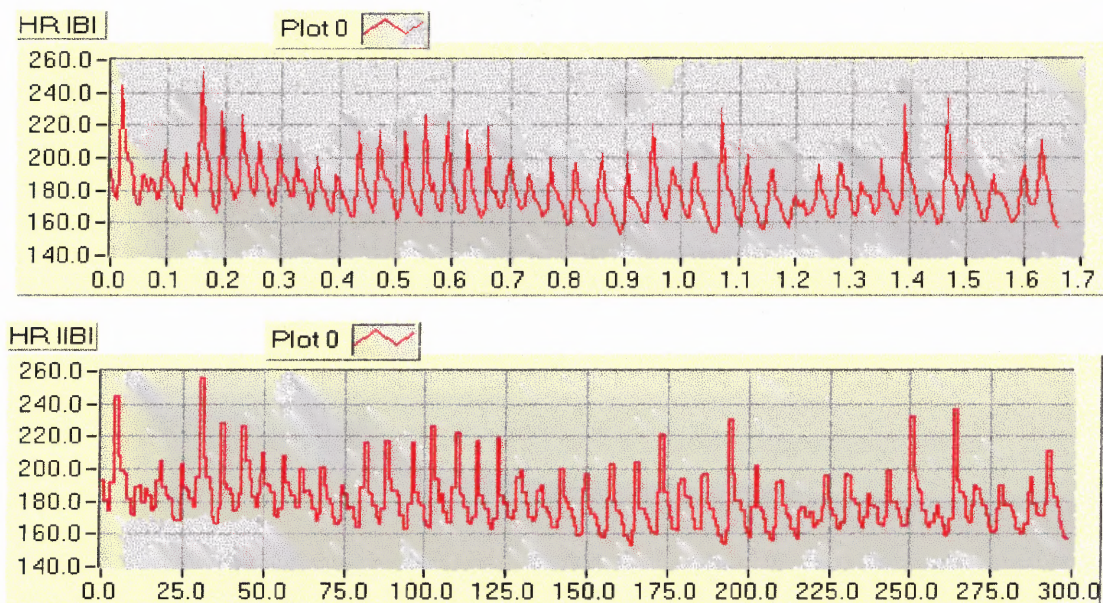


Figure 3.7 IBI and IIBI signals of heart rate.

The final step to obtain the power spectrum of HRV is to take the FFT of the detrended IIBI signal. In the existing software, this is done by decimating the IIBI signal by a factor of ten (the ECG is sampled at 200 Hz) and taking an 8192 point FFT of the decimated IIBI signal. When the signal is decimated by a factor of ten, every tenth point of the original signal is kept, and the nine points in between every tenth point are not used. In a time series of samples, every tenth point occurs at the same time as in the undecimated signal, except that there are no samples in between. In effect, decimating is similar to down-sampling. In other words, because the length of the IIBI signal is approximately the same length of the sampled ECG, which is acquired using a sampling frequency of 200 Hz, decimating the IIBI by a factor of 10, is similar to sampling the IIBI at 20 Hz. This can be done because the IIBI signal contains no frequency components above 6 Hz.

The software is programmed to take an 8192-point FFT by default regardless of the input signal length. In the experiments, 300 seconds of ECG were collected. At a sampling frequency of 200 Hz, this corresponds to 60,000 samples. Recall that the IIBI is approximately the same length as the ECG. If an 8192-point FFT were taken, only the first one-eighth of the IIBI would be represented in the spectrum. In addition, the frequency resolution would be $200/8192 = 0.0244$ Hz and the spectrum would be between 0Hz and 100 Hz. However, the spectrum of the IIBI, the heart rate variability spectrum, consists of low frequencies less than 6 Hz; therefore, the spectrum does not need to be calculated up to 100 Hz. As a result, the IIBI is decimated by a factor of ten. In this case, the IIBI signal would then be 6,000 samples long for a 300-sec long ECG signal. Note in Figure 3.6 that the length of the IIBI signal is 6,000 points long. The

length of the IBI signal depends on the number of heartbeats. Now, in order to take an 8192-point FFT of a signal that has only 6,000 samples, a technique called zero padding must be used. Essentially all samples from 6001 to 8192 are given the value of zero. The only effect this has on the spectrum is that it increases the frequency resolution. When the FFT is calculated, the spectrum is limited from 0 Hz up to 10 Hz. The frequency resolution is now $20/8192=0.00244$ Hz. Once the power spectrum is obtained, it is smoothed twice by applying a modified Daniel Rectangular smoothing algorithm. Figure 3.8 illustrates the power spectrum of the IIBI signal in Figure 3.7.

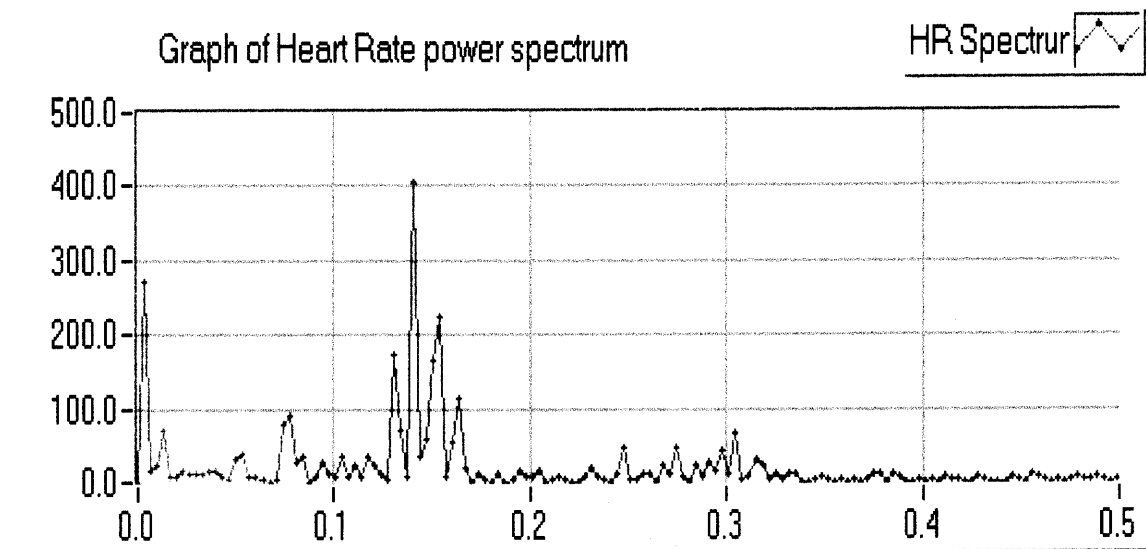


Figure 3.8 Power spectrum of the heart rate IIBI signal in Figure 3.7.

It should also be noted that when performing the FFT, the IIBI signal is windowed by applying a split cosine bell taper. The taper begins at 20 percent from each end of the time signal. The application of the split cosine bell taper is done before the zero padding takes place so as to provide a smooth transition to zero rather than the window's abrupt changes from one to zero.

It should be noted that if the window were a simple rectangular function, the sharp one to zero changes are the cause of the side lobes in the FFT output sinc function ($\sin(x)/x$). To minimize the spectral leakage caused by those sidelobes, one has to reduce the sidelobe amplitudes by using window functions other than the rectangular window. The purpose of the split cosine bell taper window is to reduce any additional spectral components that result from the shape of the window. Multiplying the time signal by the window function does the windowing. The split cosine bell taper for a 6,000-point long signal is shown in Figure 3.9.

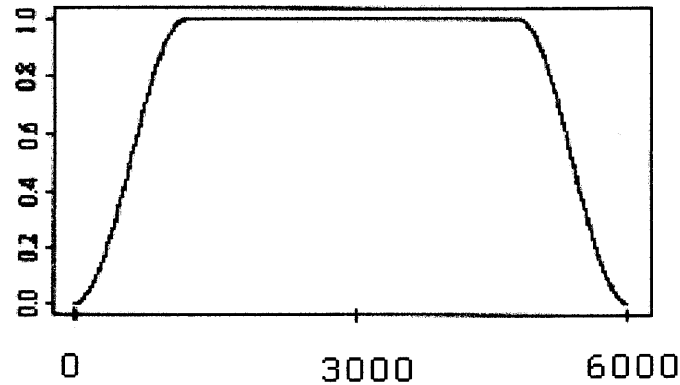


Figure 3.9 Plot of the split cosine bell taper used as a window for FFT calculation.

Past research in power spectral analysis of heart rate variability correlates three distinct frequency regions peaks with certain physiological parameters [14] as illustrated by a more classical power spectrum of the IIBI signal in Figure 3.10. The very low frequency band (0.003-0.04 Hz) is associated with vasomotor control and temperature control. The low frequency band (0.04-0.15 Hz) is associated with baroreceptor-mediated blood pressure control. The high frequency band (0.15-0.5 Hz) has been linked with respiration.

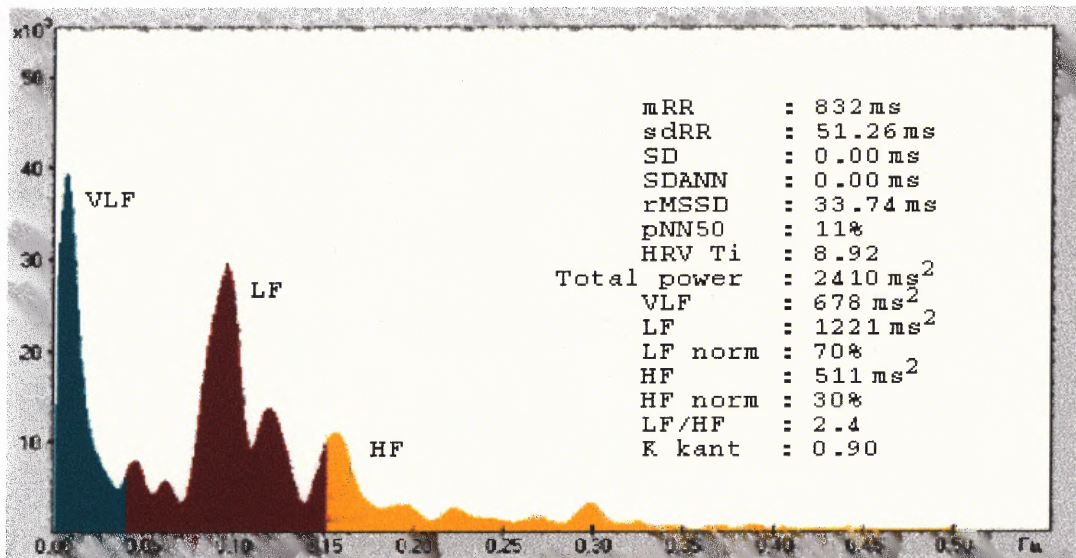


Figure 3.10 Example of power spectral density of HRV. Blue: power of spectrum of RR interval in VLF range, red: power in LF range and yellow: power in HF range. (From www.skyaid.org/Skyaid%20Org/Medical/HRV_Courses.htm, 12/2001.)

To date, the best-known and best-defined peak in power spectral analysis of heart rate variability is the high frequency peak. The high frequency peak reflects changes in the interbeat interval that cycles up and down at the same frequency as respiration. This influence of respiration on heart rate has been known for more than one century and is called respiratory sinus arrhythmia (RSA). Properly defined, RSA is a rhythmical fluctuation in heart periods at the respiratory frequency that is characterized by a shortening and lengthening of heart periods in a phase relationship with inspiration and expiration, respectively [15]. RSA is being used increasingly as a measure of vagal control of the heart. As a result, the high frequency peak, which often occurs at the same frequency as the respiration peak, corresponds approximately to the RSA and it is purely parasympathetic in origin [17]. From experience, one might contest that the frequency of respiration is not limited to within the narrow band of 0.15 Hz to 0.4 Hz.

The normal respiration rate can be as low as only a few breaths per minute at rest and as high as up to 40 breaths per minute during intense exercise [15]. This stresses the fact that, when doing research on heart rate variability to determine parasympathetic activity, the frequency of respiration must be known. More specifically, the power spectrum of the respiration waveform should be computed. Once the power spectrum of the respiration is obtained, the coherence between the respiration spectrum and the heart rate variability spectrum could be computed. Frequencies with a high coherence (i.e. >0.9) could then be considered of parasympathetic origin. Although this is the theoretical approach, in the field, the area under the frequencies of 0.15 to 0.4 Hz is considered parasympathetic in origin.

Unlike parasympathetic activity, the sympathetic activity is not easily separated from the power spectrum of heart rate variability [14]. It has been hypothesized that the low frequency peak (0.04 to 0.15 Hz) is a mixture of both parasympathetic activity and sympathetic activity. A better concept that is used to isolate the sympathetic activity is that of "sympatho-vagal balance" which recognizes both reciprocal and non-reciprocal parasympathetic and sympathetic influences on heart rate by computing the low frequency to high frequency ratio [49]. An increase in the low frequency to high frequency ratio indicates either an increase of sympathetic activity, a decrease in parasympathetic activity, or a reciprocal change in both.

3.9 Power Spectral Analysis of Blood Pressure

The necessary steps required to obtain the power spectrum of the blood pressure variability are similar to those of HRV with the exception of obtaining the blood pressure IBI signal. Similar to R-wave detection of heart rate, the systolic blood pressure peaks are also detected by the LabVIEW program and the analyst can also manually correct any error during detection. Once all the systolic blood pressure peaks are properly detected, a BP interbeat interval (BP IBI) signal can be constructed. To obtain the BP IBI signal, the height of the systolic BP peak becomes the amplitude of the BP IBI signal at that specific beat. See Figure 3.11 for a presentation. The BP IBI signal is then interpolated in the same manner as the ECG IBI signal to get the BP interpolated interbeat interval (BP IIBI) and the same steps are used to obtain the BP power spectrum waveform. See Figure 3.12 for the illustration of the power spectrum of the BP IIBI signal.

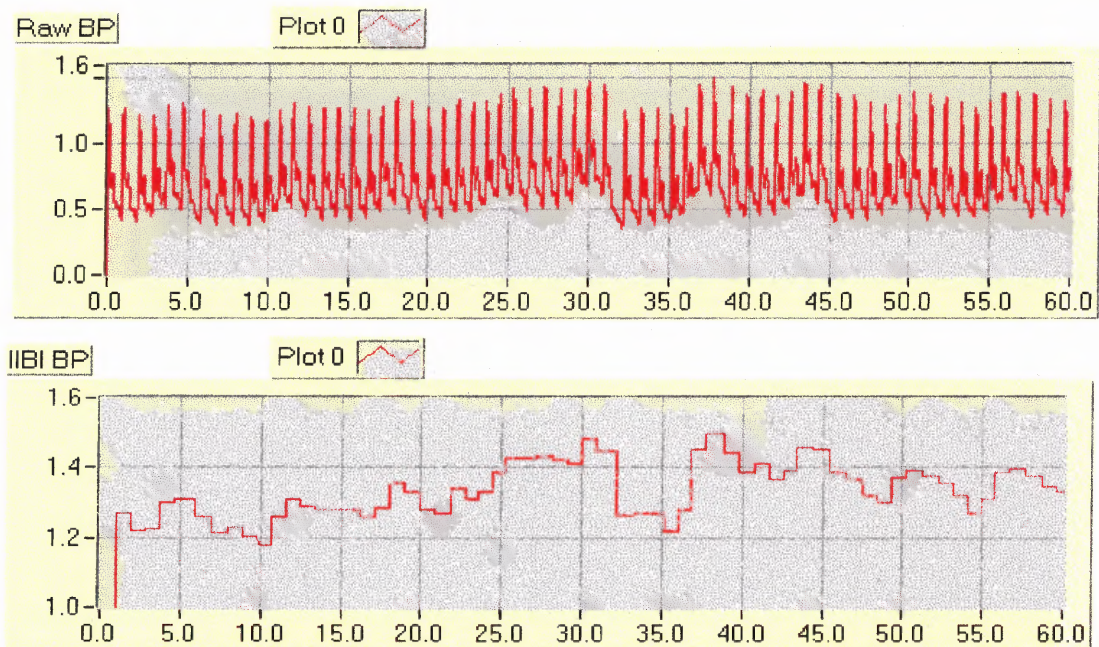


Figure 3.11 One-minute plot of raw blood pressure and its IIBI signal.

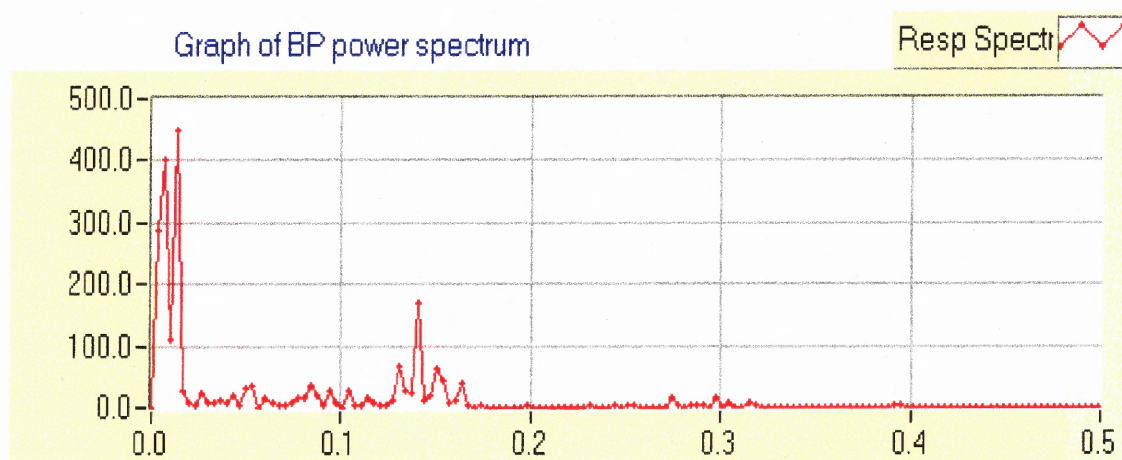


Figure 3.12 Power spectrum of BP IIBI in Figure 3.10.

3.10 Coherence Analysis

Within the present framework, the dependence between two signals can be characterized by parameters, which assess the correlation between the signals. In the frequency domain it is customary to consider the magnitude squared of the correlation between the Fourier transforms of the two signals under consideration. For the bivariate point processes (N_0, N_1) this leads to [61][62]

$$\lim_{T \rightarrow \infty} |corr\{F_{N_1}(\omega), F_{N_0}(\omega)\}|^2 \quad (3.84a)$$

as a measure of the correlation between processes N_0 and N_1 . This quantity is called the *coherence function* [63], denoted by $|\gamma_{10}(f)|^2$, estimates of which provide a measure of the strength of correlation between N_0 and N_1 as a function of frequency. The definition of the correlation $corr\{F_{N_1}(\omega), F_{N_0}(\omega)\}$ between the Fourier transforms of the two point processes N_0 and N_1 in terms of variance and covariance, given by the expression: $corr\{F_{N_1}(\omega), F_{N_0}(\omega)\} = cov\{F_{N_1}(\omega), F_{N_0}(\omega)\} / \sqrt{\text{var}\{F_{N_1}(\omega)\} \text{var}\{F_{N_0}(\omega)\}}$, leads to the alternative definition for the coherence function between point processes N_0 and N_1 as

$$|\gamma_{10}(\omega)|^2 = \frac{|P_{10}(\omega)|^2}{P_{11}(\omega)P_{00}(\omega)} \quad (3.84b)$$

Coherence functions provide a normative measure of linear association between two processes on a scale from 0 to 1, with 0 occurring in the case of independent processes [61][62]. Equation (3.84b) leads to an estimation procedure by substitution of the appropriate spectral estimates to give

$$|\hat{\gamma}_{10}(\omega)|^2 = \frac{|\hat{P}_{10}(\omega)|^2}{\hat{P}_{11}(\omega)\hat{P}_{00}(\omega)} \quad (3.84c)$$

where $|\hat{\gamma}_{10}(\omega)|^2$ denotes an estimate of $|\gamma_{10}(\omega)|^2$. A similar procedure can be used to estimate the coherence between a time series x and point process N_1

$$|\hat{\gamma}_{x1}(\omega)|^2 = \frac{|\hat{P}_{x1}(\omega)|^2}{\hat{P}_{xx}(\omega)\hat{P}_{11}(\omega)} \quad (3.84d)$$

and the coherence between two time series $x(t)$ and $y(t)$, $|\gamma_{xy}(\omega)|^2$, can be estimated in a similar manner to give:

$$MSC = |\gamma_{xy}(\omega)|^2 = \frac{|P_{xy}(\omega)|^2}{P_{xx}(\omega)P_{yy}(\omega)} \quad (3.85a)$$

When computing the coherence using equation (3.85a), the important step is to compute the coherence by means of averaged estimates based on segments of the original signals. In other words, the signals $x(t)$ and $y(t)$ are broken up into N segments of equal length and the power spectra ($P_{xx}(\omega)$ and $P_{yy}(\omega)$) and cross spectrum ($P_{xy}(\omega)$) are estimated on the basis of averages taken from the individual spectra of the segments. To increase the number of individual spectra, which increases the accuracy, the segments may overlap. In addition, care must be taken to assure that the segments are long enough to obtain an accurate spectrum. Therefore, there is a compromise required in the choice of the segment length. It must be long enough to obtain accurate frequency resolution, but short enough to allow a sufficient number of segments in the average. In addition, each segment must be extracted using a time-domain window to control the sidelobes in the frequency domain. To make things more complicated, if too many

segments are taken then the accuracy declines due to a greater correlation between segments.

Coherence estimates obtained in this way all have the same large sample properties for any combination of point process and/or time series data [64]. A confidence interval at the 100% point which is based on the assumption of independence, i.e. $|\gamma_{x1}(f)|^2=0$, is given by the value $1 - (1 - \alpha)^{1/(L-1)}$, where L is the number of disjoint sections used to estimate the second order spectra [65][66]. Therefore an upper 95% confidence limit can be set at the constant level

$$1 - (0.05)^{1/(L-1)} \quad (3.85b)$$

and estimated values of coherence below this level can be taken as evidence for a lack of correlation between the two processes at a particular frequency. The setting of confidence limits about the estimated values of coherence when significant correlation is present is discussed in [64].

Coherence estimates assess the magnitude of correlation between two signals in the frequency domain. Information relating to timing can be obtained by examining the phase difference between the two signals. For point process N_1 and time series x , the *phase spectrum*, $\Phi_{x1}(f)$ is defined as the argument of the cross-spectrum

$$\Phi_{x1}(f) = \arg\{P_{x1}(f)\} \quad (3.85c)$$

Similarly, the estimated function is given as:

$$\hat{\Phi}_{x1}(f) = \arg\{\hat{P}_{x1}(f)\} \quad (3.85d)$$

Phase spectra between other combinations of point-process and/or time series data can be defined and estimated in similar fashion. Phase estimates are only valid

when there is significant correlation between the two signals. In practice $|\hat{\gamma}_{x1}(f)|^2$ can be used to indicate the regions where $\hat{\Phi}_{x1}(f)$ has a valid interpretation. Phase estimates can be interpreted as the phase difference between harmonics of N_1 and x at frequency f . The arctan function can be used to obtain the argument of the cross-spectrum, resulting in a phase estimate over the range $[-\pi/2, \pi/2]$ radians. However, the signs of the real and imaginary parts of $\hat{P}_{x1}(f)$ can be used to determine in which quadrant the arctangent falls, so extending the range to $[-\pi, \pi]$ radians.

Phase estimates can often be interpreted according to different theoretical models. A useful model is the phase curve for two signals, which are correlated with a fixed time delay, where the theoretical phase curve is a straight line, passing through the origin (0 radians at 0 frequency) with slope equal to the delay, and a positive slope for a phase lead, and negative slope for a phase lag (see [67]). In situations where there is significant correlation over a wide range of frequencies and a delay between two signals, it is reasonable to extend the phase estimate outside the range $[-\pi, \pi]$ radians, which avoids discontinuities in phase estimates. Such a phase estimate is often referred to as an *unconstrained phase estimate*. The representation of phase estimates is discussed in [66]. Different theoretical phase curves for other forms of correlation structure are discussed in [67]. Details for the construction of confidence limits about estimated phase values can be found in [64]. In situations where the correlation structure between two signals is dominated by a delay it is possible to estimate this delay from the phase curve. Such an approach, based on weighted least squares regression, is described in the Appendix in [62]. This method has the advantage of providing an estimate of the

standard error for the estimated delay. In this dissertation, phase spectra are not being considered. However, these studies of the phase curves and their slopes obtained from correlation between two physiological signals such as HR and Respiration, BP and Respiration or HR and BP can be performed in the future. This will help in understanding the time delay, phase lead or phase lag between the regulatory systems that cause the changes in HR, BP and respiration.

3.11 Weighted Coherence

Weighted coherence is defined by Porges et al. (1980) as the proportion of the total variance of one signal that is shared with the other signal within a certain frequency band [51]. It can be computed easily from the values of the coherence function and the spectral density values of one of the signals in that frequency region. It has the advantage that one measure can be derived for a whole frequency band of interest, for example the low or high frequency band of the heart rate variability spectrum. The weighted coherence function can be computed by the following formula:

$$CW_{XY}(f1, f2) = \frac{\sum_{f_1}^{f_2} Coh_{XY}(f) * P_{YY}(f)}{\sum_{f_1}^{f_2} P_{YY}(f)} \quad (3.86)$$

In which:

$CW_{XY}(f1, f2)$ = Weighted coherence in the frequency band between f1 and f2

$Coh_{XY}(f)$ = Coherence between the signals x and y for frequency f

$P_{YY}(f)$ = Power spectral density of the signal y for frequency f.

3.12 Partial Coherence Analysis

3.12.1 Multivariate Analysis

The above methods can be extended to examine the correlation structure between several simultaneously recorded signals. This is called a multivariate analysis, and is equivalent to *multivariate regression analysis*, except that parameters are estimated at each frequency of interest.

Two related questions which can be addressed by such analysis are 1) whether the correlation between two signals results from the common (linear) influence of a third signal, and 2) whether a third signal is capable of predicting the correlation between two signals. Both these questions can be addressed by estimating the *partial coherence*, and *partial phase* which characterize the correlation between the two original signals after removing the common linear effects of the third (predictor) signal from each. This multivariate analysis can be performed on any combination of point process and/or time series data [64].

3.12.2 Partial Spectra

The starting point for the multivariate analysis is the estimates of second order spectra described in Section 3.10 of the coherence analysis, with the requirement of three simultaneously recorded signals and spectral estimates which have been estimated with the same segment length, T . For example, to estimate the partial correlation between point process N_0 and time series x , with time series y as predictor, one starts by defining partial spectra, estimates of which are then used to construct estimates of the other

partial parameters. The *partial cross-spectrum* between N_0 and x , with y as predictor, is defined as [66]

$$P_{x0/y}(\omega) = P_{x0}(\omega) - \frac{P_{xy}(\omega)P_{y0}(\omega)}{P_{yy}(\omega)} \quad (3.87)$$

The *partial auto-spectra*, $P_{xx/y}(\omega)$, is defined as

$$P_{xx/y}(\omega) = P_{xx}(\omega) - \frac{P_{xy}(\omega)P_{yx}(\omega)}{P_{yy}(\omega)} = P_{xx}(\omega) - \frac{|P_{xy}(\omega)|^2}{P_{yy}(\omega)} \quad (3.88)$$

The other partial auto-spectrum, $P_{00/y}(\omega)$, is defined in a similar manner. These partial spectra can be used to estimate the first order *partial coherence* between N_0 and x , with y as predictor, denoted by $|\gamma_{x0/y}(\omega)|^2$, as

$$|\gamma_{x0/y}(\omega)|^2 = \frac{|P_{x0/y}(\omega)|^2}{P_{xx/y}(\omega)P_{00/y}(\omega)} \quad (3.89)$$

This equation has a similar form to that for the ordinary coherence function, (3.85a). The corresponding first order *partial phase* is defined as

$$\Phi_{x0/y}(\omega) = \arg\{P_{x0/y}(\omega)\} \quad (3.90)$$

This function provides information about the timing relation of any residual coupling between N_0 and x after the removal of the common effects of process y . Partial coherence functions, like ordinary coherence functions, are bounded measures of association, with values between 0 and 1 [61, 62, 64, 66].

An alternative definition of the first order partial coherence, $|\gamma_{x0/y}(\omega)|^2$, as the magnitude squared of the correlation between the finite Fourier transforms of N_0 and x ,

after removal of the effects of process y from each, may be written (suppressing the dependencies on ω) as [61, 62, 64, 66].

$$|\gamma_{x0/y}|^2 = \lim_{T \rightarrow \infty} \left| \text{corr} \left\{ F_x(\omega) - \left(\frac{P_{xy}}{P_{yy}} \right) F_y(\omega), F_{N_0}(\omega) - \left(\frac{P_{0y}}{P_{yy}} \right) F_y(\omega) \right\} \right|^2 \quad (3.91)$$

Expansion of this expression in a similar manner to (3.84a) leads to equation (3.89). The two terms (P_{xy}/P_{yy}) and (P_{0y}/P_{yy}) represent the regression coefficients which give the *optimum linear prediction* of $F_x(\omega)$ and $F_{N_0}(\omega)$, respectively, in terms of $F_y(\omega)$. Estimates of $|\gamma_{x0/y}(\omega)|^2$ test the hypothesis that the coupling between N_0 and x can be predicted by process y , in which case the parameter will have the value zero. The partial coherence defined in (3.89) and (3.91) is a first order partial coherence, which examines the correlation between two signals after removing the common effects of a single predictor. This framework can be extended to define and estimate partial coherence functions of any order. Full details, including estimation procedures and the setting of confidence limits can be found in [64].

For further in-depth details about these calculations, see Bendat and Piersol [50]. For all the partial coherence equations used in the LabVIEW program, refer to Appendix C.

3.13 System Identification

Measuring the frequency response of a linear system is a typical first step in characterizing its dynamic behavior. To understand a system and its signal processing often demand information beyond the frequency response. Underlying differential and/or difference equations provide a concise mathematical description defining all other dynamic behavior. The task of estimating these equations from measurements of the input and output signals is referred to in the control literature as the process of System Identification (SID).

In 1971 two Swedish researchers, Åström and Eykhoff, published a paper that started the field of System Identification (SID) [53]. Although many advances have been made in unifying the underlying theories, there continues to be a wide variety of approaches promoted in technical journals, textbooks, and conferences over three decades after the original paper.

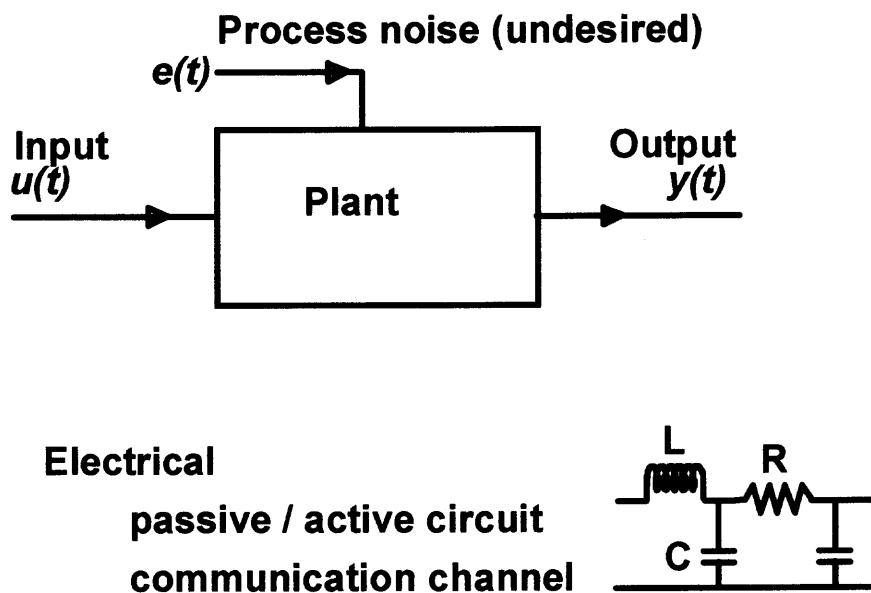


Figure 3.13 Examples of typical plant.

The bulk of the theory and applications of SID evolved from control systems research. In control language, the dynamic system being identified (or modeled) is called the **plant**. The plant can take on a wide variety of forms. In general, a plant is an object or collection of objects, producing an output by modifying an input. The input to the plant could be temperature, pressure, voltage, current, position, velocity, acceleration, and so on. The input can also contain more than one variable (e.g., several signals from transducers measuring various conditions of an engine). The output from the plant can be in the form of any of the inputs (temperature, pressure, position, etc.) and it also can contain several signals.

Single-input, single-output (**siso**) plants are addressed here since they are the most prevalent. The siso models can be combined to create multi-input, multi-output models if necessary.

Figure 3.13 depicts an example of an electrical plant. The plant can be accurately described mathematically by linear constant/coefficient, differential equations. A plant described by these equations is said to be Lumped-Linear-Time-Invariant (LLTI). Even plants that are mildly non-linear, slowly time varying, and possibly distributed in nature (e.g., those requiring partial differential equations for a full description) can often be adequately modeled using these LLTI assumptions.

3.13.1 Estimating Transfer Functions of Non-linear Systems

Accurate transfer function estimation of linear, noise-free, dynamic systems is typically an easy task. Often, however, the system being analyzed is noisy or not perfectly linear. All real-world systems suffer from these deficiencies to a degree, but biological systems

are particularly bad in this regard. Dealing with the combination of noise and non-linearity requires the understanding of the necessary measurement tradeoffs to assure an accurate transfer function estimation.

3.13.1.1 Imperfections in Dynamic Systems. Biological control systems typically have higher noise and less linearity than the typical electrical or purely mechanical system. The non-linear behavior is often due to the physiological components involved in the system. The measurement noise is often a result of the system being characterized under actual operating conditions.

3.13.1.2 Balancing Noise and Non-linearity. To make a transfer function measurement on a dynamic system, an excitation is supplied to the system and the system's response to this excitation is measured. If the system is noisy but linear, the excitation level can be increased to improve the signal to noise ratio by simply overpowering the noise. If the system is non-linear (for example at high excitation amplitudes), but noise free, the excitation can be lowered to a point where the linearity is acceptable.

When the system is both non-linear and noisy, a tradeoff must be made balancing the poor signal-to-noise ratio at low excitation amplitudes with the non-linear system behavior at high excitation amplitudes.

There are two possible approaches of transfer function estimation: swept-sine and a broadband FFT based network analyzer.

The swept sine (or more accurately stepped-sine) estimation technique is the least affected by noise and non-linear system behavior. The tradeoff with the swept-sine

technique is measurement time. The transfer function is estimated over a user defined frequency range at a single frequency point at a time.

In measurement situations where there is reasonable linearity and good signal to noise ratio, the broad-band FFT based network analyzer provides the transfer function estimate in a fraction of the time that is normally needed by the swept sine approach. The excitation is usually a periodic chirp or bandlimited random signal, but the adventuresome user has full control over the excitation including user defined (arbitrary) excitation.

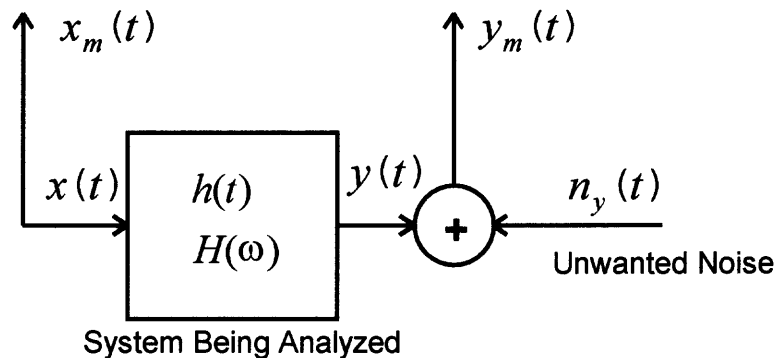


Figure 3.14 Optimal data acquisition measurement system.

In the end, the amount of time required for a transfer function estimate is set by five factors:

- 1) the system's noise
- 2) the system's linearity
- 3) the number of frequency points in the estimate
- 4) the accuracy required
- 5) the time for basic data acquisition

3.13.1.3 The Optimal Measurement Configuration. The main goal here is to determine the system transfer function $H(\omega)$ from measurements on the system. The optimal measurement configuration is shown in Figure 3.14. There is no assumption made at this point as to what kind of system is being characterized, biological system or otherwise.

This configuration allows the excitation (often called the reference) signal to the system being analyzed, to be measured with negligible error. This is a valid assumption when the output source is measured directly by an input channel as shown in Figure 3.14. Often in biomedical work, the excitation to the system is not in the form of voltage (as is assumed in Figure 3.14). Transducers must be used to convert the system excitation into a voltage which can be measured by the acquisition system. For instance, a force-to-voltage transducer would be used to measure the force in a muscle study. In cases such as this, precautions must be taken to insure that minimal electrical noise corrupts the signal from the electrodes or transducer and that they are operated in their linear region.

As shown in Figure 3.14, the entire measurement uncertainty is accounted for in the response signal $y_m(t)$ by the additional (unwanted) noise term $n_y(t)$. There are no assumptions about the character of this noise other than when the excitation is zero, the response of the system $y(t)$ is zero, and it is left with $y_m(t) = n_y(t)$. It is important to note that $n_y(t)$ is usually not an actual external source but merely a representation of the system output when there is no excitation.

At first it might seem that the restriction of having a noiseless reference channel is an unreasonable measurement condition. In practice, however, this requirement is

usually attainable. The key point is that an *unbiased* estimate of the transfer function is relatively easy to obtain if an accurate measurement of the reference channel is made.

The transfer function estimation, $\hat{H}(\omega)$, is computed from cross and auto power spectra estimates as shown in (3.92):

$$\hat{H}(\omega) = \frac{\hat{P}_{xy}(\omega)}{\hat{P}_{xx}(\omega)} \quad (3.92)$$

where $\hat{P}_{xy}(\omega)$ is the cross power spectrum between the excitation $x_m(t)$ and response $y_m(t)$ and $\hat{P}_{xx}(\omega)$ is the auto power spectrum of the excitation signal.

These spectral estimates ($\hat{P}_{xx}(\omega), \hat{P}_{xy}(\omega)$) are computed in MatLab or Lab VIEW using the FFT, windowing, and frequency-domain averaging. When more averaging is used, more data is acquired and processed to refine these estimates.

As the amount of averaging used in the computations of the cross and auto power spectra are increased, the estimate $\hat{H}(\omega)$ will converge to the actual transfer function $H(\omega)$. This is the key property of an unbiased estimator. The amount of averaging required to attain a given accuracy for the transfer function is a function of the noise $n_y(t)$: less noise, less averaging.

The coherence is an auxiliary computation often made in conjunction with the transfer function estimate. The coherence calculation in (3.93) gives an indication of the portion of the systems output power due to the input excitation.

$$\hat{C}(\omega) = \frac{|\hat{P}_{xy}(\omega)|^2}{\hat{P}_{xx}(\omega)\hat{P}_{yy}(\omega)} \quad (3.93)$$

The quantity $\hat{C}(\omega)$ has a range of 0.0 to 1.0, where 1.0 indicates that all of the measured output power is due to the input excitation. This is the most desirable situation and will only be true at frequencies where the spectral energy of the noise $n_y(t)$ is negligible. The coherence can therefore be viewed as a measurement quality indicator. When a significant portion of the measured output is not related to the excitation, a low coherence results. This indicates that for a given amount of averaging, the variance of the transfer function at these frequencies will be higher than the variance where there is good coherence (closer to 1.0).

It is important to recognize that since this estimator is unbiased, given sufficient averaging, the transfer function estimate will converge to the system's actual transfer function in spite of possibly low coherence.

The above transfer function and coherence estimation calculations are calculated in Lab VIEW and/or MatLab System Identification Toolbox.

3.13.2 The ARX Models

The timing of electrical and mechanical events within the heart is vital to its function. In “normal” healthy humans, a bundle of spontaneously depolarizing cells located on the right atrium of the heart, called the sino-atrial (SA) node, acts as the pacemaker for the heart. Through an upward drift in electrical potential, the cells spontaneously reach a threshold potential, at which point the cells rapidly depolarize, or “fire”, as a group. This is followed by a reset which marks the start of a new cycle. The firing initiates the spread of electrical activity through the heart, and therefore initiates the contraction that is necessary for blood to be delivered to the rest of the body. Although temporal

variability exists in the propagation of the electrical activity across the tissue of the heart, the primary interest is in the temporal variability from “beat-to-beat”, which can be captured through observations of a distinct electrical event contained within each cycle. The spontaneous depolarization of SA nodal cells has an intrinsic rate that is modulated by direct input from the two branches of the autonomic nervous system (ANS). The basal activity of each branch has an effect on the mean rate of depolarization, but also the vast majority of variability in the timing of the electrical events of the heart is produced via this autonomic innervation by varying how quickly the SA nodal cells reach the threshold and “fire”. Activity of the respiratory rhythm generator has been shown to modulate the rate of depolarization of SA nodal cells at the respiratory frequency via the parasympathetic branch, and baroreflex feedback mechanisms have been shown to modulate the rate through both branches at sub respiratory frequencies. The goal of the modeling, therefore, will be to capture the dynamics of these mechanisms in a relatively simple ARX-modeling scheme, which has direct physiological interpretation.

Here two models are used for this study. The first model is an open loop input driven ARX model which can capture the characteristics of the “heart rate” variability. One input is simply a filtered Gaussian white process, for which several nice results will be developed. Other inputs correspond directly to autonomic mediation specifically related to respiration and blood pressure related modulation. The other model includes a feedback that allows one to investigate the feedback mechanisms in the ARX model, which will lay the groundwork for capturing the effect of baroreflex activity on heart rate variability.

3.13.2.1 Open-loop Input Driven ARX Model. The Open-loop Input Driven ARX Model is shown in Figure 3.15. The inputs to the model are [54]:

Respiration $V_t(n)$.

Systolic blood pressure, $SBP(n)$

The output of the model is:

Heart Rate, $RR(n)$.

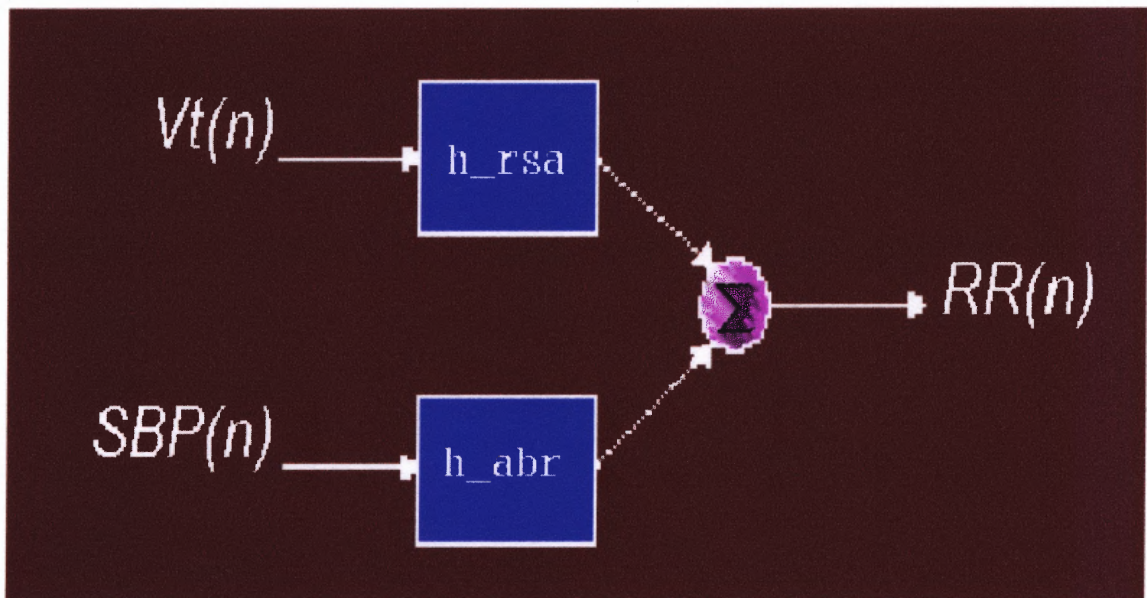


Figure 3.15 Open-loop input driven ARX model.

This figure shows an open-loop model-based approach that enables the dynamic effects of respiration and arterial systolic blood pressure on heart rate to be estimated in both COPD and normal subjects. This method is based on a two-compartment model of respiratory sinus arrhythmia (RSA), which includes a vagally mediated central component (h_rsa), and an arterial baroreflex (h_abr) component driven by both vagal and sympathetic systems. A parametric linear AutoRegressive representation with

eXogenous input (ARX) was used to estimate the impulse responses (IR) and transfer function (TF) of the two couplings in the model. A number of indexes derived from the IR's (peak magnitude, time of peak, delays) and TF's (gains and phases in the frequency bands of interest) were used for subsequence statistical analysis and the assessment of autonomic function.

$$\Delta RR(n) = \frac{B_1(q)}{A(q)} \Delta V_r(n - N_{V_r}) + \frac{B_2(q)}{A(q)} \Delta SBP(n - N_{ABP}) + \frac{1}{A(q)} W_{RR}(n) \quad (3.93a)$$

The two-compartment model of RSA in the Figure is described as an ARX representation by the equation. The coefficient of each polynomials (B_i , A) were estimated from the data by least square minimization of the prediction error W_{RR} . The orders and the delays of the model were chosen by finding the model that minimized the cross-correlation of each input and the prediction error, as well as the Minimum Description Length (MDL)

3.13.2.2 Feedback Closed-loop ARX Model. In this section a more realistic physiological model involving baroreflex and feedback loop. The depolarization, and therefore contraction, of the ventricles is associated with the ejection of blood into the aorta during systole. If one made the assumption that the volume of ejected blood is roughly the same for each contraction, then the arterial pressure will only be a function of the timing of the contractions. If several contractions occur close together, arterial pressure builds, causing simultaneous stimulation and inhibition of the parasympathetic and sympathetic branches of the ANS, respectively, resulting in a decrease in the rate of depolarization of the SA nodal tissue. A cascade of contractions that occur further apart

in time will result in a reduction of arterial pressure, causing simultaneous stimulation and inhibition of the sympathetic and parasympathetic branches of the ANS, respectively, producing an increase in the rate of depolarization.

Obviously, the arterial pressure varies in many ways. During systole the ventricles contract, causing the pressure to build, and during diastole the ventricles relax and the pressure drops. However, the mean arterial pressure fluctuates in a much slower manner, and it is this activity that dictates the level of baroreflex response.

In an effort to capture the dynamics of the baroreflex mechanism, it therefore becomes necessary to extend the previous models to include a class of systems that exhibit negative feedback, as shown in Figure 3.16. With the extended model to include a feedback loop and through the baroreflex mechanism, it will provide the baro-related heart rate variability in the lower frequency range (LF) through the intrinsic oscillations of the system.

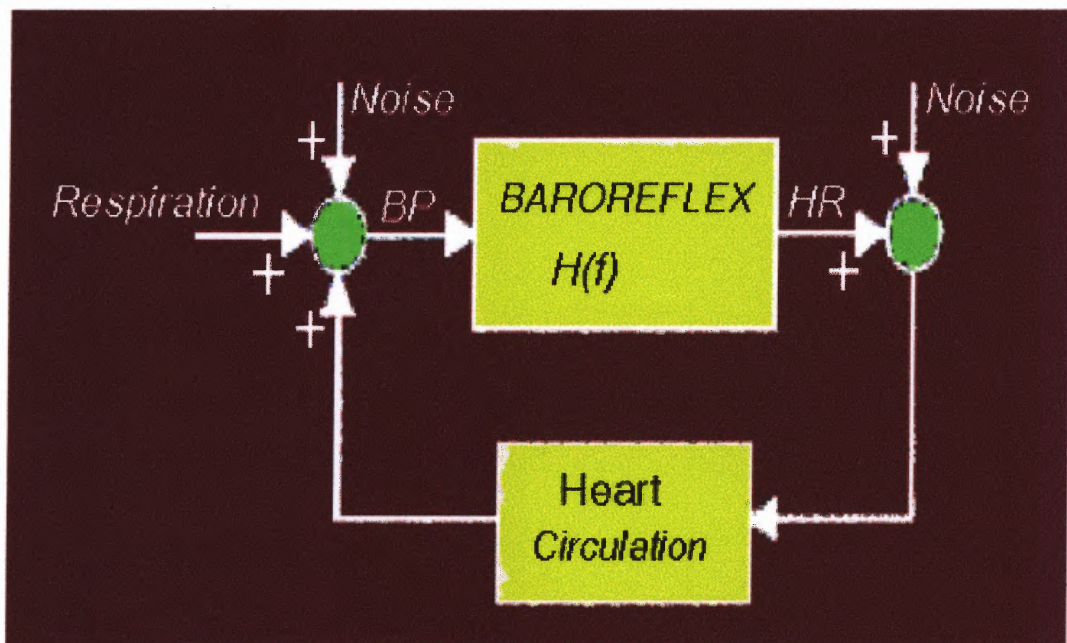


Figure 3.16 Feedback closed-loop ARX model.

The baroreflex, an autonomic reflex which controls heart rate through efferent vagal and sympathetic nerves by afferent inputs from pressure sensitive baroreceptors, is still mostly unknown. The neural control of the total cardiovascular system with several closed loops, of which the baroreflex is only a part, is very complex and that makes it difficult to assess characteristics of this reflex. If one was able to create a large enough broadband input signal and measure the input Blood Pressure (BP) as well as the output Heart Rate (HR), one could estimate from spectral calculations of input, output and cross- correlation, the amplitude and phase frequency characteristics of the baroreflex.

Respiration is known to modulate BP as well as HR, the latter phenomenon called respiratory sinus arrhythmia (RSA). However, the precise relationships are still under debate. Respiration affects primarily HR by central cardio-respiratory coupling and changes BP through variations in cardiac output. Respiration also directly modulates BP through mechanical effects of changing intrathoracic pressure on cardiac filling, which through the baroreflex causes HR variations at the respiration frequency. Recent studies [1][3] showed that respiration to a large extent primarily modulates BP and through the baroreflex, HR. The baroreflex with the respiratory influence can therefore schematically be visualized as in Figure 3.16. Under these assumptions one does have the possibility to "control" baroreflex input (BP) by letting a person breathe voluntarily according to a sinusoid on several fixed frequencies or a slowly changing frequency (sweep). Here it is desirable to prove the possibility of assessing gain and phase relations of the transfer function of BP and HR in a human, over a wide frequency range by voluntarily breathing at predetermined frequencies.

The results of this ARX model will prove to be a powerful analytical tool for relating the spectral characteristics of the sequence of observed intervals to the nature of the input and noise, which serves as a diagnostic for the underlying autonomic nervous system activity.

3.14 Principal Component Analysis

Principal component analysis is performed in order to simplify description of a set of the interrelated variables. In principal component analysis the variables are treated equally; i.e., they are not divided into independent and independent variables, as in regression analysis.

The technique can be summarized as a method of transforming the original variables into new, uncorrelated variables. The new variables are called the principal components. Each principal component is a linear combination of the original variables. One measure of the amount of information conveyed by each principal component is its variance. For this reason the principal components are arranged in order of decreasing variance. Thus the most informative principal component is the first, and the least informative is the last (a variable with zero variance does not distinguish between the members of the population).

The investigator may wish to reduce the dimensionality of the problem, i.e., reduce the number of variables without losing much of the information. This objective can be achieved by choosing to analyze only the first few principal components. The principal components not analyzed convey only a small amount of information since their variances are small. This technique is attractive for another reason, namely, that

the principal components are not intercorrelated. Thus instead of analyzing a large number of the original variables with complex interrelationships, the investigator can analyze a small number of uncorrelated principal components.

The selected principal components may also be used to test for their normality. If the principal components are not normally distributed, then neither are the original variables. Another use of the principal components is to search for outliers. A histogram of each of the principal components can identify those individuals with very large or very small values; these values are candidates for outliers or blunders.

In regression analysis it is sometimes useful to obtain the first few principal components corresponding to the X variables and then perform the regression on the selected components. This tactic is useful for overcoming the problem of multicollinearity since the principal components are uncorrelated [55].

Principal component analysis is considered to be an exploratory technique that may be useful in gaining a better understanding of the interrelationships among the variables. The original application of principal component analysis was in the field of educational testing. Hotelling [56] developed this technique and showed that there are two major components to responses on entry-examination tests: verbal and quantitative ability. Principal components analysis is also used extensively in psychological applications in an attempt to discover underlying structure. In addition, principal components analysis has been used in biological and medical applications [57] [58].

3.14.1 Basic Concepts of Principal Components Analysis

Suppose that there is a random sample of N observations on X_1 and X_2 . For ease of interpretation the sample mean is subtracted from each observation, thus obtaining

$$x_1 = X_1 - \bar{X}_1 \quad (3.94)$$

$$x_2 = X_2 - \bar{X}_2 \quad (3.95)$$

Note that this technique makes the means of x_1 and x_2 equal to zero but does not alter the sample variances S_1^2 and S_2^2 or the correlation r . The basic idea is to create two new variables, C_1 and C_2 , called the principal components. These new variables are linear functions of x_1 and x_2 and can therefore be written as

$$C_1 = a_{11}x_1 + a_{12}x_2 \quad (3.96)$$

$$C_2 = a_{21}x_1 + a_{22}x_2 \quad (3.97)$$

It should be noted that for any set of values of the coefficients a_{11} , a_{12} , a_{21} , a_{22} , one can introduce the N observed x_1 and x_2 and obtain N values of C_1 and C_2 . The means and variances of the N values of C_1 and C_2 are

$$\text{mean}C_1 = \text{mean}C_2 \quad (3.98)$$

$$\text{Var}C_1 = a_{11}^2S_1^2 + a_{12}^2S_2^2 + 2a_{11}a_{12}rS_1S_2 \quad (3.99)$$

$$\text{Var}C_2 = a_{21}^2S_1^2 + a_{22}^2S_2^2 + 2a_{21}a_{22}rS_1S_2 \quad (3.100)$$

where $S_i^2 = \text{Var}X_i$. Equation 3.98 is true because the means of x_1 and x_2 are zero.

The coefficients are chosen to satisfy three requirements:

1. The $\text{Var}C_1$ is as large as possible.
2. The N values of C_1 and C_2 are uncorrelated.

$$3. \quad a_{11}^2 + a_{12}^2 = a_{21}^2 + a_{22}^2 = 1.$$

The mathematical solution for the coefficients was derived by Hotelling [56]. The solution is illustrated graphically in Figure 3.17. Principal components analysis amounts to rotating the original X_1 and X_2 axes to new C_1 and C_2 axes. The angle of rotation is determined uniquely by the requirements just stated. For a given point x_1, x_2 (see Figure 13.2) the values of C_1 and C_2 are found by drawing perpendicular lines to the new C_1 and C_2 axes. The N values of C_1 thus obtained will have the greatest variance according to requirement 1. The N values of C_1 and C_2 will have a zero correlation.

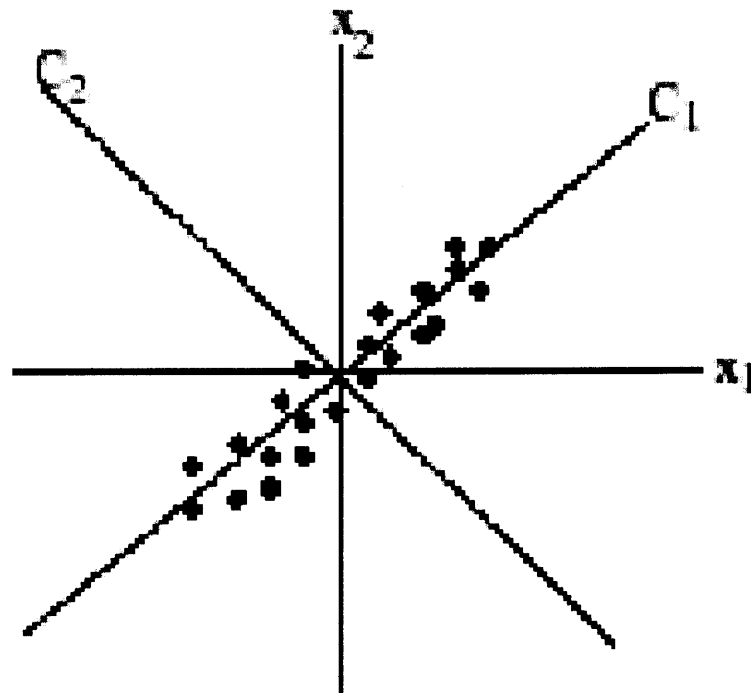


Figure 3.17 Principal component analysis illustration.

These ideas are easily extended to the case of P variables x_1, x_2, \dots, x_p . Each principal component is a linear combination of the x variables. Coefficients of these linear combinations are chosen to satisfy the following three requirements:

1. $VarC_1 \geq VarC_2 \geq \dots \geq VarC_p$.
2. The values of any two principal components are uncorrelated.
3. For any principal component the sum of the squares of the coefficients is one.

In other words, C_1 is the linear combination of the largest variance. Subject to the condition that it is uncorrelated with C_1 , C_2 is the linear combination with the largest variance. Similarly, C_3 has the largest variance subject to the condition that it is uncorrelated with C_1 and C_2 , etc. The $VarC_i$ are the eigenvalues. These P variances add up to the original total variance. In some literature the set of coefficients of the linear combination for the i th principal component is called the i th eigenvector (also known as the characteristic or latent vector).

3.15 Cluster Analysis

The term *cluster analysis* (first used by Tryon, 1939) actually encompasses a number of different classification algorithms. A general question facing researchers in many areas of inquiry is how to organize observed data into meaningful structures, that is, to develop taxonomies. For example, biologists have to organize the different species of animals before a meaningful description of the differences between animals is possible. According to the modern system employed in biology, man belongs to the primates, the mammals, the amniotes, the vertebrates, and the animals. Note how in this classification, the higher the level of aggregation the less similar are the members in the respective class. Man has more in common with all other primates (e.g., apes) than it does with the more "distant" members of the mammals (e.g., dogs), etc.

Note that one talks about clustering algorithms and does not mention anything about statistical significance testing. In fact, cluster analysis is not as much a typical statistical test as it is a "collection" of different algorithms that "put objects into clusters." The point here is that, unlike many other statistical procedures, cluster analysis methods are mostly used when priori hypotheses are not available, and it is still in the exploratory phase of the research. In a sense, cluster analysis finds the "most significant solution possible." Therefore, statistical significance testing is really not appropriate here, even in cases when p-levels are reported (as in ANOVA).

Clustering techniques have been applied to a wide variety of research problems. Hartigan (1975) provides an excellent summary of the many published studies reporting the results of cluster analyses [59]. For example, in the field of medicine, clustering diseases, cures for diseases, or symptoms of diseases can lead to very useful taxonomies.

In the field of psychiatry, the correct diagnosis of clusters of symptoms such as paranoia, schizophrenia, etc. is essential for successful therapy. In archeology, researchers have attempted to establish taxonomies of stone tools, funeral objects, etc. by applying cluster analytic techniques. In general, whenever one needs to classify a "mountain" of information into manageable meaningful piles, cluster analysis is of great utility.

3.15.1 Joining (Tree Clustering)

The examples given in previous sections illustrate the goal of the joining or tree clustering algorithm. The purpose of this algorithm is to join together objects (e.g., animals) into successively larger clusters, using some measure of similarity or distance. A typical result of this type of clustering is the hierarchical tree.

3.15.2 Hierarchical Tree

Consider a *Vertical Hierarchical Tree Plot* (see Figure 3.18 below), on the horizontal axis of the plot; one begins with each object in a class by itself. Now imagine that, in very small steps, one "relaxes" the criterion as to what is and is not unique. Put another way, the threshold regarding the decision is lowered when declaring two or more objects to be members of the same cluster. As a result more and more objects are linked together and aggregate (*amalgamate*) larger and larger clusters of increasingly dissimilar elements. Finally, in the last step, all objects are joined together. In these plots, the vertical axis denotes the linkage distance (in *Horizontal Icicle Plots*, the horizontal axis denotes the linkage distance). Thus, for each node in the graph (where a new cluster is

formed) one can read off the criterion distance at which the respective elements were linked together into a new single cluster.

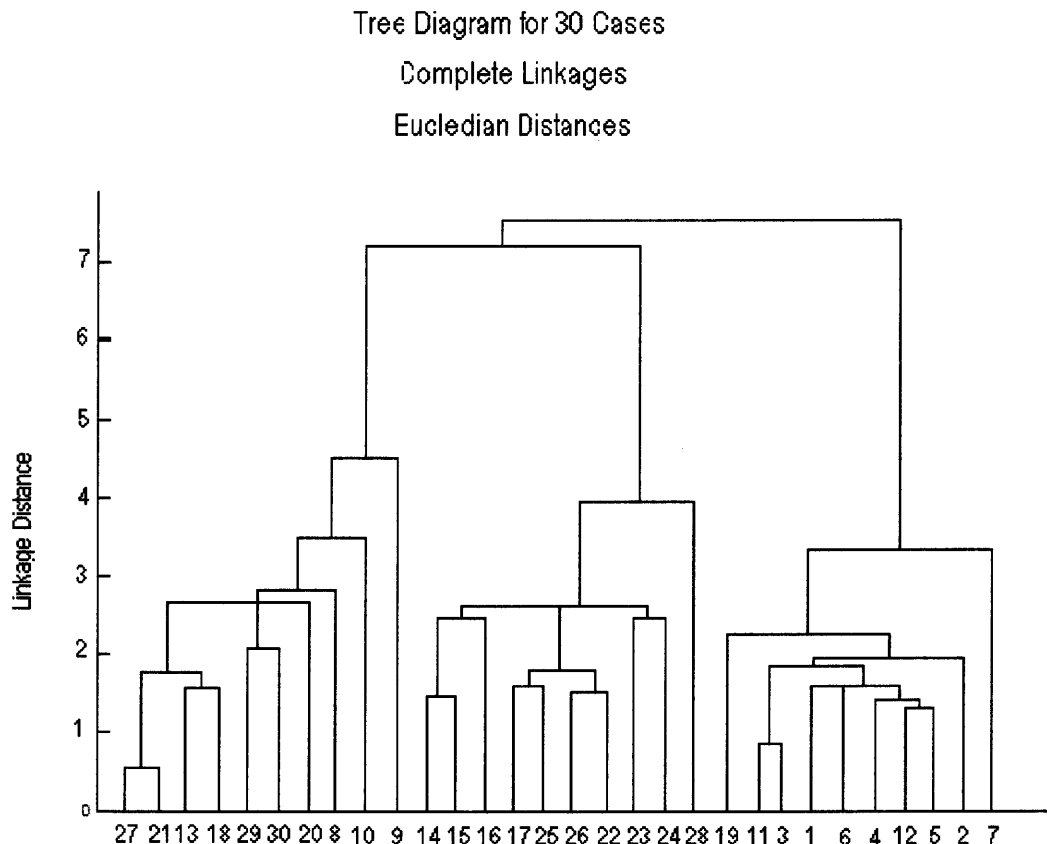


Figure 3.18 Vertical hierarchical tree plot.

When the data contain a clear "structure" in terms of clusters of objects that are similar to each other, then this structure will often be reflected in the hierarchical tree as distinct branches. As the result of a successful analysis with the joining method, one is able to detect clusters (branches) and interpret those branches.

3.15.3 Distance Measures

The joining or tree clustering method uses the dissimilarities or distances between objects when forming the clusters. These distances can be based on a single dimension

or multiple dimensions. For example, if fast foods were clustered, one could take into account the number of calories they contain, their price, subjective ratings of taste, etc. The most straightforward way of computing distances between objects in a multi-dimensional space is to compute Euclidian distances. If one had a two- or three-dimensional space this measure is the actual geometric distance between objects in the space (i.e., as if measured with a ruler). However, the joining algorithm does not "care" whether the distances that are "fed" to it are actual real distances, or some other derived measure of distance that is more meaningful to the researcher; and it is up to the researcher to select the right method for his/her specific application.

3.15.4 Euclidian Distance

This is probably the most commonly chosen type of distance. It simply is the geometric distance in the multidimensional space. It is computed as:

$$\text{distance}(x,y)=\{\sum_i (x_i - y_i)^2\}^{1/2} \quad (3.101)$$

Note that Euclidian (and squared Euclidian) distances are usually computed from raw data, and not from standardized data. This method has certain advantages (e.g., the distance between any two objects is not affected by the addition of new objects to the analysis, which may be outliers). However, the distances can be greatly affected by differences in scale among the dimensions from which the distances are computed. For example, if one of the dimensions denotes a measured length in centimeters, and one then converts it to millimeters (by multiplying the values by 10), the resulting Euclidian or squared Euclidian distances (computed from multiple dimensions) can be greatly affected, and consequently, the results of cluster analyses may be very different.

3.15.5 Squared Euclidian Distance

One may want to square the standard Euclidian distance in order to place progressively greater weight on objects that are further apart. This distance is computed as (see also the note in the previous paragraph):

$$\text{distance}(x,y)=\sum_i (x_i - y_i)^2 \quad (3.102)$$

3.15.6 City-block (Manhattan) Distance

This distance is simply the average difference across dimensions. In most cases, this distance measure yields results similar to the simple Euclidian distance. However, note that in this measure, the effect of single large differences (outliers) is dampened (since they are not squared). The city-block distance is computed as:

$$\text{distance}(x,y)=\sum_i |x_i - y_i| \quad (3.103)$$

3.15.7 Chebychev Distance

This distance measure may be appropriate in cases when one wants to define two objects as “different” if they are different on any one of the dimensions. The Chebychev distance is computed as:

$$\text{distance}(x,y)=\text{Maximum}|x_i - y_i| \quad (3.104)$$

3.15.8 Power Distance

Sometimes one may want to increase or decrease the progressive weight that is placed on dimensions on which the respective objects are very different. This can be accomplished via the *power distance*. The power distance is computed as:

$$\text{distance}(x,y)=\left(\sum_i |x_i - y_i|^p\right)^{1/r} \quad (3.105)$$

where r and p are user-defined parameters. Parameter p controls the progressive weight that is placed on differences on individual dimensions; parameter r controls the progressive weight that is placed on larger differences between objects. If r and p are equal to 2, then this distance is equal to the Euclidian distance.

3.15.9 Percent Disagreement

This measure is particularly useful if the data for the dimensions included in the analysis are categorical in nature. This distance is computed as:

$$\text{distance}(x,y)=\frac{(\text{Number of } x_i \neq y_i)}{i} \quad (3.106)$$

3.15.10 Amalgamation or Linkage Rules

At the first step, when each object represents its own cluster, the distances between those objects are defined by the chosen distance measure. However, once several objects have been linked together, how does one determine the distances between those new clusters? In other words, one needs a linkage or amalgamation rule to determine when two clusters are sufficiently similar to be linked together. There are various possibilities: for example, one could link two clusters together when *any* two objects in the two clusters are closer together than the respective linkage distance. Put another way, the "nearest neighbors" across clusters were used to determine the distances between clusters; this method is called *single linkage*. This rule produces "stringy" types of clusters, that is, clusters "chained together" by only single objects that happen to be close together.

Alternatively, one may use the neighbors across clusters that are furthest away from each other; this method is called *complete linkage*. There are numerous other linkage rules such as these that have been proposed.

3.15.11 Single Linkage (nearest neighbor)

As described above, in this method the distance between two clusters is determined by the distance of the two closest objects (nearest neighbors) in the different clusters. This rule will, in a sense, *string* objects together to form clusters, and the resulting clusters tend to represent long “chains.”

3.15.12 Complete Linkage (furthest neighbor)

In this method, the distances between clusters are determined by the greatest distance between any two objects in the different clusters (i.e., by the “furthest neighbors”). This method usually performs quite well in cases when the objects actually form naturally distinct “clumps.” If the clusters tend to be somehow elongated or of a “chain” type nature, then this method is inappropriate.

3.15.13 Unweighted pair-group Average

In this method, the distance between two clusters is calculated as the average distance between all pairs of objects in the two different clusters. This method is also very efficient when the objects form natural distinct “clumps,” however, it performs equally well with elongated, “chain” type clusters. Note that in their book, Sneath and Sokal

introduced the abbreviation UPGMA to refer to this method as *unweighted pair-group method using arithmetic averages* [60].

3.15.14 Weighted pair-group Average

This method is identical to the *unweighted pair-group average* method, except that in the computations, the size of the respective clusters (i.e., the number of objects contained in them) is used as a weight. Thus, this method (rather than the previous method) should be used when the cluster sizes are suspected to be greatly uneven. Note that in their book, Sneath and Sokal introduced the abbreviation *WPGMA* to refer to this method as *weighted pair-group method using arithmetic averages* [60].

3.15.15 Unweighted pair-group Centroid

The *centroid* of a cluster is the average point in the multidimensional space defined by the dimensions. In a sense, it is the *center of gravity* for the respective cluster. In this method, the distance between two clusters is determined as the difference between centroids. Sneath and Sokal used the abbreviation *UPGMC* to refer to this method as *unweighted pair-group method using the centroid average* [60].

3.15.16 Weighted pair-group Centroid (median)

This method is identical to the previous one, except that weighting is introduced into the computations to take into consideration differences in cluster sizes (i.e., the number of objects contained in them). Thus, when there are (or one suspects there to be) considerable differences in cluster sizes, this method is preferable to the previous one.

Sneath and Sokal used the abbreviation *WPGMC* to refer to this method as *weighted pair-group method using the centroid average* [60].

3.15.17 Ward's Method

This method is distinct from all other methods because it uses an analysis of variance approach to evaluate the distances between clusters. In short, this method attempts to minimize the Sum of Squares (SS) of any two (hypothetical) clusters that can be formed at each step. Refer to Ward [46] for details concerning this method. In general, this method is regarded as very efficient, however; it tends to create clusters of small size.

3.15.18 Two-way Joining

Previously, this method has been discussed in terms of “objects” that are to be clustered (as in Joining (Tree Clustering)). In all other types of analyses the research question of interest is usually expressed in terms of cases (observations) or variables. It turns out that the clustering of both may yield useful results. For example, imagine a study where a medical researcher has gathered data on different measures of physical fitness (variables) for a sample of heart patients (cases). The researcher may want to cluster cases (patients) to detect clusters of patients with similar syndromes. At the same time, the researcher may want to cluster variables (fitness measures) to detect clusters of measures that appear to tap similar physical abilities.

Given the discussion in the paragraph above concerning whether to cluster cases or variables, one may wonder why not cluster both simultaneously? Two-way joining is useful in (the relatively rare) circumstances when one expects that both cases and

variables will simultaneously contribute to the uncovering of meaningful patterns of clusters.

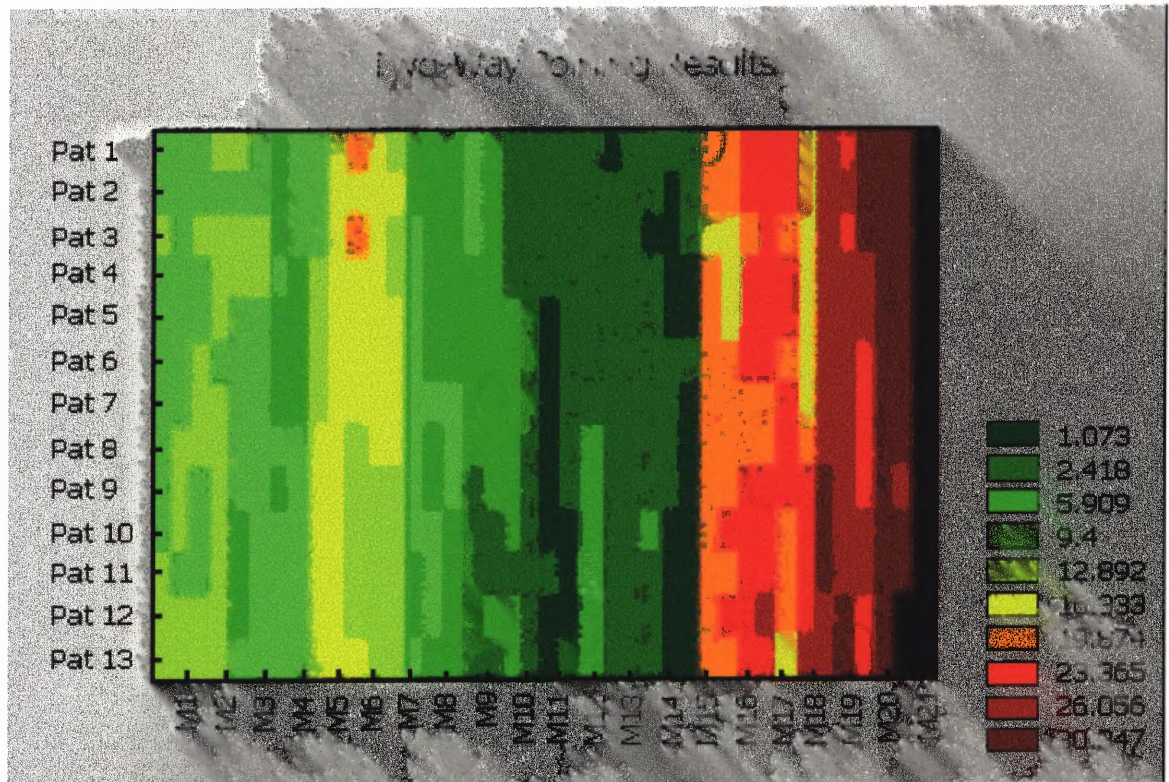


Figure 3.19 Contour graph of a two-way joining clustering. (From Statistic Manual, the SAS Institute, 2001).

For example, returning to the example of Figure 3.19 above, the medical researcher may want to identify clusters of patients that are similar with regard to particular clusters of similar measures of physical fitness. The figure shows the 13 physical fitness patterns on the y axis and the different heart cases in the x axis. The measures of similarity or distance values are indicated by using various color intensities. The difficulty with interpreting these results may arise from the fact that the similarities between different clusters may pertain to (or be caused by) somewhat different subsets of variables. Thus, the resulting structure (clusters) is by nature not homogeneous. This

may seem a bit confusing at first, and, indeed, compared to the other clustering methods described (Joining (Tree Clustering) and K- means Clustering), two-way joining is probably the one least commonly used. However, some researchers believe that this method offers a powerful exploratory data analysis tool (for more information refer to the detailed description of this method in Hartigan [52]).

3.15.19 K-means Clustering

This method of clustering is very different from the Joining (Tree Clustering) and Two-way Joining. Suppose that one already has the hypotheses concerning the number of clusters in one's cases or variables. The computer may be told to form exactly 3 clusters that are to be as distinct as possible. This is the type of research question that can be addressed by the k- means clustering algorithm. In general, the k-means method will produce exactly k different clusters of greatest possible distinction.

In the physical fitness example (in *Two-way Joining*), the medical researcher may have a "hunch" from clinical experience that her heart patients fall basically into three different categories with regard to physical fitness. One might wonder whether this intuition can be quantified, that is, whether a k-means cluster analysis of the physical fitness measures would indeed produce the three clusters of patients as expected. If so, the means on the different measures of physical fitness for each cluster would represent a quantitative way of expressing the researcher's hypothesis or intuition (i.e., patients in cluster 1 are high on measure 1, low on measure 2, etc.).

3.15.20 Computations

Computationally, one may think of this method as analysis of variance (ANOVA) “in reverse.” The program will start with k random clusters, and then move objects between those clusters with the goal to (1) minimize variability within clusters and (2) maximize variability between clusters. This is analogous to “ANOVA in reverse” in the sense that the significance test in ANOVA evaluates the between group variability against the within-group variability when computing the significance test for the hypothesis that the means in the groups are different from each other. In k-means clustering, the program tries to move objects (e.g., cases) in and out of groups (clusters) to get the most significant ANOVA results.

3.15.21 Interpretation of Results

Usually, as the result of a k-means clustering analysis, one would examine the means for each cluster on each dimension to assess how distinct our k clusters are. Ideally, one would obtain very different means for most, if not all dimensions, used in the analysis. The magnitude of the F values from the analysis of variance performed on each dimension is another indication of how well the respective dimension discriminates between clusters.

CHAPTER 4

METHODS

The purpose of this chapter is to thoroughly explain the methods used to acquire the biological signals of interest, namely the electrocardiogram (ECG), the systolic blood pressure, and the respiration signal, as well as to explain the equipment used to acquire these signals. Also included in this chapter is an explanation of the experimental protocol, and the different signal processing analysis techniques, which were developed for system identification.

4.1 Experimental Protocols

4.1.1. Study Procedures

The subject populations of the study include:

- 1) Patients with severe pulmonary disease that were being enrolled into the National Emphysema Treatment Trial (NETT) to study lung volume reduction surgery (LVRS) as well as the elective population undergoing lung volume reduction surgery.
- 2) Normal individuals with no known cardiac or pulmonary disease.

Since the study of COPD subjects is a long-term (up to 5 years) project, the population of COPD patients can be up to several hundred. The data collection for the COPD population can be as large as required. However, data of 47 COPD subjects were analyzed for this dissertation. On the other hand, the population of volunteered normal

subjects is somewhat limited so the data of 8 recruited normal subjects were used for this study.

The testing of all the subjects was done in the Human Performance Laboratory in Atchley room 327 of the Columbia Presbyterian hospital in New York City, NY and included a Pulmonary Stress test on 30% supplemental oxygen as per the NETT Protocol and HRV, BPV, and BRS.

The autonomic testing was performed in the following manner, as described in each of the separate subsections below.

4.1.2 Data Acquisition

All exercise stress testing was performed on a bicycle ergometer with a SensorMedics Vmax 229 series workstation. The protocol was a ramp exercise test with 5-minute baseline data collection, followed by a three-minute warm-up at no load and then a maximum exercise test at 5 Watts per minute ramp. All exercise was done on 30% supplemental oxygen. The autonomic biopotentials were obtained through an interface board (BNC 2080, National instruments Co., Austin TX) and fed into a 12-bit analog-to-digital (A/D) converter (DAQCard-700, National instruments Co., Austin TX) and then into a Pentium computer (Hitachi Vision Book Plus, San Jose, California). Five-minute resting data collections were also done in a counter-balanced order on room air and 30% supplemental oxygen. Post acquisition data analyses were carried out separately. The data were stored on the hard drive of the computer and daily backups were made to Iomega Zip 100 Mbytes cartridges.

4.1.2.1 Autonomic Testing. HR Variability and BP Variability: These tests were carried out for rest, deep breathing, Valsalva maneuver, isometric contraction, and exercise. These were established noninvasive methods for the quantitative assessment of autonomic activity based on the analysis of the variability of the cardiac R-R interval through the assessment of parasympathetic (PNS), sympathetic (SNS), and sympathovagal balance (S/V). Our laboratory used an established and validated routine for the spectral decomposition of heart rate variability. Specifically, interbeat (IBI) intervals were derived from the electrocardiogram (ECG) using a peak detection routine. The sequence of the IBI was interpolated to provide a continuous data stream, and the resulting IBI data were detrended using a robust locally weighted regression procedure. The resulting data were split in sections, and each section is tapered using a split cosine window. Finally, the data were transformed into frequency spectra using fast Fourier transform algorithms and smoothed across blocks of frequencies to produce a spectrum.

The power of the heart rate variability is calculated by measuring the area under the spectra in the established frequency bands. Power spectra within the 0.04 to 0.15 Hz range were defined as low frequency components, whereas those at the frequency of 0.15 to 0.40 Hz were defined as the high frequency components. The ratio between low frequency (LF) and high frequency (HF) components is considered representative of the sympathovagal balance.

4.1.2.2 Parasympathetic Activity and Sympathovagal Balance Assessment.

1) Rest: Subjects were seated, at rest, and post absorptive for at least four hours, and refrained from consuming alcohol and caffeinated beverages for at least 12 hours prior to the test. ECG recordings were made using lead II and lead V, with an electrocardiographic machine (Marquette Max-1, Marquette Medical Systems, Milwaukee, WI). The subject's beat-by-beat blood pressure recordings were made using a wrist cuff via a noninvasive oscillometric device (Model 7000, Colin Medical Instruments Corp., San Antonio, TX). Blood pressure recordings were made with the left arm supported at heart level. In addition, respiration was recorded from respiratory induced temperature changes using a thermistor (YSI reusable temperature probe, Yellow Springs, OH) placed under the right nostril. During rest subjects were instructed to maintain normal breathing patterns. Two data gathering episodes were made while seated in an upright position, each five minutes in duration (one on room air, another on 30% oxygen). Total test duration was approximately 25 minutes (2 trials with equilibration on oxygen in between).

2) Deep Breathing: Subjects breathed at 0.2 Hz (12 breaths/minute), as this breathing rate has been shown to stimulate the respiratory sinus arrhythmia, a noninvasive marker of parasympathetic activity. Subjects were trained until satisfactory tracings were obtained. This protocol consisted of 2 trials, each of one minute in duration. Total test duration was approximately 5 minutes (2 trials with rest in between).

3) Valsalva Maneuver: Subjects breathed at a normal rate for 15 seconds, then were asked to blow against a fixed resistance to a pressure of 20 mm Hg for 15 seconds, and then were asked to breathe normally for a 30 second interval. Continuous measurement

of heart rate, blood pressure, respiratory rate, and oxygen saturation were done over the one-minute trial. Subjects were trained until satisfactory tracings were obtained. This protocol consisted of 2 trials, each of one minute in duration. Total test duration was approximately 5 minutes (2 trials with rest in between). This was done twice, once on room air, and once on 30% supplemental oxygen, for a total duration of 10 minutes for the two trials.

4.1.2.3 Baroreceptor Sensitivity Assessment. The spontaneous beat-by-beat interactions of systolic blood pressure (SBP) and R-R interval reflect true baroreflex events rather than random interactions. In the cases of the more severe COPD subjects who could not perform the Valsalva maneuver, the following baroreceptor sensitivity assessment method was used instead. With the subjects in a seated position, and after a 20-minute equilibrium time in a quiet room, R-R interval and SBP data were recorded for a total of 1024 beats. The subjects were to breathe naturally, at a frequency at or above 12 breaths/minute (0.2 Hz). The R-R intervals were measured by the standard electrocardiograph. The spontaneous baroreflex response was determined from the beat-to-beat changes in the R-R interval and SBP by a modification of the technique of Bertinieri, et al. [61]. Linear regression was performed on any episodes of three consecutive beats with R-R interval lags in the same direction (either up or down), and the resultant data yielded an evaluation of the baroreflex sensitivity.

4.1.2.4 Interventions. All the patients underwent a full course of pulmonary rehabilitation prior to randomization (NET) or surgery (Non-NETT). This rehabilitation was done under the same protocol, and was as follows.

Six-week program of intensive outpatient rehabilitation

- Program 3-5 times a week at hospital program
- Supervised portion of exercise to be done with the following:

Two-hour sessions

- Cross training
- 30 min. continuous treadmill exercise at modified Borg level 7.5
- 15 min. on arm ergometer at modified Borg level 7.5
- 15 min. on stair stepper/bicycle ergometer at modified Borg level 7.5 or with Karvonen's target heart rate intensity factor 0.6
- Pulse oximetry (Supplemental O₂ as needed to maintain SpO₂ > 90 %)
- Telemetry
- Blood pressure monitoring
- Patient education sessions with 6 basic topics
 - Basic breathing techniques
 - Anatomy/Physiology
 - Medications
 - Stress and relaxation
 - Nutrition
 - Armchair aerobics
- Patient specific training in breathing and relaxation techniques

The patients who underwent LVRS were given their surgery within a month after the completion of the initial rehabilitation program. The surgery was to be done as per the surgeon and/or the NETT protocol. This testing and analysis had no bearing on the surgical plans for the patients. After surgery, the patients were given treatment and physical rehabilitation as needed to insure that they could be remobilized. Both the surgical and medical patients then received a second six-week course of rehabilitation. The subjects were then followed at 3-month intervals for a year and then for 4 years at 6-month intervals, out to 60 months (5 years). It should be noted that the whole time the patient participated in the study, qualified personnel with appropriate emergency equipment and emergency facilities were readily available to treat any problems that may occur.

4.2 Data Analysis

All signal processing techniques were performed with the LabVIEW graphical programming language and MATLAB. This section describes the use of both LabVIEW and MATLAB and the algorithms by which the different physiological signals were analyzed. All the programs for spectral analysis, the Wigner time-frequency analysis program (Sympar.vi), coherence, weighted coherence and partial coherence were written in LabVIEW. The time-frequency analysis (Cohen's class and wavelets), system identification techniques, principal component analysis and cluster analysis were performed using the MATLAB System Identification and Statistics toolboxes.

4.2.1 Wigner Time-Frequency Analysis

As mentioned previously, the Wigner time-frequency analysis program (Sympar.vi) was written in LabVIEW. The time-frequency analysis was performed using raw ECG data. The ECG signal was read from a spreadsheet file acquired together with other signals such as respiration, blood pressure and Oxygen volume consumption. All of these signals were represented in spreadsheet form as columns of space delimited data. The ECG data was filtered through a high-pass filter (HP_FILT.vi) after which point the R wave locations were detected automatically (Search BP.vi). The array of R wave locations was then used to calculate the heart rate and to generate graphs of both the ECG signal with detected R waves and of the heart rate, respectively. The raw ECG signal was then displayed with markers at each corresponding detected R wave along with the newly calculated corresponding heart rate. These graphs appear on the control

panel of the Correct.vi. It was in the Correct.vi block that a cursor was provided allowing the user to manually detect missing peaks or undetect "bad" peaks by turning the "Modify" marker on or off. Missing peaks were results of saturation, motion, or noise artifact during acquisition of the ECG signal. Consequently, peaks must be manually interpolated in place of the missing data. "Bad" peaks consist of peaks that were not characteristically R waves, such as those generated by noise artifact. Manual detection of R waves continued until the user clicks the "Done" button on the control panel of the Correct.vi, indicating to the program that all detection of R waves was complete. The output of the Correct.vi consists of the IBI as calculated from consecutive R waves detected in the ECG, which was then saved to a spreadsheet file to be utilized for further analysis. The IBI was interpolated and decimated (Interpolation & Decimation.vi) to generate a decimated IIBI waveform which was analyzed utilizing the Wigner distribution (Symbar (Wigner).vi). After execution of the final subVI in this program, two-dimensional time-frequency graphs of both parasympathetic (HF) activity and of the combined parasympathetic and sympathetic (LF) activity were generated on the control panel of Symbar (Wigner).vi. The control panel also displayed graphs of the decimated IIBI waveform, as well as the LF/HF ratio with respect to time.

4.2.2 Power Spectrum Analysis of Heart Rate Variability

The power spectrum analysis program, also written in LabVIEW, consists of several subVIs that ultimately generate graphs of the LF area and HF area of the corresponding ECG signal. As with the Wigner program, the signal was read from a spreadsheet file as a single column of space delimited data (Read From Spreadsheet File.vi). However, in

this case the data consisted of the previously recorded IBI of the heart rate obtained from the Correct.vi block in the Wigner time-frequency analysis program rather than the raw ECG signal. The use of the IBI array was justified because the subVIs utilized by the Wigner program to obtain this array was duplicated in the power spectrum analysis program. Furthermore, the sequence of data flow through these subVIs was identical in both programs. Therefore, it would follow that the IBI generated by the Wigner time-frequency analysis program was equivalent to that generated by the power spectrum analysis program. Essentially, the use of the previously generated IBI provides several benefits, such as saving time in the analysis process, and more importantly, it provides consistency in the data being analyzed. This factor was significant when considering the possibility of variation resulting during the manual interpolation of missing data in the ECG signal.

The IBI data flowed through the Spectrum1.vi block where it was interpolated. Here, the IBI underwent a series of analyses and mathematical calculations through subVIs that were provided by LabVIEW programming language. First, the IBI was input into the Mean.vi block, where the mean average was computed, and then the resulting output was zero padded (Zero Padder.vi). After this point, the power spectrum was computed and divided to display the graph of the heart rate power spectrum as well as the values of the LF area, the HF area, and the length of the data file in minutes. The graph and calculated data were displayed on the control panel. Because of its interactive nature, the program allowed for adjustment of sampling frequency as well as the upper and lower bounds for the VLF, LF, and HF ranges.

4.2.3 Power Spectrum Analysis of Blood Pressure Variability

The power spectrum of the blood pressure (BP) signal was also obtained from a VI written in LabVIEW. Again, the physiological signals were read from the same spreadsheet data file (Read From Spreadsheet File.vi). Each of the raw ECG and blood pressure signals was independently analyzed and displayed on the control panel.

Similar to the raw ECG signal, the raw blood pressure signal passed through a high-pass filter (HP_FILT.vi) and successively into a peak detection block (Search BP.vi). The filtered BP array was then analyzed for the detection of each systolic peak. Unlike the peak detection block for the ECG signal, the location of each consecutive peak of the blood pressure signal was not directly detected, but rather it was the peak amplitude of the systolic blood pressure waveform, which was of importance. It was the detection of the amplitude of each peak that indicates the peak location. Detection of the BP peak location was dependent upon the maximum amplitude of the peak, i.e. the y-axis. The first maximum value of amplitude that occurred in the peak was detected. This value was interpolated over the interval until the next successive peak amplitude was detected. The BP IBI was then interpolated to generate the IIBI. Each peak amplitude value was interpolated over the period of time between each successive peak amplitude detection. For example, if the first peak in succession has an amplitude of 1.135, the next detected peak has an amplitude of 0.850, and there was a period of 200 points between the two detected peaks, then the value of the first detected peak, or 1.135, was interpolated over the 200 points so that each point possesses this amplitude until the next detection at 0.850. The resulting array then underwent a series of analyses and mathematical calculations, similar to the heart rate IIBI, to graphically display the

BP power spectrum. This graph in addition to graphs of the heart rate power spectrum, the raw BP signal, and the BP IBI were displayed on the control panel. In addition to the graphical displays, the calculated values of the LF area, the HF area, and the length of the data file in minutes could be found on the control panel. Because of its interactive nature, the program allowed for adjustment of sampling frequency as well as the upper and lower bounds for the VLF, LF, and HF ranges.

4.2.4 Coherence and Weighted Coherence Analysis of Heart Rate and Respiration

The coherence and weighted coherence analysis between heart rate and respiration were performed using the `coherenc.vi` of LabVIEW. Again, the physiological signals were read from a spreadsheet file (`Read From Spreadsheet File.vi`) as consecutive, space delimited data columns, where one column consisted of the raw ECG signal and the other column consisted of the raw respiration signal. Each signal was independently analyzed and displayed on the control panel. The raw ECG signal was again passed through a high-pass filter (`HP_FILT.vi`) and successively into peak detection (`Search (BP).vi`) and correction (`Correct.vi`) blocks. The user then manually detected and corrected the bad or missing R peaks as before to generate the IIBI array. This IIBI array just obtained from the detection and correction of the raw ECG was then input together with the filtered raw respiration signal into the `coherenc.vi` where the power spectra and cross-power spectrum of the ECG IIBI and the raw respiration signal were calculated. From these power spectra a coherence plot between the derived heart rate and respiration was generated and the weighted coherence value was calculated. Two movable cursors on the coherence plot allow the user to selectively choose and obtain a

weighted-average value of the coherence between the range of frequencies f_1 and f_2 . This value was calculated according to equation 3.85 discussed in section 3.10 before and would be used as a parameter in the system identification analysis.

4.2.5 Coherence and Weighted Coherence Analysis of HR and Blood pressure

This analysis is similar to the coherence analysis of heart rate and respiration just described above with the exception that the blood pressure IBI (detected and corrected the same way as the blood pressure spectral analysis) was used instead of the raw respiration signal. The heart rate IIBIs and the blood pressure IIBIs were input into the `coherenc.vi` to create the coherence plot and the weighted coherence value in the same fashion as the coherence and weighted coherence analysis of heart rate and respiration.

4.2.6 Partial Coherence

This analysis was similar to the coherence analysis. The heart rate IIBIs, the blood pressure IIBIs and the respiration signal were inputted into the `pcoherenc.vi` to create the partial coherence plots and the weighted coherence values in the same fashion as the coherence and weighted coherence analysis but using the equations 3.86 - 3.91 described in section 3.11 and 3.12.

4.2.7 Time-frequency Analysis

The original time-frequency analysis program for STFT, SPWD, CWD and BJCD was written by Adib [45] in 1995 and was intended to analyze electromyogram (EMG) data in the frequency range from 20 Hz to 500 Hz. In order to use the same program to analyze HRV data in the frequency range of 0.05 – 0.4 Hz, modifications to the 3D mesh and contour graphic routine were made for this program to display the plots with enough frequency resolution even in the low frequency range between 0.05 – 0.4 Hz.

The wavelet analysis programs used were taken from the MATLAB wavelet toolbox (The Math Works Inc., Natick, MA, 2000) also with the appropriate modification to fit the low frequency range required for HRV, systolic BP and RESP signals of the study in this dissertation. The main MATLAB m-file used was the cwt.m file. This program computed and plotted the wavelet coefficients for the physiological signals with positive scales, using the wavelets: morl (Morlet), meyr (Meyer), dB4 (Daubechies 4), mexh (Mexican Hat) and haar (Haar). The program also ran other wavelets whose names appeared as shown in Table 4.1.

Basically, the process used in the cwt.m file was as follows:

Let $s(t)$ be the analyzed signal and Ψ the wavelet. The wavelet coefficient of s at scale a and position b is defined by:

$$C_{a,b} = \int_R s(t) \frac{1}{\sqrt{a}} \overline{\Psi\left(\frac{t-b}{a}\right)} dt \quad (4.1)$$

Since $s(t)$ is a discrete signal, one can use a piecewise constant interpolation of the $s(k)$ values, $k=1$ to $\text{length}(s)$ where s is the total number of data points of the analyzed signal rounded up to the nearest power of two.

For each given scale a within the vector scales, the wavelet coefficient $C_{a,b}$ were computed for $b=1$ to $ls=length(s)$, and were stored in $COEFS(i,:)$ if $a=scales(i)$. Output argument $COEFS$ is a la -by- ls matrix where la is the length of scales. $COEFS$ is a real or complex matrix depending on the wavelet type. The steps of calculating the $COEFS$ were:

$$C_{a,b} = \int_R s(t) \frac{1}{\sqrt{a}} \overline{\Psi\left(\frac{t-b}{a}\right)} dt \quad (4.2)$$

Since $s(t)=s(k)$, if $t \in]k,k+1]$ then

$$C_{a,b} = \sum_k \int_k^{k+1} s(t) \frac{1}{\sqrt{a}} \overline{\Psi\left(\frac{t-b}{a}\right)} dt \quad (4.3)$$

$$C_{a,b} = \frac{1}{\sqrt{a}} \sum_k s(k) \int_k^{k+1} \overline{\Psi\left(\frac{t-b}{a}\right)} dt \quad (4.4)$$

$$C_{a,b} = \frac{1}{\sqrt{a}} \sum_k s(k) \left[\int_{-\infty}^{k+1} \overline{\Psi\left(\frac{t-b}{a}\right)} dt - \int_{-\infty}^k \overline{\Psi\left(\frac{t-b}{a}\right)} dt \right] \quad (4.5)$$

For any scale a , the wavelet coefficients $C_{a,b}$ for $b=1$ to $length(s)$ could be obtained by convolving the signal s and a dilated and translated version of the integrals of the form $\int_k^{k+1} \overline{\Psi(t)} dt$ (given by `intwave.m`), and taking the finite difference using `diff.m`.

One of the objectives in studying the HRV in this dissertation was to compare the time frequency representations of the Short time Fourier transform, Smoothed Pseudo Wigner-Ville, Choi-William and Born-Jordan-Cohen distributions to the wavelet

distribution. However, the wavelet distribution gave plots in time and scale instead of a time-frequency axis. In order to make good comparison, the scale axis of the wavelet distribution had to be converted to a frequency axis. But how frequency and scale are related?

The scale of the wavelet distribution refers to the width of the wavelet. As the scale increases and the wavelet gets wider, it includes more of the time series, and the finer details get smeared out. The scale can be defined as the distance between oscillations in the wavelet (e.g. for the Morlet), or it can be some average width of the entire wavelet (e.g. for the Haar or Mexican hat).

The period (or inverse frequency) is the approximate Fourier period that corresponds to the oscillations within the wavelet. For all wavelets, there is a one-to-one relationship between the scale and period. The relationship can be derived by finding the wavelet transform of a pure cosine wave with a known Fourier period, and then computing the scale at which the wavelet power spectrum reaches its maximum.

For some wavelets, the period has more meaning than others. For the Morlet wavelet, which has several smooth oscillations, the period is a well-defined quantity, which measures the approximate Fourier period of the signal. For the Daubechies, which has irregularly-spaced oscillations, the period has less meaning and should probably be ignored.

In the MATLAB wavelet toolbox, the relationship between scale and frequency is referred to in terms of the pseudo-frequency corresponding to a scale. The idea is to associate with a given wavelet a purely periodic signal of frequency F_c . The frequency maximizing the FFT of the wavelet modulus is F_c . If one agrees to associate the

frequency F_c to the wavelet function, then the wavelet is dilated by a factor a , and this center frequency becomes F_c / a . Lastly, if the underlying sampling period is Δ , it is natural to associate to the scale a the frequency:

$$F_a = \frac{\Delta * F_c}{a} \quad (4.6)$$

The `cwt.m` file of the MATLAB wavelet toolbox has been modified to provide time-frequency plots instead of time-scale plots so that the comparison of the wavelet distribution and the time-frequency distributions can be easily performed as seen in the next chapter.

Table 4.1 Wavelet Names Available for Analysis (94+)(From Wavelet Toolbox User's Guide, Version 2, The MathWorks, Inc., 9/2000)

Group	Wavelet Names
Haar (1)	haar
Daubechies db (11+)	db1 db2 db3 db4 db5 db6 db7 db8 db9 db10 db**
Symlets sym (8+)	sym2 sym3 sym4 sym5 sym6 sym7 sym8 sym**
Coiflets coif (5)	coif1 coif2 coif3 coif4 coif5
BiorSplines bior (15)	bior1.1 bior1.3 bior1.5 bior2.2 bior2.4 bior2.6 bior2.8 bior3.1 bior3.3 bior3.5 bior3.7 bior3.9 bior4.4 bior5.5 bior6.8
ReverseBior rbio (15)	rbio1.1 rbio1.3 rbio1.5 rbio2.2 rbio2.4 rbio2.6 rbio2.8 rbio3.1 rbio3.3 rbio3.5 rbio3.7 rbio3.9 rbio4.4 rbio5.5 rbio6.8
Meyer (1)	meyr
DMeyer (1)	dmey
Gaussian gaus (9+)	gaus1 gaus2 gaus3 gaus4 gaus5 gaus6 gaus7 gaus8 gaus**
Mexican_hat (1)	mexh
Morlet (1)	morl
Complex Gaussian cgau (6+)	cgau1 cgau2 cgau3 cgau4 cgau5 cgau**
Shannon shan (6+)	shan1-1.5 shan1-1 shan1-0.5 shan1-0.1 shan2-3 shan**
Frequency B-Spline fbsp (7+)	fbsp1-1-1.5 fbsp1-1-1 fbsp1-1-0.5 fbsp2-1-1 fbsp2-1- 0.5 fbsp2-1-0.1 fbsp**
Complex Morlet cmor (7+)	cmor1-1.5 cmor1-1 cmor1-0.5 cmor1-1 cmor1-0.5 cmor1-0.1 cmor**

4.2.8 System Identification Analysis

All the system identification tasks were performed using the commercially available MATLAB System Identification Toolbox (The MathWorks, Inc.). The physiological data acquired from COPD and normal subjects were used for building simplified models of complex systems from respiration signals as noisy time-series data. The mathematical ARX models of dynamic cardiovascular systems based on observed input/output data were obtained. The time and frequency response plots as well as the pole-zero plots were also acquired. The control parameters of the estimated models such as ARX coefficients, the model order, and the transfer function parameters such as the overall gain, DC gain, 3 dB points and phase responses were tabulated for each subject.

4.2.9 Analysis of generation of Broadband respiration signal

Part of the method of investigation for noninvasively characterizing the ANS in humans was to determine the system response at all frequencies of interest simultaneously through the use of broadband input waveforms. Berger, Saul, et al. [44] described a simple method for eliciting a broadband respiration signal without significantly altering the normal ventilatory mechanics. In their study the broadband respiratory signal was obtained by instructing the subject to start inhale/exhale as cued by a sequence of beeps (100 ms long), which is generated by a PDP-11/23 computer. The computer programs then beep evenly at a preset rate λ_0 for a few minutes so that the subject can find a comfortable depth of inspiration. The computer then switches to a mode in which the beeps were spaced at irregular intervals chosen randomly from a given distribution but

having the same mean occurrence rate λ_0 for the period of data collection (typically 6 minutes). The algorithm that the computer used to set the timing of the beeps was as follows [44]. A Gaussian white-noise (GWN) signal was obtained by constructing a sequence of Gaussian-distributed random numbers. To confine the GWN signal energy to the spectral band of interest, the signal was digitally processed with a low-pass filter in which the corner frequency was typically set to 0.7 Hz. The resulting band-limited GWN signal $f(t)$ represented the desired instantaneous pulse frequency and its reciprocal $1/f(t)$ the instantaneous inter-pulse interval. An internal clock kept track of the time T that elapsed since the last pulse produced. Whenever T exceeded $1/f(t)$, a new pulse was produced and T was reset to zero. Stylized representations of the band-limited GWN signal, its theoretical power spectrum and probability distribution, and the corresponding GWN frequency-modulated (GWNFM) pulse train are shown in Fig. 4.1. Importantly, the mean f_{mean} and variance σ_f of the (GWN) modulator signal were specified for each 6-min experimental run.

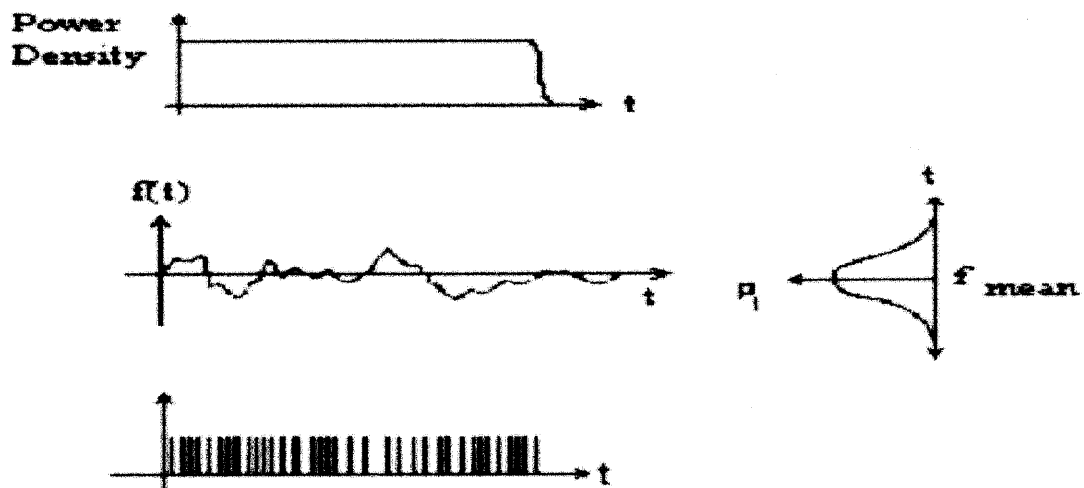


Figure 4.1 Theoretical power spectrum, time series, and probability distribution of band-limited Gaussian white noise and corresponding frequency-modulated pulse train.

In this study a simpler approach was chosen. A box with 16 light-emitting diodes (LED) was built to perform the similar task as described above. LEDs light source is used since a beeping sound was experienced as an annoyance and could alter the subject's autonomic activities. The subject was instructed to start the inhale/exhale cycle as the lighted LED moved from top to bottom and then reversed direction from bottom to top. Subjects had found that paced-breathing by following the LED movement also provided a more comfortable and therapeutic experience.

Two different boxes were constructed for this portion of the study. The first box was built such that the LEDs move at the preset rate λ_0 (selected by the user) for a few minutes so that the subject could find a comfortable depth of inspiration. The user then switched to a random mode in which the LEDs were spaced at irregular intervals chosen randomly from a uniformly distributed function but having a mean occurrence rate $\lambda_A = 14.5 \text{ bpm}$ (breaths per minute) for a short period. This would give a flat power spectrum over the frequencies of interest. The random interval was repeated over and over for the entire duration of data collection. The rate of 14.5 bpm was chosen because it is a good approximate mean breathing rate for all COPD subjects. This first box was built this way because of its ease of implementation.

Later, a second box was also built such that the LEDs move at the preset rate λ_0 for a few minutes at the subject's comfortable rate of inspiration similar to the first box. The user then switched to a random mode in which the LEDs were spaced at irregular intervals chosen randomly from a uniformly distributed function the same as in the first box. However, the random sequence was generated in such a way that it had the mean occurrence rate λ_0 for which the subject was comfortable. This irregular interval was

again repeated over and over for the entire duration of data collection. Hence each COPD subject breathed at the random rate at which the subject was comfortable and still gave a flat power spectrum over the frequencies of interest.

These boxes were used for convenience and simplicity without changing the objective of broadband respiration signal generation.

4.2.10 Principal Component Analysis

The central idea of Principal component analysis (PCA) is to reduce the dimensionality of the data set while retaining as much as possible the variation in the data set. Principal components (PC's) are linear transformations of the original set of variables. PC's are uncorrelated and ordered so that the first few PC's contain most of the variations in the original data set [63]. The first PC has the geometric interpretation that it is a new set of the coordinate axes that maximizes the variation of the projections of the data points onto the new coordinate axes.

In this dissertation a data set obtained from real data and analysis results (coherence, partial coherence) that contained 15 parameters is shown in Table 4.2. The first three parameters were the actual rate values taken from acquired data of normal and COPD subjects (i.e. heart rate in beats per minute, respiration in breaths per minute and blood pressure in beats per minute). The other parameters were obtained from LF and HF weighted values of the coherence/partial coherence cross-spectral analyses.

Table 4.2 Parameters That Make Up the Data Set Used for PCA and Cluster Analysis

Parameter	Name
Respiration	RSP
Heart Rate	HR
Blood Pressure	BP
LF Coherence HR-RESP	LF_coh_HR_rsp
LF Coherence HR-BP	LF_coh_HR_BP
LF Coherence BP-RESP	LF_coh_BP_rsp
HF Coherence HR-RESP	HF_coh_HR_rsp
HF Coherence HR-BP	HF_coh_HR_BP
HF Coherence BP-RESP	HF_coh_BP_rsp
LF Partial Coherence HR-RESP	LF_pcoh_HR_rsp
LF Partial Coherence HR-BP	LF_pcoh_HR_BP
LF Partial Coherence BP-RESP	LF_pcoh_BP_rsp
HF Partial Coherence HR-RESP	HF_pcoh_HR_rsp
HF Partial Coherence HR-BP	HF_pcoh_HR_BP
HF Partial Coherence BP-RESP	HF_pcoh_BP_rsp

The data set was entered into the Matlab PCA program. The results are three principal components with associated eigenvalues of the covariances calculated from the data set. The range of the eigenvalues was normalized to -1 , $+1$ and the parameter with the highest positive eigenvalues was the principal component of the data set. In the example shown in table 4.3, the three PC's of a fictitious data set were:

1. PC1 = **BP** with eigenvalue 0.3800
2. PC2 = **HF_coh_BP_rsp** with eigenvalue 0.4961
3. PC3 = **RSP** with eigenvalue 0.3099

Table 4.3 Principal Components from Normal and COPD Data Set

P1	P2	P3	Categories
0.0351	-0.3625	0.3099	RSP
0.2960	-0.1943	0.0928	HR
0.3800	0.0271	-0.0793	BP
0.2729	-0.2367	0.1637	LF_coh_HR_rsp
0.2725	-0.0886	-0.3849	LF_coh_HR_BP
0.3349	0.2178	-0.0244	LF_coh_BP_rsp
0.3416	0.0691	-0.0556	HF_coh_HR_rsp
0.1389	0.1252	-0.5128	HF_coh_HR_BP
0.1924	0.4961	0.0194	HF_coh_BP_rsp
0.3386	-0.2607	0.0482	LF_pcoh_HR_rsp
0.0449	0.0540	-0.0351	LF_pcoh_HR_BP
0.3341	0.1433	0.0701	LF_pcoh_BP_rsp
0.2954	-0.2978	0.2039	HF_pcoh_HR_rsp
-0.0170	-0.2281	-0.5558	HF_pcoh_HR_BP
0.1308	0.4691	0.2969	HF_pcoh_BP_rsp

4.2.11 Cluster Analysis

The same data used for PCA in the previous section were also used for cluster analysis in separating the normal and COPD subjects and severity classification. The data set was entered into the Matlab clustering program. The program executed according to the following syntax:

```
T = clusterdata(X,cutoff)
```

where:

X was a matrix of size m by n , interpreted as m observations of n variables.

$cutoff$ was a threshold value that determines how the cluster function creates clusters.

The value of $cutoff$ determined how `clusterdata` interpreted it.

If $0 < cutoff < 1$, $cutoff$ was interpreted as the threshold for the inconsistency coefficient. The inconsistency coefficient quantified the degree of difference between objects in the hierarchical cluster tree. If the inconsistency coefficient of a link was greater than the threshold, the cluster function would use the link as a boundary for a cluster grouping.

If $cutoff \geq 1$ $cutoff$ was interpreted as the maximum number of clusters to retain in the hierarchical tree.

The output, T , was a vector of size m that identifies, by number, the cluster in which each object was grouped. The program used the `clusterdata` function to compute the distances between items in the dataset and create a hierarchical cluster tree from the dataset. Finally, the `clusterdata` function grouped the items in the dataset into the number of cluster specified by the value “ $cutoff$ ”.

CHAPTER 5

RESULTS

5.1 Spectral Analysis: A Method for Describing Periodic Processes

Spectral analysis is the natural tool for answering questions regarding periodic or rhythmic processes. Respiration, heart rate variability and blood pressure variability signals are inherently rhythmic. For example, the physiological construct of a central respiratory drive is periodic and is often described in terms of specific frequencies. Spectral analysis is merely a method of quantifying the periodicity and partitioning the total variance of the series into components associated with specific rhythms.

Although respiratory frequencies may be identified by observing a time domain record, the frequency components of heart rate and blood pressure activities are more difficult to identify. The heart is driven and controlled by various neural, mechanical, and biochemical factors. Hypothetically, each factor may be associated with a specific periodicity.

Compare the sinusoidal characteristics of the temporal changes in the respiration signal plotted in Figures 5.1 (a) and 5.2 (a) with the time interval plot between heart rate IIBI signal in Figure 5.1 (b) and blood pressure IIBI signal in Figure 5.2 (b) of a COPD subject sitting at rest, breathing at 16 bpm (0.267 Hz) for 5-minutes. These figures are time domain representations of the respiration, heart rate and blood pressure physiological processes. Time domain representations are often the sum of the component sinusoids. As a general rule, with the exception of processes that are manifested by relatively pure sinusoids (e.g., respiration), it is difficult or impossible to identify rhythms by viewing the time series in the time domain of the heart rate and blood pressure variability signals. By

viewing the time series of sequential heart periods and blood pressure in the frequency domain, spectral analysis decomposes the summed sinusoids into constituent frequencies.

The frequencies of interest in the study of RSA are the frequencies associated with the normal spontaneous respiratory activity. If the breathing were constant at a rate of 16 times a min, each breath would take appropriately 3.745 sec and would have a frequency of 0.267 cycles/sec (0.267 Hz). In Figures 5.1 (c) and 5.2 (c), the power density spectra for each frequency of heart rate and blood pressure are plotted. These analyses were conducted on the data plotted in Figures 5.1 and 5.2 (b). Note that both series exhibit a peak power density estimate at the same frequency, representing the dominant or most characteristic respiratory frequency of 0.267 Hz.

Even though the spectral decomposition of both heart rate and blood pressure processes results in similar dominant frequencies, each process exhibits other prominent frequencies, independent of respiration, that have been theoretically associated with other physiological processes such as temperature and hormonal fluctuations [19].

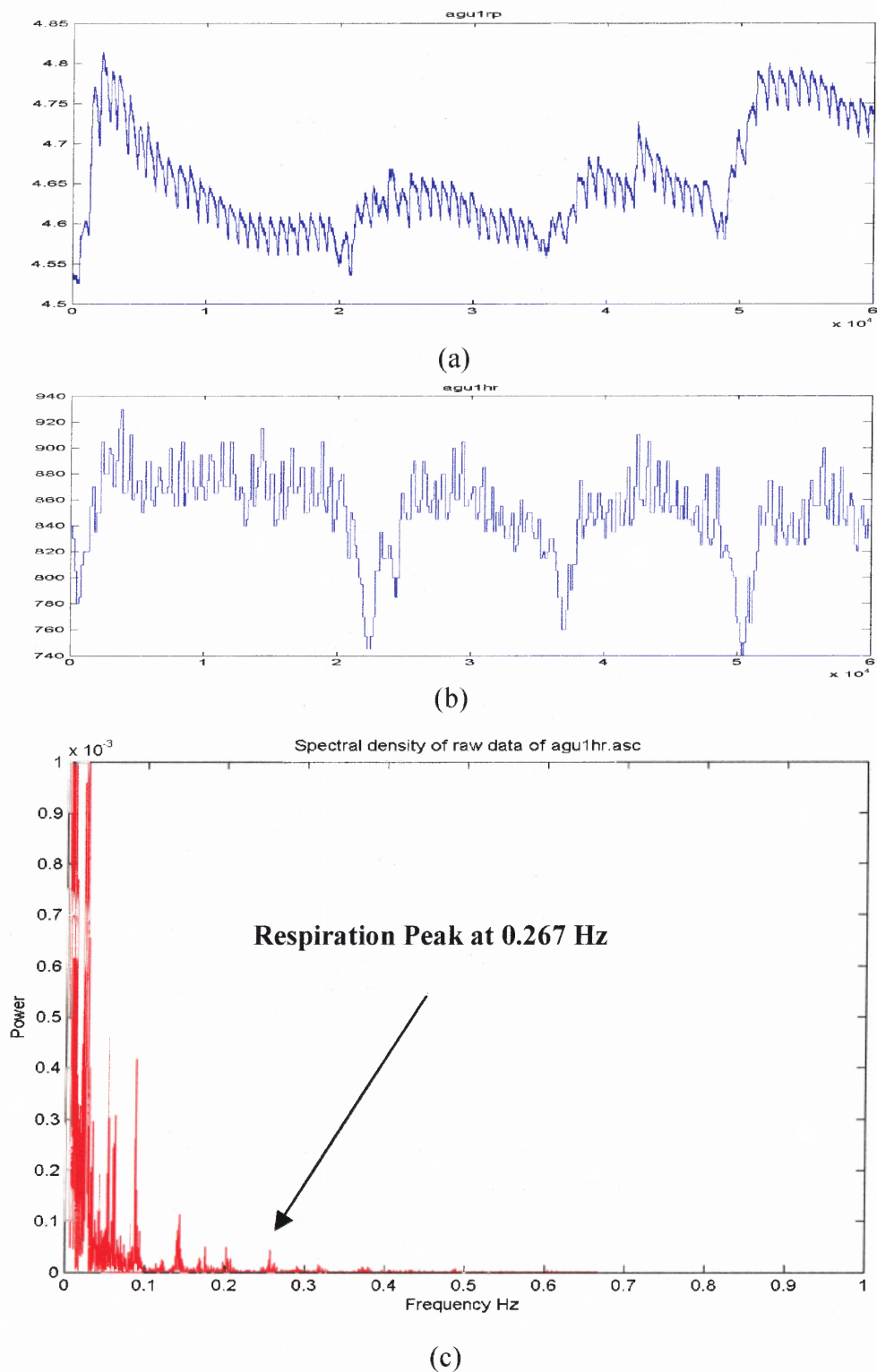


Figure 5.1 HRV analysis of a COPD subject.

(a) Raw respiration signal, 5-minute rest at 16 bpm (0.267 Hz)

(b) Heart rate IIBI signal.

(c) Frequency spectrum of HR IIBI signal.

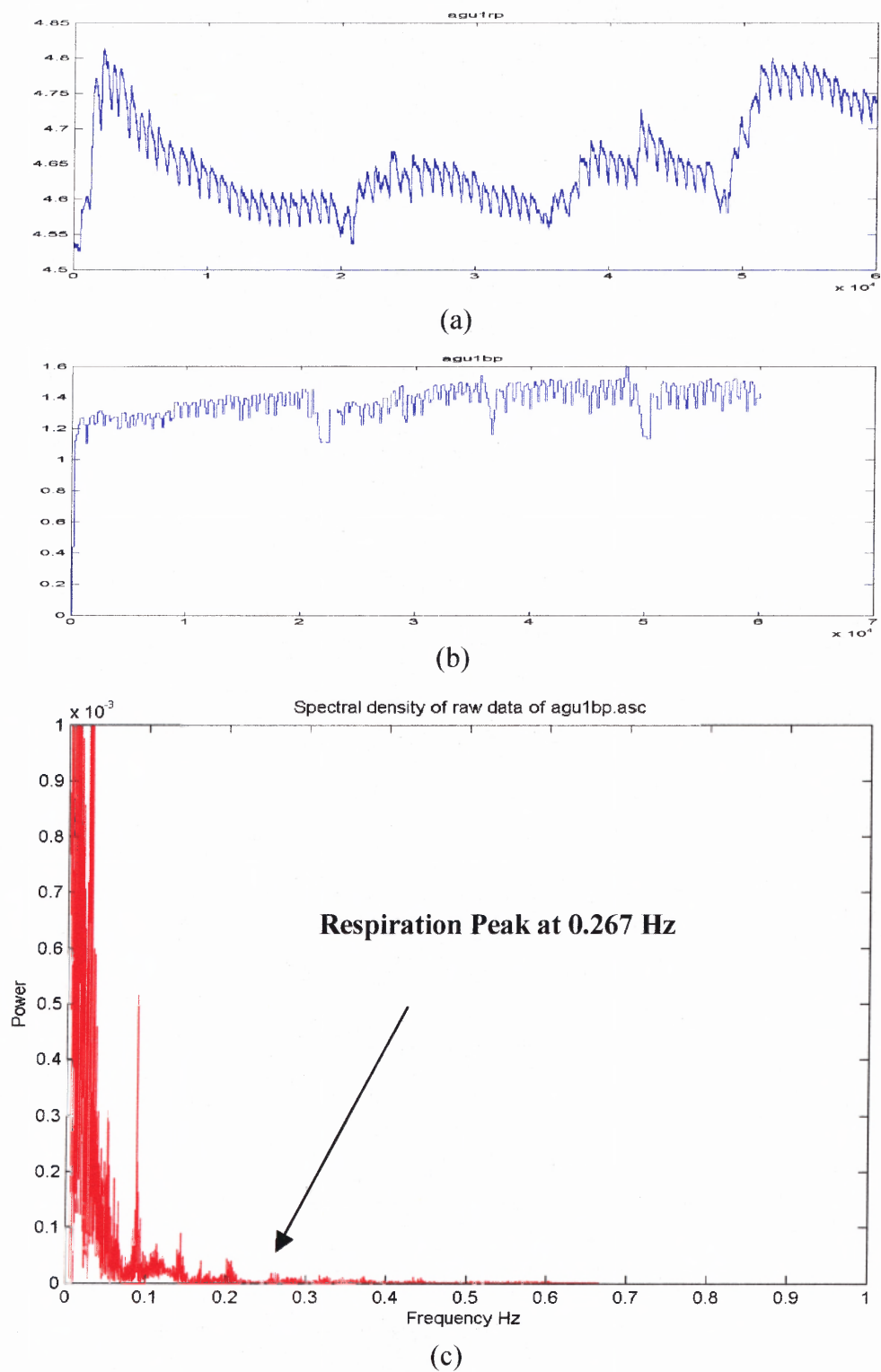


Figure 5.2 BPV analysis of a COPD subject.

(a) Raw respiration signal, 5-minute rest at 16 bpm (0.267 Hz)

(b) Blood pressure IIBI signal.

(c) Frequency spectrum of BP IIBI signal.

Similar spectral analysis is also performed on the heart rate and blood pressure variability signals of a “normal” subject at rest and breathing at 10 bpm (0.167 Hz). The HRV and BPV spectral analysis plots are shown in Figures 5.3 and 5.4. The same strongly influenced respiration frequency peaks of 0.167 Hz can be seen from both the heart rate and blood pressure power spectral density plots of Figures 5.3 and 5.4 (c). As with the COPD subject shown in Figures 5.1 and 5.2, even though the spectral decomposition of both heart rate and blood pressure processes results includes the respiration frequency peaks, each process also exhibits other prominent frequencies, theoretically associated with other physiological processes.

The spectral analysis approach, however, has disadvantages. To illustrate this point, the heart rate power spectral density plots and the blood pressure power spectral plots of both the COPD and normal are plotted side by side for comparison, as shown in Figures 5.4.1 and 5.4.2, respectively. Besides some of the obvious differences between the power spectral density plots such as the amplitude of the components at 0.1 Hz, 0.167 Hz, 0.2 Hz, 0.267 Hz, 0.3 Hz and 0.4 Hz etc., there are no other information from these plots that can help to distinguish the COPD subject from the normal subject. These conventional power spectra clearly fail to reflect an appropriate representation of the signal characteristics of the heart rate and blood pressure variability signals. All time information is completely lost; hence there is no way to quantitatively differentiate COPD from normal. Fortunately, there are other techniques such as time-frequency analysis and cross-spectral analysis, which will be presented in later sections, which can overcome these limitations

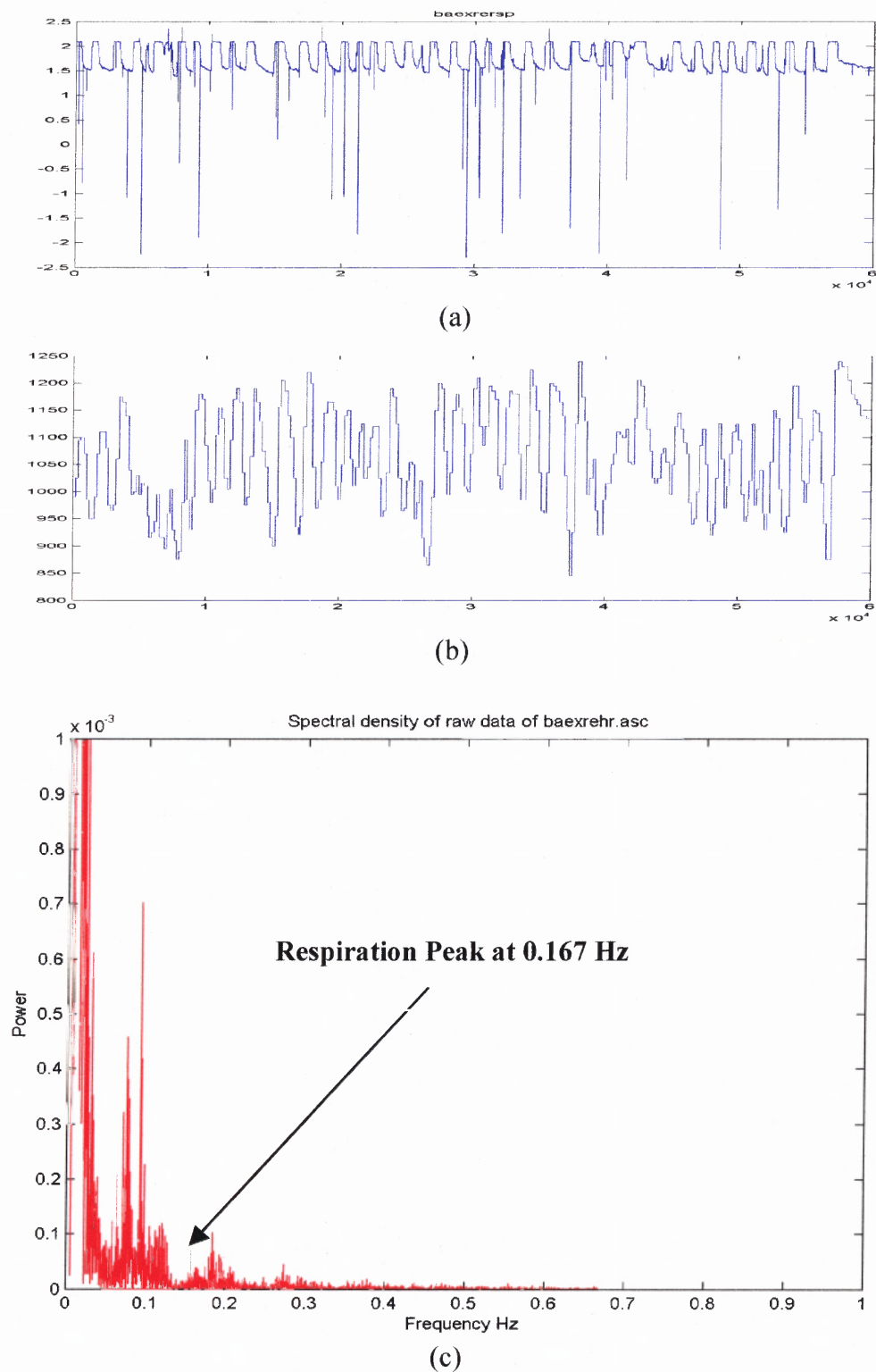


Figure 5.3 HRV analysis of a normal subject.

(a) Raw respiration signal, 5-minute rest at 10 bpm (0.167 Hz)

(b) Heart rate IIBI signal.

(c) Frequency spectrum of HR IIBI signal.

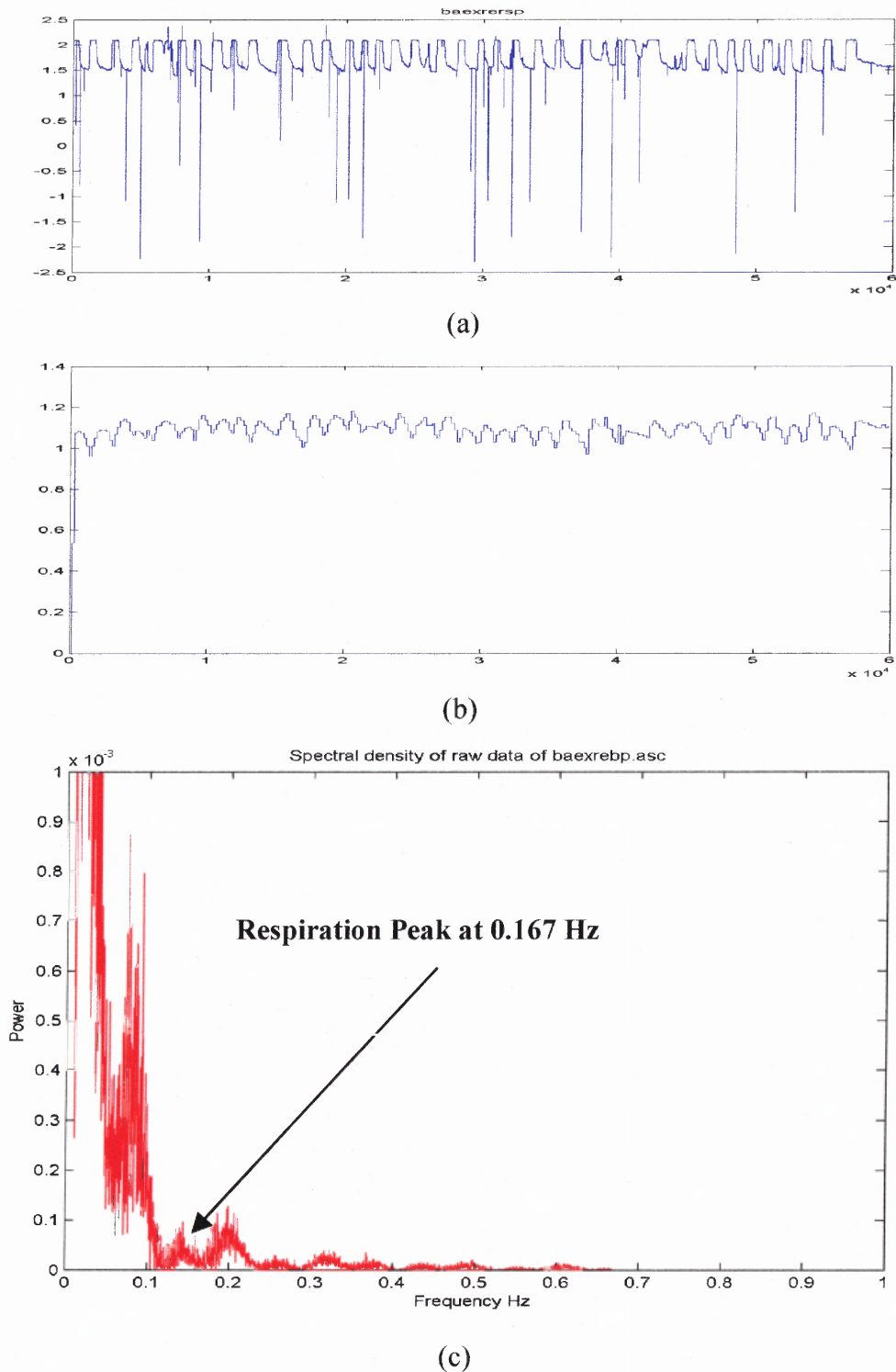
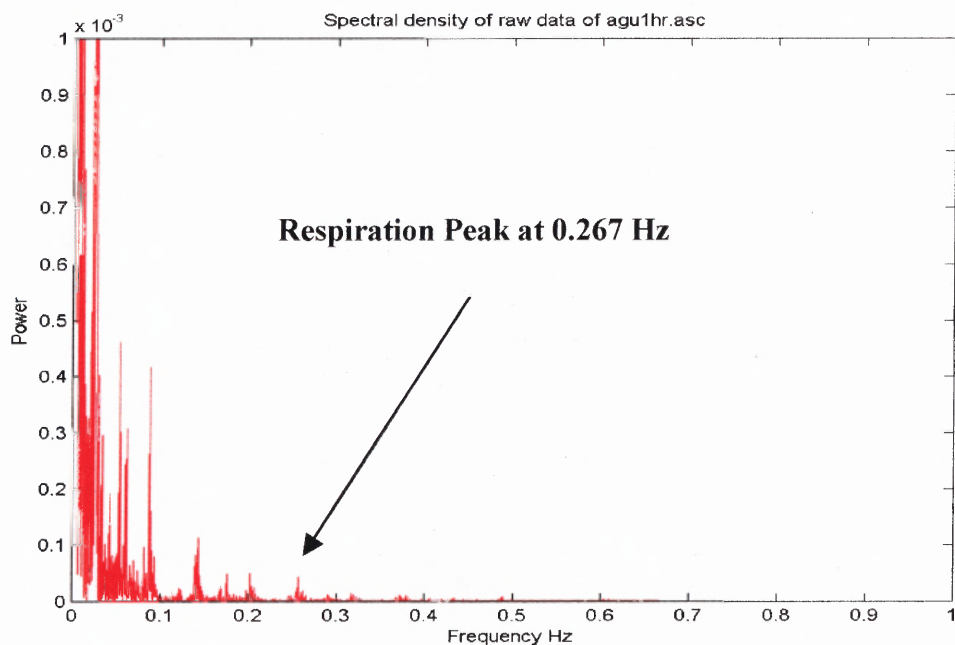


Figure 5.4 BPV analysis of a normal subject.

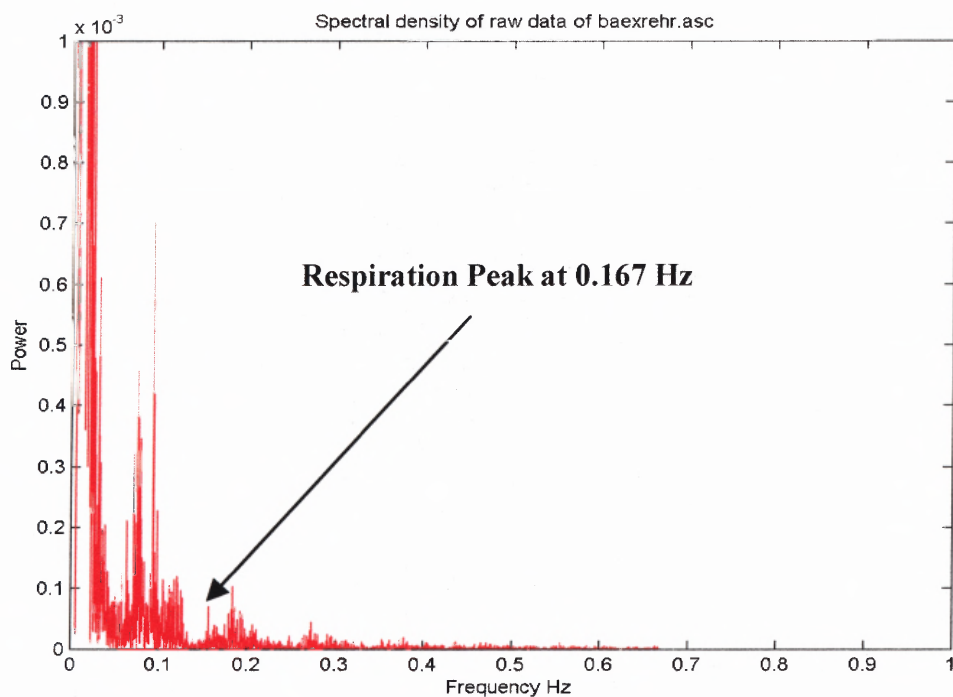
(a) Raw respiration signal, 5-minute rest at 10 bpm (0.167 Hz)

(b) Blood pressure IIBI signal.

(c) Frequency spectrum of BP IIBI signal.



(a)

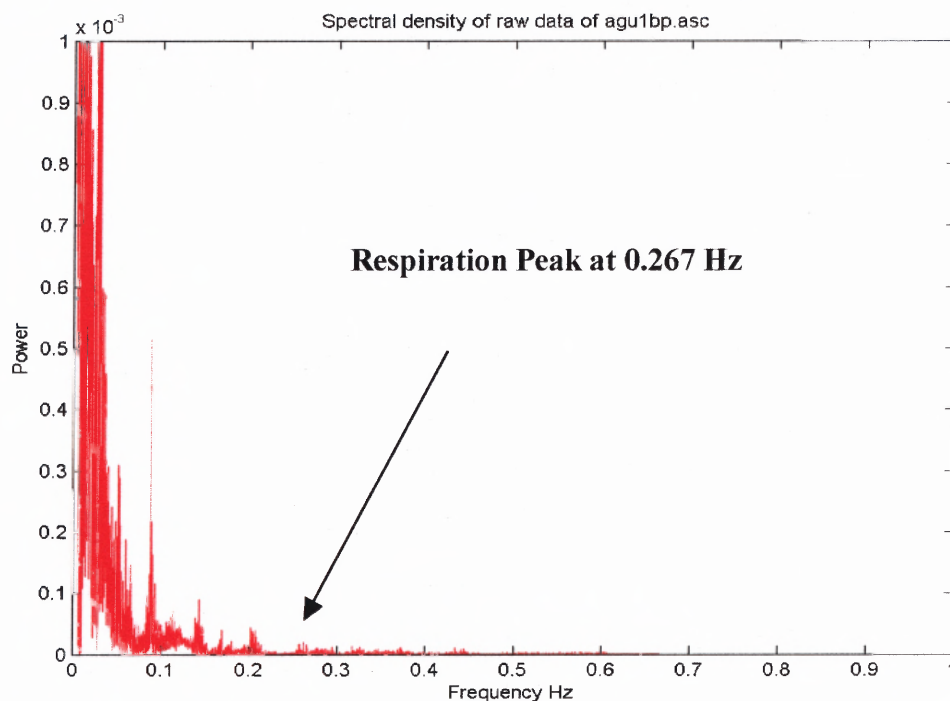


(b)

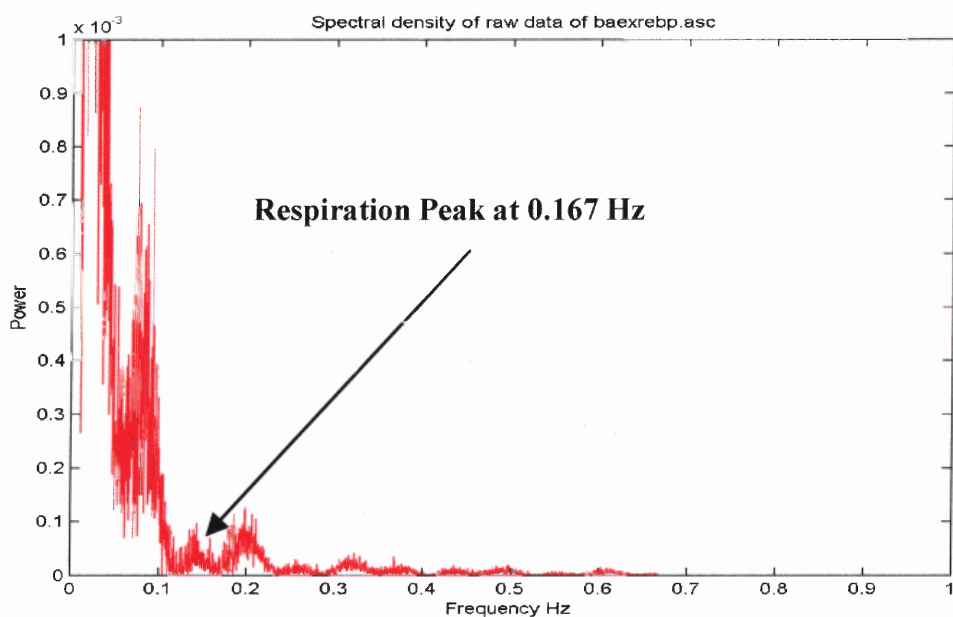
Figure 5.4.1 Comparison of the HRV frequency spectra of COPD and normal subject during 5 minutes rest.

(a) COPD breathing at 16 bpm (0.267 Hz).

(b) Normal breathing at 10 bpm (0.167 Hz).



(a)



(b)

Figure 5.4.2 Comparison of the BPV frequency spectra of COPD and normal subject during 5 minutes rest.

(a) COPD breathing at 16 bpm (0.267 Hz).

(b) Normal breathing at 10 bpm (0.167 Hz).

5.2 Time Frequency Analysis

One of the reasons that the time-frequency analysis (TFA) has enjoyed a tremendous popularity and phenomenal development in the past three decades is that TFA has overcome some of the shortcomings of the widely used Fourier transform of spectral analysis. The Fourier transform describes the spectral properties of a time signal [23]. It provides frequency information that can only be extracted for the complete duration of the signal. It gives no information about the local variations in time and requires the signal to be stationary. There is no way of knowing whether the value of the power spectral density of a signal at a particular frequency is derived from frequencies present throughout the life of the signal or during one or a few selected periods. The TFA, with its ability to perform local time-frequency decomposition (as long as it satisfies the Heisenberg's Uncertainty Principle as mentioned in section 3.2), is able to measure the time dependent variations of the instantaneous frequency contents of a nonstationary signal.

5.2.1 Time Frequency Analysis Applied to Sine Waves

Before seeing how TFA perform on real data, the advantages and disadvantages of the four time frequency distributions (the Short Time Fourier Transform, Smoothed Pseudo-Wigner Ville, Choi-Williams and Born-Jordan-Cohen distributions) used in this dissertation are more clearly seen when applied to signals with known spectra. Since all time frequency analyses used for heart rate variability studies in this dissertation were in the frequency range between 0.04 Hz to 0.5 Hz, a test signal was constructed with three

sine waves (0.3, 0.1 and 0.5 Hz sampled at 200 samples per second) as shown in Figure 5.5.

All four time-frequency distributions are shown as 3D mesh and contour plots with time axis in seconds and frequency axis in Hertz. The results are shown in Figure 5.6. All four time-frequency distributions' shapes showed the expected pattern. However, the Choi-Williams has a clearer frequency representation at 0.3, 0.1 and 0.5 Hz on the contour plot than the Short Time Fourier Transform (STFT), Smoothed Pseudo-Wigner Ville, and the Born-Jordan-Cohen distributions; even though the Smoothed Pseudo-Wigner Ville is a close second. On the 3D mesh plots the 0.3 Hz component of the Choi-William and the Smoothed Pseudo-Wigner Ville distributions stop smearing at 0.7 Hz while the STFT and the BJCD smear out to 0.8 Hz and 1 Hz respectively. The CWD is better than the BJCD because there is less power smearing at 0.9, 0.6 and 1 Hz of the 0.3, 0.1 and 0.5 Hz components (shown as yellow-green on the contour plots) respectively. The criterion for a clear representation will be discussed in section 5.2.3. All four distributions show the amplitudes of the 0.3, 0.1 and 0.5 Hz peaks spread out to other frequencies, even though the amplitude of the original test signal is the same throughout and the frequencies of the three sine waves are clearly at 0.3, 0.1 and 0.5 Hz.

The Continuous Wavelet Transform plot is shown in Figure 5.7 (a)-(e) in 3D mesh and 2D contour with time axis in seconds and the pseudo-frequency axis in Hertz. The term "pseudo" frequency is used here because in reality wavelet distributions are plotted in terms of time and scale and frequency is inversely proportional to scale.

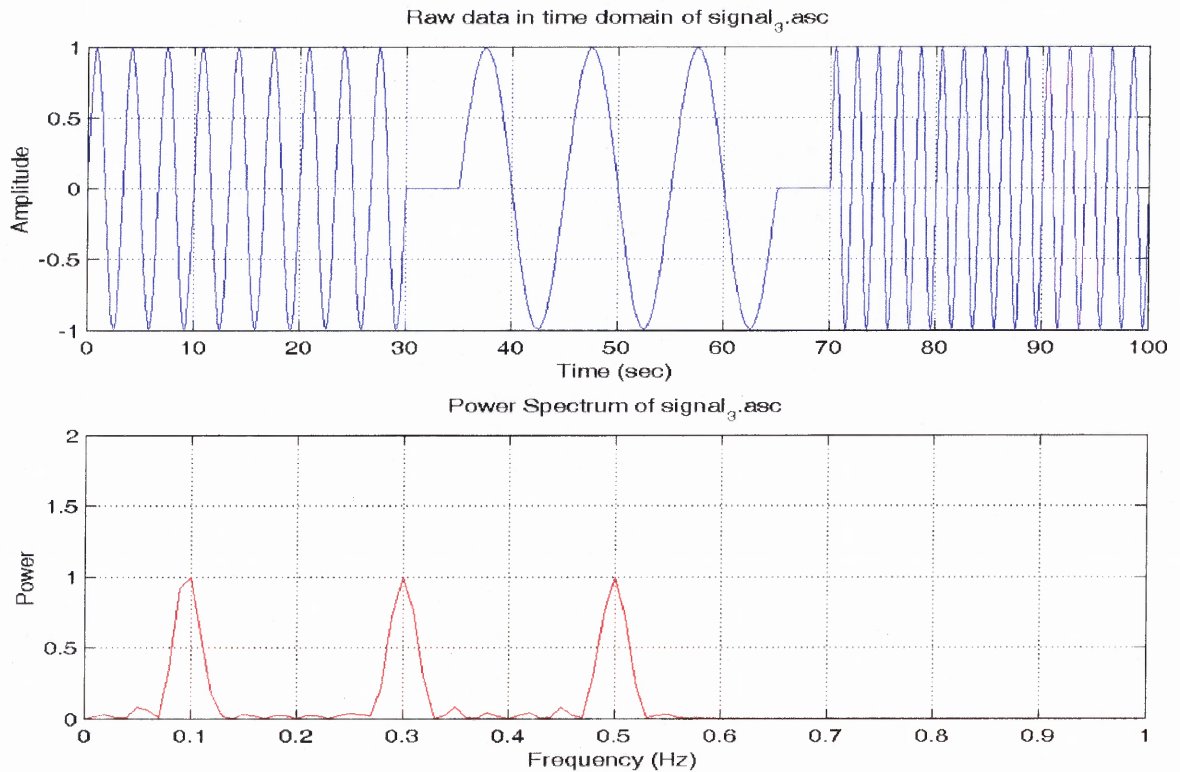


Figure 5.5 Test signal with 3 sine waves at 0.3, 0.1 and 0.5 Hz (top) and its power spectrum (bottom).

The Morlet wavelet, as well as the Meyer, Daubechies 4, Mexican Hat and Haar wavelet used, clearly shows the more defined pictures of the 3 sine waves representation with little interference (or cross-terms) when compared side-by-side with the STFT, PWVD, CWD and BJCD of the time-frequency representations. The Morlet wavelet may still not be the best wavelet type used in analyzing the low frequency range (below 2 Hz) of HRV but still is better than the other time-frequency representations presented here.

The results obtained from the test signal indicate that the linear time-frequency representations (CWD and wavelets) are the preferred time frequency distributions and the Morlet wavelet analysis is the better method to use for HRV.

Mesh & Contour of signal_3.asc using Short Time Fourier Transform distribution

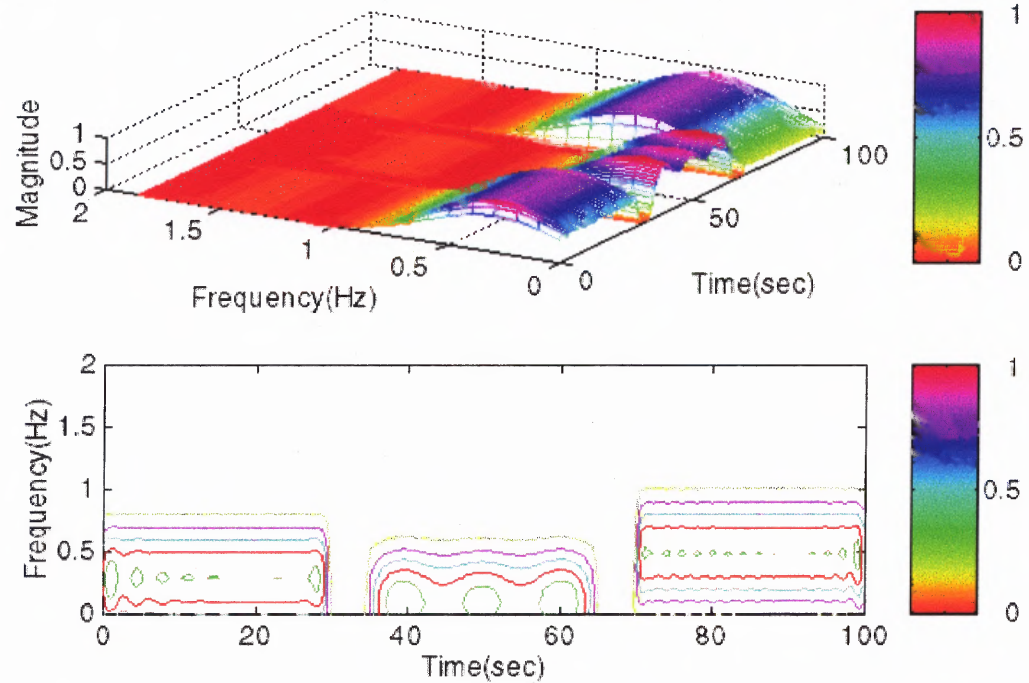


Figure 5.6 (a) STFT of a signal with 3 sine waves at 0.3, 0.1 and 0.5 Hz.

Mesh & Contour of signal_3.asc using smoothed WVD distribution

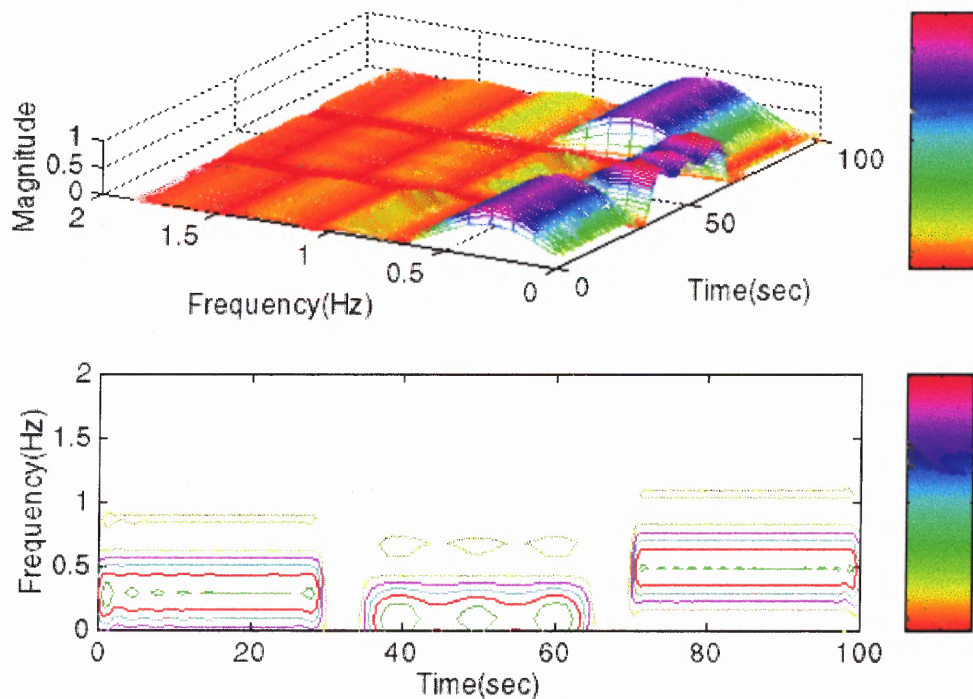


Figure 5.6 (b) SWVD of a signal with 3 sine waves at 0.3, 0.1 and 0.5 Hz.

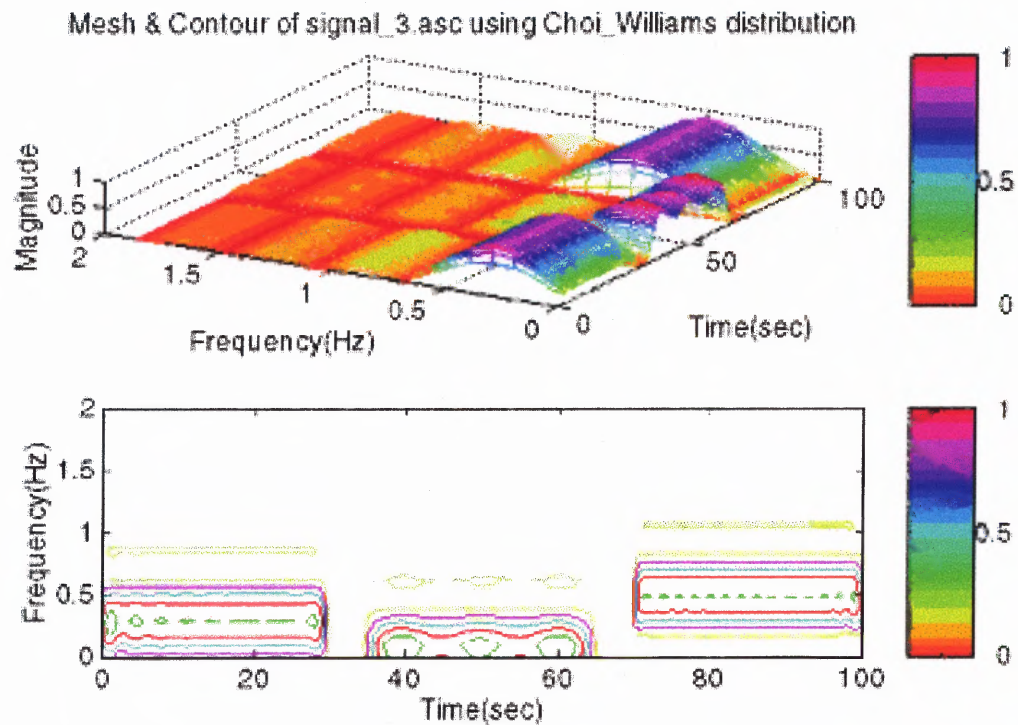


Figure 5.6 (c) CWD of a signal with 3 sine waves at 0.3, 0.1 and 0.5 Hz.

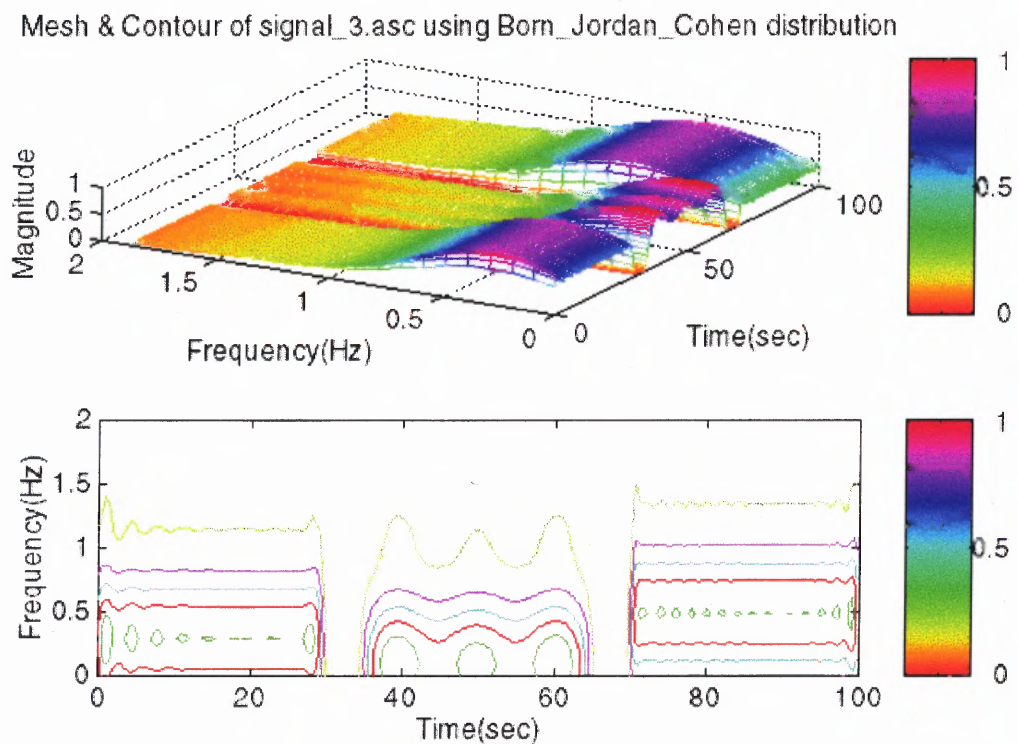


Figure 5.6 (d) BJCD of 3 sine waves at 0.3, 0.1 and 0.5 Hz.

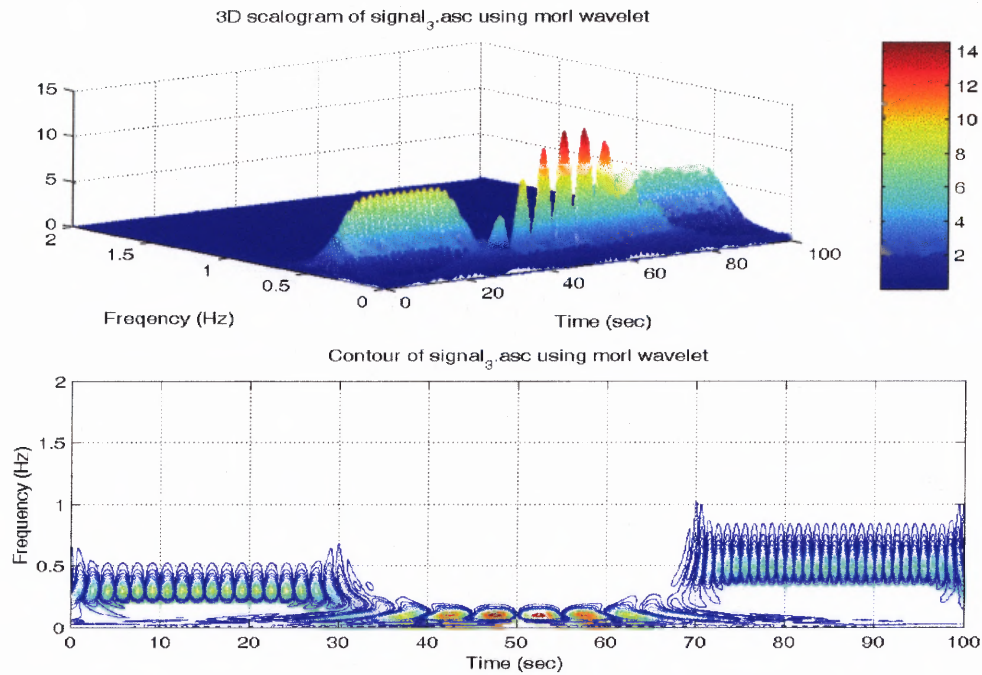


Figure 5.7 (a) WT (Morlet wavelet) of a signal with 3 sine waves at 0.3, 0.1 and 0.5 Hz.

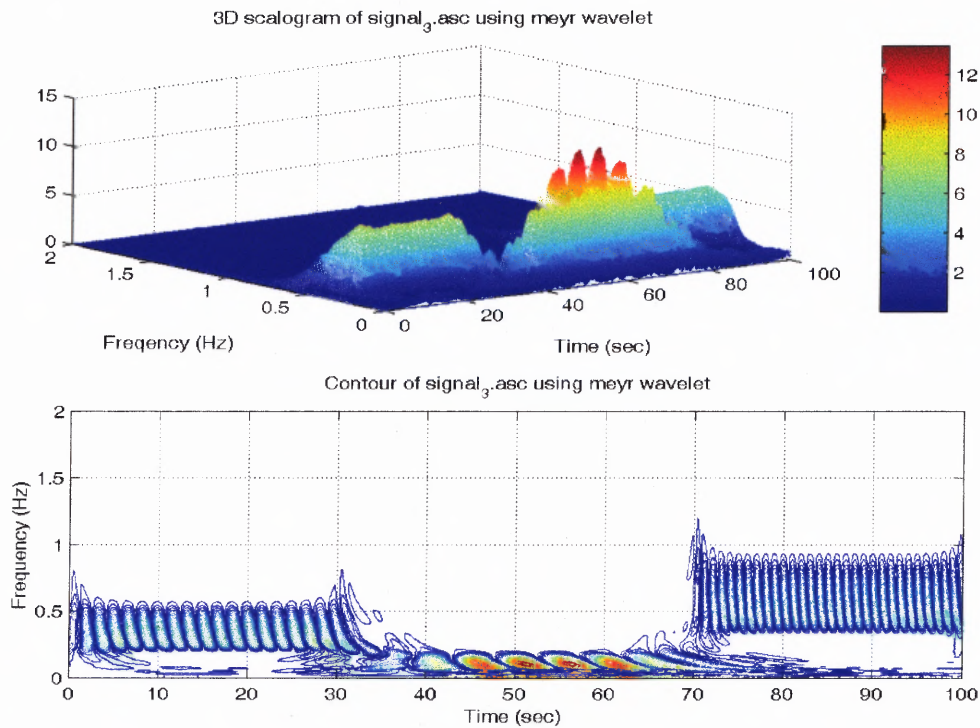


Figure 5.7 (b) WT (Meyer wavelet) of a signal with 3 sine waves at 0.3, 0.1 and 0.5 Hz.

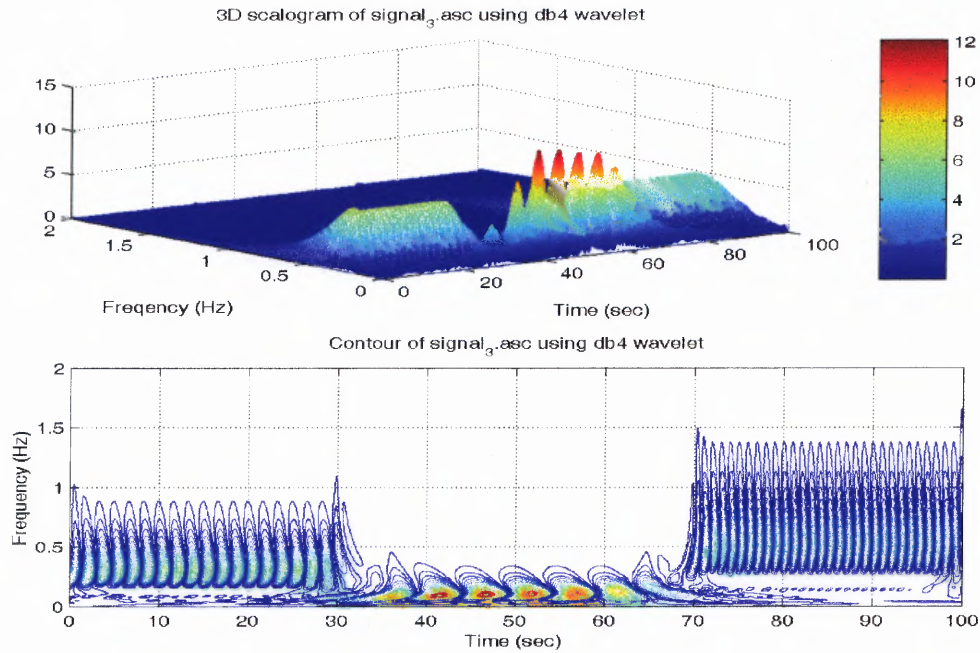


Figure 5.7 (c) WT (db4 wavelet) of a signal with 3 sine waves at 0.3, 0.1 and 0.5 Hz.

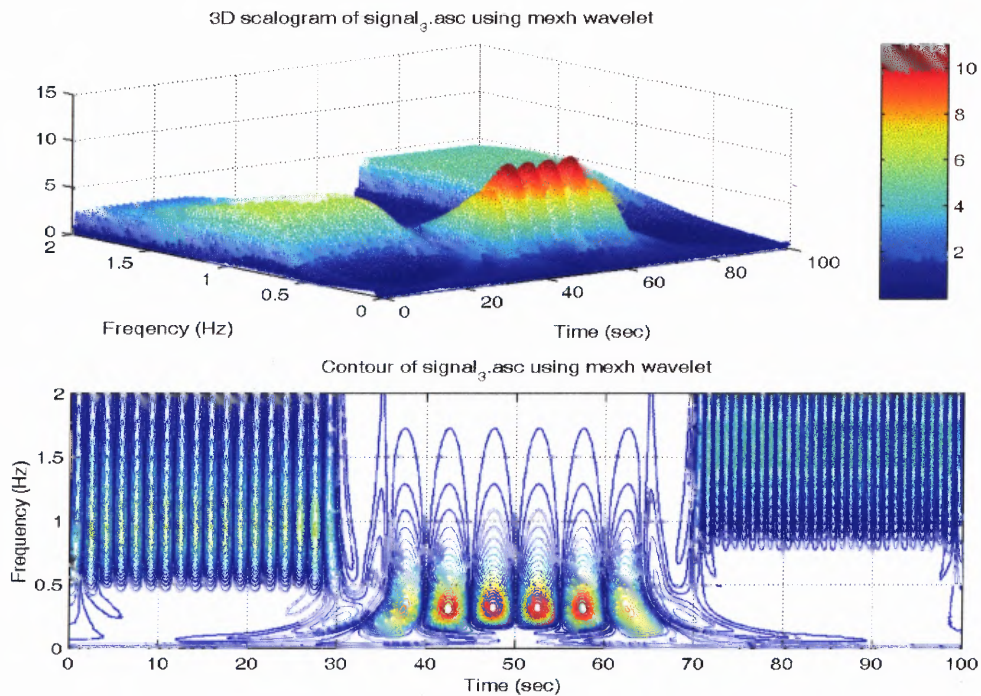


Figure 5.7 (d) WT (Mexican Hat wavelet) of a signal with 3 sine waves at 0.3, 0.1 and 0.5 Hz.

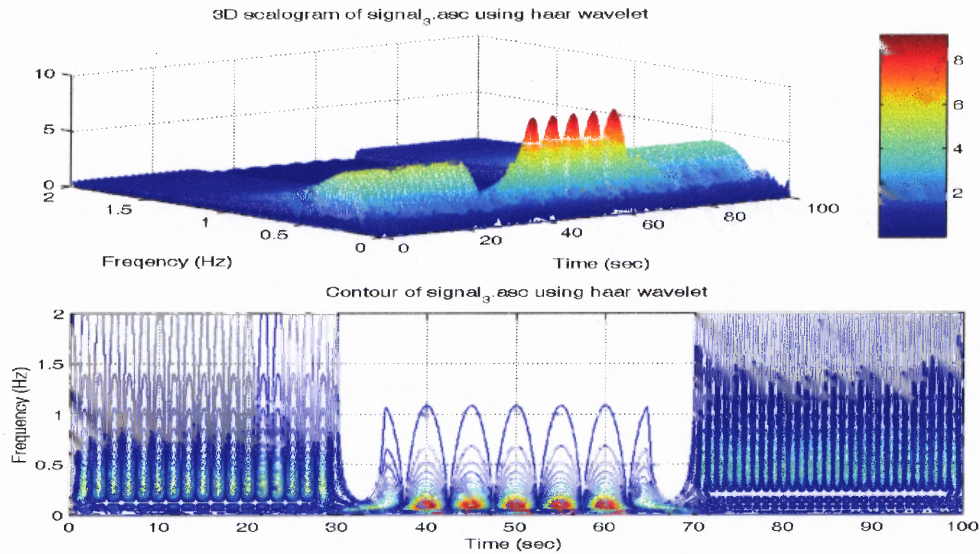


Figure 5.7 (e) WT (Haar wavelet) of a signal with 3 sine waves at 0.3, 0.1 and 0.5 Hz.

5.2.2 Time-frequency Analysis of Heart Rate Variability

The first goal of this research work is dedicated to the use of time-frequency analysis of heart rate variability as a new and innovative approach to investigate the physical attributes of both normal and COPD subjects.

Although time-frequency analysis has been extensively studied and universally used, there is not much experience in its application to very low frequency ranges (less than 2 Hz). In the previous section, each distribution used: the short time Fourier transform (STFT), the smoothed pseudo Wigner-Ville (SPWV), The Choi-Williams (CW), and the Born-Jordan-Cohen (RID), has unique characteristics which affect the amount of smoothing and the generation of crossterm interference as applied to sinusoid test signals in the HRV frequency range. The STFT and Cohen's class distributions (SPWD, CWD and BJCD) provided adequate time frequency representations for low frequency signals of HRV analysis. However, with the wavelet transform applied to

HRV more information about HRV activities in both time and frequency domains can now be revealed and be waiting for researcher's new and appropriate interpretations.

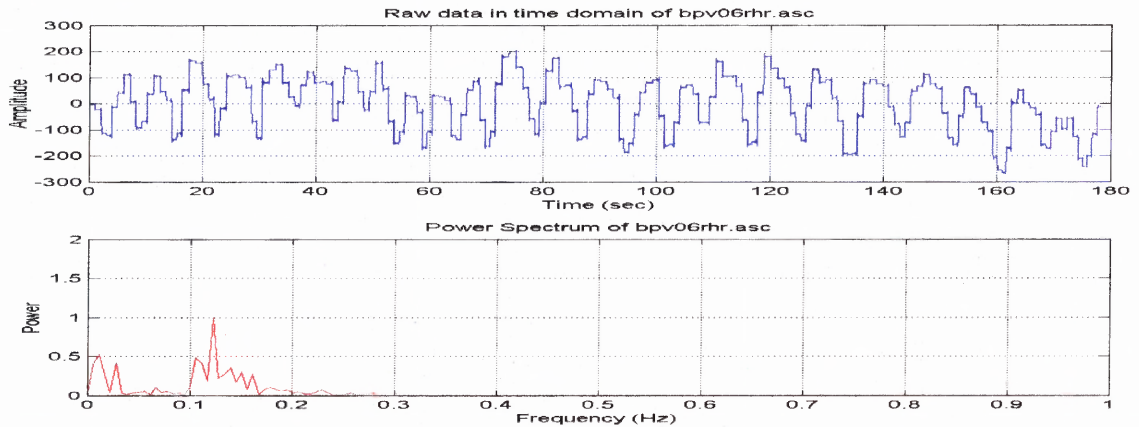


Figure 5.8 HR IIBI and power spectrum plots of a normal subject at 3 min rest paced breathing at 8 bpm.

Figure 5.8 illustrates the case of a file from a normal subject paced breathing at 8 bpm during a 3 minutes rest period. The HRV analysis was performed using the four different distributions with the same specifications (length of analysis window equal to 256, the length of the FFT analysis is 1024 and time resolution of 0.195 seconds). Even though this was a poor choice of resolution, other resolutions showed even worse results. It is evident from looking at the results in the figures that all the distributions show the effect of respiration on HRV at about the respiration frequency of 0.133 Hz (due to paced-breathing at 8 breaths per minute). Figures 5.9 (a) – (d) all show a band at 0.133 Hz and they all smear to other frequencies in various amounts. The 0.133 Hz bands of the SPWV and CW distributions in figures 5.9 (b) and (c) show less smearing than the STFT or the BJC distribution. When comparing the contour plots of the SPWV and CW distributions, it is clear that CW shows the 0.133 Hz band with more intensity and much sharper than the SPWV distribution. From these observations, the CW is the best distribution of the four time-frequency distributions.

Mesh & Contour of bpv06rat.asc using Short Time Fourier Transform distribution

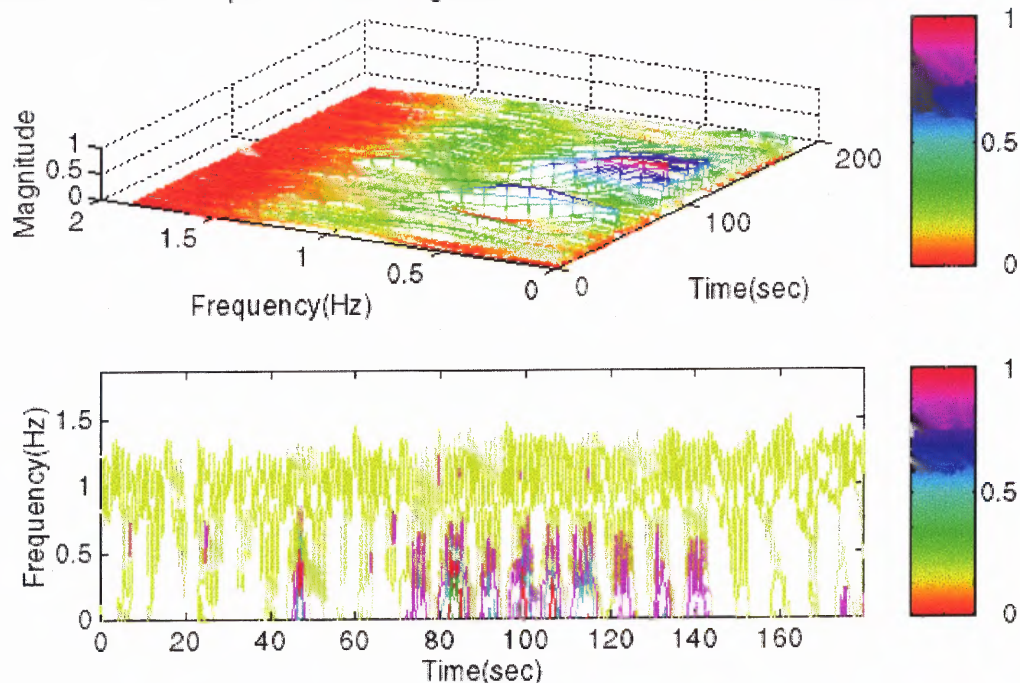


Figure 5.9 (a) STFT plots of a normal subject at 3 min rest paced breathing at 8 bpm.

Mesh & Contour of bpv06rat.asc using smoothed WVD distribution

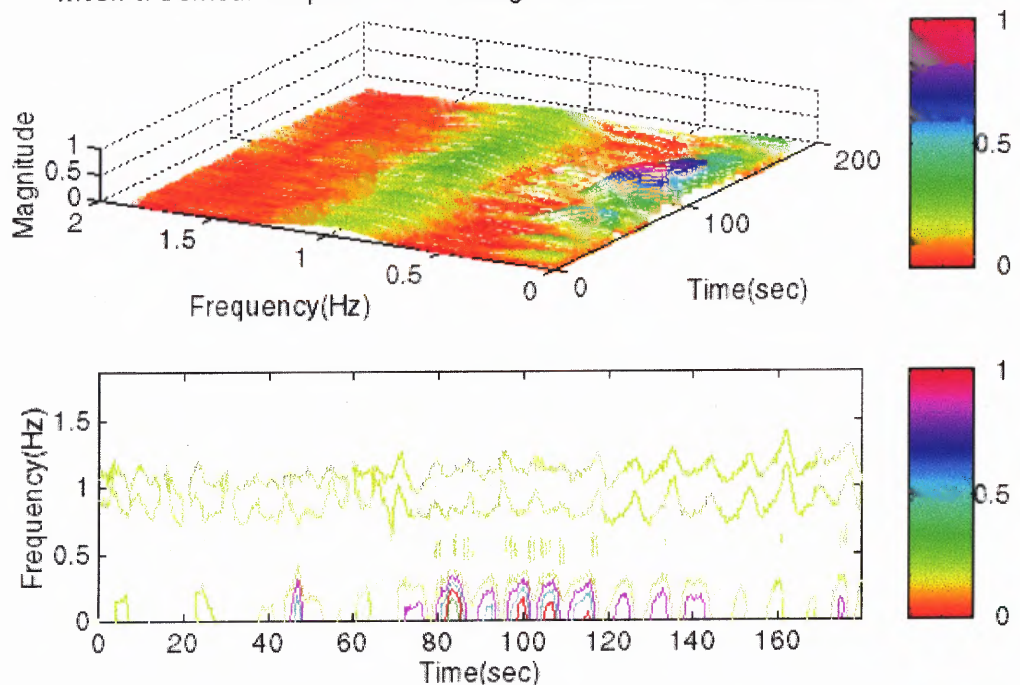


Figure 5.9 (b) SWVD plots of a normal subject at 3 min rest paced breathing at 8 bpm.

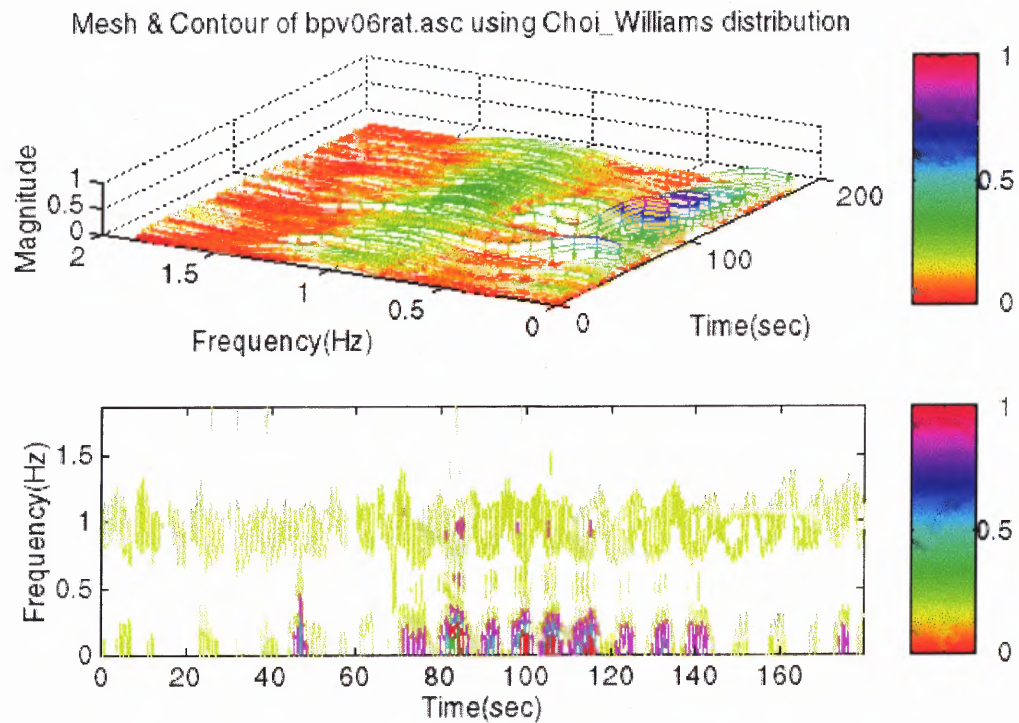


Figure 5.9 (c) CWD plots of a normal subject at 3 min rest paced breathing at 8 bpm.

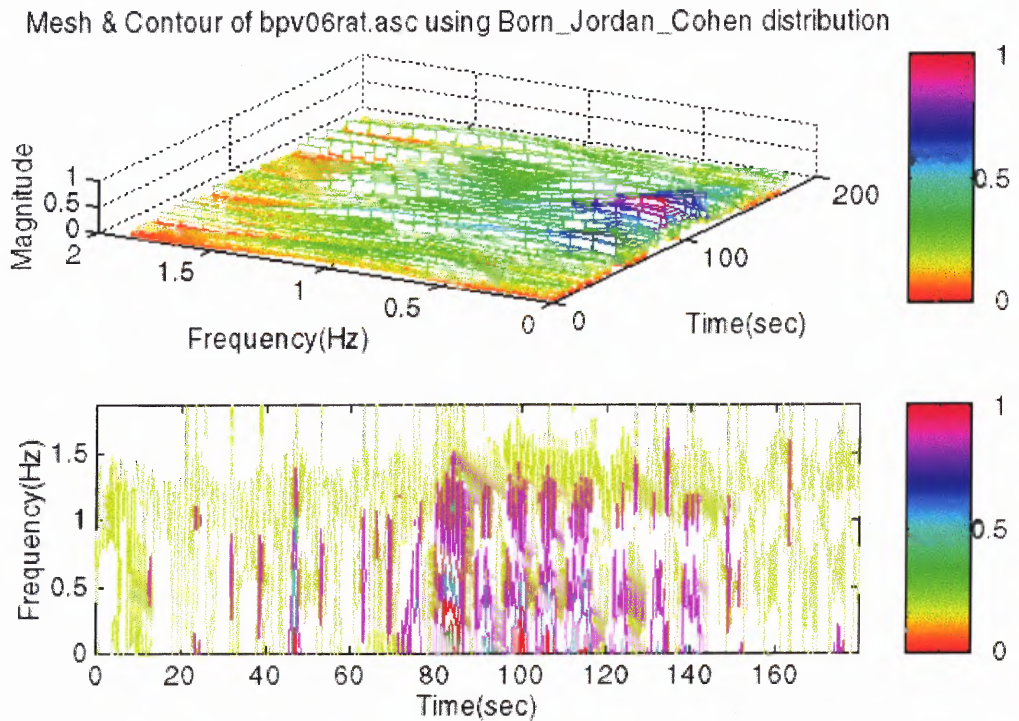


Figure 5.9 (d) BJCD plots of a normal subject at 3 min rest paced breathing at 8 bpm.

The time-frequency plots using the Morlet wavelet is shown in figure 5.10. Figure 5.10 (a) shows the 3D plot in time (seconds), frequency (Hertz) and wavelet coefficient (power). Figure 5.10 (b) and (c) are contour plots of figure 5.10 (a) looking along the z-axis (wavelet coefficients, power). Figure 5.10 (b) shows a relatively straight band at the 1024 scale, which corresponds, to 0.133 Hz due to paced breathing at 8 bpm. Furthermore, the plot also shows another band of high amplitude at 128-256 scales, which corresponds to 0.635-1.27 Hz; the same is also shown on all other time-frequency plots. The meaning of this band may possibly be due to the 1 Hz cyclic modulation of the ECG rhythm that is out of our frequency range of interest. When zooming into a closer frequency range as illustrated in figure 5.10 (c) the 0.1333 Hz band is not a straight band but varies in frequencies from 0.09 Hz and up to 0.2 Hz. This information exists on all time-frequency plots except it is much better represented on all plots using the wavelet transform. This band is also not solid but made up of many lobes called the cones of influence. Each cone of influence occurs at the minimum and maximum points of the original HR IIBI signal being analyzed which is shown in figure 5.10 (d) again for ease of observation. Figure 5.10 (c) also shows another band of cones of influence along the lower frequency range of 0.01 – 0.05 Hz that mimics the trend of the lower frequency modulation present in the HR IIBI signal. This is additional information about the trend of HRV signals, which is shown for the first time using wavelet analysis. This information is totally absent when using the Cohen's class time-frequency representations such as SPWD, CWD or BJCD.

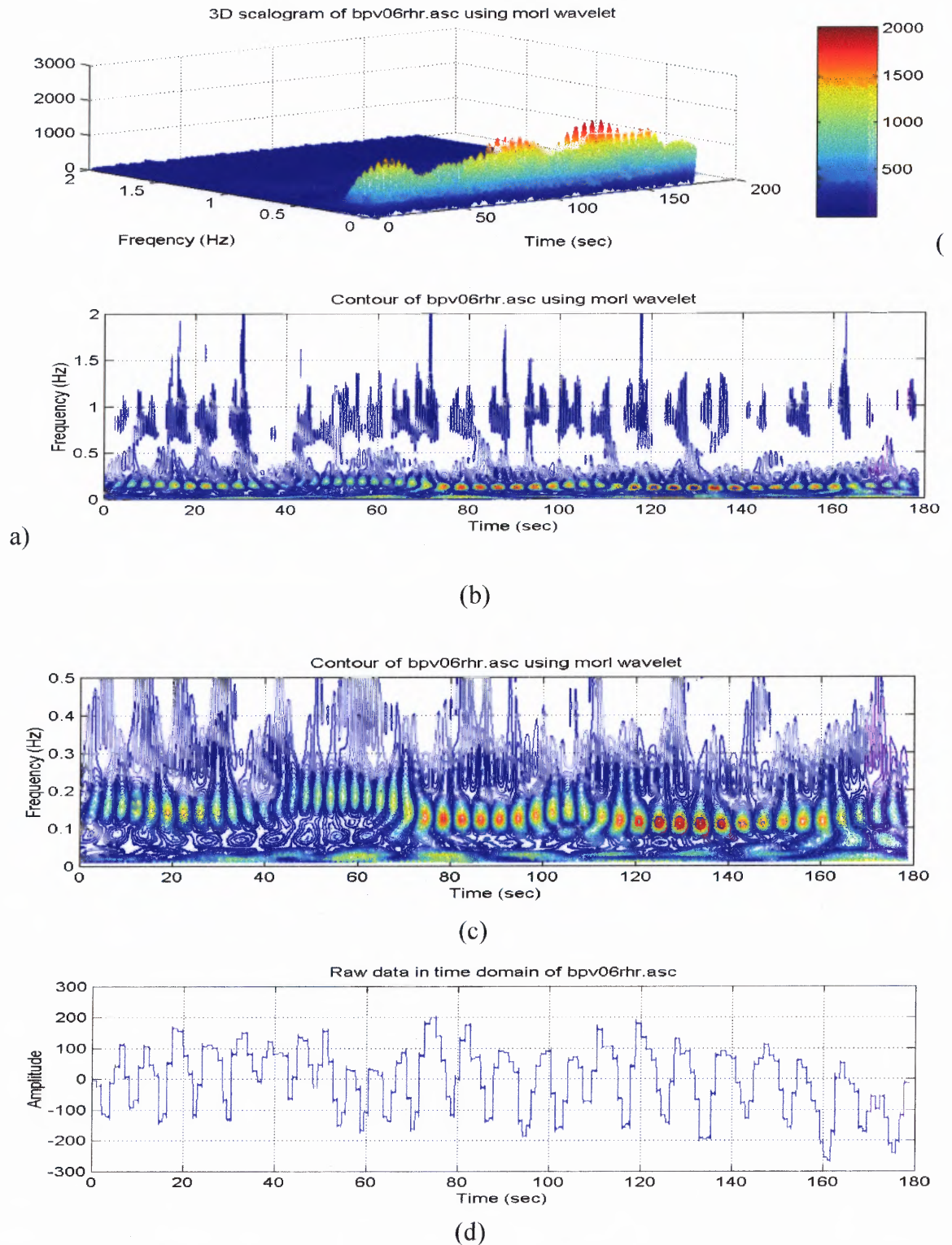


Figure 5.10 CWT (Morlet) HRV plot of a normal subject at 3 min rest paced breathing at 8 bpm. (a) 3D time frequency plot. (b) Contour plot. (c) Zoom contour plot to frequency of respiration. (d) HR IIBI signal being analyzed (shown to point out cones of influence).

5.2.3 Time-Frequency Analysis (Wavelet) of COPD HRV data

In order to analyze COPD HRV signals, it was necessary to use digitized HRV data sets. One example of the digitized HRV signals is from a COPD subject resting and paced-breathing at 16 breaths per minute. Figure 5.11 illustrates the HR IIBI and its power spectrum plots for the case of a file from a COPD subject paced breathing at 16 bpm during a 5 minutes rest period. The HRV analysis was performed using the five different wavelet distributions (Morlet, Meyer, Daubechies 4, Mexican Hat and Haar) with the same specifications (length of analysis window equal to 200 and the length of the FFT analysis of 256).

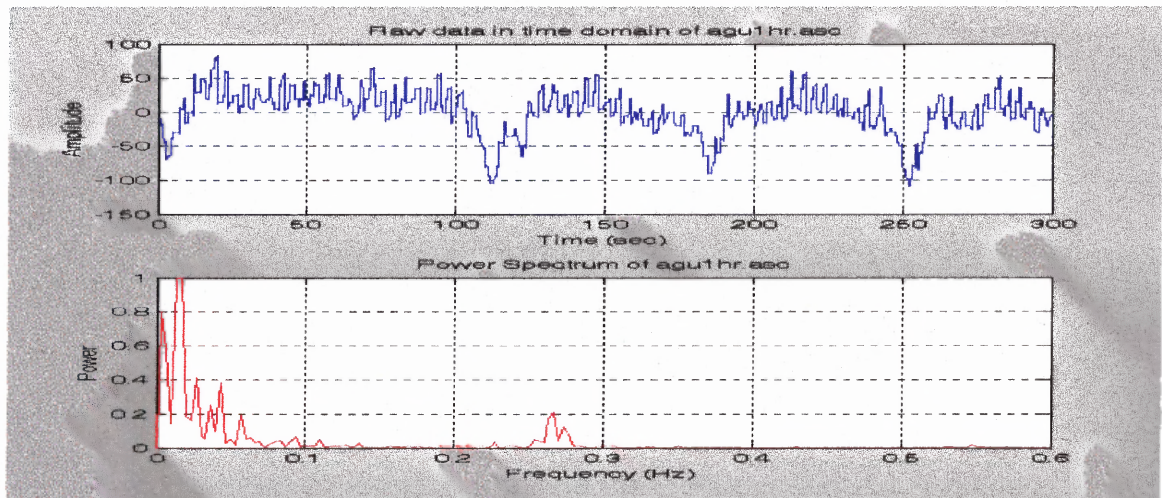


Figure 5.11 HR IIBI and power spectrum of a COPD subject at rest breathing at 16 bpm.

There are an infinite number of possible functions that satisfy the criteria for a wavelet. For a function to be a wavelet, it must integrate to zero and must be localized in time. These requirements are shown in equation form below:

$$\int_{-\infty}^{\infty} \Psi(t) dt = 0 \quad (5.1)$$

$$\lim_{t \rightarrow \infty} |\Psi(t)| = 0 \quad (5.2)$$

The following figures show the results of these transforms. The purpose of this is to show that, although the output for different wavelets varies, the fundamental characteristics of the wavelet transform are the same.

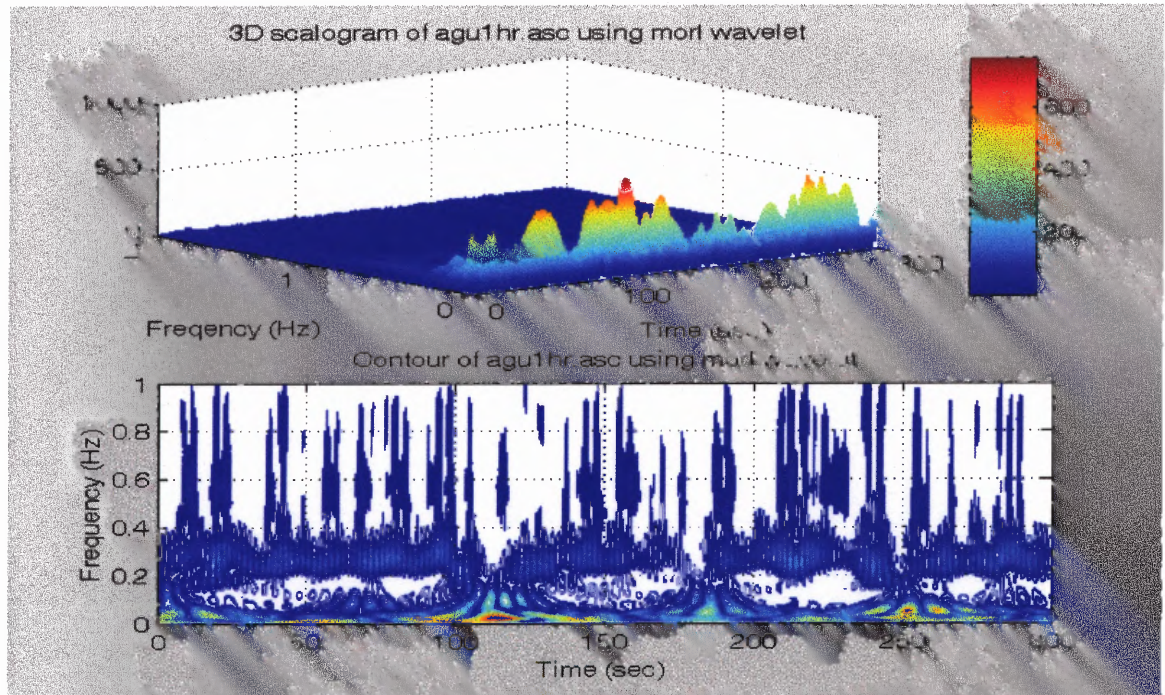


Figure 5.12 CWT (Morlet) HRV plot of a COPD subject at 5 min rest paced breathing at 16 bpm. (a) 3D time frequency plot. (b) Contour plot.

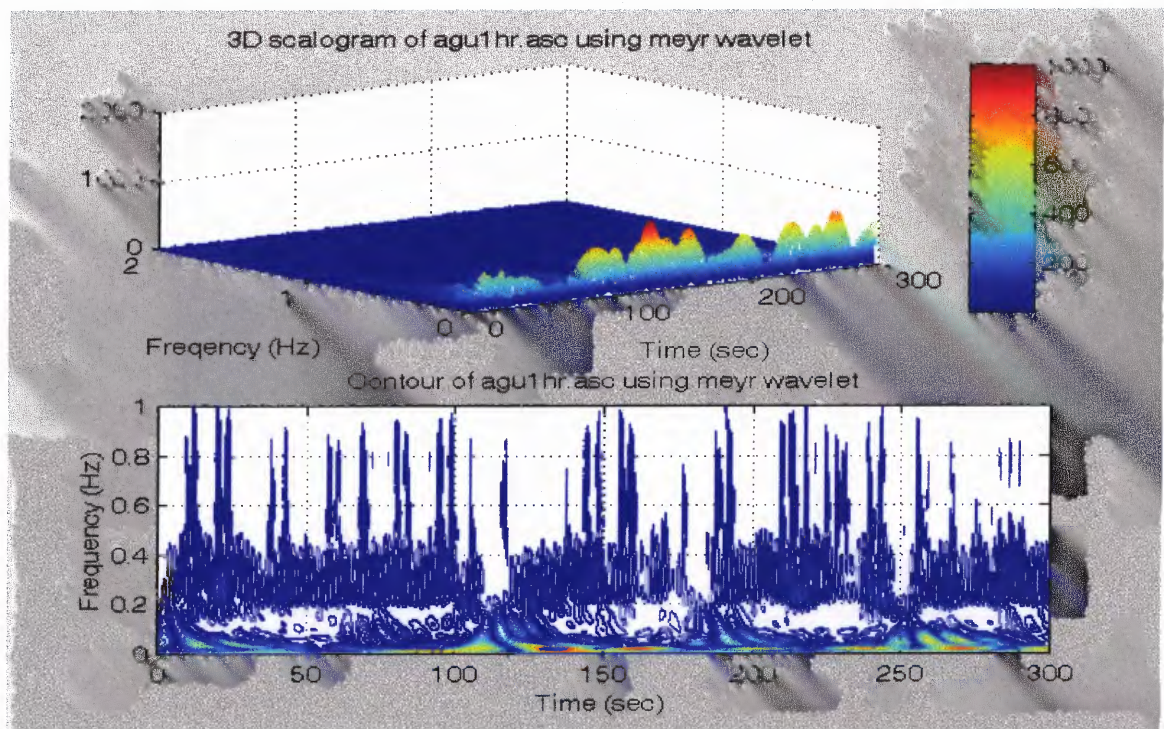


Figure 5.13 CWT (Meyer) HRV plot of a COPD subject at 5 min rest paced breathing at 16 bpm. (a) 3D time frequency plot. (b) Contour plot.

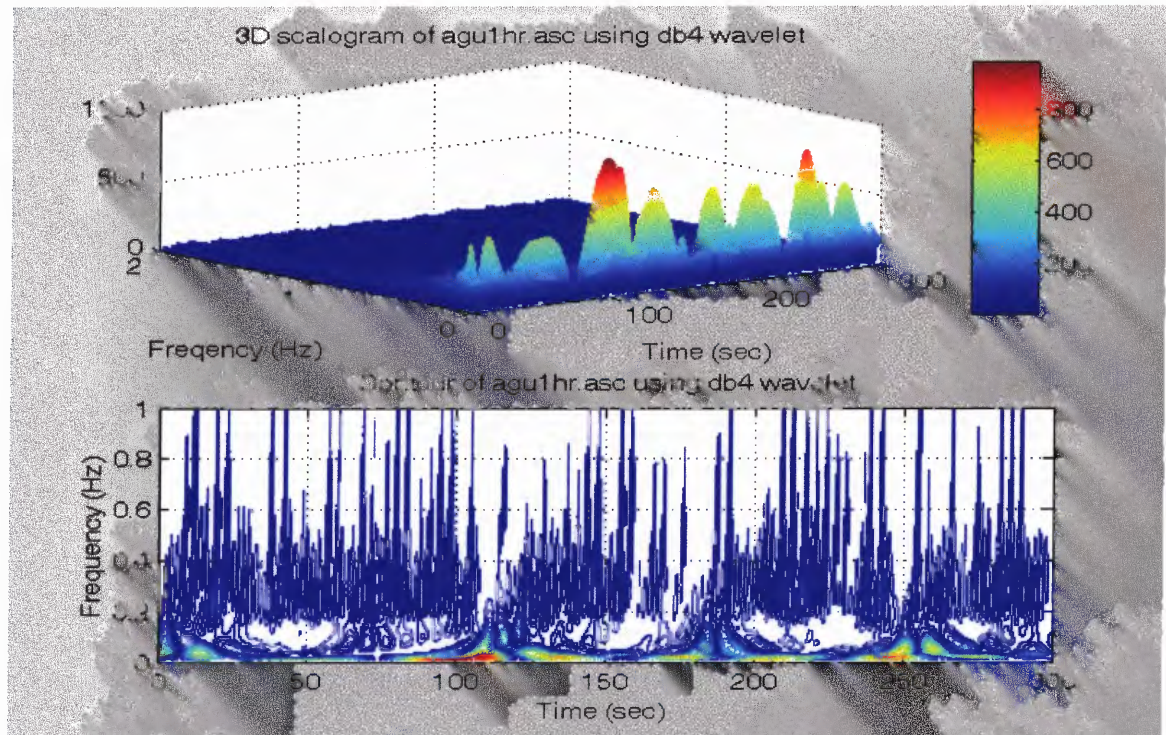


Figure 5.14 CWT (dB4) HRV plot of a COPD subject at 5 min rest paced breathing at 16 bpm. (a) 3D time frequency plot. (b) Contour plot.

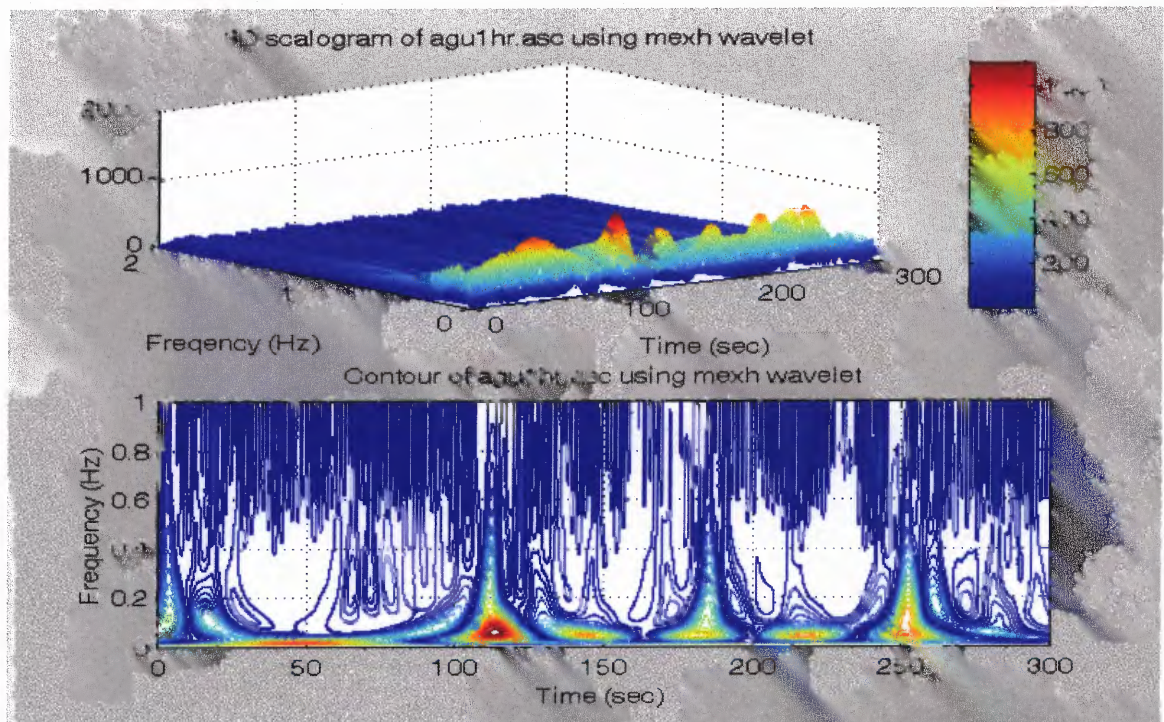


Figure 5.15 CWT (Mexican Hat) HRV plot of a COPD subject at 5 min rest paced breathing at 16 bpm. (a) 3D time frequency plot. (b) Contour plot.

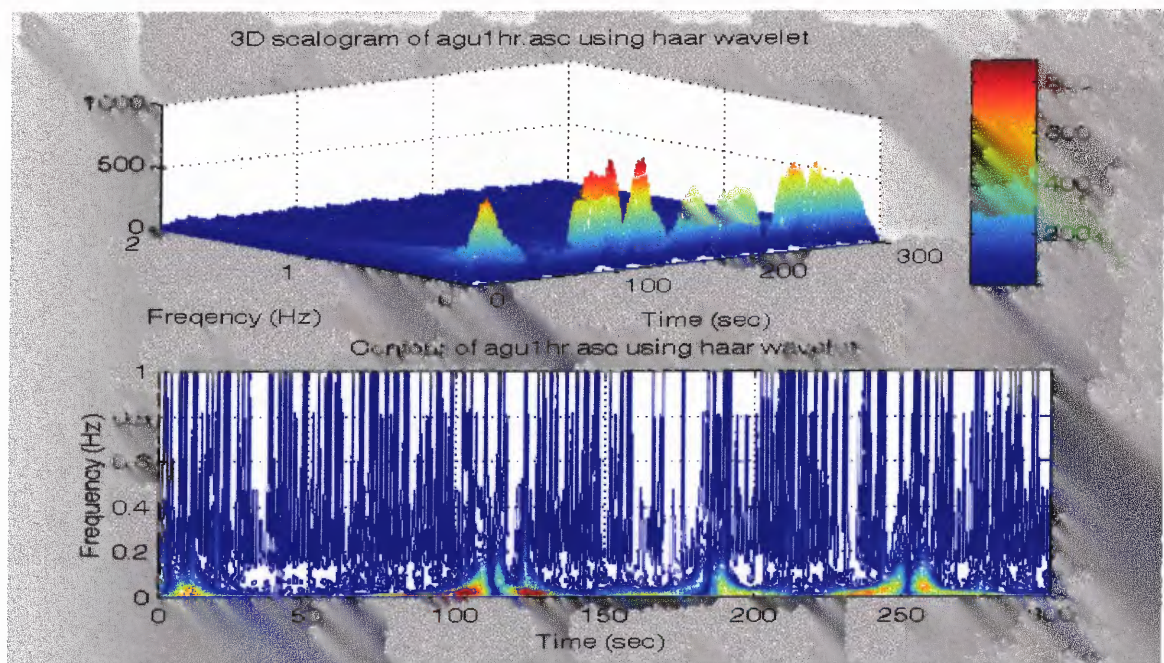


Figure 5.16 CWT (Haar) HRV plot of a COPD subject at 5 min rest paced breathing at 16 bpm. (a) 3D time frequency plot. (b) Contour plot.

All of the WT time-frequency representations shown in Figures 5.12 - 5.16 are somewhat similar. A band of cones of influence corresponding to each minimum and maximum points on the HR IIBI signal at the frequency of respiration (16 bpm, 0.266667 Hz) appears in each wavelet transform representation. However, the power intensity of the band is not as high as the similar band shown in the normal subject case investigated in section 5.2.2. Another band of cones of influence in the very low frequency range (0.01 – 0.15 Hz) also exists with higher energy and in longer time (from 10 seconds to 120 seconds, to 180 seconds, to 250 seconds). Among the wavelets, the Morlet wavelet provides the best representation in terms of time, frequency resolution and meaningful details. The band of the cones of influence at 0.266667 Hz is modulated slightly indicating that the respiration is not a stationary signal.

5.2.4 Best Time-Frequency Representations for HRV Study

In this part of the study, one chooses the best of four time-frequency representations and a wavelet distribution to analyze the HRV signal. The criterion for the best selection of distribution includes:

1. Sharp frequency band representation without smearing to the next frequency band.
2. Little or no interference (cross-term).
3. High amplitude representation that corresponds well with amplitude of original signal.

These criteria are used basically in visual inspection of the 3D and contour time-frequency plots. However, a more scientifically accepting method is needed that will be presented in the next section.

5.2.5 Best Wavelet Selection for HRV Time-frequency Representation

Wavelet representations show more details than the classical time frequency representation such as the Cohen's class distributions. Among the different wavelets used in the analysis, the Morlet wavelet seems to be the right choice of wavelet for analyzing the actual physiological signals of BP, respiration and heart rate variability signal (derived from the ECG) when visual inspection was performed. Here the author proposes using the cross-correlation to help make this decision.

The technique of cross-correlation was used to compare the power spectrum derived wavelet coefficients (power) versus frequency obtained from the 3D scalogram representations of the HRV IIBI signals of COPD subjects to the power spectrum of the same signal using Fourier analysis. The Fourier analysis power spectrum was used because Fourier analysis provided the perfect representation of the signal power in the frequency domain. Any wavelet representation considered as best representation must have the highest cross-correlation index value when comparing the wavelet power spectrum with the Fourier power spectrum. The cross-correlation between two signals measures the way the signals change with respect to one another. In other words, if $f(x)$ always increases and decreases as $g(x)$ increases and decreases, then $f(x)$ and $g(x)$ are positively correlated. The correlation of two continuous functions $f(x)$ and $g(x)$, denoted as $f(x) \bullet g(x)$, is defined by the following equation [25]:

$$f(x) \bullet g(x) = \int_{-\infty}^{\infty} f(x)^* g(x + \lambda) dx \quad (5.3)$$

where $*$ is the complex conjugate. For this study, the power spectrum signals were not complex. Therefore, to calculate the cross-correlation, the function $g(x)$ is shifted, by

different values of λ , over the length of $f(x)$, the signals are multiplied, and the area under the product of the two signals is computed. If the cross-correlation function is normalized by the product of the square root of the auto cross-correlation of each function, then the normalized cross correlation will have a range from 0 to 1. For two signals that are the same, the cross-correlation at zero lag (when $\lambda = 0$) is equal to 1. The closer the cross-correlation value is to 1, the more similar the waveforms are to one another.

It should be pointed out that the power spectra (Fourier and wavelets) in this study are not continuous, but discrete. Therefore, to compute the discrete cross-correlation, the following equation was used [26]:

$$C_{fg}(\lambda) = \frac{\frac{1}{N-1} \sum_{n=1}^N (f(n) - \bar{f})(g(n+\lambda) - \bar{g})}{\sqrt{\frac{1}{N-1} \sum_{n=1}^N (f(n) - \bar{f})^2 \frac{1}{N-1} \sum_{n=1}^N (g(n) - \bar{g})^2}} \quad (5.4)$$

where N is the number of points in the signal. To compute the cross-correlations for this section, a Matlab program was written and is listed in Appendix B.

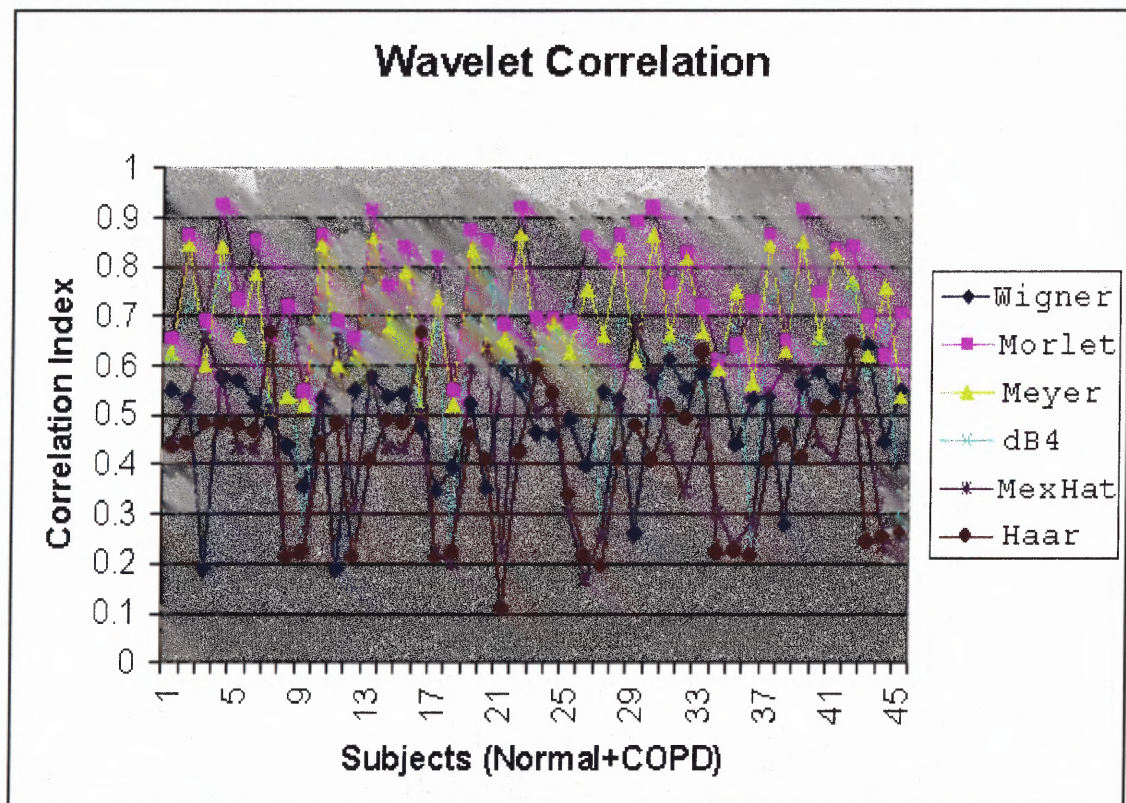
Based on the cross-correlation method presented, the cross-correlation coefficient between the Fourier power spectrum and the wavelet power spectrum was calculated for each COPD subject. Table 5.1 tabulates the cross-correlation results. It should be noted that the table displays the maximum absolute value of the cross-correlation function. From the table and the graph in figure 5.17, the values are from 0.2 to over 0.9 but all values indicated that the Morlet wavelet is the best representation.

Table 5.1 Correlation Indices of Wavelet Representations

Subject	Wigner	Morl	Meyer	dB4	Mex Hat	Haar
1	0.551	0.655	0.625	0.613	0.443	0.436
2	0.532	0.864	0.845	0.725	0.523	0.441
3	0.189	0.690	0.600	0.662	0.659	0.484
4	0.577	0.926	0.841	0.797	0.579	0.483
5	0.571	0.733	0.661	0.676	0.434	0.479
6	0.524	0.857	0.789	0.611	0.430	0.466
7	0.487	0.661	0.516	0.516	0.500	0.665
8	0.438	0.720	0.537	0.684	0.221	0.211
9	0.357	0.547	0.521	0.259	0.222	0.222
10	0.532	0.864	0.845	0.725	0.523	0.441
11	0.189	0.690	0.600	0.662	0.659	0.484
12	0.551	0.655	0.625	0.613	0.314	0.211
13	0.577	0.917	0.865	0.711	0.579	0.408
14	0.537	0.760	0.681	0.686	0.434	0.491
15	0.544	0.840	0.793	0.616	0.432	0.485
16	0.476	0.661	0.516	0.516	0.500	0.665
17	0.348	0.820	0.737	0.684	0.221	0.211
18	0.395	0.550	0.523	0.256	0.200	0.222
19	0.524	0.875	0.835	0.755	0.593	0.461
20	0.352	0.852	0.640	0.780	0.635	0.408
21	0.593	0.682	0.652	0.599	0.229	0.109
22	0.554	0.921	0.866	0.556	0.627	0.425
23	0.463	0.698	0.609	0.627	0.504	0.593
24	0.461	0.697	0.688	0.659	0.531	0.544
25	0.492	0.686	0.629	0.727	0.305	0.339
26	0.399	0.861	0.755	0.623	0.167	0.214
27	0.548	0.820	0.662	0.267	0.261	0.195
28	0.531	0.865	0.836	0.691	0.520	0.411
29	0.260	0.892	0.600	0.702	0.682	0.478
30	0.573	0.918	0.865	0.502	0.581	0.409
31	0.613	0.765	0.661	0.641	0.436	0.517

Table 5.1 (Cont.) Correlation Indices of Wavelet Representations

Subject	Wigner	Morl	Meyer	dB4	Mex Hat	Haar
32	0.554	0.828	0.817	0.656	0.346	0.490
33	0.584	0.720	0.668	0.539	0.487	0.629
34	0.603	0.611	0.594	0.620	0.303	0.222
35	0.440	0.639	0.750	0.684	0.238	0.226
36	0.532	0.729	0.565	0.244	0.282	0.216
37	0.537	0.866	0.845	0.731	0.542	0.408
38	0.279	0.649	0.630	0.780	0.598	0.459
39	0.564	0.917	0.850	0.525	0.592	0.411
40	0.588	0.748	0.657	0.641	0.446	0.516
41	0.550	0.837	0.828	0.680	0.410	0.510
42	0.551	0.840	0.769	0.759	0.559	0.644
43	0.639	0.700	0.621	0.580	0.475	0.243
44	0.445	0.619	0.758	0.679	0.235	0.253
45	0.549	0.706	0.537	0.260	0.253	0.262

**Figure 5.17** Graph of correlation indices for wavelet representations.

5.2.6 Vagal Tone and Sympathovagal Balance via Time-Frequency Distribution of COPD Subjects

Although the inherent rhythmicity of the heart is due to a natural pacemaker situated in the sinoatrial node, continuous beat-to-beat control of the heart is dependent on the relative balance of the sympathetic and the parasympathetic impulses delivered from the brain to the sinus node. From drug studies, three discrete frequency ranges in the spectrum of HRV were found to be of importance: a very low frequency range (VLF, 0.02 to 0.04 Hz), a low frequency range (LF, 0.04 to 0.15 Hz) and a high frequency range (HF, 0.15 to 0.5 Hz). The VLF band was equated with the rennin-angiotensin system, the LF band with blood pressure and baroreflex control, and the HF band with respiration. The LF band is mediated by both the sympathetic and the parasympathetic pathways while the HF band is mediated by the parasympathetic pathways only.

Assessment of the parasympathetic activity from spectral analysis is obtained via a measurement of the area under the HF peak. Sympathetic activity is less easy to quantify using this methodology [49]. A realizable goal is that of the sympathovagal balance measurements (LF/HF ratio), which recognizes both the reciprocal and the non-reciprocal parasympathetic and sympathetic influences on heart rate. [49] Factors other than the cardiac nerves can also alter the heart rate (HR). The HR is also sensitive to changes in body temperature, plasma electrolyte concentrations and hormones. However, these factors are normally less important than the sympathetic and the parasympathetic nerve pathways to the heart [49].

This section looks at some applications of the wavelet time frequency distribution techniques. At the same time, comparisons of different wavelets are done to find the best wavelet for the sympathovagal case.

The wavelet distributions were calculated using our wavelet time frequency distribution software. The program then analyzed the representative heart rate and blood pressure IIBI signals of a COPD subject. The 3D, contour plots and the activity plots were obtained for the entire file by calculating the areas under the LF, HF ranges for each instant of time. The sympathovagal balance (the ratio of the LF to the HF range, LF:HF) was also obtained. As mentioned earlier drug studies indicate that the LF range is a mixture of sympathetic and parasympathetic division activity. The ratio is an indication of both reciprocity and non-reciprocity [50].

Figures 5.18 – 5.27 display the 5-minute activity plots of a COP subject at rest breathing at 16 breaths per minute using the Morlet, Meyer, Daubechies 4, Mexican Hat and Haar wavelet. The even figures (5.18, 5.20, 5.22, 5.24 and 5.26) present the low frequency, the high frequency and the ratio of low frequency to high frequency as obtained by summing the areas under the curves in the LF and HF bands at each instant of time throughout the whole experiment period. The odd figures (5.19, 5.21, 5.23, 5.25 and 5.27) present the normalized low frequency, the normalized high frequency and the normalized ratio of the low frequency to high frequency. The normalized LF and HF activity plots are obtained by dividing at each instant of time the LF and HF power by the sum of both as follows:

$$NLF = \frac{LF}{LF + HF} \quad \text{and} \quad NHF = \frac{HF}{LF + HF}$$

These figures basically show that at rest, the trend of the relative power is higher in the high frequency range than in the low frequency range. In addition, the oscillation in the HF range is more than double the oscillation in the LF range. Fast oscillation in the HF range indicates that the parasympathetic activity of the COPD subject had to make faster and more regular adjustments to sustain the resting state and at the same time to compensate for the higher than normal breathing rate that contributes to more power in the HF range. The ratio of the LF to HF emphasizes the dominance of the LF activity during rest even though there is a regular compensation in the HF activity due to higher respiration rate.

Figures 5.18 – 5.27 replicate the same findings using the Morlet, Meyer, dB4, Mexican Hat and Haar wavelet. The differences between these wavelets relate back to the properties of the mother wavelet. The Mexican Hat and the Haar wavelets still present the cross-term interference problem. The dB4 is the higher order Haar wavelet that improves the cross-term a little. However, the clarity of presentation and the smoothest display of Morlet wavelet have demonstrated its use as a suitable HRV time-frequency analysis method.

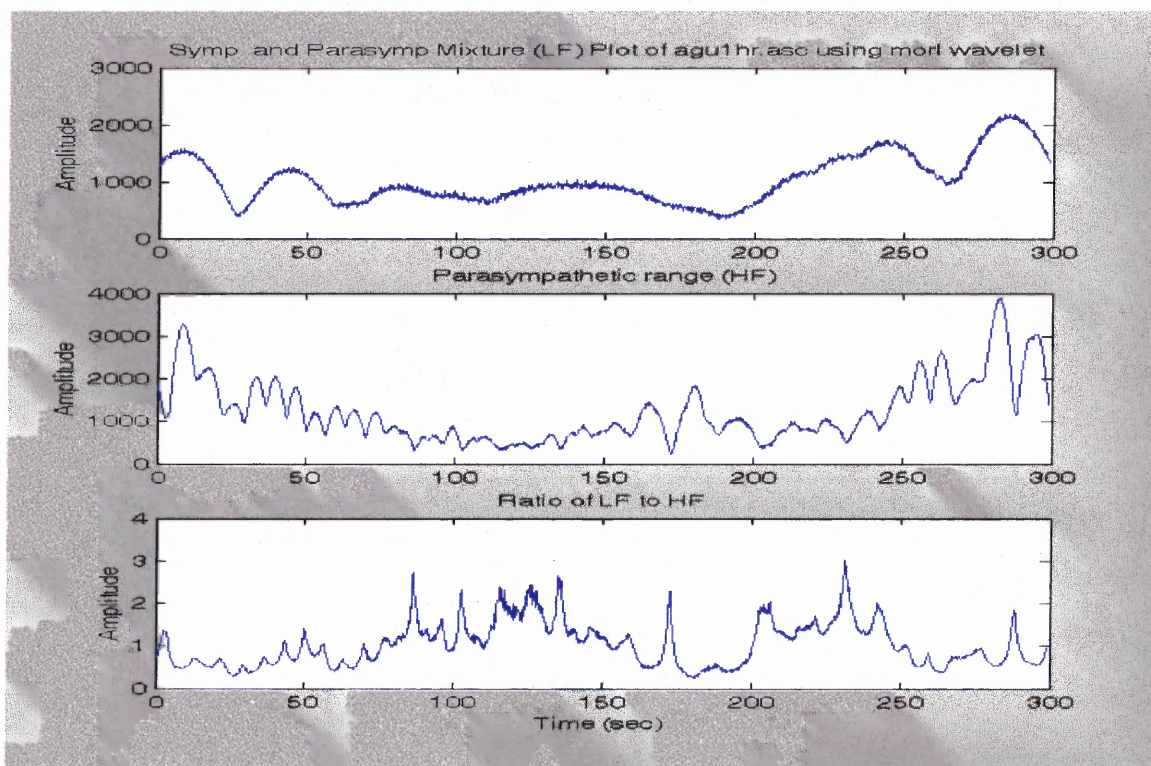


Figure 5.18 Sympathetic and parasympathetic mixture plots of HR using Morlet wavelet (COPD subject in 5 min rest, breathing at 16bpm).

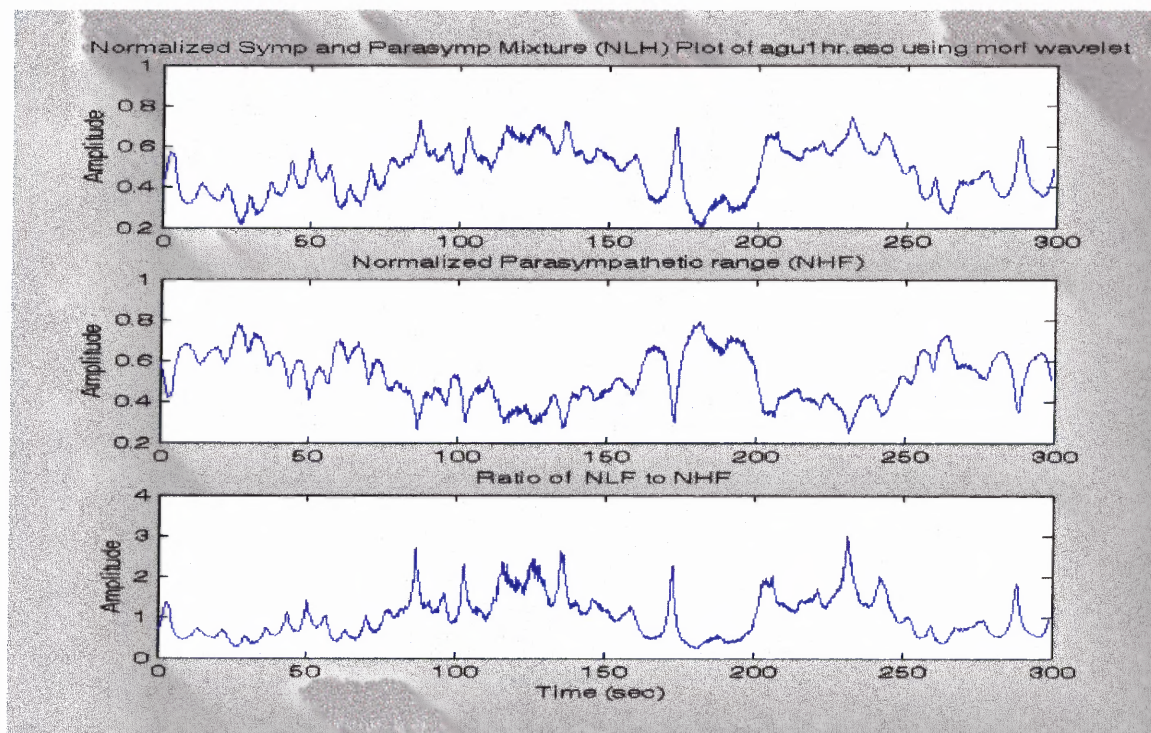


Figure 5.19 Normalized sympathetic and parasympathetic mixture plots of HR using Morlet wavelet (COPD subject in 5 min rest, breathing at 16bpm).

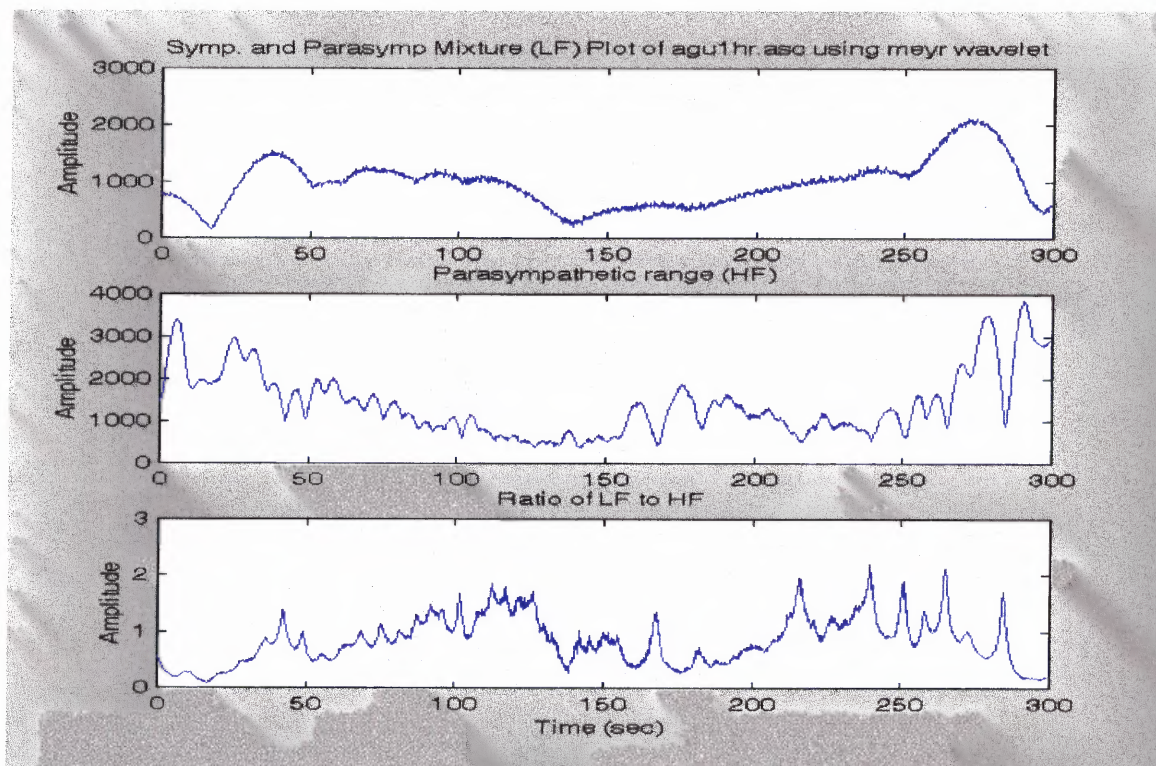


Figure 5.20 Sympathetic and parasympathetic mixture plots of HR using Meyer wavelet (COPD subject in 5 min rest, breathing at 16bpm).

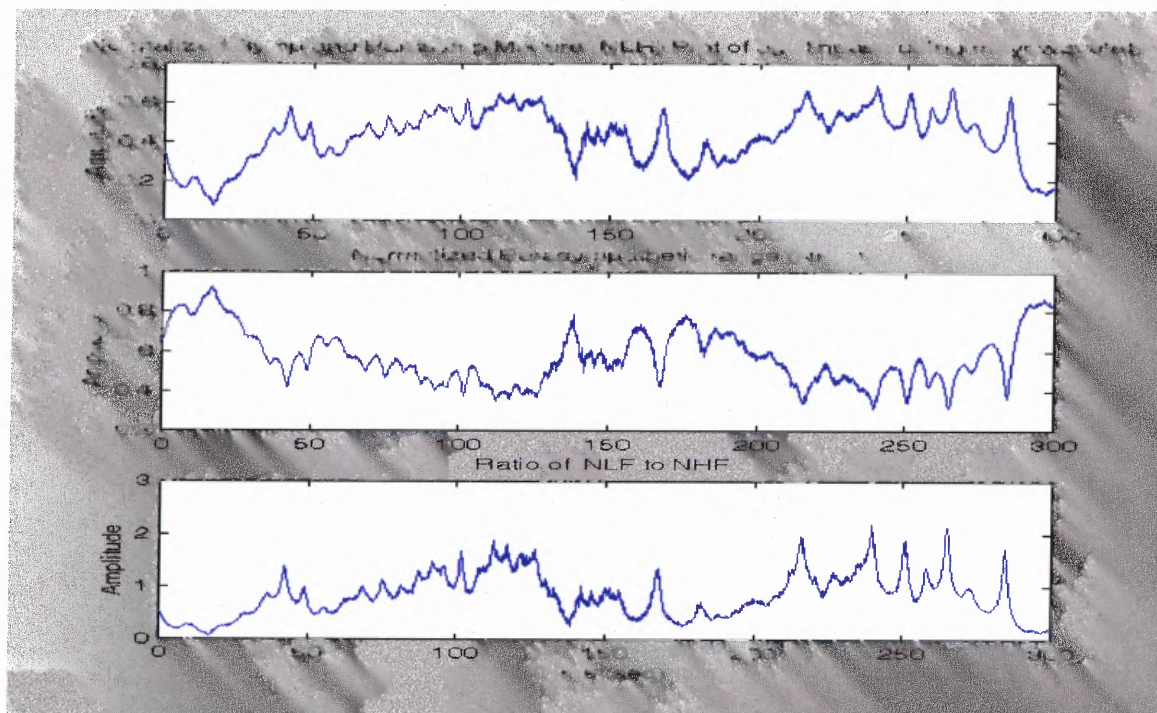


Figure 5.21 Normalized sympathetic and parasympathetic mixture plots of HR using Meyer wavelet (COPD subject in 5 min rest, breathing at 16bpm).

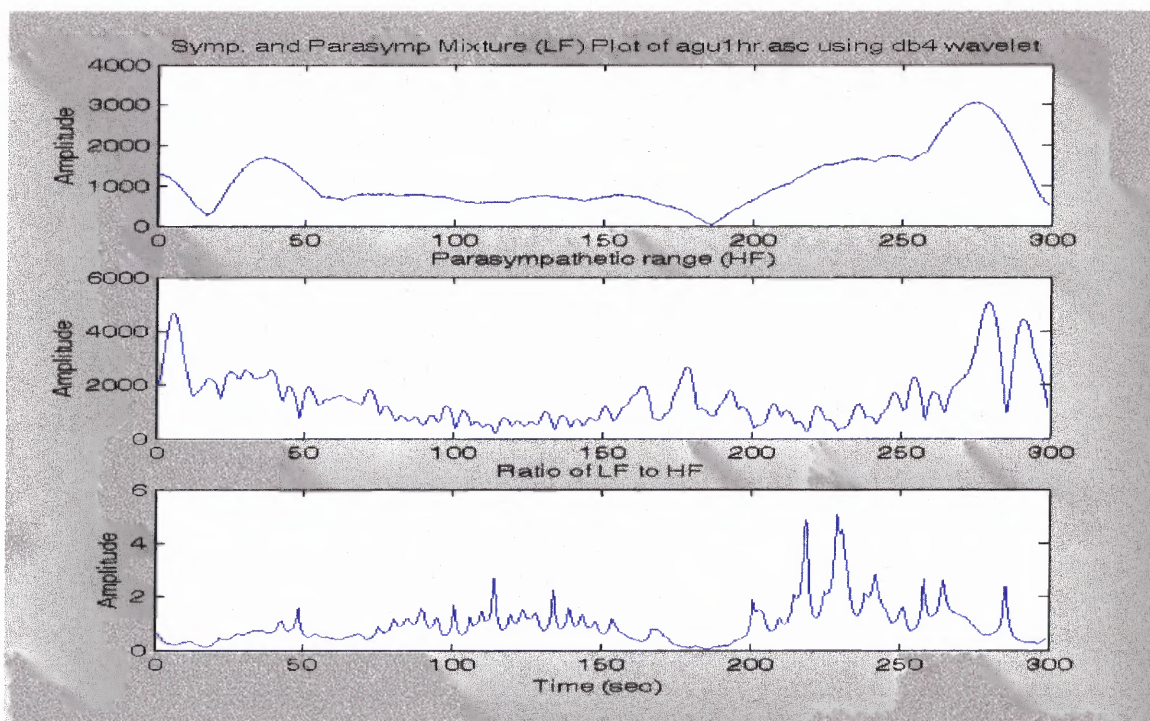


Figure 5.22 Sympathetic and parasympathetic mixture plots of HR using Daubechies 4 wavelet (COPD subject in 5 min rest, breathing at 16bpm).

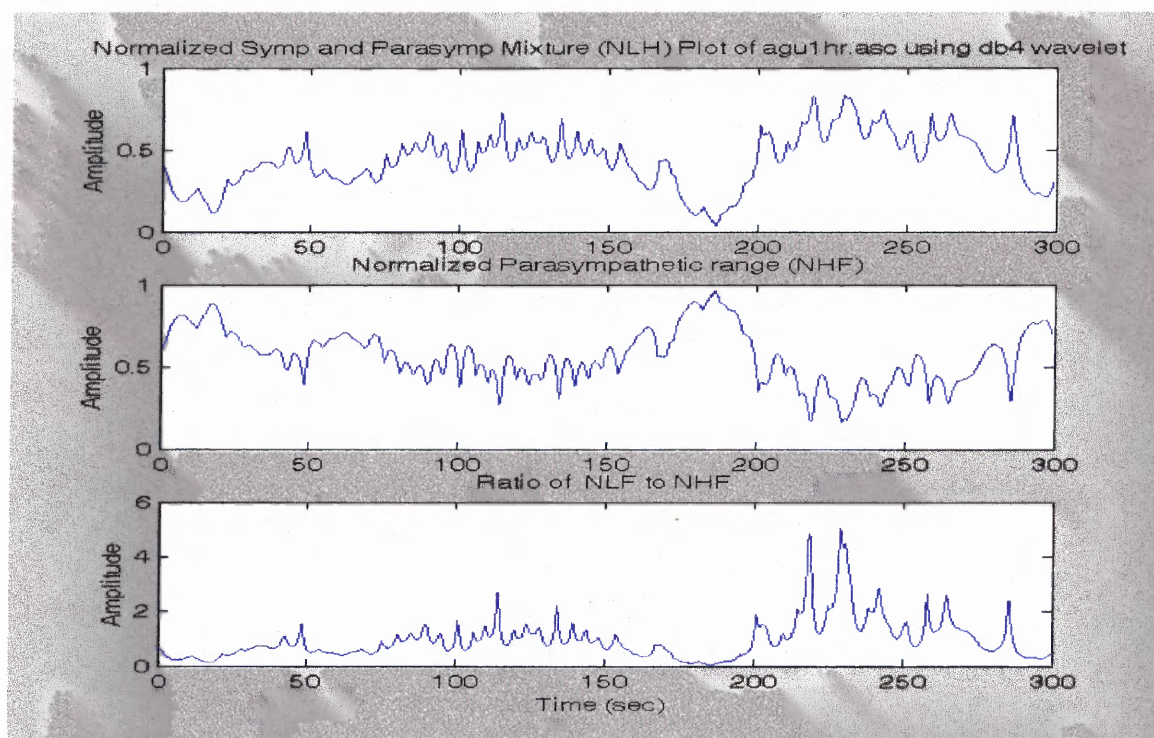


Figure 5.23 Normalized sympathetic and parasympathetic mixture plots of HR using Daubechies 4 wavelet (COPD subject in 5 min rest, breathing at 16bpm).

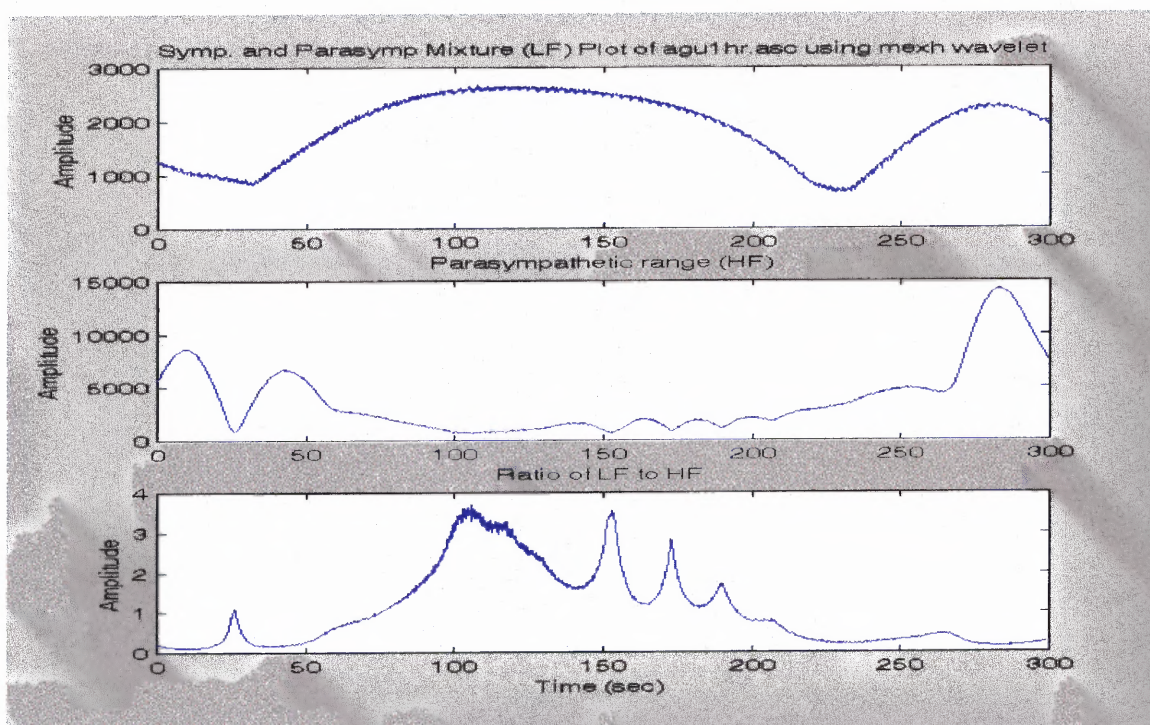


Figure 5.24 Sympathetic and parasympathetic mixture Plots of HR using Mexican Hat wavelet (COPD subject in 5 min rest, breathing at 16bpm).

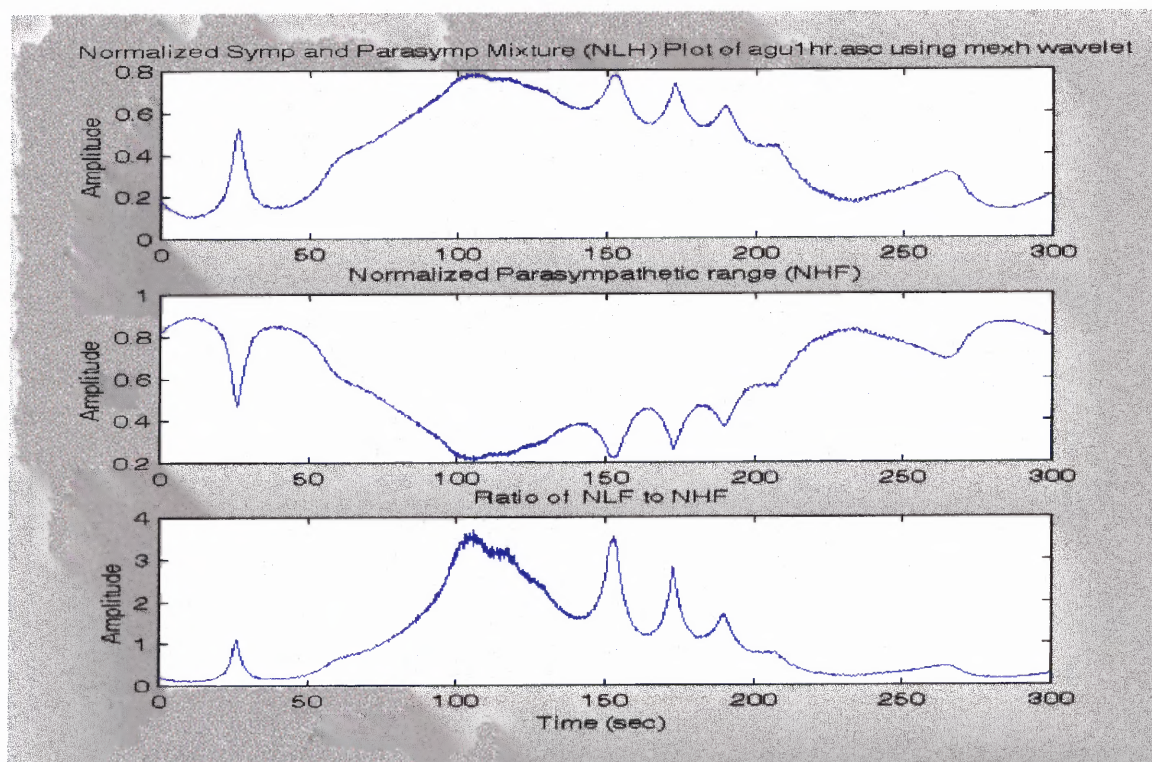


Figure 5.25 Normalized sympathetic and parasympathetic mixture plots of HR using Mexican Hat wavelet (COPD subject in 5 min rest, breathing at 16bpm).

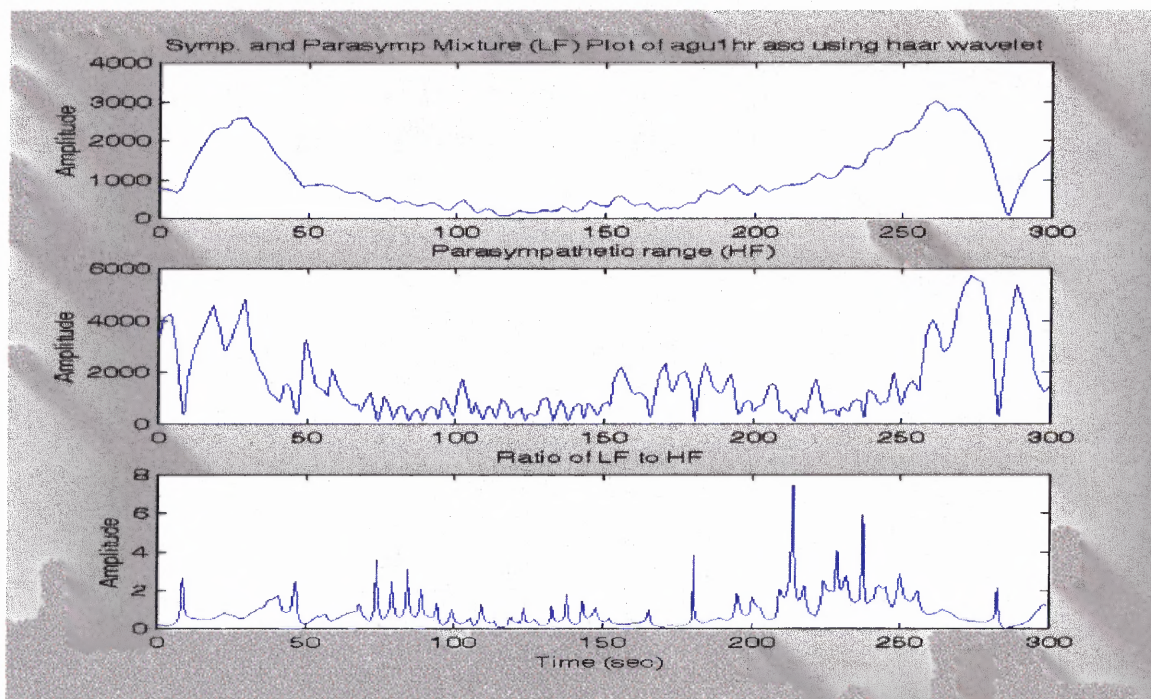


Figure 5.26 Sympathetic and parasympathetic mixture plots of HR using Haar wavelet (COPD subject in 5 min rest, breathing at 16bpm).

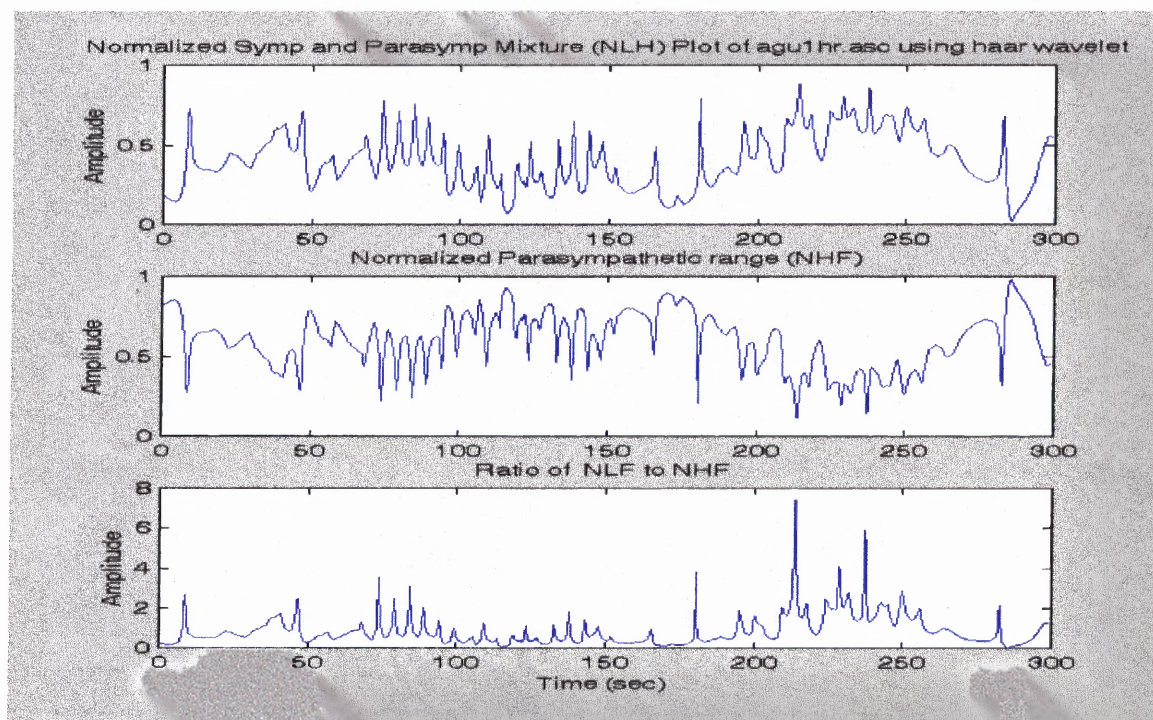


Figure 5.27 Normalized sympathetic and parasympathetic mixture plots of HR using Haar wavelet (COPD subject in 5 min rest, breathing at 16bpm).

5.2.7 Time-Frequency Analysis (Wavelet) of Blood Pressure Variability

In order to experiment with analyzing COPD BPV signals, the BP IIBI signal is used. One example of the BP IIBI signals is from a COPD subject resting and paced-breathing at 16 breaths per minute. Figure 5.28 illustrates the BP IIBI and its power spectrum plots for the case of a file from a COPD subject paced breathing at 16 bpm during a 5 minutes rest period. The BP analysis was also performed using the five different wavelet distributions (Morlet, Meyer, Daubechies 4, Mexican Hat and Haar) with the same specifications (length of analysis window equals to 200 and the length of FFT analysis of 256).

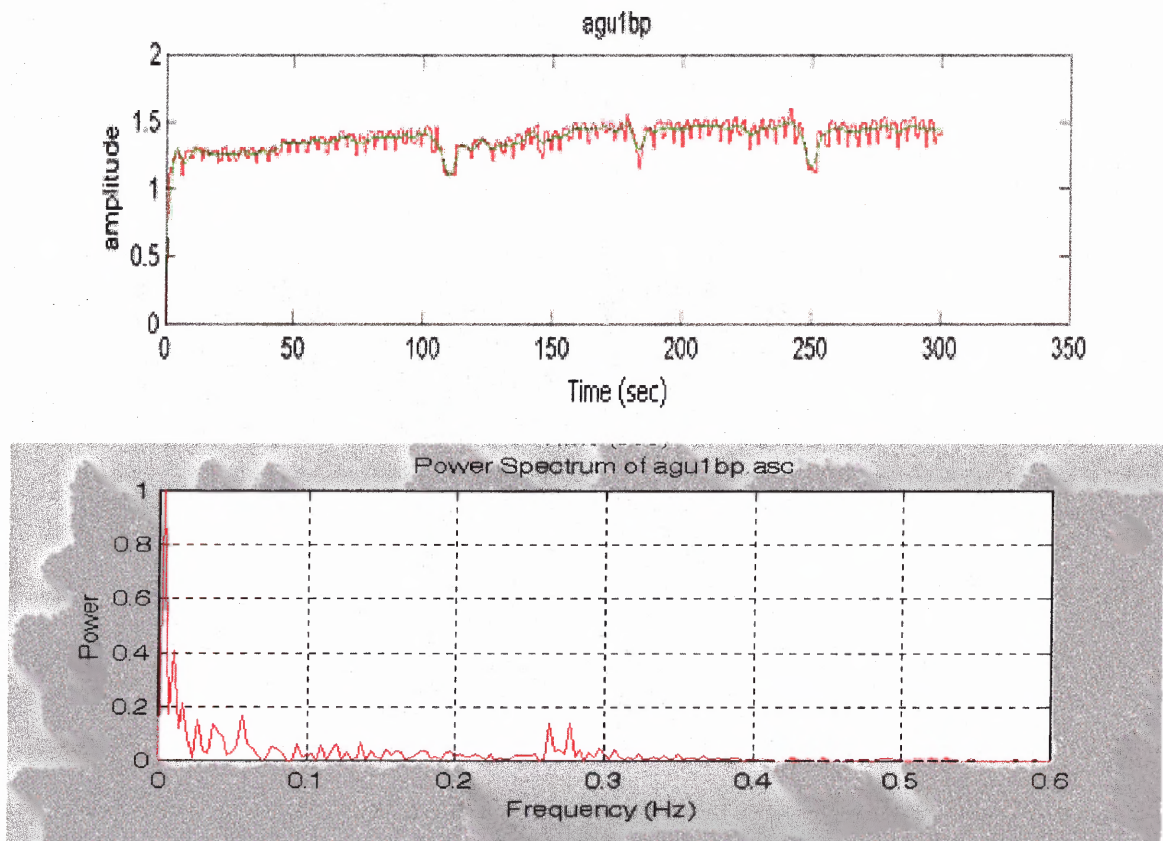


Figure 5.28 Plot of blood pressure IBI and its power spectrum using Fourier transform.

The purpose of this is to show that, although the output for different wavelets varies, the fundamental characteristics of the wavelet transform are the same. Figure 5.29 – 5.33 show the results of these transforms. A band of cones of influence corresponding to each minima and maxima on the BP IIBI signal at the frequency of respiration (16 bpm, 0.266667 Hz) appears in each wavelet transform representation. In addition, the power intensity of the band is as high as the similar band shown in the normal subject case investigated in section 5.2.2. Another band of cones of influence in the very low frequency range (0.01 – 0.15 Hz) also exists with high energy and in longer time (from 10 seconds to 120 seconds, to 180 seconds, to 250 seconds). This matches the trend of the blood pressure IIBI signal that can be seen in figure 5.28 (top panel, signal in green). Among the wavelets, the Morlet wavelet again provides the best representation in terms of time, frequency resolution and meaningful details. The band of the cones of influence at 0.266667 Hz modulated slightly indicating that the BPV is also dominated by the respiration signal and is also not a stationary signal.

There are also many interesting observations unveiled from the data and the experimental setup of the normal and COPD subjects. The first was the interplay of the two opposing physiological factors that were simultaneously revealed in the time-frequency analysis of the heart rate variability signal during stressful exercise conditions for normal subjects and during rest for COPD patients. Another was the compensation of the HR in COPD by having a cyclic modulation at about 4 to 5 minutes while normal subjects took longer to have these HR modulations and in a more random nature.

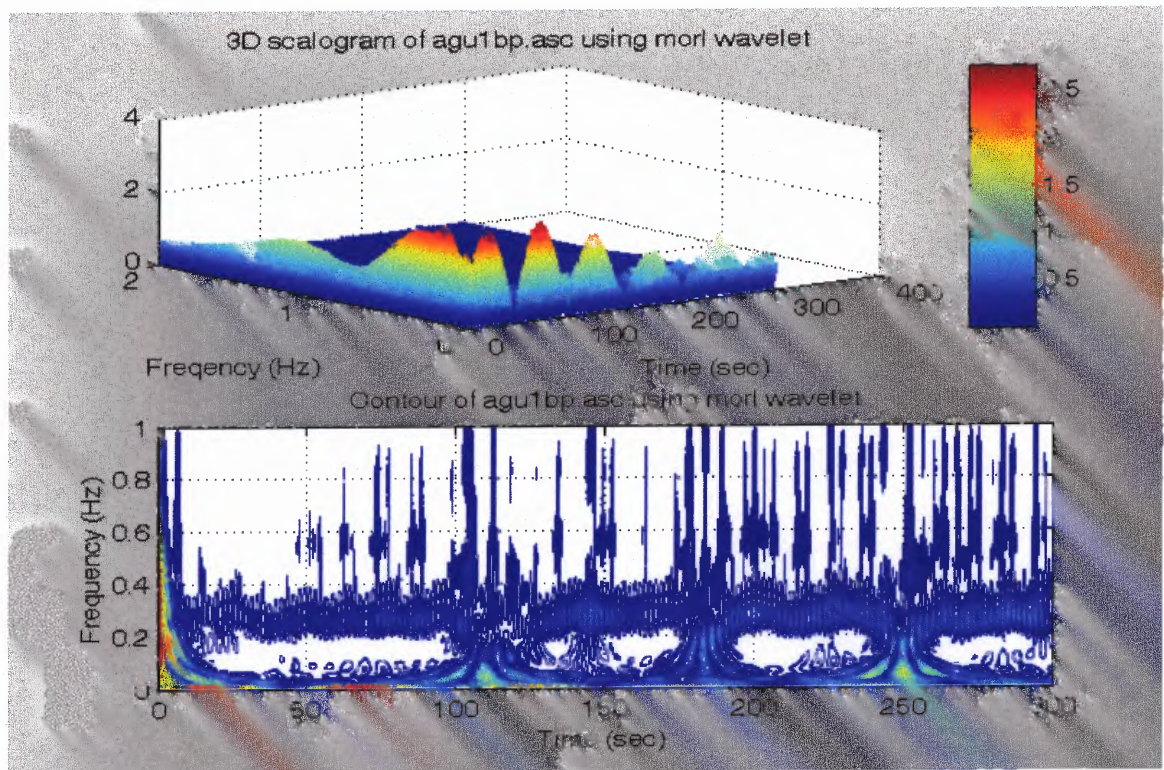


Figure 5.29 3D and contour plot of blood pressure spectrum using Morlet wavelet.

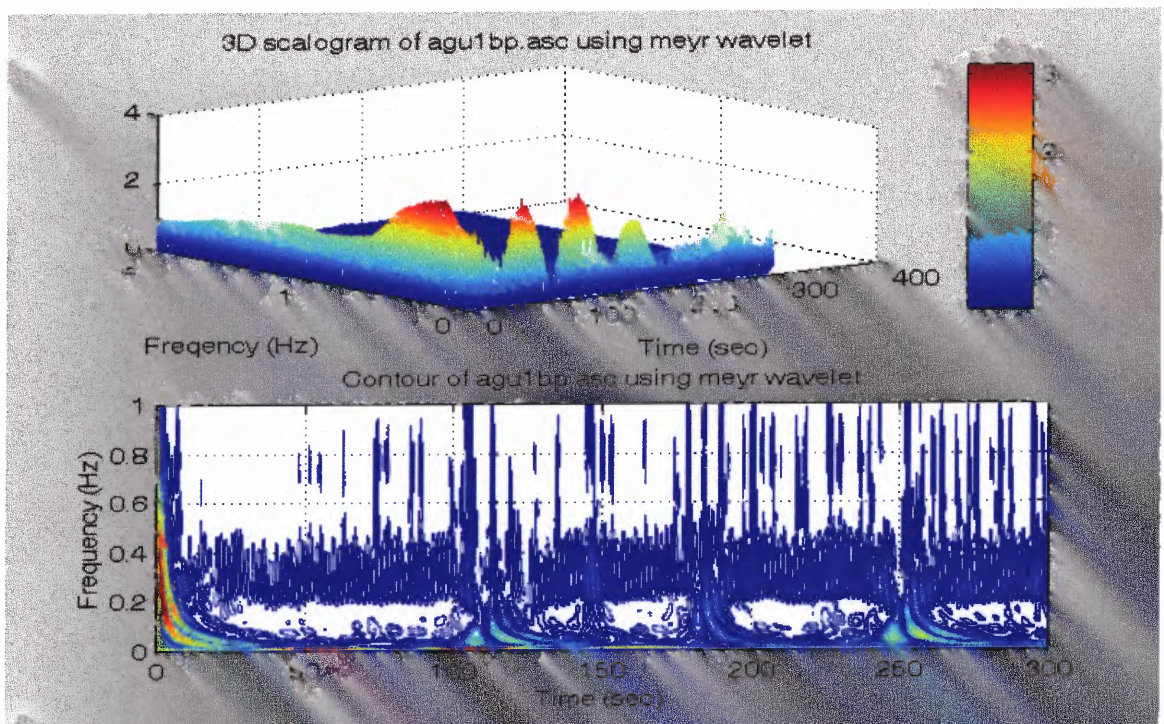


Figure 5.30 3D and contour plot of blood pressure spectrum using Meyer wavelet.

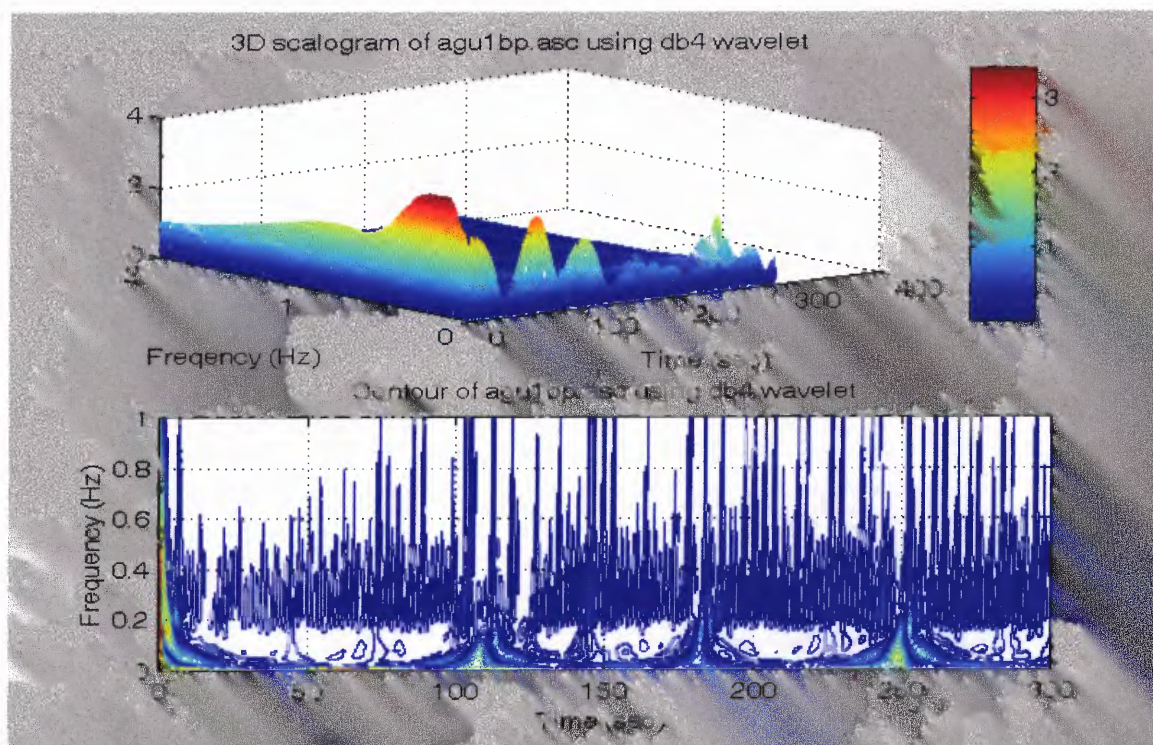


Figure 5.31 3D and contour plot of blood pressure spectrum using DB4 wavelet.

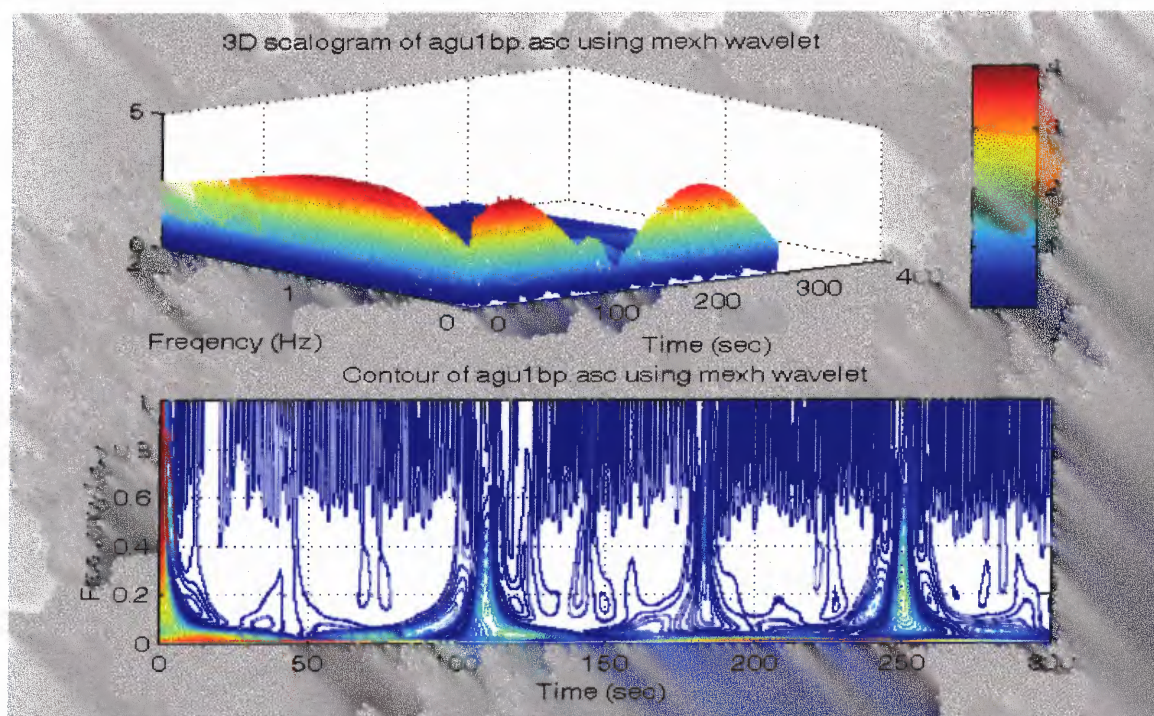


Figure 5.32 3D and contour plot of blood pressure spectrum using Mexican Hat wavelet.

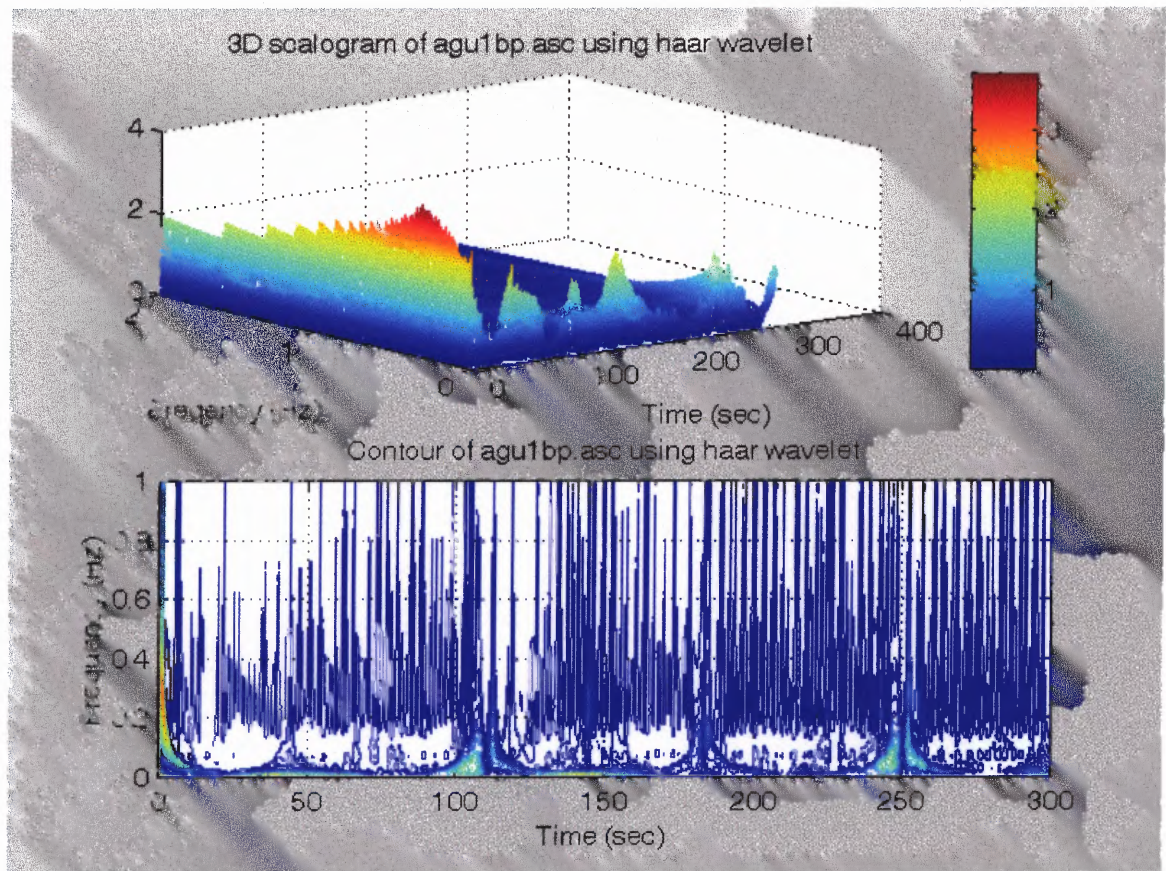


Figure 5.33 3D and contour plot of blood pressure spectrum using Haar wavelet.

Figures 5.34 – 5.43 display the 5-minute BPV activity plots of a COPD subject at rest breathing at 16 breaths per minute using the Morlet, Meyer, Daubechies 4, Mexican Hat and Haar wavelet. The figures present the non-normalized and the normalized low frequency, the high frequency and the ratio of low frequency to high frequency activity plots. At rest, the trend of the relative power is much higher in the high frequency range than in the low frequency range. However, the parasympathetic relative power cycles from high to low in two minutes and then repeats. While the LF and HF plots are different, the plots of the ratio of the LF to HF for BPV are similar to those ratio plots for HRV of the same COPD subject.

The activity plots for BPV using the Morlet, Meyer, dB4, Mexican Hat and Haar wavelet all show similar trend. The non-normalized plots paint a better picture of what is happening. The LF starts out high and decreases to near zero in about 2 minutes, then changes direction trying to get back to the beginning state. The HF also starts out high but decreases to near zero value in half the time as the LF and stays near zero for almost 4 minutes before heading back up to the beginning state. All the normalized plots of LF and HF show mirror images but totally opposite of each other. The LF/HF ratio plots all start near zero indicating that there is stronger parasympathetic effect at the beginning. However, the sympathovagal balance tries to reach to a level of twice that of the vagal tone for almost the entire 5-minute session.

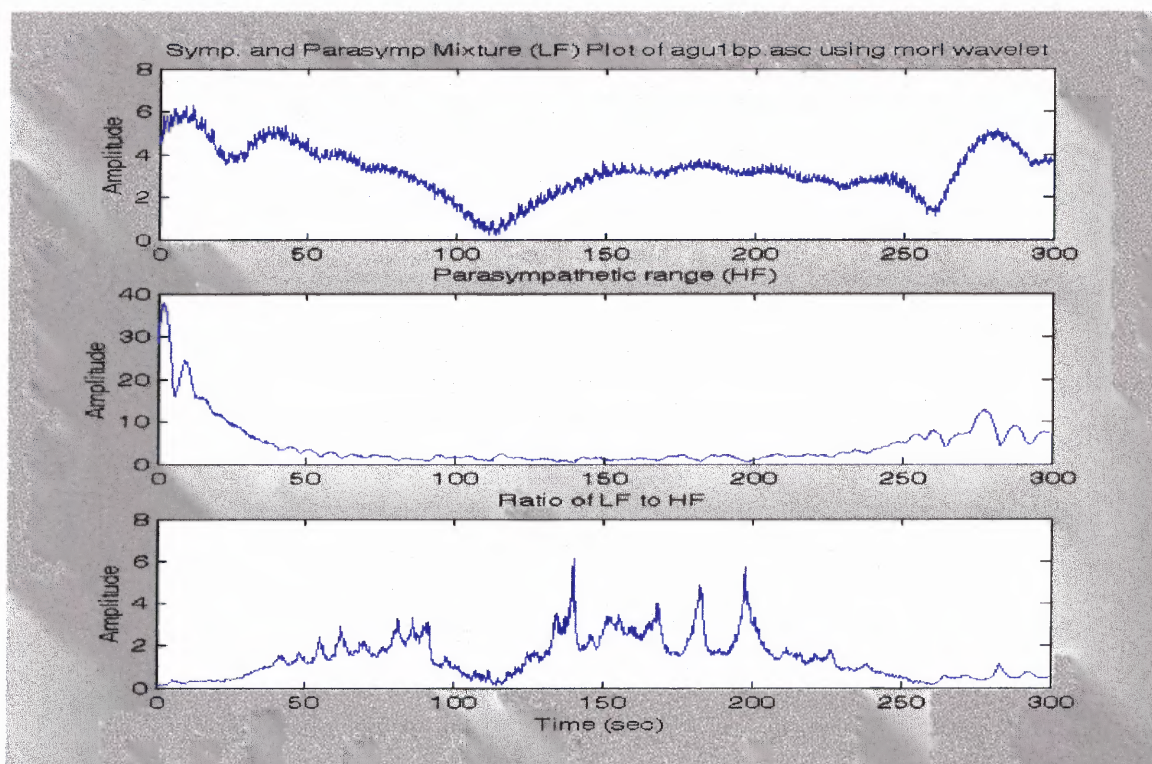


Figure 5.34 Sympathetic and parasympathetic mixture plots of BP using Morlet wavelet.

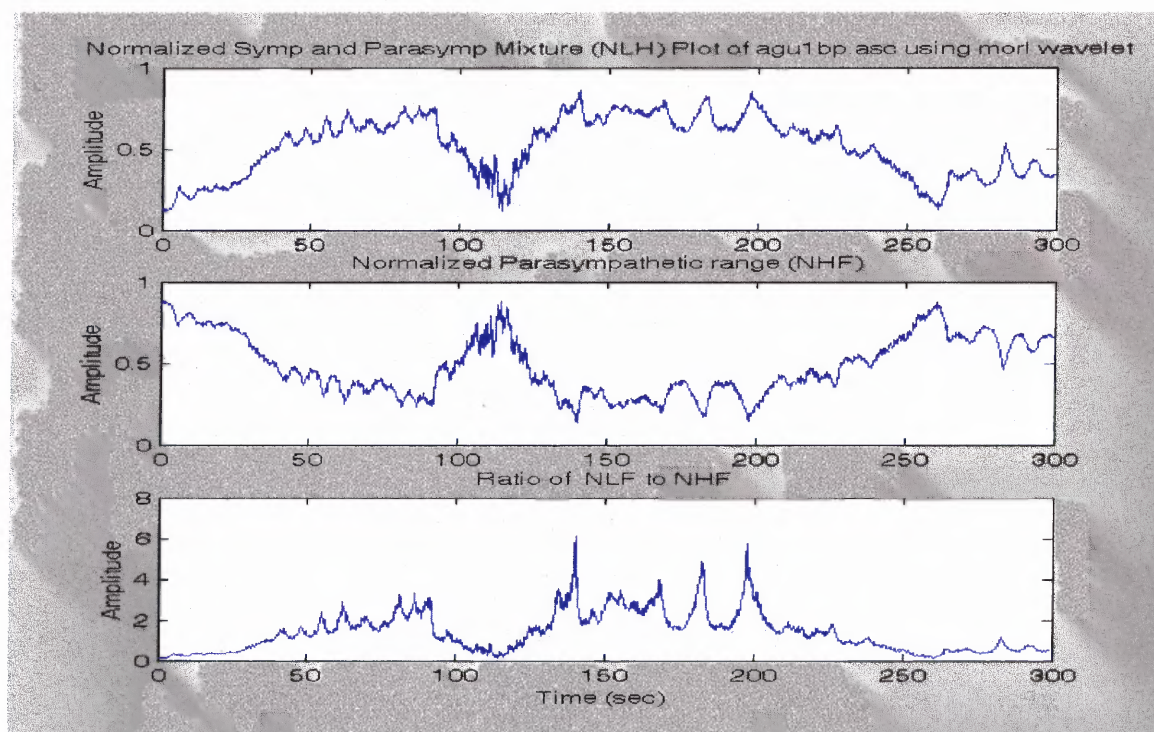


Figure 5.35 Normalized sympathetic and parasympathetic mixture plots of BP using Morlet wavelet.

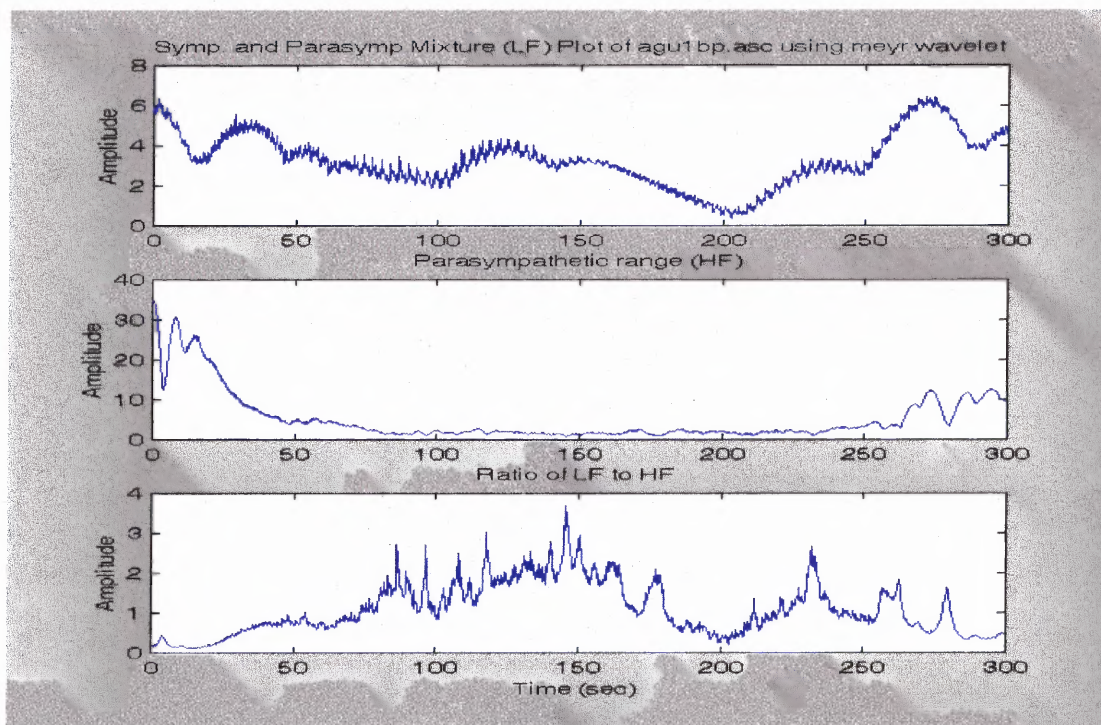


Figure 5.36 Sympathetic and parasympathetic mixture plots of BP using Meyer wavelet.

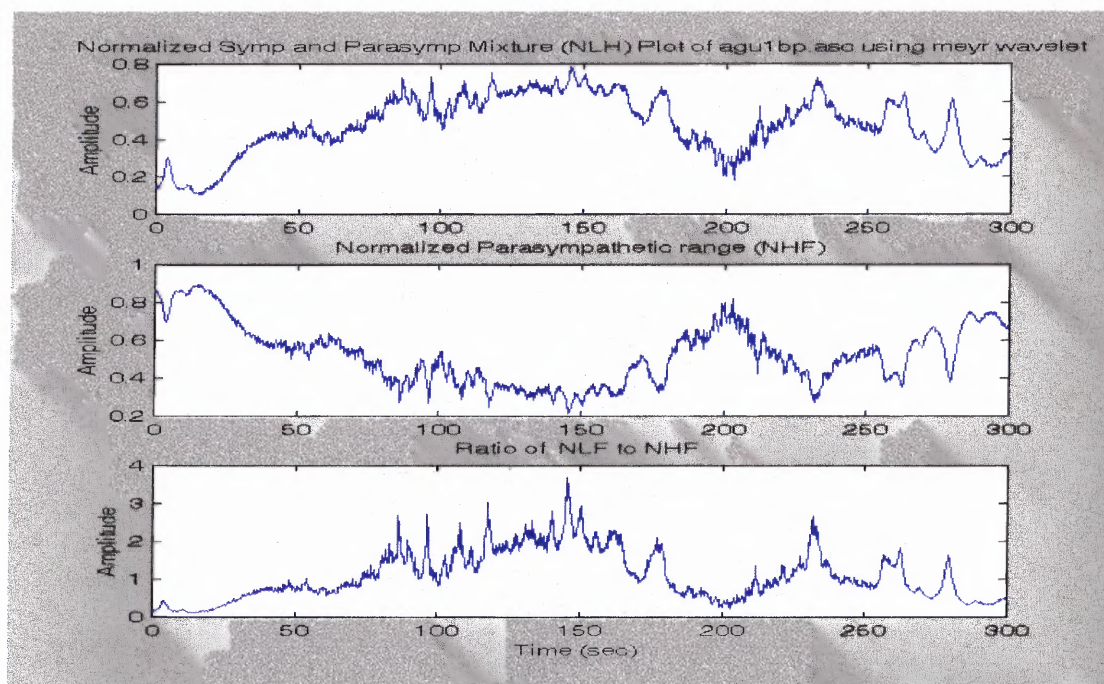


Figure 5.37 Normalized sympathetic and parasympathetic mixture plots of BP using Meyer wavelet.

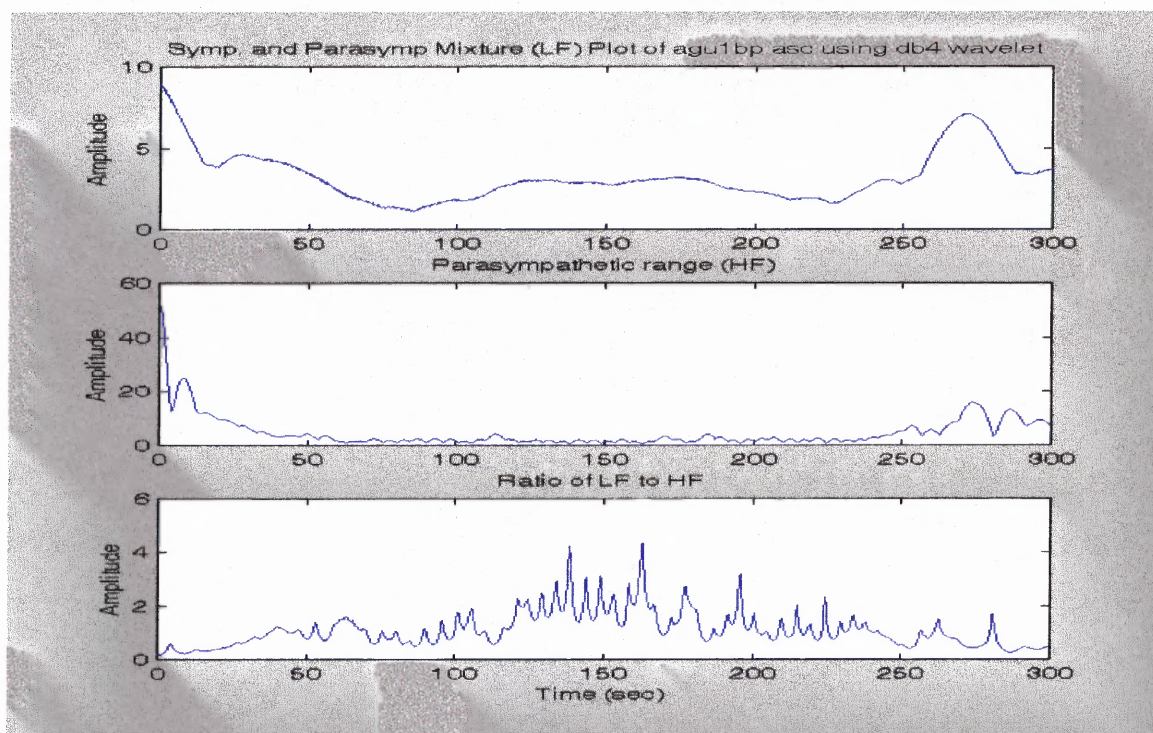


Figure 5.38 Sympathetic and parasympathetic mixture plots of BP using Daubechies 4 wavelet.

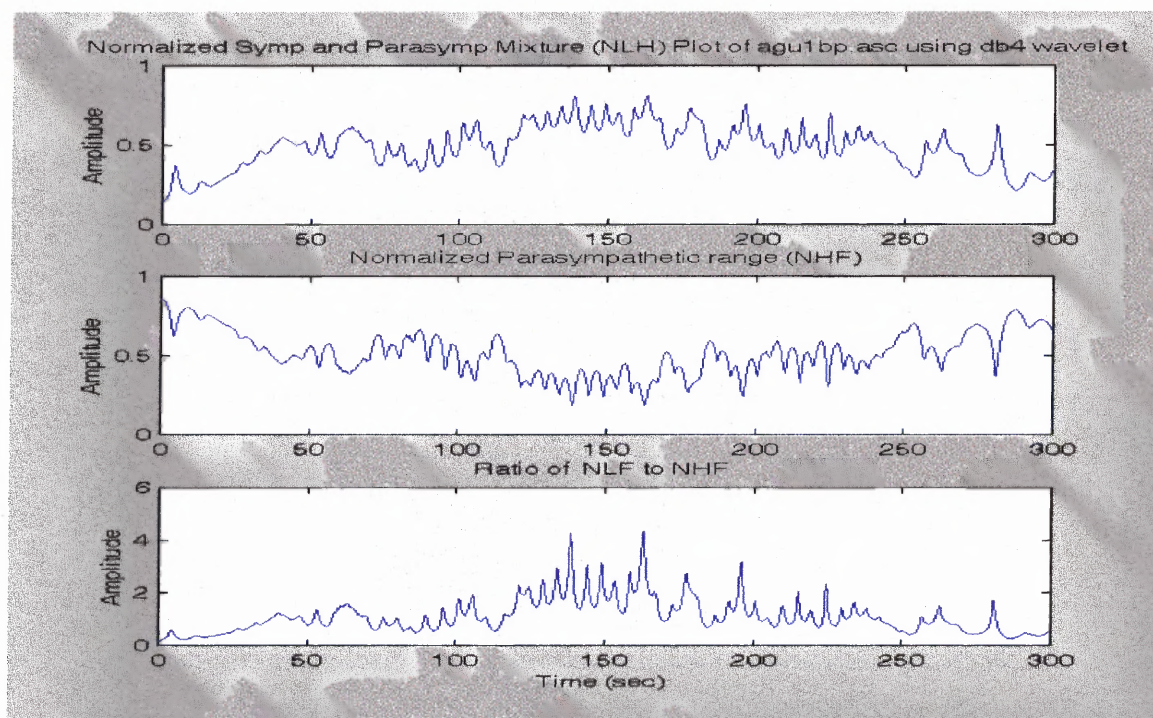


Figure 5.39 Normalized sympathetic and parasympathetic mixture plots of BP using Daubechies 4 wavelet.

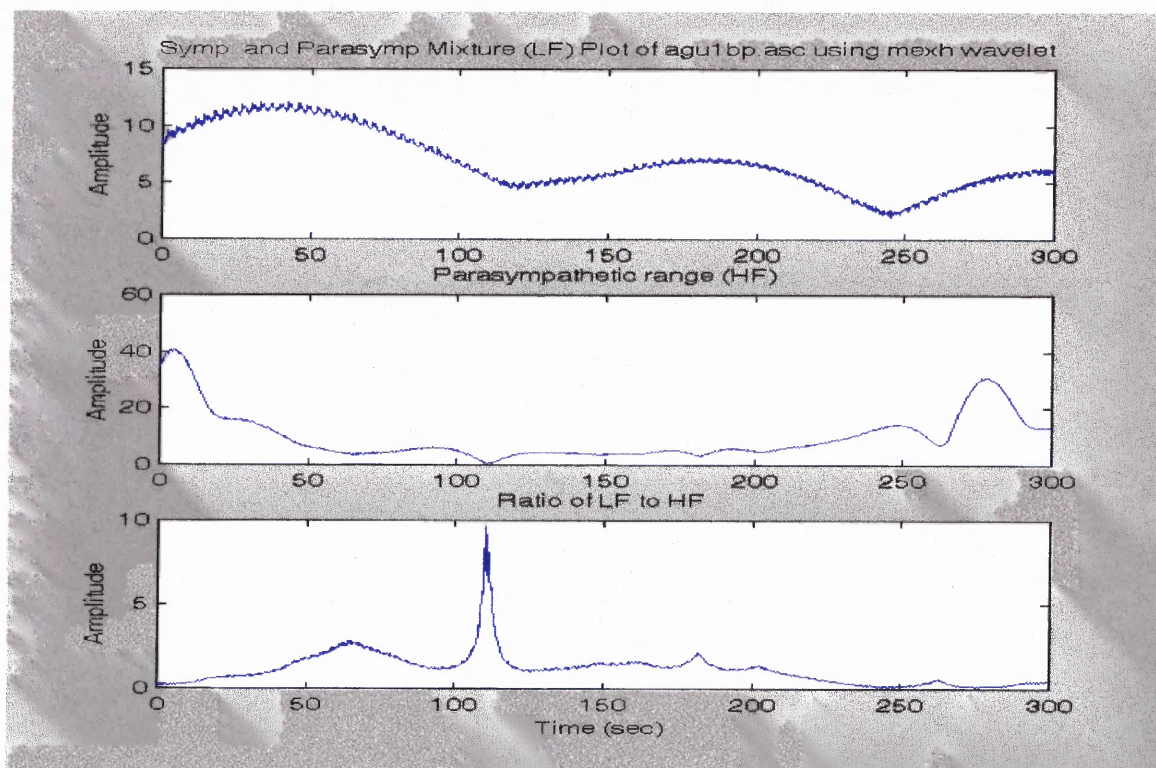


Figure 5.40 Sympathetic and parasympathetic mixture plots of BP using Mexican Hat wavelet.

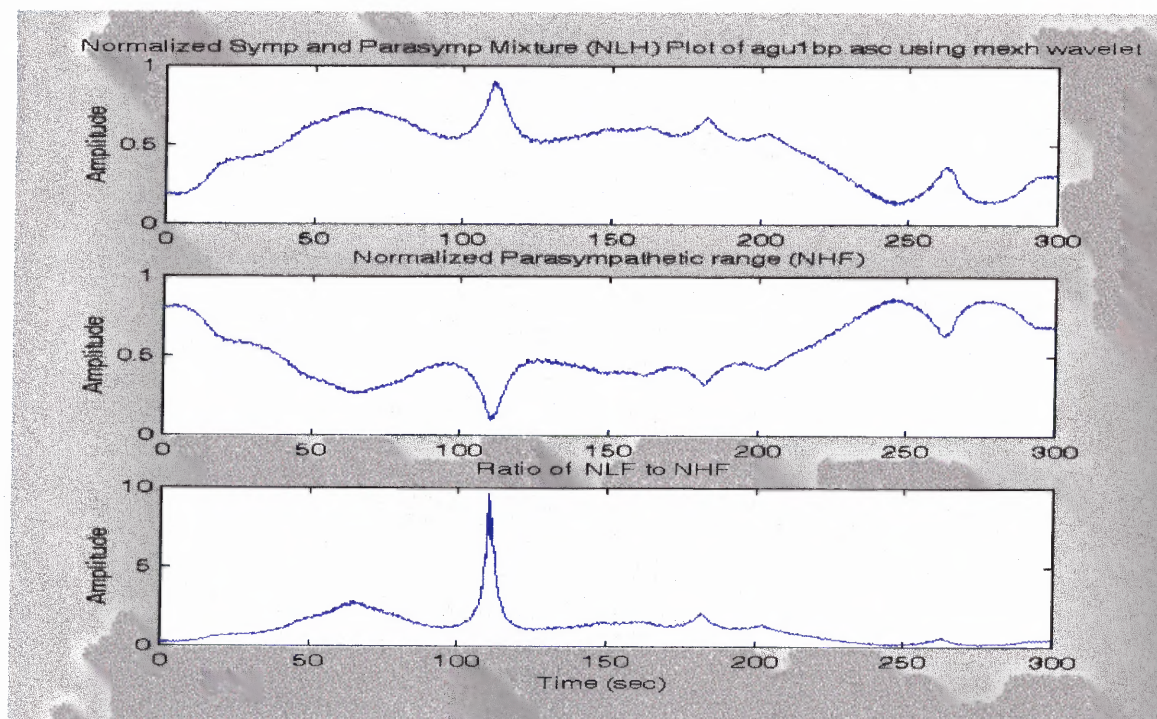


Figure 5.41 Normalized sympathetic and parasympathetic mixture plots of BP using Mexican Hat wavelet.

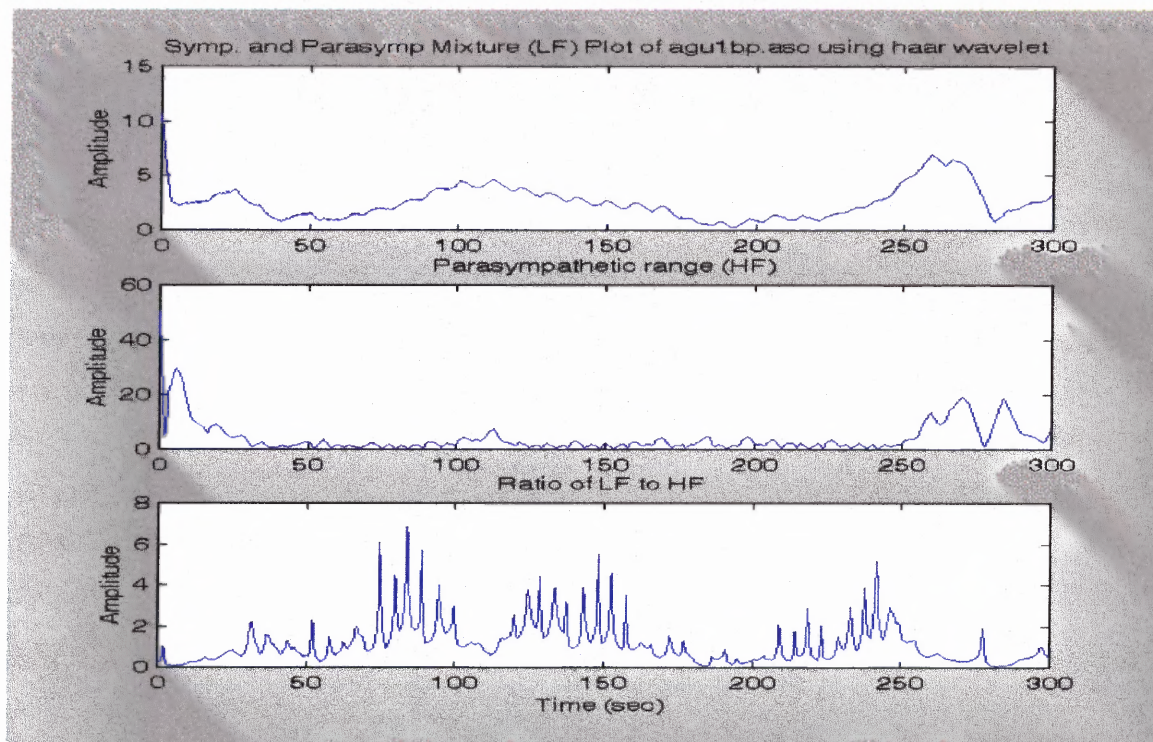


Figure 5.42 Sympathetic and parasympathetic mixture plots of BP using Haar wavelet.

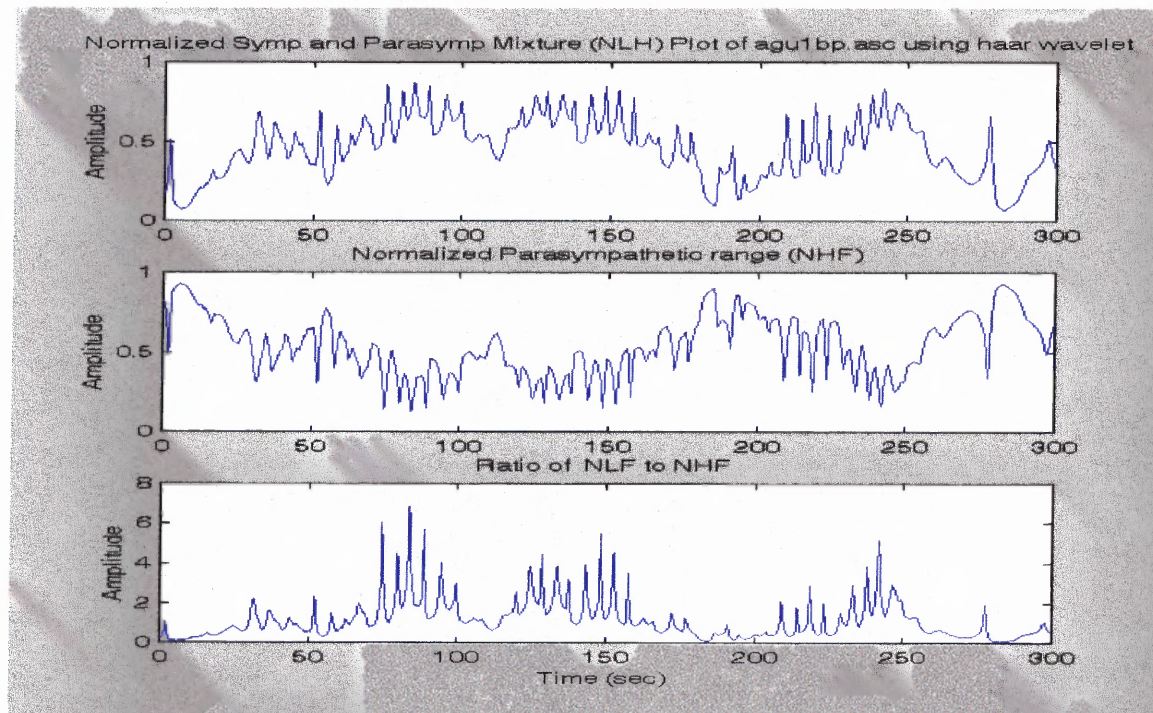


Figure 5.43 Plot of normalized LF, HF, and sympathovagal balance of blood pressure using Haar wavelet.

5.3 Coherence/Partial (Weighted) Coherence Analysis of Heart Rate Study

The typical results of the cross-spectral analysis for a subject (either normal or COPD) are shown in Figures 5.44 - 5.46. The first two panels of figure 5.44 are the plots of the raw respiration and ECG signals, respectively. The third panel is the heart rate IBI obtained from the ECG. The fourth and fifth panels show the raw blood pressure and the blood pressure IBI signals. The last two panels are the heart rate and blood pressure spectra, respectively. Figure 5.45 shows the coherence plots of HR & Resp, HR & BP and BP & Resp in the LF range with their weighted coherence values. Figure 5.46 shows the partial coherence plots of HR & Resp, HR & BP and BP & Resp in the LF range with their weighted partial coherence values. Similarly, figures 5.47 and 5.48 show the coherence and partial coherence plots in the HF range, respectively.

The analysis for all 8 normal subjects was performed and tabulated in table 5.2. The results of the coherence/partial (weighted) coherence analysis for all 47 COPD subjects was performed and tabulated in table 5.3.

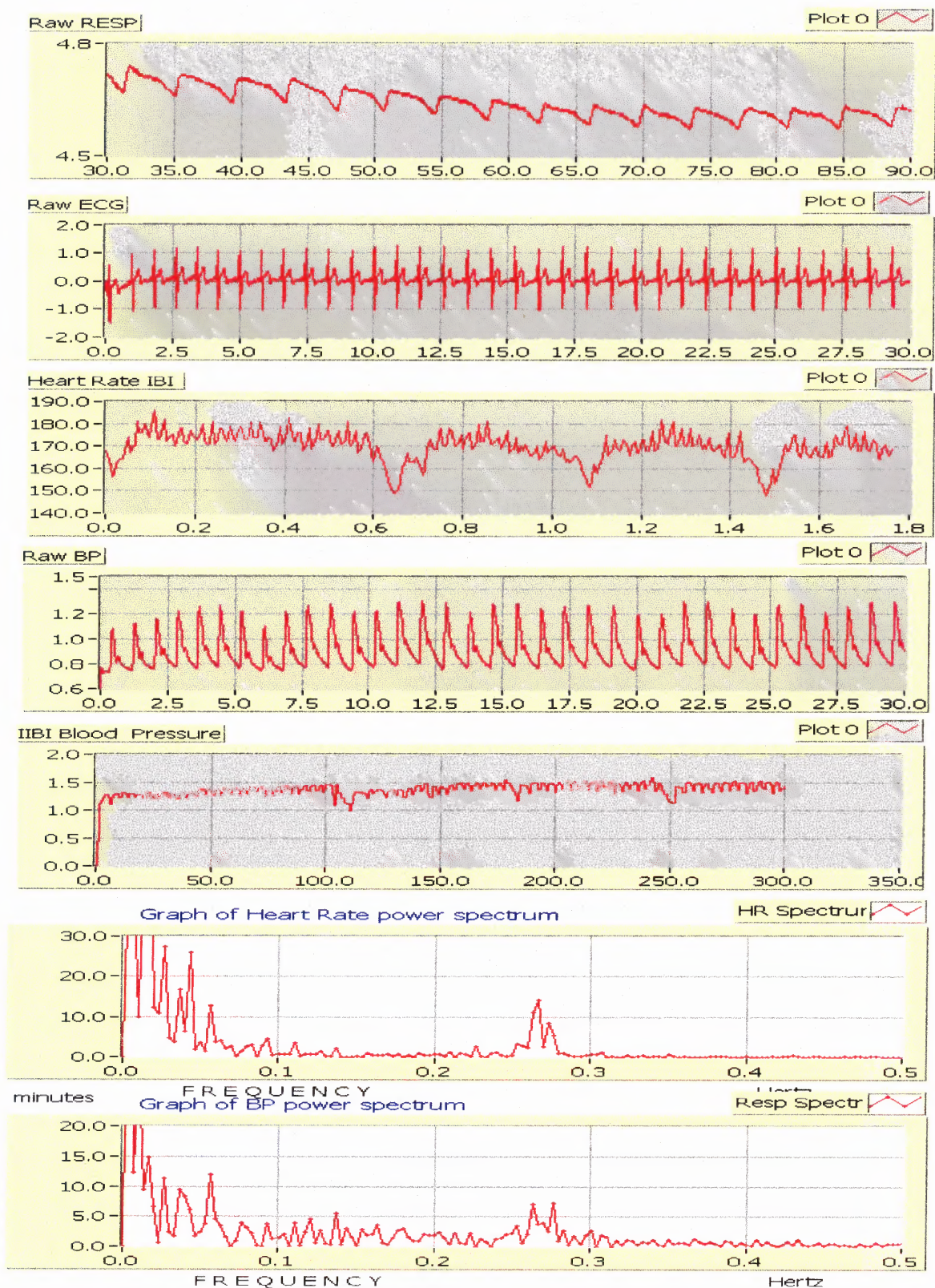


Figure 5.44 Plot of raw respiration, ECG, BP, HR IIBI, BP IIBI, HR and BP power spectrum signals of a subject (COPD subject Agu1), 5 min at rest breathing at 16 bpm.

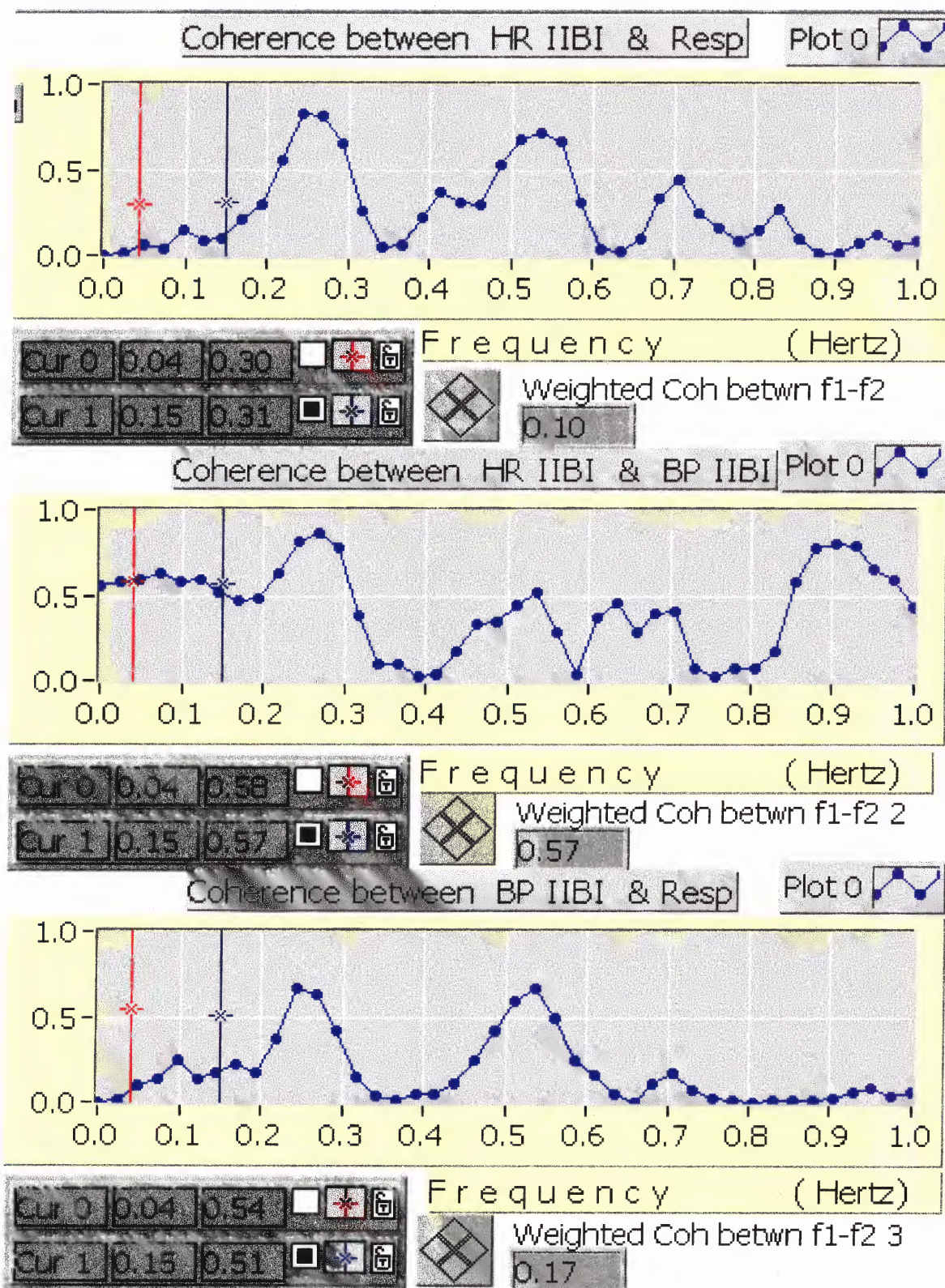


Figure 5.45 The LF coherence plots of a subject (COPD subject Agu1), 5 min at rest breathing at 16 bpm.

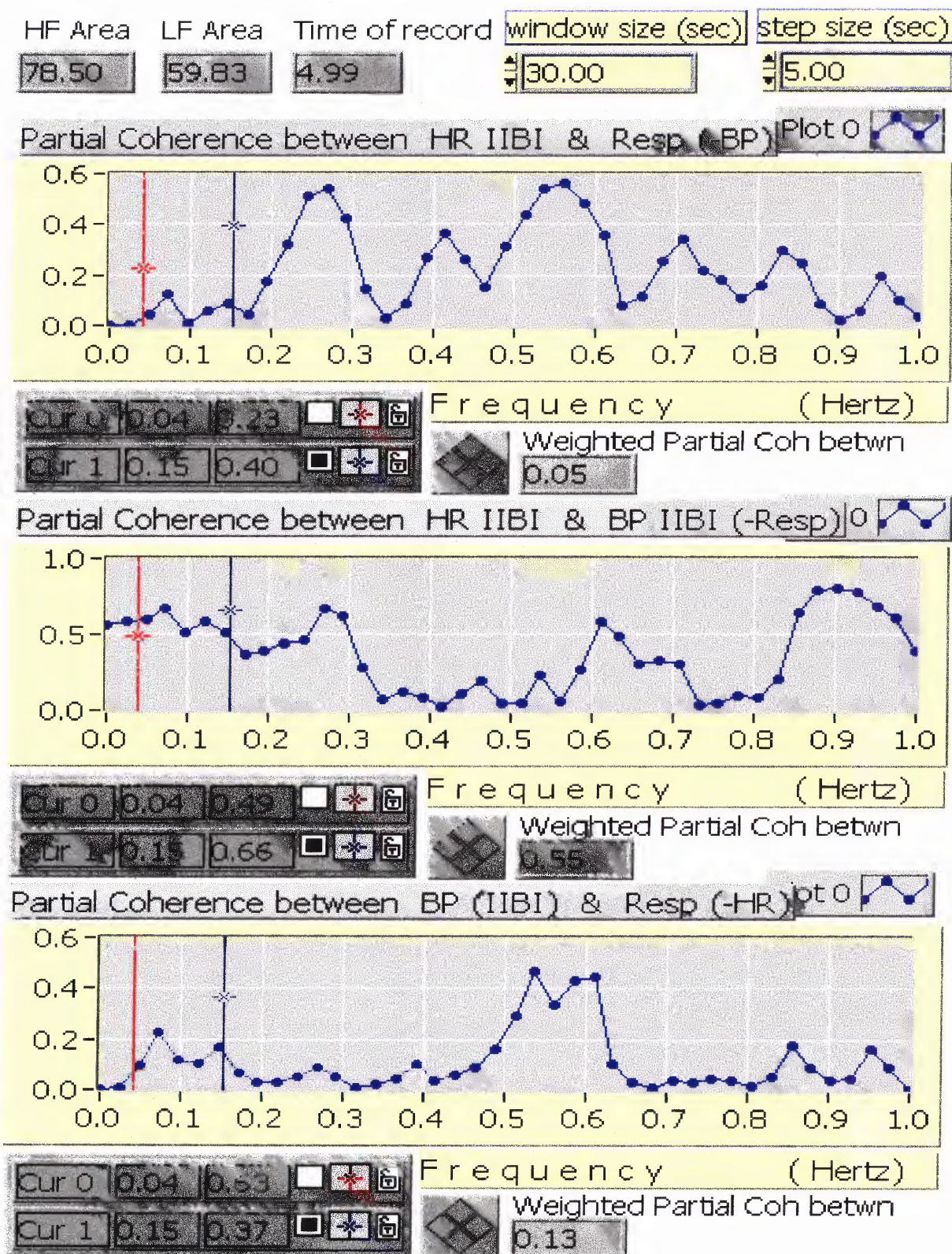


Figure 5.46 The LF partial coherence plots of a subject (COPD subject Agu1), 5 min at rest breathing at 16 bpm.

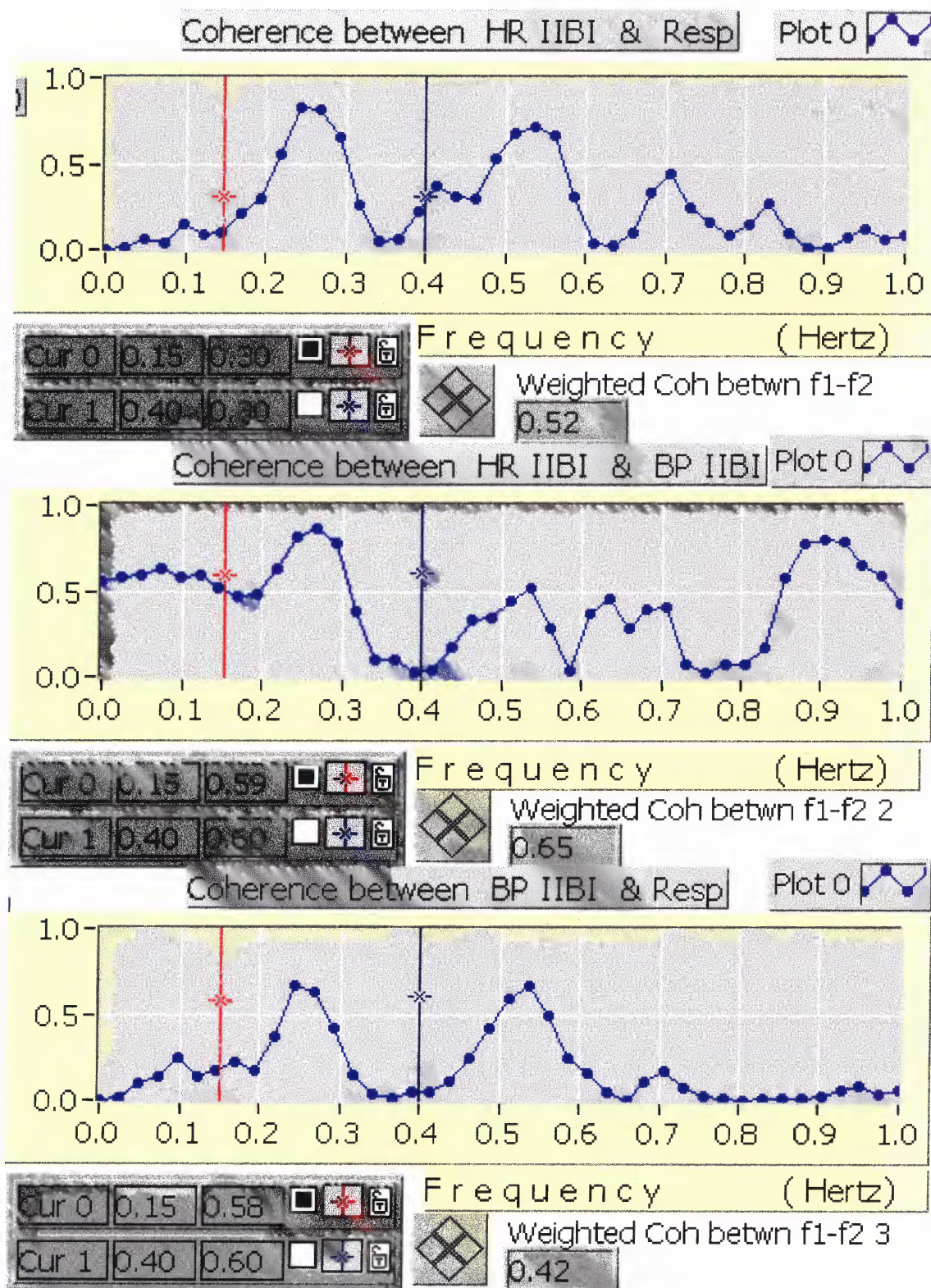


Figure 5.47 The HF coherence plots of a subject (COPD subject Agu1), 5 min at rest breathing at 16 bpm.

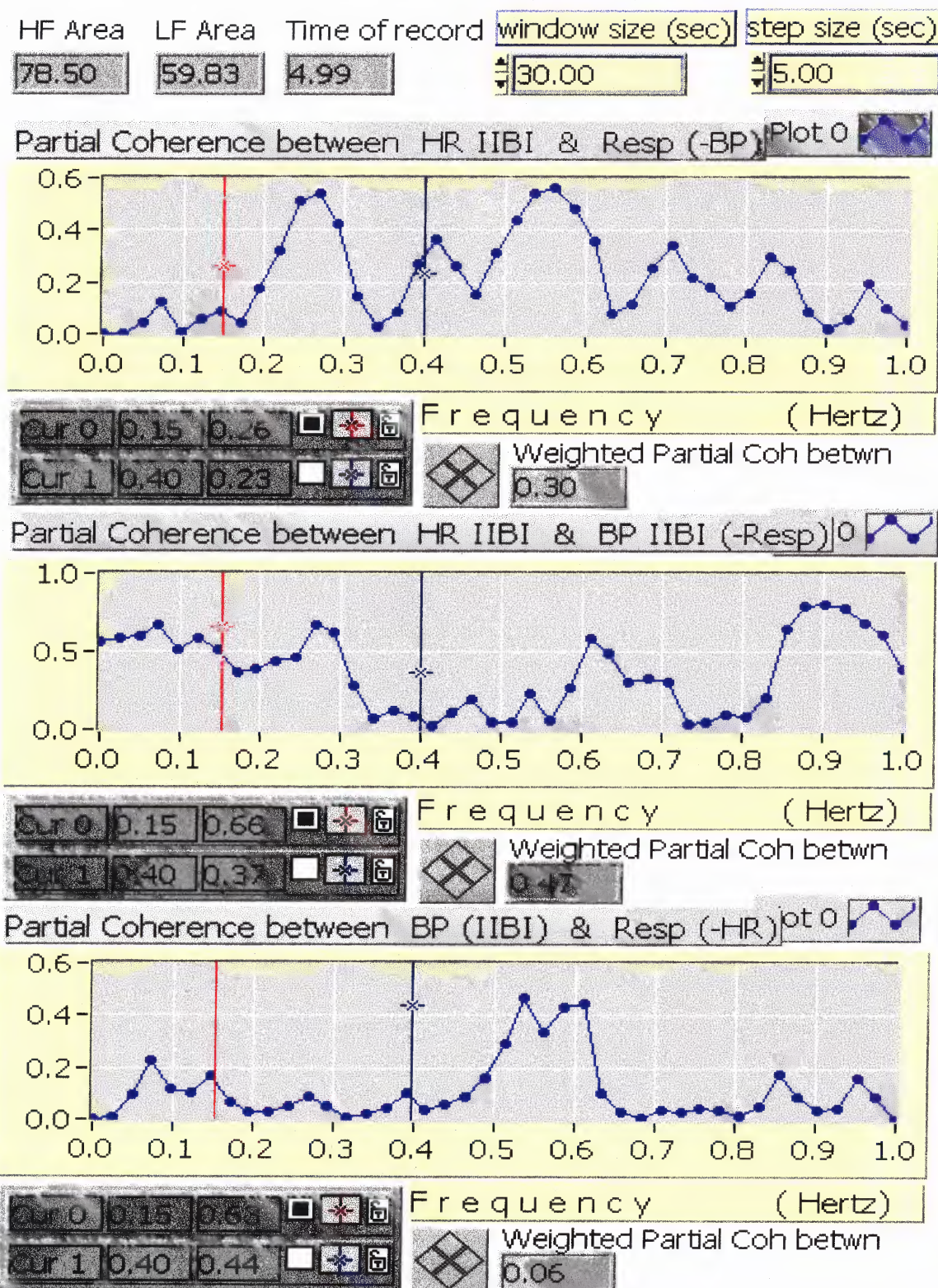


Figure 5.48 HF partial coherence plots of COPD subject AGU1, 5 min at rest breathing at 16 bpm.

Table 5.2 Cross-spectral Analysis of all 8 Normal Subjects

Names	rsp	HR	BP	LF_coh_ HR_rsp	LF_coh_ HR_BP	LF_coh_ BP_rsp	HF_coh_ HR_rsp	HF_coh_ HR_BP	HF_coh_ BP_rsp	LF_pcoh_ HR_rsp	LF_pcoh_ HR_BP	LF_pcoh_ BP_rsp	HF_pcoh_ HR_rsp	HF_pcoh_ HR_BP	HF_pcoh_ BP_rsp
ba50	18	90	94	0.35	0.25	0.35	0.6	0.27	0.1	0.3	0.1	0.18	0.6	0.27	0.15
ja50	16	118	118	0.2	0.4	0.2	0.8	0.7	0.58	0.3	0.4	0.2	0.65	0.1	0.3
rajf50	22	104	118	0.1	0.3	0.05	0.8	0.13	0.25	0.1	0.32	0.05	0.75	0.1	0.24
rajm50	22	110	112	0.25	0.25	0	0.75	0.6	0.5	0.2	0.35	0.11	0.7	0.18	0.3
ka50	18	106	106	0.35	0.2	0.15	0.65	0.55	0.8	0.28	0.08	0.1	0.35	0.16	0.55
ma50	18	114	116	0.4	0.8	0.6	0.6	0.25	0.25	0.45	0.8	0.6	0.6	0.25	0.35
ro50	30	96	96	0.45	0.8	0.58	0.62	0.3	0.4	0.45	0.8	0.58	0.62	0.3	0.4
so50	21	104	104	0.25	0.7	0.1	0.6	0.2	0.5	0.28	0.7	0.15	0.59	0.25	0.48
ba75	24	108	110	0.02	0.35	0	0.08	0.04	0.22	0.02	0.35	0	0.12	0.09	0.25
ja75	32	68	68	0.03	0.12	0.04	0.05	0.14	0.07	0.04	0.13	0.05	0.04	0.13	0.06
rajf75	26	148	142	0.03	0.08	0.02	0.22	0.09	0.03	0.02	0.08	0.02	0.23	0.1	0.04
rajm75	20	124	126	0.16	0.13	0.01	0.61	0.1	0.13	0.17	0.15	0.03	0.62	0.12	0.16
ka75	19	122	124	0.1	0.06	0.04	0.54	0.14	0.3	0.11	0.09	0.06	0.54	0.12	0.28
ma75	19	140	140	0.06	0.49	0.17	0.45	0.42	0.55	0.13	0.52	0.24	0.26	0.2	0.37
ro75	27	112	110	0.04	0.17	0.02	0.36	0.07	0.02	0.03	0.17	0.01	0.37	0.09	0.04
so75	25	134	132	0.02	0.26	0.02	0.13	0.02	0.04	0.02	0.26	0.03	0.14	0.03	0.04
ba10	34	146	142	0.02	0.1	0.03	0.06	0.02	0.03	0.02	0.1	0.03	0.06	0.02	0.03
ja10	38	70	70	0.04	0.24	0.05	0.18	0.42	0.08	0.03	0.22	0.04	0.16	0.39	0.05
rajf10	29	170	166	0.05	0.19	0.03	0.22	0.08	0.06	0.04	0.18	0.03	0.19	0.05	0.02
rajm10	25	144	142	0.03	0.15	0.08	0.19	0.13	0.13	0.05	0.17	0.1	0.2	0.14	0.15
ka10	20	144	146	0.05	0.12	0.03	0.12	0.21	0.18	0.04	0.11	0.02	0.15	0.23	0.24
ma10	24	168	168	0.13	0.61	0.1	0.2	0.24	0.76	0.08	0.59	0.05	0.03	0.07	0.7
ro10	30	134	136	0.02	0.29	0.02	0.01	0.14	0.02	0.02	0.29	0.02	0.02	0.15	0.03
so10	26	158	160	0.05	0.03	0.08	0.17	0.03	0.07	0.07	0.04	0.09	0.16	0.02	0.07

Table 5.2 Cross-Spectral Analysis of all 8 Normal Subjects (Continued)

Names	rsp	HR	BP	LF_coh_ HR_rsp	LF_coh_ HR_BP	LF_coh_ BP_rsp	HF_coh_ HR_rsp	HF_coh_ HR_BP	HF_coh_ BP_rsp	LF_pcoh_ HR_rsp	LF_pcoh_ HR_BP	LF_pcoh_ BP_rsp	HF_pcoh_ HR_rsp	HF_pcoh_ HR_BP	HF_pcoh_ BP_rsp
ba	8	54	54	0.23	0.45	0.2	0.38	0.37	0.42	0.12	0.4	0.1	0.14	0.16	0.18
ja	17	63	62	0.18	0.26	0.05	0.68	0.44	0.45	0.17	0.26	0.04	0.46	0.11	0.13
rajf	11	68	66	0.57	0.3	0.18	0.6	0.18	0.18	0.48	0.18	0.05	0.57	0.07	0.07
rajm	15	94	96	0.03	0.66	0.03	0.61	0.76	0.72	0.02	0.66	0.02	0.06	0.42	0.37
ka	15	64	64	0.09	0.4	0.11	0.67	0.68	0.76	0.11	0.4	0.12	0.24	0.37	0.43
ma	6	98	98	0.11	0.33	0.15	0.11	0.39	0.3	0.17	0.38	0.22	0.11	0.39	0.3
ro	18	62	62	0.03	0.74	0.07	0.47	0.5	0.59	0.04	0.74	0.08	0.12	0.19	0.39

Table 5.3 Cross-Spectral Analysis of all 47 COPD Subjects

Names	rsp	HR	BP	LF_coh_ HR_rsp	LF_coh_ HR_BP	LF_coh_ BP_rsp	HF_coh_ HR_rsp	HF_coh_ HR_BP	HF_coh_ BP_rsp	LF_pcoh_ HR_rsp	LF_pcoh_ HR_BP	LF_pcoh_ BP_rsp	HF_pcoh_ HR_rsp	HF_pcoh_ HR_BP	HF_pcoh_ BP_rsp
agu	17	70	70	0.09	0.56	0.15	0.48	0.63	0.35	0.05	0.54	0.11	0.28	0.47	0.03
all	12	90	90	0.04	0.15	0.11	0.03	0.04	0.45	0.03	0.14	0.1	0.04	0.03	0.5
bec	21	92	90	0.09	0.2	0.03	0.43	0.24	0.31	0.07	0.19	0.01	0.29	0.06	0.16
ben	17	68	68	0.05	0.42	0.02	0.45	0.39	0.61	0.04	0.41	0.01	0.19	0.11	0.51
bos	16	80	80	0.06	0.4	0.24	0.41	0.57	0.41	0.26	0.28	0.08	0.21	0.43	0.19
bre	18	86	74	0.03	0.22	0.03	0.06	0.08	0.07	0.05	0.24	0.05	0.05	0.07	0.06
bro	15	76	76	0.14	0.24	0.15	0.26	0.29	0.46	0.14	0.24	0.16	0.08	0.12	0.35
bur	10	76	74	0.49	0.54	0.51	0.1	0.11	0.38	0.15	21	0.19	0.04	0.06	0.34
cro	14	86	84	0.36	0.29	0.25	0.56	0.62	0.47	0.22	0.2	0.04	0.3	0.38	0.13
ecc	24	88	82	0.03	0.18	0.05	0.04	0.1	0.02	0.03	0.18	0.05	0.05	0.1	0.03
edw	12	52	52	0.2	0.3	0.15	0.67	0.66	0.71	0.09	0.23	0.16	0.31	0.38	0.22
fal	12	76	78	0.28	0.4	0.3	0.39	0.68	0.42	0.12	0.26	0.14	0.06	0.58	0.08
fan	18	68	68	0.08	0.15	0.29	0.1	0.17	0.24	0.05	0.12	0.27	0.19	0.26	0.31
fer	13	80	80	0.05	0.5	0.05	0.06	0.46	0.06	0.03	0.49	0.03	0.02	0.45	0.03
for	15	102	100	0.49	0.78	0.58	0.84	0.9	0.92	0.03	0.6	0.31	0.1	0.51	0.56
gil	10	62	62	0.12	0.23	0.27	0.3	0.29	0.58	0.02	0.14	0.22	0.04	0.03	0.54
gra	13	72	72	0.07	0.4	0.1	0.68	0.46	0.47	0.03	0.37	0.07	0.46	0.08	0.16
hay	15	70	68	0.21	0.11	0.18	0.57	0.5	0.76	0.18	0.09	0.17	0.2	0.05	0.6
hor	12	100	106	0.04	0.06	0.19	0.31	0.37	0.75	0.02	0.04	0.17	0.04	0.11	0.69
how	23	88	88	0.04	0.12	0.02	0.05	0.24	0.39	0.03	0.11	0.01	0.05	0.22	0.42
hyd	12	94	92	0.06	0.44	0.11	0.45	0.43	0.52	0.04	0.41	0.1	0.11	0.1	0.4
imr	13	102	104	0.14	0.52	0.16	0.26	0.38	0.61	0.04	0.45	0.06	0.05	0.21	0.5
joh	12	72	72	0.15	0.25	0.44	0.29	0.35	0.66	0.03	0.14	0.36	0.19	0.14	0.62

Table 5.3 Cross-Spectral Analysis of all 47 COPD Subjects (Continued)

Names	rsp	HR	BP	LF_coh_ HR_rsp	LF_coh_ HR_BP	LF_coh_ BP_rsp	HF_coh_ HR_rsp	HF_coh_ HR_BP	HF_coh_ BP_rsp	LF_pcoh_ HR_rsp	LF_pcoh_ HR_BP	LF_pcoh_ BP_rsp	HF_pcoh_ HR_rsp	HF_pcoh_ HR_BP	HF_pcoh_ BP_rsp
kle	13	82	84	0.19	0.54	0.36	0.48	0.5	0.89	0.05	0.45	0.26	0.05	0.11	0.78
kos	21	86	86	0.19	0.23	0.14	0.59	0.54	0.71	0.14	0.16	0.08	0.15	0.08	0.51
las	12	78	80	0.08	0.45	0.16	0.71	0.72	0.88	0.07	0.44	0.14	0.05	0.09	0.73
lic	12	72	74	0.08	0.19	0.1	0.25	0.26	0.42	0.04	0.15	0.06	0.19	0.17	0.36
lie	12	72	74	0.28	0.31	0.22	0.34	0.3	0.39	0.16	0.2	0.09	0.23	0.12	0.28
lin	18	76	78	0.02	0.36	0.31	0.34	0.6	0.68	0.01	0.31	0.29	0.22	0.05	0.66
loc	30	82	82	0.04	0.09	0.22	0.23	0.1	0.55	0.08	0.12	0.24	0.2	0.05	0.54
mai	18	82	84	0.28	0.48	0.33	0.6	0.62	0.77	0.04	0.32	0.15	0.15	0.23	0.51
man	12	50	50	0.04	0.05	0.03	0.4	0.27	0.44	0.05	0.06	0.03	0.23	0.07	0.3
mcg	13	84	84	0.09	0.28	0.14	0.68	0.74	0.89	0.1	0.3	0.16	0.05	0.25	0.67
mck	13	108	106	0.32	0.39	0.55	0.46	0.42	0.64	0.07	0.2	0.4	0.29	0.15	0.58
mcl	11	72	70	0.25	0.44	0.42	0.39	0.39	0.69	0.04	0.26	0.28	0.07	0.13	0.53
mcc	12	90	88	0.11	0.48	0.29	0.81	0.78	0.86	0.09	0.46	0.29	0.14	0.08	0.58
mid	12	104	106	0.24	0.57	0.12	0.77	0.79	0.86	0.18	0.54	0.07	0.3	0.25	0.33
mul	13	76	74	0.37	0.32	0.47	0.84	0.83	0.82	0.14	0.06	0.3	0.37	0.2	0.26
mli	12	82	82	0.26	0.17	0.33	0.39	0.46	0.71	0.19	0.09	0.27	0.15	0.16	0.71
mur	14	80	82	0.18	0.53	0.2	0.77	0.69	0.77	0.2	0.55	0.23	0.46	0.19	0.4
mut	9	74	76	0.19	0.55	0.17	0.71	0.72	0.71	0.08	0.48	0.05	0.19	0.29	0.26
mey	11	64	66	0.12	0.43	0.18	0.13	0.66	0.28	0.15	0.46	0.22	0.11	0.65	0.26
per	29	84	86	0.03	0.31	0.01	0.06	0.62	0.08	0.05	0.32	0.04	0.04	0.61	0.05
pri	13	64	64	0.14	0.57	0.08	0.08	0.64	0.1	0.13	0.58	0.09	0.06	0.63	0.08
qin	13	92	92	0.03	0.26	0.15	0.01	0.17	0.7	0.06	0.24	0.17	0.23	0.37	0.76
riv	12	106	106	0.02	0.63	0.03	0.38	0.83	0.37	0.02	0.62	0.03	0.05	0.8	0.02
rot	11	80	80	0.11	0.58	0.16	0.28	0.83	0.3	0.13	0.59	0.18	0.07	0.8	0.1

The LF coherences for all COPD and normal subjects are plotted in figure 5.49. The 47 COPD subjects are indicated as data points 1-47. The 8 normal subjects are shown as data points 48-55. The HF coherences for all COPD and normal subjects are plotted in figure 5.50. The LF partial coherences for all COPD and normal subjects are plotted in figure 5.51. The HF partial coherences for all COPD and normal subjects are also plotted in figure 5.52. From these figures, it is quite difficult to compare the differences of the coherence and partial coherence values for the COPD and the normal subjects. Other statistical methods are needed.

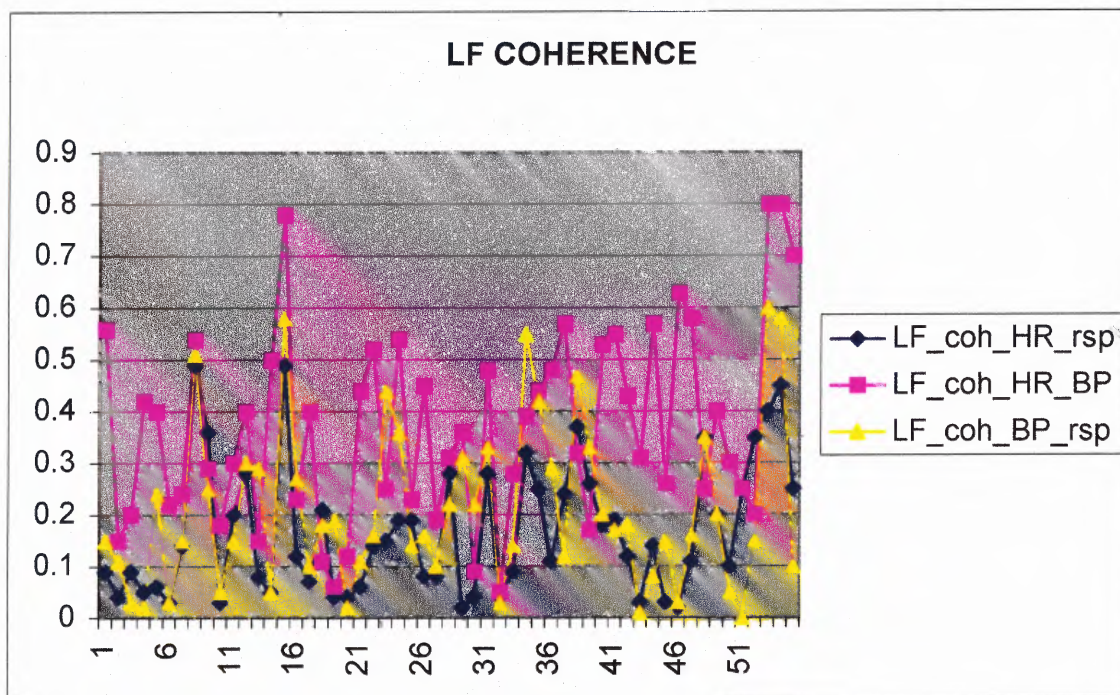


Figure 5.49 LF coherence of COPD (1-47) and normal (48-55) subjects.

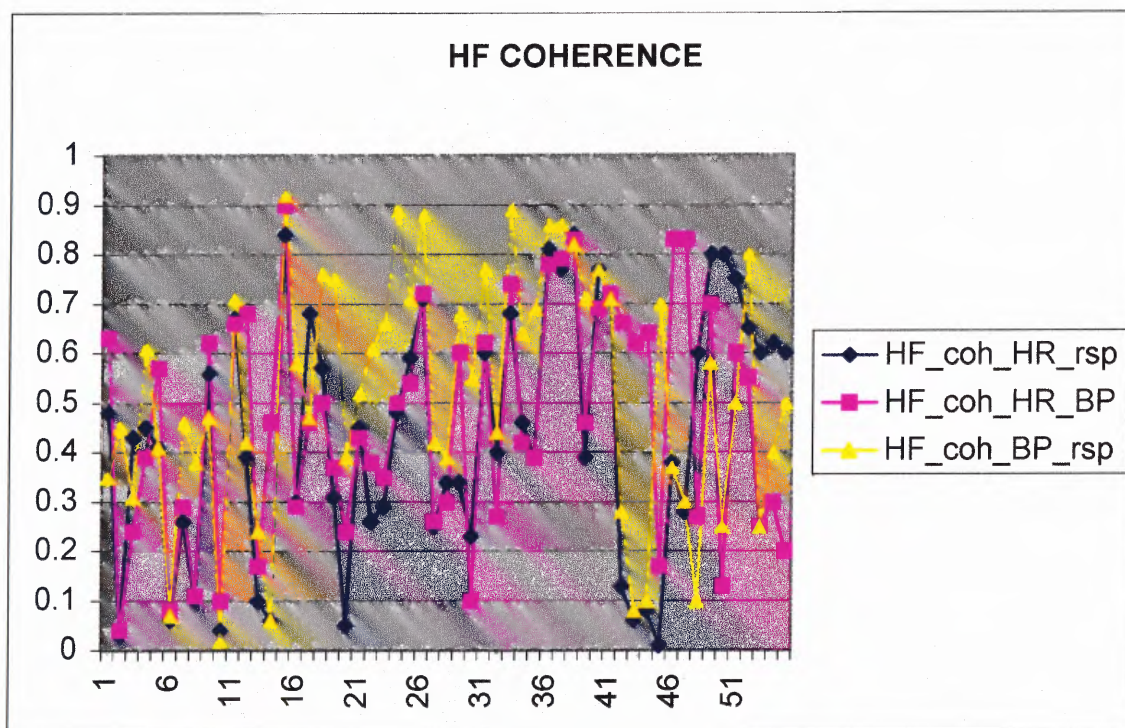


Figure 5.50 HF coherence of COPD (1-47) and normal (48-55) subjects.

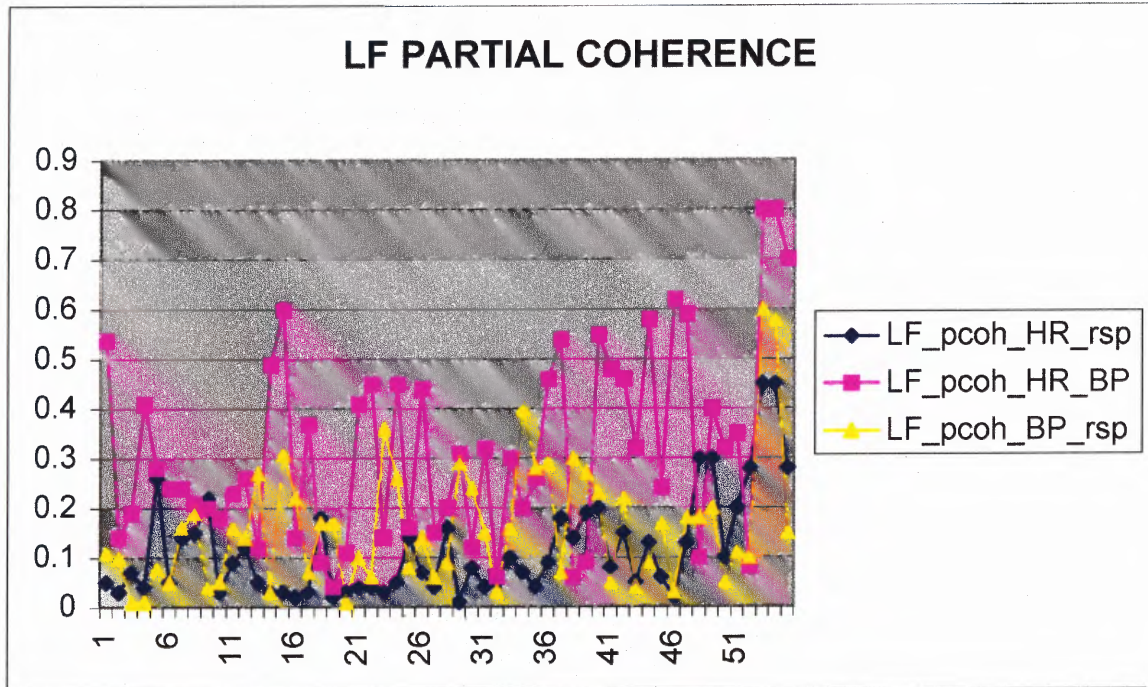


Figure 5.51 LF partial coherence of COPD (1-47) and normal (48-55) subjects.

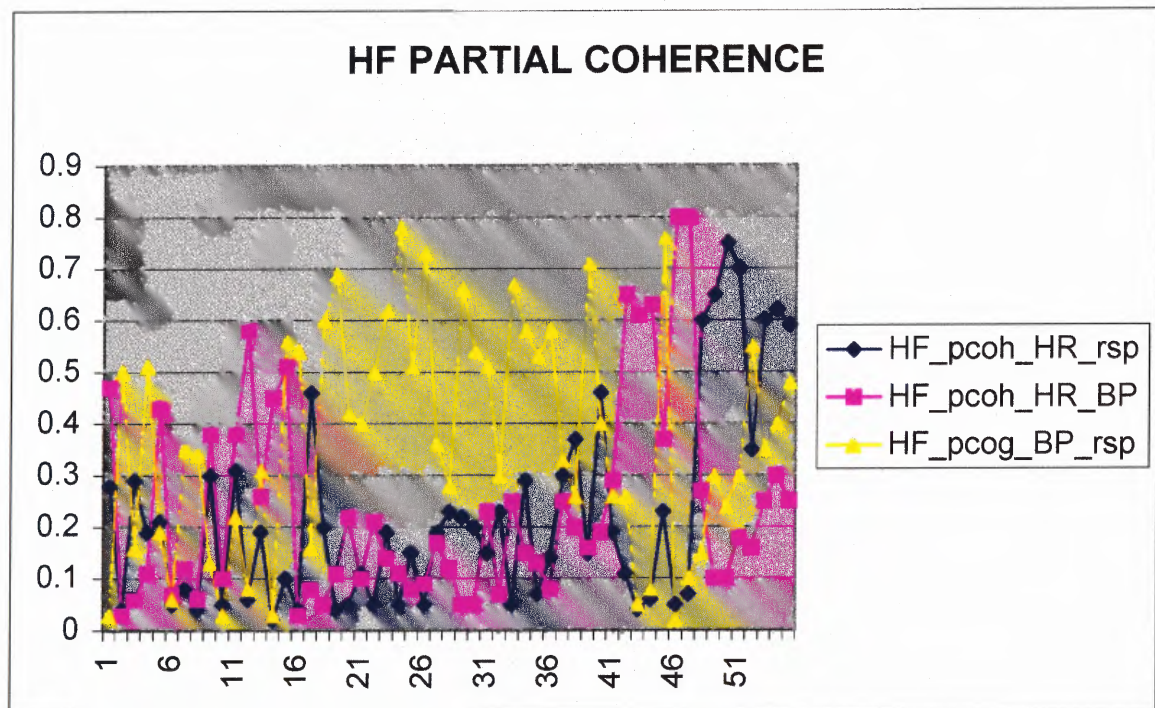


Figure 5.52 HF partial coherence of COPD (1-47) and normal (48-55) subjects.

For better presentation of the cross-spectral data, a descriptive statistical analysis is performed. The statistical analysis of coherence and partial coherence for both normal and COPD subjects is summarized in table 5.3.1. From this table, the mean weighted coherence and partial coherence values are plotted as shown in figure 5.53. From this figure, both the coherence and partial coherences in the LF range of normal subjects are almost double the values of COPD subjects. In the HF range, only the coherence and partial coherence values between HR & Rsp of normal are significantly higher than COPD subjects. These observations may indicate that heart rates in normal subjects are affected by respiration a lot more than COPD subjects. With much higher coherence/partial coherence in the LF range, both the sympathetic and parasympathetic activities of the ANS contribute much more to variation in heart rate of normal subjects than COPD subjects.

Figure 5.53 also shows higher coherence and partial coherence values between BP and respiration of COPD subjects in the HF range than those of normal subjects. This may be due to a more dominant coupling effect of the respiration signal on the blood pressure in COPD subjects while this phenomenon is absent in the normal population. Since COPD subjects breathe faster and more shallow, with the coupling effect of respiration on blood pressure, it causes the blood pressure to have less variability which in turn causes less changes in heart rate variability in COPD subjects.

Table 5.3.1 Statistical Analysis of Coherence and Partial Coherence for Normal and COPD Group

COPD	LF_coh_HR_rsp	LF_coh_HR_BP	LF_coh_BP_rsp	HF_coh_HR_rsp	HF_coh_HR_BP	HF_coh_BP_rsp
Mean	0.14913	0.349783	0.20413	0.39587	0.469783	0.539783
Standard Error	0.017977	0.025188	0.021862	0.036615	0.034153	0.036509
Median	0.115	0.34	0.165	0.39	0.46	0.565
Mode	0.04	0.4	0.15	0.06	0.62	0.71
Standard Deviation	0.121926	0.170834	0.148273	0.248333	0.231637	0.247615
Sample Variance	0.014866	0.029184	0.021985	0.061669	0.053656	0.061313
Normal	LF_coh_HR_rsp	LF_coh_HR_BP	LF_coh_BP_rsp	HF_coh_HR_rsp	HF_coh_HR_BP	HF_coh_BP_rsp
Mean	0.273333	0.475556	0.243333	0.633333	0.425556	0.408889
Standard Error	0.041197	0.08216	0.073276	0.052414	0.082817	0.070385
Median	0.25	0.4	0.16	0.62	0.3	0.4
Mode	0.35	0.25	#N/A	0.6	#N/A	0.25
Standard Deviation	0.123592	0.246481	0.219829	0.157242	0.248451	0.211154
Sample Variance	0.015275	0.060753	0.048325	0.024725	0.061728	0.044586

COPD	LF_pcoh_HR_rsp	LF_pcoh_HR_BP	LF_pcoh_BP_rsp	HF_pcoh_HR_rsp	HF_pcoh_HR_BP	HF_pcoh_BP_rsp
Mean	0.084565	0.292391	0.148043	0.159348	0.232174	0.382391
Standard Error	0.009277	0.024424	0.015353	0.016949	0.028933	0.033675
Median	0.055	0.25	0.14	0.15	0.155	0.38
Mode	0.03	0.14	0.01	0.05	0.11	0.03
Standard Deviation	0.062918	0.165653	0.104129	0.114957	0.19623	0.228397
Sample Variance	0.003959	0.027441	0.010843	0.013215	0.038506	0.052165
Normal	LF_pcoh_HR_rsp	LF_pcoh_HR_BP	LF_pcoh_BP_rsp	HF_pcoh_HR_rsp	HF_pcoh_HR_BP	HF_pcoh_BP_rsp
Mean	0.276667	0.46	0.238889	0.547778	0.267778	0.318889
Standard Error	0.040791	0.092421	0.06818	0.070154	0.070765	0.048633
Median	0.28	0.4	0.18	0.6	0.25	0.3
Mode	0.3	0.8	0.18	0.6	0.1	0.3
Standard Deviation	0.122372	0.277263	0.204539	0.210462	0.212296	0.145898
Sample Variance	0.014975	0.076875	0.041836	0.044294	0.045069	0.021286

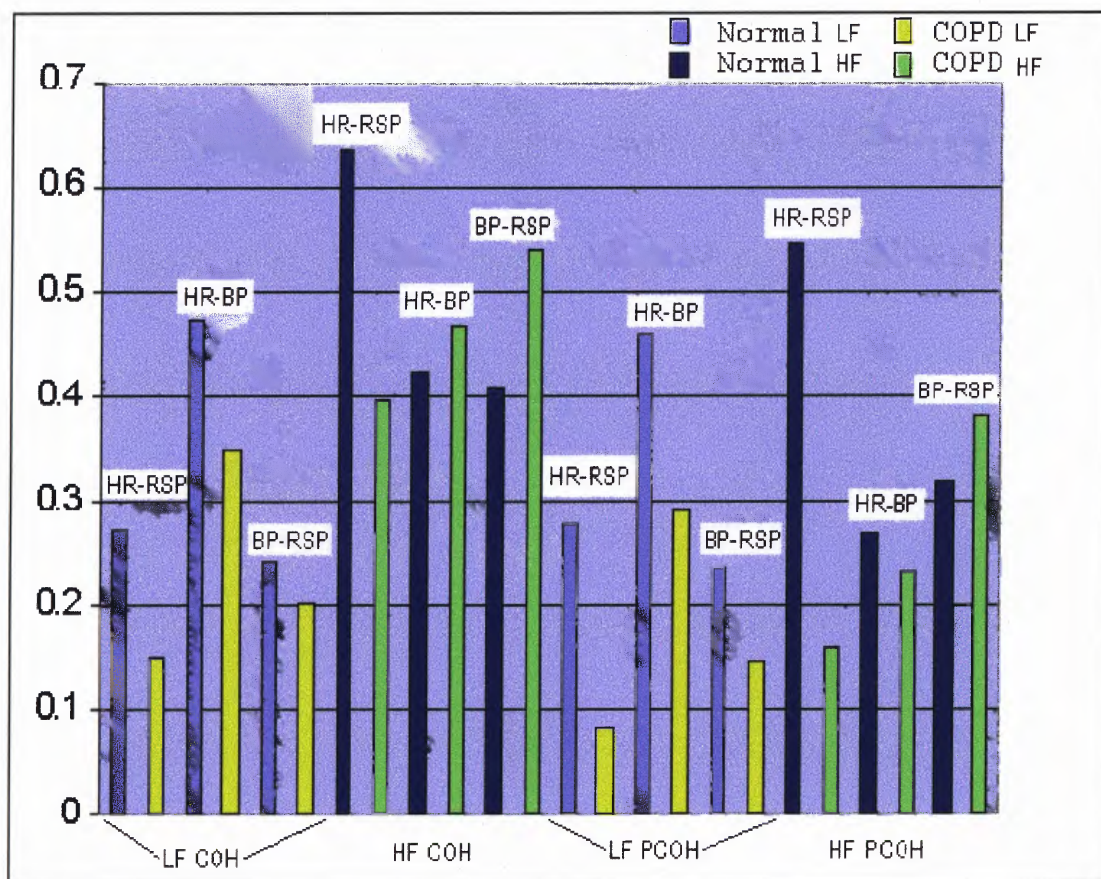


Figure 5.53 Coherence and partial coherence comparison between normal and COPD.

5.4 Cardiovascular System Models for Normal Subjects

A model of heart rate (HR) and arterial blood pressure (ABP) control similar to that shown in Figure 5.54 has recognized the complex interactions between HR and ABP during closed-loop operation of the cardiovascular system. This model has been previously proposed and now widely accepted as a simple feedback and control model of the cardiovascular system [29].

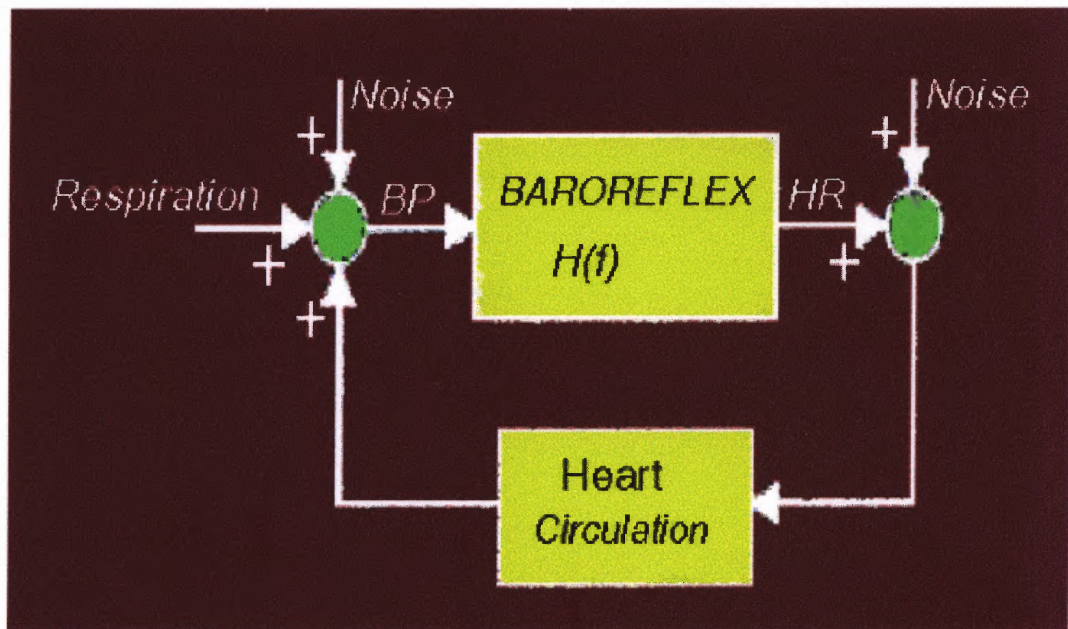


Figure 5.54 Simple feedback and control model of ABP and HR regulation. Respiration enters as input, ABP and HR are outputs.

Previous studies have successfully used non-parametric transfer function analysis in combination with broadband noise sources to address the following problems:

1. Identification of the transfer relations between HR, ABP and the respiratory noise sources experimentally has been limited during spontaneous operation because the frequency content of the noise sources is relatively narrow-band and provides insufficient excitation energy at any relevant physiological frequencies.

2. Interpretation of the transfer relations has been limited by insufficient characterization of the central and peripheral mechanisms, which mediate these relations (e.g. – the sino-atrial (SA) nodal responses, the mechanical coupling relations, and the baroreceptors).

In this research the author uses the same model of the cardiovascular system for normal subjects using the experimental data taken from ten normal healthy subjects. In the HRV modeling task, the transfer functions of the HRV model is estimated from a black box model using the actual respiration (rsp) data as input and

- 1) The iibi signal derived from the actual ECG as output, and/or
- 2) The actual blood pressure data as output.

In previous studies the transfer or frequency response functions were all calculated using the cross spectral method. The autospectra of the input signal (e.g. respiration), $S_{ii}(f)$ and of the output signal (e.g. – HR), $S_{oo}(f)$ were estimated. The cross-spectra, $S_{io}(f)$, between the input and output signals were also computed. Then, the complex transfer function, $H(f)$, and its magnitude and phase, $|H(f)|$ and $\theta(f)$ were estimated using the relations,

$$H(f) = \frac{S_{io}(f)}{S_{ii}(f)} \quad (5.8)$$

$$|H(f)| = \{[H_R(f)]^2 + [H_I(f)]^2\}^{1/2} \quad (5.9)$$

$$\theta(f) = \tan^{-1} \frac{H_I(f)}{H_R(f)} \quad (5.10)$$

where R and I are the real and imaginary components of the complex transfer function.

In addition, group-average transfer function estimates were derived for all the studies by using a weighting algorithm based on the coherence estimates $\gamma^2(f)$ for each individual transfer function [29].

$$\gamma^2(f) = \frac{|S_{xy}(f)|^2}{S_{xx}(f)S_{yy}(f)} \quad (5.11)$$

However, in this research the MATLAB System Identification toolbox is used to estimate the transfer function. As one can see below, with minor modification to the programs in the toolbox, the model transfer function can be easily obtained and the results are quite acceptable. Once the transfer function is obtained, the cardiovascular system model for normal subjects is estimated. It can now be examined and be used for further investigation. This estimated model of normal subjects would also be used as reference in developing the diseased cardiovascular model for COPD patients.

Figures 5.55 – 5.59 present the case of a file from a normal subject resting and breathing at 14 breaths per minute (bpm). The HRV iibi signal was derived from the ECG signal and the first half of this signal was used as output of the cardiovascular model while the first half of the respiration signal was used as the single input. The two halves of the input/output were used to calculate the coefficients of the transfer function for the model.

Figure 5.55 shows the rsp input and the iibi signal derived from the actual ECG as output. Below the figure are the transfer function coefficients of the estimated model in System Identification format. The basic format for representing models in the System Identification Toolbox is called the *theta format*. It stores all relevant information about the model structure used, including the values of the estimated parameters, the estimated

covariances of the parameters, and the estimated variance and so on. It also contains some information about how and when the model was created.

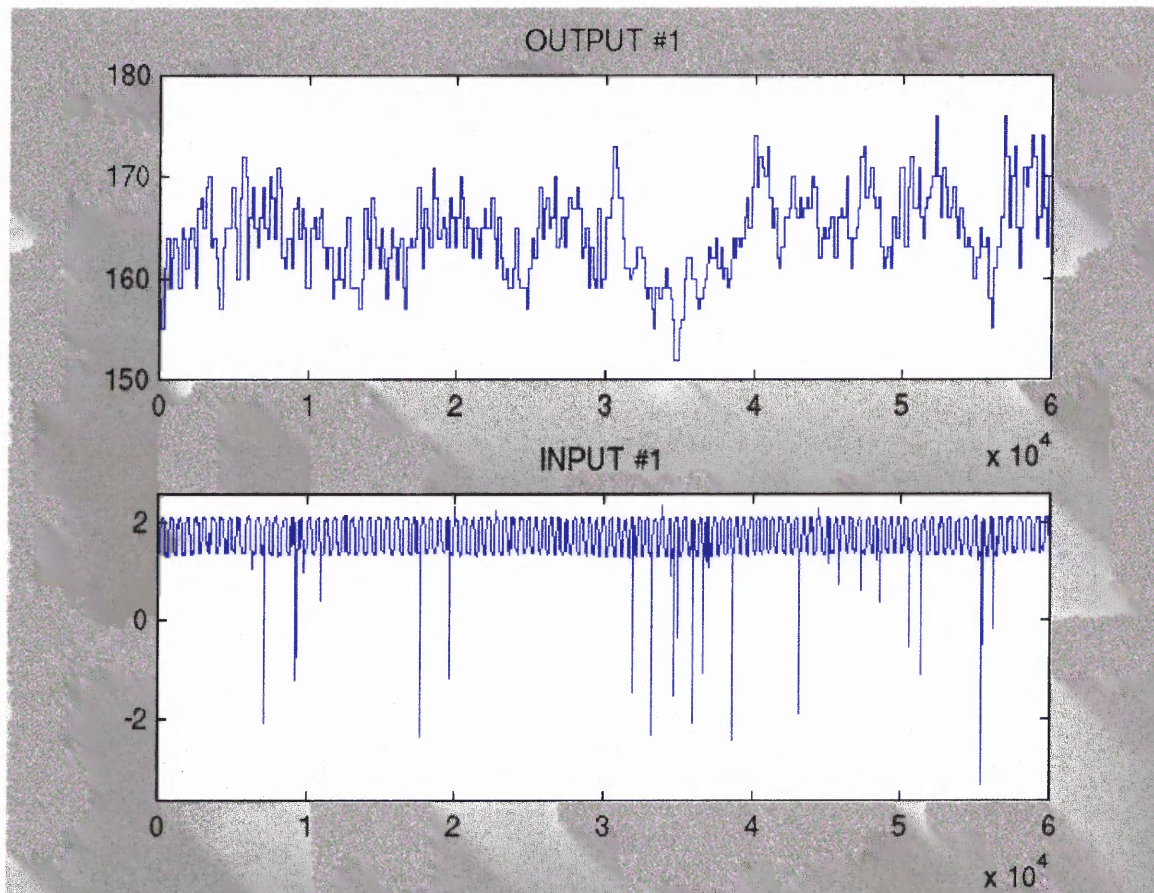


Figure 5.55 Plot of output HR IIBI (Top) and input RSP (Bottom) signals.

» present(th);

This matrix was created by the command ARX on 4/16 2001 at 5:55

Loss fcn: 0.071384 Akaike's FPE: 0.071431 Sampling interval 0.005

The polynomial coefficients and their standard deviations are:

B =

Columns 1 through 7

0	0	0	-0.0072	-0.0103	-0.0008	-0.0003
0	0	0	0.0174	0.0177	0.0180	0.0181

Columns 8 through 13

```
-0.0114  0.0063  0.0139  0.0169  0.0216  0.0175
 0.0182  0.0182  0.0181  0.0180  0.0177  0.0174
A =
```

Columns 1 through 7

```
1.0000 -0.9960 -0.0000 -0.0000 -0.0000 -0.0000 -0.0000
      0   0.0041  0.0058  0.0058  0.0058  0.0058  0.0058
```

Columns 8 through 11

```
-0.0000  0.0000  0.0000 -0.0019
 0.0058  0.0058  0.0058  0.0041
```

```
>>
```

The information in the theta format is displayed by the present command `present(th)` and the results are shown above. This spells out the information in the calculated model `th`. Depending on the character of the underlying model structure, the information is given

1. in terms of the polynomials in $A(q)y(t) = \frac{B(q)}{F(q)}u(t - nk) + \frac{C(q)}{D(q)}e(t),$

2. in terms of the matrices in $x(kT + T) = Ax(kT) + Bu(kT) + Ke(kT)$

$$y(kT) = Cx(kT) + Du(kT) + e(kT)$$

$$x(0) = x_0, \text{ or}$$

3. in terms of the ARX polynomials in $A(q)y(t) = B(q)u(t) + e(t).$

Estimated standard deviations for the parameters are always supplied. For multivariable ARX models and for state-space matrices, the standard deviations are given as imaginary numbers added to the parameters. For the polynomials they are given as a second row. For the case shown above, the polynomial coefficients and their standard

deviations are interpreted as $A(q) = 1 - 0.9960q^{-1} - 0.0019q^{-10}$ and the standard deviation of “1” is zero (naturally enough, since it is not estimated). The standard deviation of a_1 is 0.0041, a_2 through a_9 is 0.0058 and a_{10} is 0.0041.

Note that leading zeros in the $B(q)$ polynomial indicate the delay. In this case, $B(q) = -0.0072q^{-3} - 0.0103q^{-4} - 0.0008q^{-5} - 0.0003q^{-6} - 0.0114q^{-7} + 0.0063q^{-8} + 0.0139q^{-9} + 0.0169q^{-10} + 0.0216q^{-11} + 0.0175q^{-12}$ and the standard deviation of b_0 , b_1 , and b_2 are zeros and of b_3 through b_{12} are 0.0174, 0.0177, 0.0180, 0.0181, 0.0182, 0.0182, 0.0181, 0.0180, 0.0177, and 0.0174 respectively.

Figure 5.56 shows the actual iibi output (derived HRV signal) (blue) and the estimated model simulated output (green). From this figure, it is cleared that the simple ARX model does not estimate the amplitude of the HRV output well. However, the period of the simulated output mimics the heart rate variability period very closely. The period of the iibi signal is the desired information needed to be obtained from the model and the amplitude needs not be matched exactly since the iibi of the ECG gives twice the HRV information. The estimated model provides the period variation information and this is all one can ask for out of the simple ARX model provided by the System Identification.

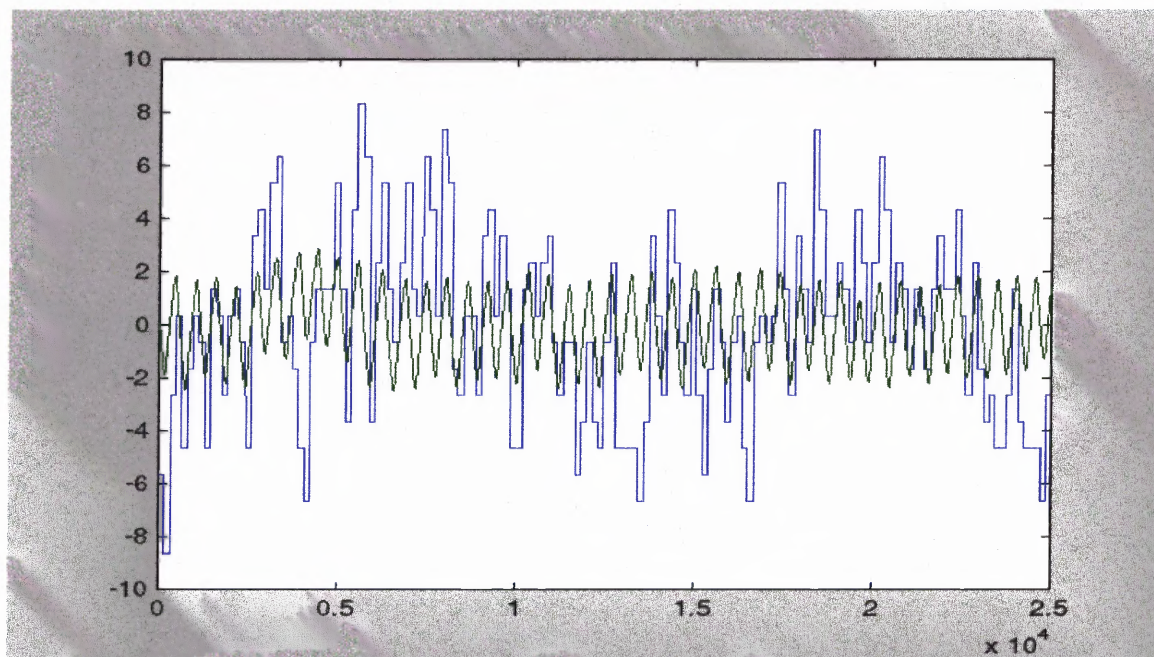


Figure 5.56 ARX model of HRV using RSP as input and HR IIBI as output.

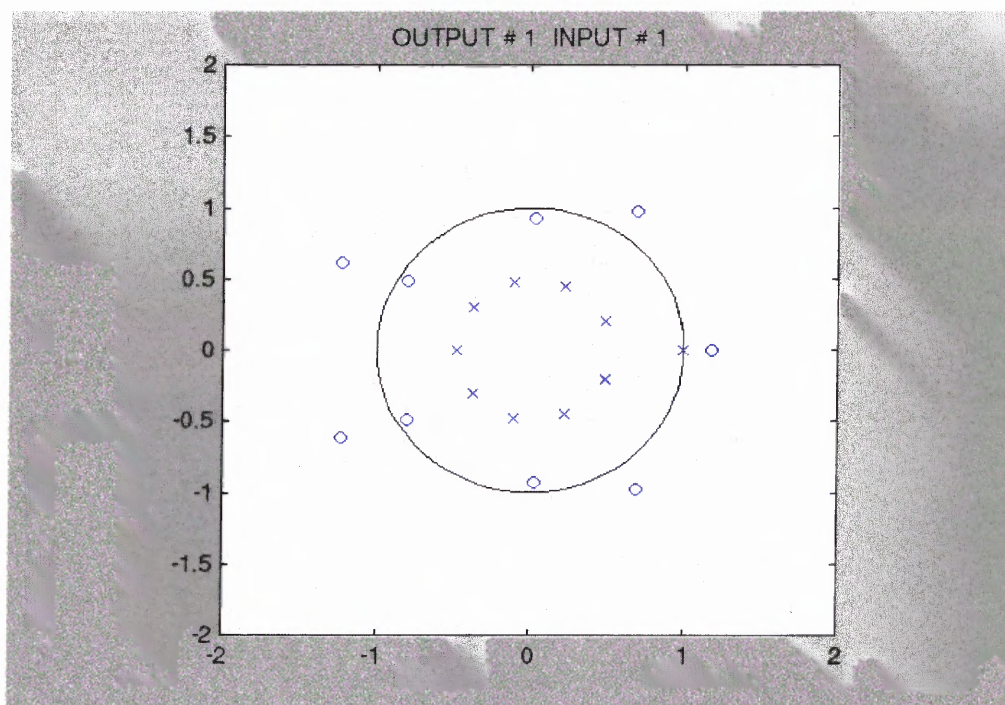


Figure 5.57 Poles and zeros graph of the HRV model using RSP as input and HR IIBI as output.

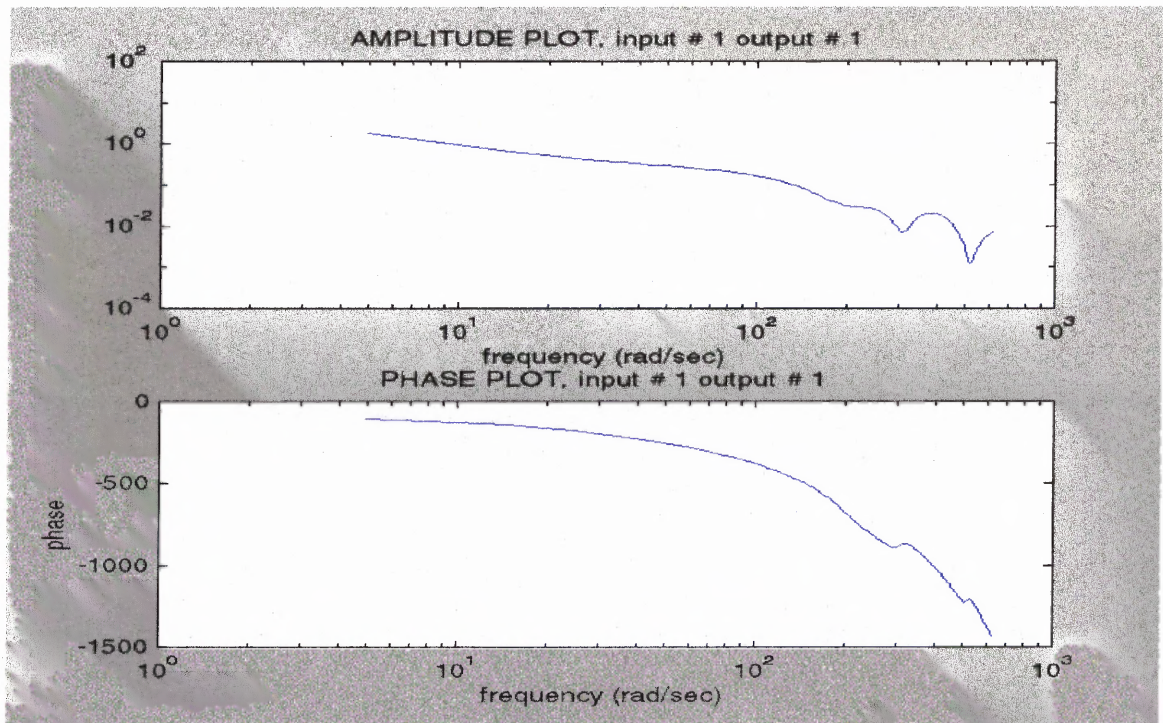


Figure 5.58 Bode plot of the HRV model using RSP as input and HR IIBI as output.

Figures 5.58 and 5.59 show the poles/zeros plot and the Bode plot of the blackbox model calculated using the rsp as input and iibi as output. Figure 5.60 indicates the comparison between the system and the simulated amplitude and phase response. Notice that even with a simple ARX model, the amplitude and the low frequency phase of the Bode plot of the system and the simulated model match relatively well. The phase plot of the real system and the simulated model seem to diverge greatly for frequencies beyond the cut-off frequency.

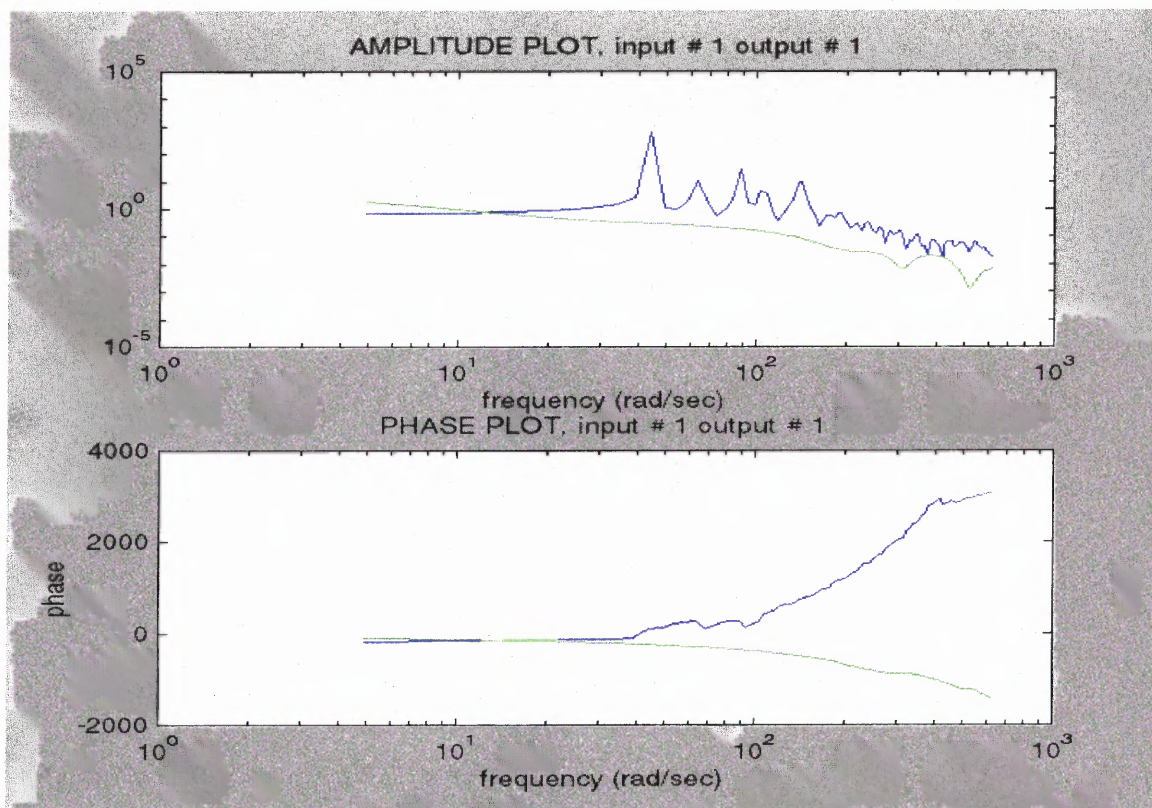


Figure 5.59 Compare the estimate of the transfer function by spectral analysis (Blue) and by model (Green) using RSP as input and HR IIBI as output.

The data for all 8 normal subjects were analyzed, tabulated and statistically summarized as shown in table 5.4:

Table 5.4 Gain and Phase Data of Normal Subjects

	3dB Gain	3dB Freq Hz	-45 (Hz)	-90 (Hz)	-180 (Hz)
Mean	243.83	0.0735	0.0808	0.7062	5.7767
Std Error	51.31	0.0152	0.0188	0.2835	1.1347
Median	185.42	0.0670	0.0796	0.4216	4.77
STD	162.26	0.0480	0.0593	0.8965	3.8840
Variance	26327.25	0.0023	0.00352	0.8037	12.8764

In this section a simple model of cardiovascular-respiratory interaction in humans is presented. The data analyzed, ECG, BP and respiratory signals, have these features:

1. The physiological signals have different forms (respiration is a narrow-band signal, while BP and ECG can be reduced to spike pulse trains);
2. The characteristic time scales of the signals are different (there are always several heart beats or BP cycles per respiratory cycle) and vary within each data recording period.
3. Oscillation coupling is probably related to modulation of the HR and BP by respiration.

From table 5.4 one cannot give much insight to what is happening until this table is compared to a similar table obtained from the COPD model in section 5.5

5.5 Cardiovascular System Models for COPD Subjects

The next goal of this research was to use system identification techniques to develop a HRV model first for healthy normal subjects and then use this normal cardiovascular model as reference for the design of the diseased model that can represent the physical attributes of the COPD patients using an adaptive controller. An adaptive controller differs from an ordinary controller in that the controller parameters are variable, and there is a mechanism for adjusting these parameters online based on signals in the system. In this research the author used the so-called Model-Reference Adaptive Control (MRAC) model. A schematic of the MRAC system is represented in Figure 5.59.1. It is composed of four parts: a plant of the COPD cardiovascular system containing unknown parameters, a reference model of the cardiovascular system for compactly specifying the desired output (e.g. HR and ABP) of the control system, a feedback control law containing adjustable parameters, and an adaptation mechanism for updating the adjustable parameters [50].

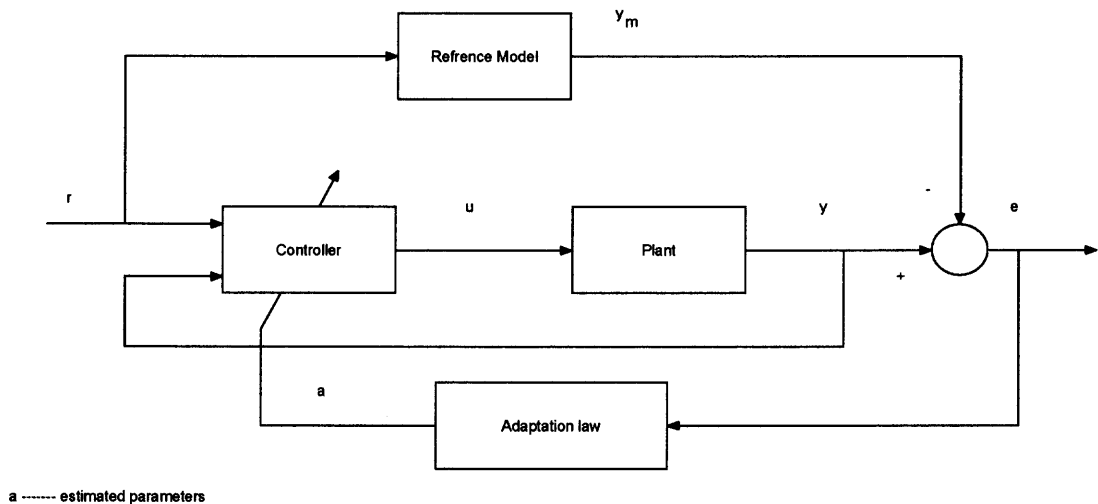


Figure 5.59.1 An adaptive COPD cardiovascular system model.

The data for all 47 COPD subjects were also analyzed, tabulated and statistically summarized as shown in table 5.5:

Table 5.5 Gain and Phase Data of COPD Subjects

	3dB Gain	3dB Freq Hz	-45 (Hz)	-90 (Hz)	-180 (Hz)
Mean	213.42	0.0857	0.1633	0.6722	93.1328
Std Error	35.84	0.0215	0.0838	0.8285	5.3413
Median	195.11	0.0730	0.0918	0.2356	11.47
STD	181.42	0.0512	0.0633	0.8657	8.8880
Variance	6147.49	0.0048	0511	0.8792	20.4733

Comparing tables 5.4 and 5.5, the 3dB gains and 3dB frequencies of the normal and COPD subjects are similar. However, all three phase data points at -45, -90 and -180 degrees of COPD show a significant lag in response time. The lag time is commonly referred to as propagation time or dead time because no output is produced during this time.

The gain and phase data obtained from cardiovascular modeling of normal and COPD show definite changes in the way the baroreflex behaved in normal and COPD subjects. Since the COPD model represents a disease state, it is obvious that the lag time affects the stability of a control system. Although lag time in COPD cannot be eliminated from the model, it may certainly be reduced. In addition, the system loop gain may be adjusted until the system is stable. This is verified from the fact that the cardiovascular system still works in COPD and that the COPD 3dB gain is slightly smaller than that of normal subjects.

5.6 Principal Component Analysis

As mentioned in section 3.14, the principal components were arranged in order of decreasing variance with the most informative principal component listed first, and the least informative listed last. The dimensionality of the problem was reduced, i.e., reduces the number of variables without losing much of the information. Thus instead of analyzing a large number of the original variables with complex interrelationships, the data could be analyzed by a small number of uncorrelated principal components.

Figure 5.60 presented a principal component plot of the data set containing 48 COPD and 8 normal subjects at rest. The data set gave the following principal components (PC):

1st PC: LF_coh_HR_rsp – Coherence of HR and respiration signals in the LF range (0.04 - 0.15 Hz).

2nd PC: HF_coh_BP_rsp – Coherence of BP and respiration signals in the HF range (0.15 - 0.4 Hz).

3rd PC: rsp – The respiration rate.

This indicated that the largest variance between COPD and normal subjects was the interrelationships between heart rate and respiration. The second largest variance was the interrelationships between blood pressure and respiration. The third largest variance was the respiration rate itself.

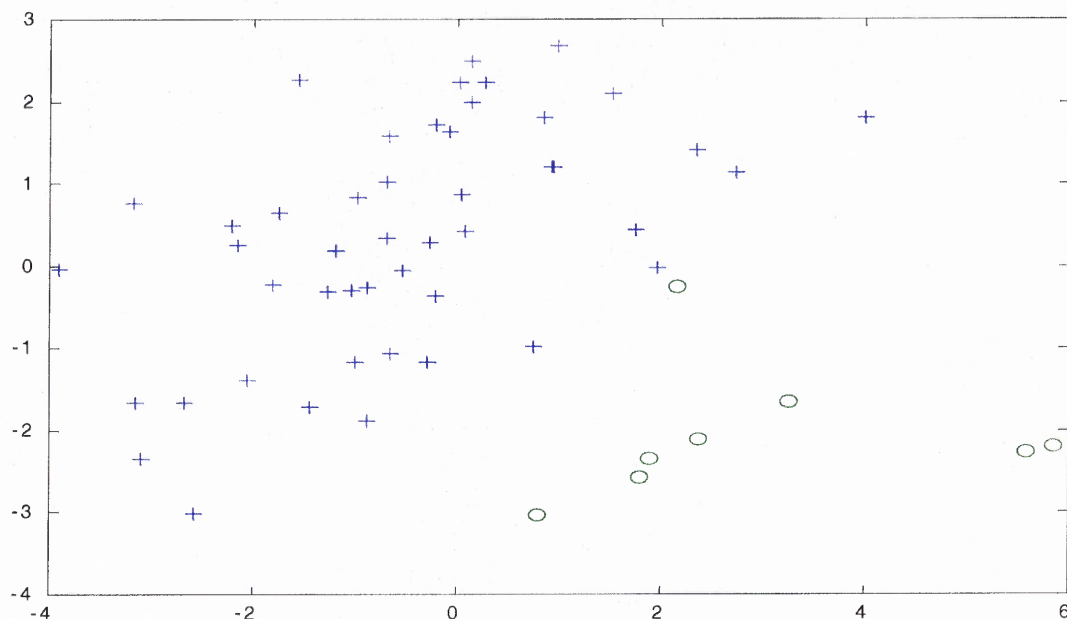


Figure 5.60 Normal and COPD classification using principal component analysis (PCA).

Note: (o: Normal; +: COPD)

Table 5.6 Principal Components from Normal and COPD Data

P1	P2	P3	Categories
0.0351	-0.3625	0.3099	rsp
0.2960	-0.1943	0.0928	HR
0.2729	-0.2367	0.1637	BP
0.3800	0.0271	-0.0793	LF_coh_HR_rsp
0.2725	-0.0886	-0.3849	LF_coh_HR_BP
0.3349	0.2178	-0.0244	LF_coh_BP_rsp
0.3416	0.0691	-0.0556	HF_coh_HR_rsp
0.1389	0.1252	-0.5128	HF_coh_HR_BP
0.1924	0.4961	0.0194	HF_coh_BP_rsp
0.3386	-0.2607	0.0482	LF_pcoh_HR_rsp
0.0449	0.0540	-0.0351	LF_pcoh_HR_BP
0.3341	0.1433	0.0701	LF_pcoh_BP_rsp
0.2954	-0.2978	0.2039	HF_pcoh_HR_rsp
-0.0170	-0.2281	-0.5558	HF_pcoh_HR_BP
0.1308	0.4691	0.2969	HF_pcoh_BP_rsp

Figure 5.61 presents a principal component plot of the data set containing 47 COPD at rest and 8 normal subjects at 50%, 75% and 100% load. The data set gave the following principal components (PC):

1st PC: rsp – The respiration rate.

2nd PC: $HF_coh_HR_BP$ – Coherence of HR and BP IIBI signals in the HF range (0.15 - 0.4 Hz).

3rd PC: $HF_pcoh_HR_BP$ – Partial Coherence of HR and BP IIBI signals in the HF range (0.15 - 0.4 Hz).

This indicated that the largest variance between COPD at rest and normal subjects during exercise was the breathing rate (respiration). The second largest variance was the interrelationships between HR and blood pressure in the HF range. The third largest variance was the partial interrelationships between HR and blood pressure in the HF range. The 1st PC of the respiration indicated that the higher breathing rate of the COPD subjects was not the same in the HRV sense even though normal subjects increased their respiration rate to a similar level. Once the respiration PC was removed, the residual interrelationship was that between HR and blood pressure in the HF range.

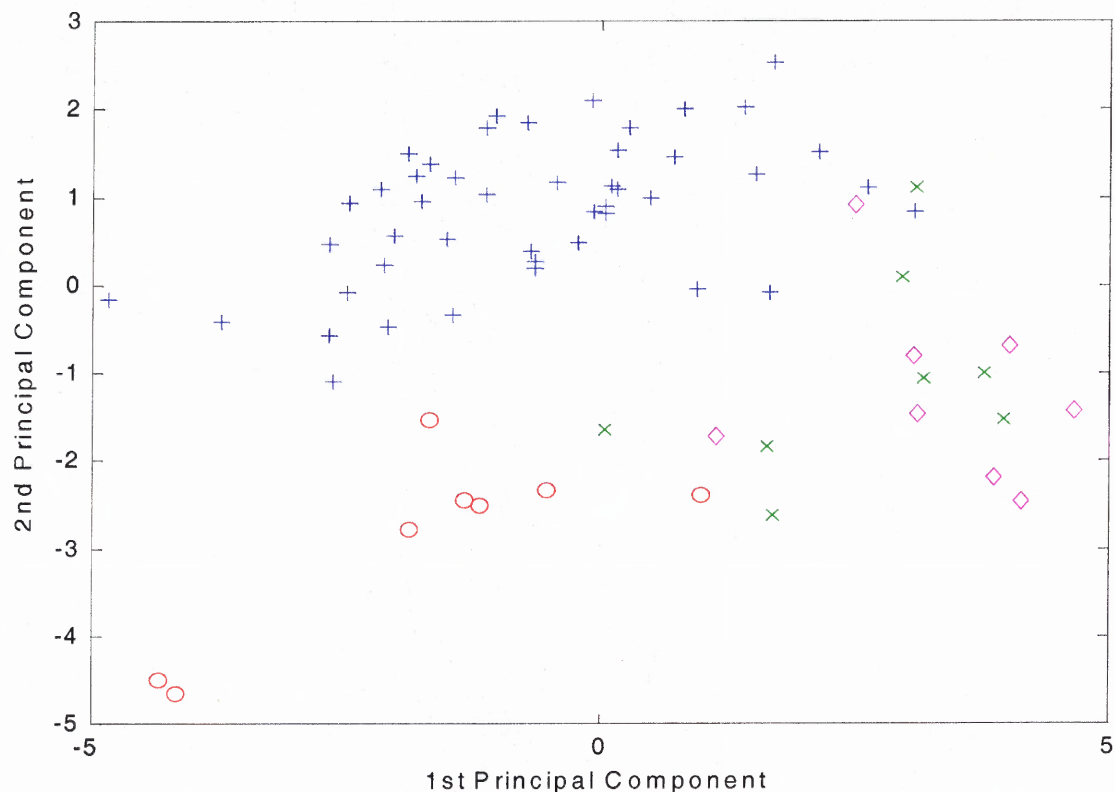


Figure 5.61 Normal and COPD classification using principal component analysis (PCA).
Note: (+: COPD; others: Normal).

Table 5.7 Principal Components from Normal and COPD Data

P1	P2	P3	Categories
0.2786	-0.2679	0.0641	rsp
0.1821	-0.4329	-0.0664	HR
0.2003	-0.4289	-0.0794	BP
-0.3381	-0.2261	0.0720	LF_coh_HR_rsp
-0.2748	-0.0542	0.2845	LF_coh_HR_BP
-0.3504	-0.1026	-0.0994	LF_coh_BP_rsp
-0.3003	-0.2006	0.0039	HF_coh_HR_rsp
-0.3012	0.1989	0.2501	HF_coh_HR_BP
-0.3300	0.1176	-0.3431	HF_coh_BP_rsp
-0.2354	-0.3680	0.2052	LF_pcoh_HR_rsp
-0.0736	-0.0101	-0.0148	LF_pcoh_HR_BP
-0.3184	-0.1643	-0.1079	LF_pcoh_BP_rsp
-0.1085	-0.4427	0.1169	HF_pcoh_HR_rsp
-0.1080	0.1885	0.5983	HF_pcoh_HR_BP
-0.2463	0.0679	-0.5323	HF_pcoh_BP_rsp

Figure 5.62 presents a principal component plot of the data set of 8 normal subjects exercised at 50%, 75% and 100% load. The data set gave the following principal components (PC):

1st PC: rsp – The respiration rate.

2nd PC: BP – The blood pressure rate.

3rd PC: LF_pcoh_HR_BP – Partial Coherence of HR and BP IIBI signals in the LF range (0.04 - 0.15 Hz).

This indicated that the largest variance between normal subjects during exercise was the breathing rate (respiration). The second largest variance was the blood pressure. The third largest variance was the partial interrelationships between HR and blood pressure in the LF range. The 1st PC of the respiration showed the obvious indication of exercise in normal subjects with increased breathing rate followed by the increased in blood pressure in order to meet the increased oxygen demand. Once the respiration PC was removed, the residual interrelationship was that between HR and blood pressure in the LF range.

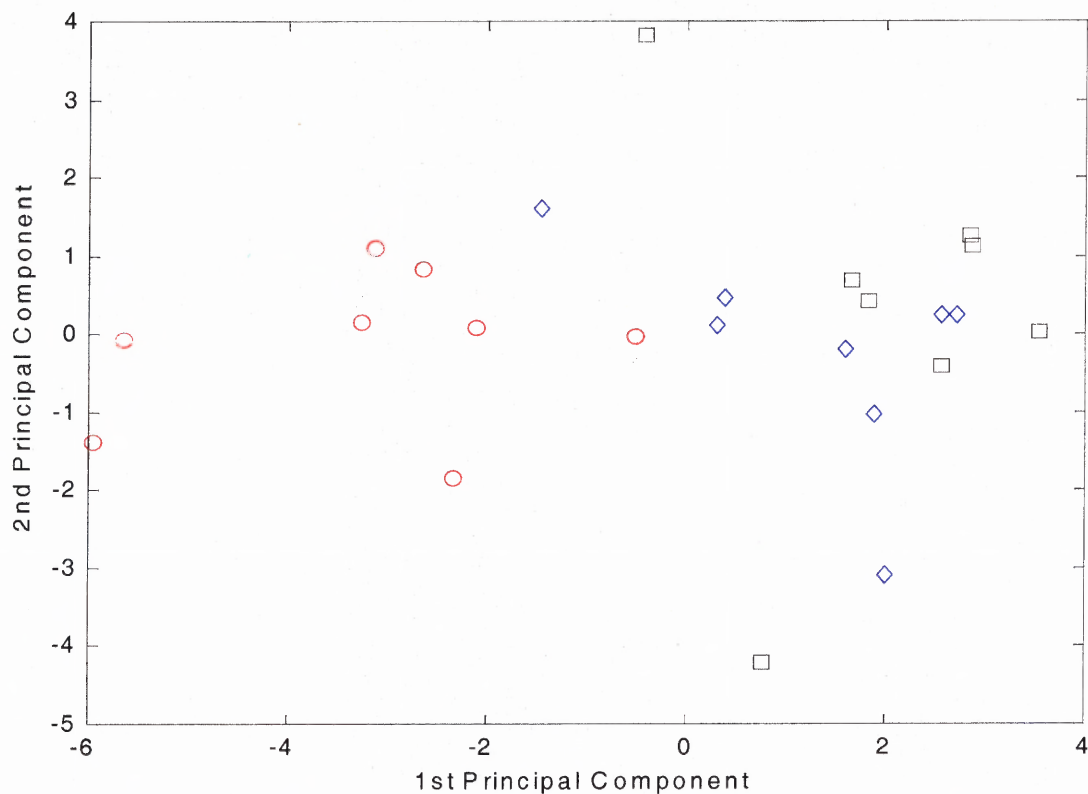


Figure 5.62 Normal classification using principal component analysis (PCA).
Note: (red: 50%, blue: 75% and black: 100% AT exercise).

Table 5.8 Principal Components from Normal Exercise Data

P1	P2	P3	Categories
0.1808	-0.3223	0.3405	rsp
0.1516	0.5183	0.1746	HR
0.1428	0.5321	0.1498	BP
-0.3332	-0.0238	-0.0139	LF_coh_HR_rsp
-0.2823	0.0823	0.3773	LF_coh_HR_BP
-0.2901	-0.0642	0.3060	LF_coh_BP_rsp
-0.2851	0.0547	-0.3642	HF_coh_HR_rsp
-0.2326	0.0083	-0.2892	HF_coh_HR_BP
-0.2361	0.3173	-0.1673	HF_coh_BP_rsp
-0.3458	-0.0110	0.0223	LF_pcoh_HR_rsp
-0.2652	0.0979	0.3797	LF_pcoh_HR_BP
-0.2982	-0.0385	0.3181	LF_pcoh_BP_rsp
-0.2627	-0.0339	-0.3151	HF_pcoh_HR_rsp
-0.2155	-0.3432	0.0706	HF_pcoh_HR_BP
-0.2523	0.3145	-0.0252	HF_pcoh_BP_rsp

Table 5.9 Principal Components of Different Population Groups

	PC1	PC2	PC3
Normal (Exercise)	RSP	BP	LF_PCOH_HR_BP
Normal + COPD1	RSP	HF_COH_HR_BP	HF_PCOH_HR_BP
Normal + COPD2	LF_COH_HR_RSP	HF_COH_BP_RSP	RSP

Table 5.9 shows the summary of the principal component analysis for the three cases of the HRV study for both normal and COPD subjects. The data set for normal subjects during exercise shows the respiration rate was first principal component (PC); the blood pressure was the second PC and the partial coherence value between heart rate and blood pressure in the low frequency range was the third PC. When the first set of data that combined the COPD and normal data was used, only the first PC of respiration was the same and the other two PC's were different. When the second set of the combined COPD-normal data was used, the three PC's were completely different. This fact indicates that the PCA method is not “event” dependent but the technique is only adaptive to the actual data used.

5.7 Cluster Analysis

The purpose of using principal component analysis (PCA) and cluster analysis (CA) is illustrated by the results of figures 5.63 and 5.64 and summarized in Table 5.10. First, PCA-CA was used to blindly separate the normal subjects and COPD patients using a data set that contained the physiological data such as heart rate, blood pressure rate and respiration rate as well as the cross-spectral results of the (weighted) coherence and partial coherence in both the LF and HF range. Figure 5.63 clearly shows the separation between the COPD group (green squares and blue pluses) from the normal group (red circles). In the same figure, one red circle of a normal subject was placed near a blue plus and a green square of the COPD subject. The reason for this may be that the COPD subjects represented by blue plus and green square may only be at risk of the disease. Hence, their physiological parameters placed them near that of the normal subject. The COPD group is represented in green and blue markers because their data came from the same COPD group, but were from two different testing trials. This proves that cluster analysis could separate the normal and COPD subjects and the results were reproducible, i.e. same results for the same COPD group even with different data sets from different experimental trials.

Figure 5.64 shows the results of not only normal and COPD blind separation but also the COPD severity classification. When the desired number of clusters was set prior to running the cluster analysis program to separate the normal group (cluster 1) from the “at risk” group (cluster 2), the “mild” group (cluster 3), the “moderate” group (cluster 4) and the “severe” group (cluster 5), the result was the graph of figure 5.64. This is the first attempt at this type of blind separation and classification. Another more fine-tuned

attempt by adjusting the threshold of the correlation coefficients would provide a better and more defined group of clusters. However, this would defeat the purpose of blind separation and classification.

The COPD assignment of the 47 COPD and 8 normal subjects are presented in Table 5.10. When compared to the clinical classification using FEV1 over FVC data the PCA-CA classification technique produces very high accuracy results. It has been shown to separate the COPD from the normal population with 100% accuracy. It can also classify the COPD population into “at risk”, “mild”, “moderate” and “severe” stages with 100%, 90%, 88% and 100% accuracy respectively. As a result, cluster and principal component analysis can be used to separate COPD and normal subjects and can be used successfully in COPD severity classification.

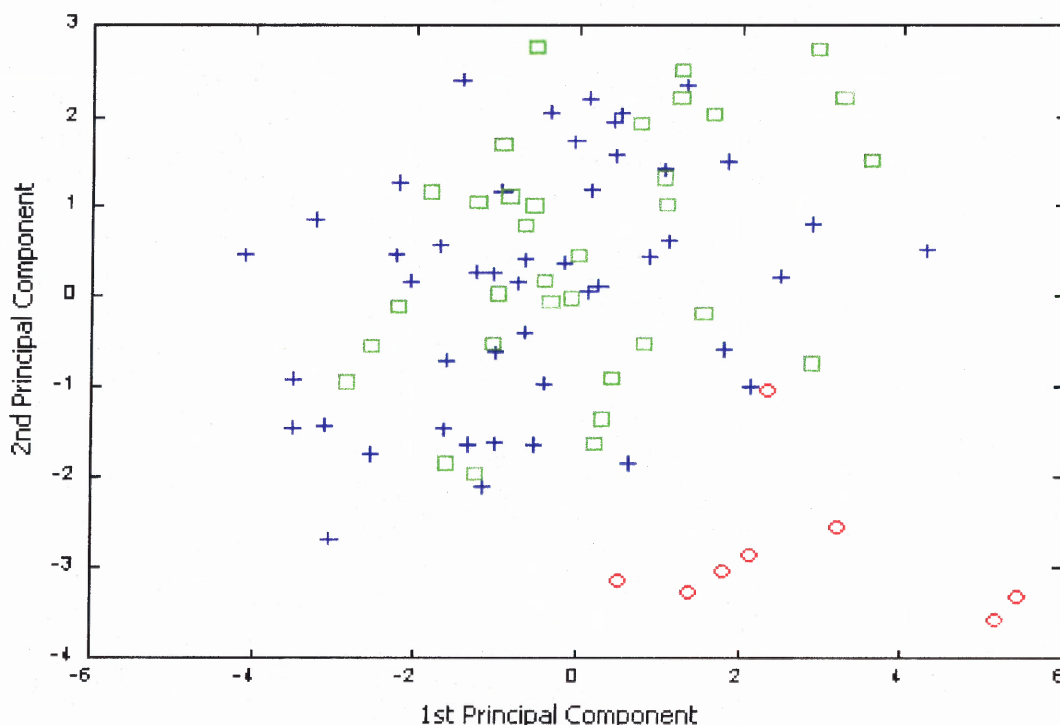


Figure 5.63 Separation of normal (Red) from COPD subjects (Blue/Green).

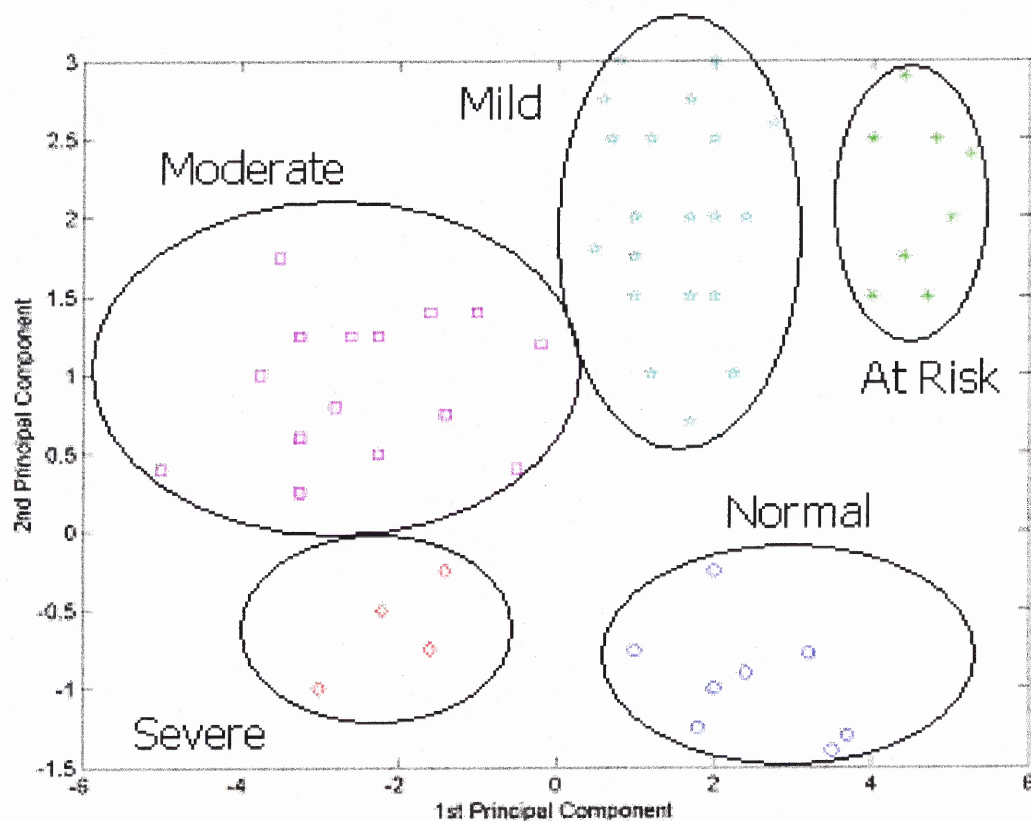


Figure 5.64 Severity classification of normal and COPD subjects. (Normal: blue circle, At Risk: green star, Mild: cyan pentagon, Moderate: magenta square and Severe: red diamond).

Table 5.10 Summary of Normal-COPD Severity Classification

Stage	Clinical	PCA-CA	% Accuracy
Severe	4	4	100.00
Moderate	17	15	88.23
Mild	18	20	90.00
At Risk	8	8	100.00
Normal	8	8	100.00

CHAPTER 6

CONCLUSIONS

Recently, joint time-frequency signal representation has received considerable attention as a powerful tool for analyzing a variety of signals and systems of biological origin, which do not comply with the stationarity assumptions. The time-frequency representations of signals can be classified as linear and quadratic. The linear time-frequency representations (TFR) include the short-time Fourier transform (STFT) and the wavelet transform. All linear TFR's satisfy the superposition or linearity principle. On the other hand, the quadratic TFR's provide a time-frequency energy distribution or instantaneous power spectrum [27]. They are called quadratic since the energy is a quadratic signal representation. An energy distribution-based TF representation combines the instantaneous power and the spectral energy density. The temporal and spectral correlations can also be combined as an alternative quadratic representation [27].

In reality signals may have unknown spectral components. In that case, TFR's may suffer significantly from cross-terms of these spectral components. This problem may be partially overcome by designing specific kernels for the signal at hand. In this dissertation, the author explored the possibility of better representation of three particular biological signals, heart rate variability, blood pressure variability and respiration. The author evaluated the use of time-frequency analysis to investigate the physical and respiratory effects attributed to COPD.

In the first phase of this work, the application of five different bilinear representations on modeled HRV test signals, and experimental HRV and BPV signals of

both the normal and COPD subjects were evaluated. Each distribution: the short time Fourier transform (STFT), the smoothed pseudo Wigner-Ville (SPWVD), the Choi-Williams (CWD) and the Born-Jordan-Cohen (BJCD), has unique characteristics which was shown to affect the amount of smoothing and the generation of cross-terms differently. The same biological signals were also analyzed using five different types of wavelets: the Morlet, Meyer, Daubechies 4, Mexican Hat and Haar wavelets. The resulting 3D and contour plots were compared: first, visually and second, by using the proposed correlation indices of the Wigner distribution, which was cited in the literature [38] as the best distribution of the Cohen's class, and five presented wavelets. Although four Cohen's class distributions and five wavelets were used to analyze the physiological data, it was found that the Morlet wavelet was consistently proven to be the best time-frequency technique for HRV, BPV and respiration analysis.

In all, the difficulty with TF analysis was the ability to extract the relevant information. The resulting time-dependent spectra contained a lot of information and knowing how to extract the information was crucial to the interpretation of the physiology. By expanding the concept of spectral analysis of heart rate variability (HRV) into time-frequency analysis, one was able to quantitatively assess the parasympathetic (HF) and sympatho-vagal balance (LF:HF) changes as a function of time. As a result, the reassessment of the autonomic nervous system during rapid changes was made. The results also demonstrated that TF analysis provided temporal and spectral localization that could not be revealed by the use of standard spectral methods. The five wavelets were chosen for further application because of overcoming the drawbacks of the other distributions by

providing higher resolution in time and frequency while suppressing interferences between the signal components.

The respiration analysis validated the physiological states the COPD subjects were in. With shortness of breath, the breathing rate has to increase to supply the body with more oxygen and remove more carbon dioxide, thus shifting the frequency of respiration into higher ranges that could reach as high as 0.55 Hz (33 bpm). The HRV analysis of normal subjects showed that with rest the average heart rate slows down while the variability in the heart rate increases. On the other hand, with exercise, the average heart rate speeds up while the variability in the heart rate decreases. Both the time-frequency and statistical analysis of the HRV signals showed that a stressful exercise level drastically changed the HRV signal and that there was a significant difference between the three states of rest, exercise, and recovery.

In the second phase of this research, the cross spectral analyses (i.e. coherence, weighted coherence and partial coherence) were used to investigate the increase or decrease of the HRV, BPV or any of the combinations of HRV, BPV and respiration that changed the behavior in the autonomic nervous system. Examination of the results for the 47 COPD and 8 normal subjects presented some real challenge because the peaks of the ECG R-waves, blood pressure peaks and even respiration signals of COPD patients were difficult to detect and analyze. However, the interrelationships between heart rate and respiration, heart rate and blood pressure, and blood pressure and respiration could be quantified and helped in understanding the various coupling effects between various systems inside the body.

In summary, COPD subjects had higher respiratory rate, heart rate and blood pressure while HRV and BPV were always lower than those of normal subjects.

From examining the transfer function and frequency response of the cardiovascular system ARX models from both normal and COPD subjects, COPD models showed a similar DC gain response (slightly less). However, there was a significant lag in phase (at -180°) for COPD models as compare to those of normal subjects.

In the last phase, a new methodology was proposed that used principal component analysis and cluster analysis to identify diseased subjects from a normal population. This method combines the techniques of principal component analysis (PCA) and cluster analysis (CA) and has been shown to separate the COPD from the normal population with 100% accuracy. It can also classify the COPD population into “at risk”, “mild”, “moderate” and “severe” stages with 100%, 90%, 88% and 100% accuracy respectively. As a result, cluster and principal component analysis can be used to separate COPD and normal subjects and can be used successfully in COPD severity classification.

In conclusion, wavelets as time-frequency representation provide great visual benefit in analyzing HRV, BPV and other biological signals. Using cross-spectral techniques such as coherence, partial coherence, and modeling transfer function analysis also provided important insights to understanding the behavior of complex physiological systems. Statistical techniques such as PCA and CA could be used as accurate tools of severity classification and could be a great help in diagnosing different disease states non-invasively.

6.1 Future Work

The applications of time-frequency analysis are countless. The constantly improving wavelet algorithms have provided more insight into a large number of clinical applications in quantifying rapid (transient) changes in biological signals. One application may be the assessment of exercise in athletes in order to find ways to induce an increase in the parasympathetic activity during or immediately after strenuous exercise. It may also be used to study electromyographical changes during various conditions or to assess autonomic nervous system damage. A future project may be the assessment of the autonomic nervous system in spinal cord injury patients. Comparison of the rate of change of the vagal tone during a provocation of healthy subjects to spinal cord injured subjects may allow us to categorize the severity of the injury as well as increase our understanding of the nervous system dysfunction in spinal cord injured people. At last there are now many new methods available to biomedical researchers to help them in their research.

In this dissertation, many signal processing techniques in time domain, frequency domain, time-frequency domain as well as statistical techniques have helped providing more insights to the heart rate variability field. Other helpful insights that might affect the variability in the data are the gender, smoking, and fitness conditions, which should be included in normal data for future research. With such a small sample of participants (eight), these conditions should be limited to one gender and one fitness level, with no smoking to assess better the findings in a specified population.

APPENDIX A

EXERCISE PHYSIOLOGY

A.1 Borg Perceived Exertion Scale

Figure A.1 shows the Borg scale of perceived exertion. The original Borg scale of perceived exertion has been modified. The number from 6 to 10 are in green, the numbers from 11 to 15 are in yellow, and the numbers from 16 to 20 are in red, similar in concept to traffic lights.

A.2 The Karvonen Formula

The Karvonen's Formula is an accurate way to calculate your desired aerobic training intensity. The required information:

1. Your age in years.
2. Resting Heart Rate – in beats per minute. Take your resting heart rate in the morning. Lie quietly and take a one-minute pulse. Do this for three mornings in a row to record the average.
3. Percentage of Maximum Heart Rate. The American College of Sport Medicine recommends exercising between 60% and 90% of your Maximum Heart Rate.

6	very, very light
7	
8	
	very light
9	
10	
	fairly light
11	
12	
	somewhat hard
13	
14	
15	hard
16	
17	
	very hard
18	
19	
	very very hard
20	

Figure A.1 The Borg scale of perceived exertion.

A.3 Figure Out Your Target Heart Rate!

To get the maximum benefit from exercise, it is best to work at a pre-determined target heart rate.

A.3.1 Taking your Pulse

The pulse is most commonly taken either at the carotid artery on the neck or at the wrist. Use your index finger and middle finger to locate your pulse (never use your thumb). Use a very light touch and avoid pressing too hard. You may use a 6 or 10 second pulse check, then multiply by the appropriate number (10 or 6 respectively) to get a 60 second count.

A.3.2 Maximum heart rate

This heart rate generally declines with age from about 220 beats per minute in childhood to about 160 beats per minute at age 60. This fall in heart rate is fairly linear, decreasing by approximately 1 beat per minute per year. There is no strong evidence to suggest that training influences the decline in maximal heart rate. It should be remembered that individuals of the same age might have quite different maximal heart rates. Therefore it is more accurate to calculate this value by undergoing a stress test than by using an age-related formula. On the other hand, resting heart rate is greatly influenced by endurance training.

A.3.3 Resting Heart Rate

This is your heart rate at complete rest. To determine this, take your pulse for 60 seconds just before you get out of bed...or take it for 30 seconds and multiply by 2. The typical adult has a resting heart rate of about 72 bpm whereas highly trained runners may have readings of 40 bpm or lower.

A.3.4 Target Heart Rate Range

Training intensity should range from 40% - 85% of adjusted maximal heart rate. Beginning exercisers should work between 50% - 65%. More advanced exercisers may be comfortable in the 70% - 80% range. Very fit exercisers may tolerate a level up to 85%.

A.3.5 Calculate

For your age, use a whole year. (Between 0 and 100)

Put your Resting Heart Rate. (Between 30 and 100)

Enter your maximum heart rate if you know it (use a number between 50 and 85)

Otherwise use an estimate as follows:

Males: $214 - (0.8 * \text{age})$.

Females: $209 - (0.7 * \text{age})$.

Calculate your target heart rate using the Karvonen's formula:

$$\text{HeartRate} = \frac{(\text{MaxHR} - \text{RestingHR}) * \text{TargetHR}}{100} + \text{RestingHR} \quad (\text{A.1})$$

APPENDIX B

ANALYSIS PROGRAM LISTINGS

The analysis programs were written in both LabVIEW and MATLAB. The cross-spectral analysis which calculated and provided the weighted coherence and weighted partial coherence values between heart rate and respiration, heart rate and blood pressure and blood pressure and respiration was included in one LabVIEW program. The LabVIEW graphical program is presented in Section B.1. All the time-frequency representations (linear and bilinear), the PCA, cluster analysis and correlation index calculation for choosing the best time-frequency distributions were written in MATLAB as shown in Section B.2.

B.1 Cross-Spectral Analysis Steps

This section outlines the procedure for performing heart rate variability (weighted) coherence and partial coherence between heart rate and blood pressure, heart rate and respiration, and blood pressure and respiration combination. The programs are written in LabVIEW using the data file that includes ECG, BP and respiration signals as input. The outputs of the front panel include the plots of the raw data for the respiration, ECG and blood pressure signals. The graphs of the derived heart rate, blood pressure IIBI, and the respective power spectra of each as well as the values of the areas under the heart rate spectral curves in the LF and HF ranges are also shown in the front panel. The outputs of the coherence-partial coherence panel are the coherence and partial coherence plots with the appropriate weighted values for each coherence/partial coherence combination.

As an example, the procedure of the cross-spectral analysis using a data file of a COPD subject in text format acquired using the National Instrument data acquisition system, saved as file name `agu1baseline.txt` is presented below:

- 1) Find the data acquisition sampling frequency, `sf`, of the data file. Use WinEdit or Notepad to open the data file. A single integer number on line 1 of the data file is the sampling frequency of the file. Record this number for reference. In all studies used for this dissertation, the sampling frequency is 200 samples per second.
- 2) Next, the information of what signal on what channel is needed. Click on the LabVIEW icon to start running LabVIEW. The National Instrument LabVIEW dialog box opens. Click on Open VI bar to select the data file to load. The Choose the VI to open: dialog box opens. Click on the down arrow of the Look in: bar to navigate the windows directory and select the VI program. Double click to select `4dsp.vi`. The `4dsp.vi` front panel is displayed. Click on the right arrow on the command bar to run the LabVIEW (`4dsp.vi`) program. The choose file to read dialog box appears. Use the down arrow button in the Look in: bar to navigate the directory to select the data file to be analyzed (in the example, the data file is `agu1baseleine.txt`). Double click on the data file name to run the program.
- 3) In a few seconds, the plots of all four data signals are displayed. Resize the x-axis on each plot to zoom in to a small section of the signal. Record the signals and their channel numbers for reference. (In the example, the channels are shown below)

Signal	Channel
CO2	0
BP	1
Resp	2
ECG	3

- 4) Click on file, close to exit the 4dsp.vi program. Click No when the save changes dialog box appears.
- 5) Click on open VI of the LabVIEW dialog box. Use the down arrow button of the Look in: task bar to select partcoh3.llb library of LabVIEW programs. Use the mouse to move the up/down bar until the partial coherence between HR, BP & RESP vi file appears. Double click on this file to run the LabVIEW program.
- 6) Enter the SF, ECG, BP and RESP in the text boxes on the front panel with the information obtained in steps 1 and 3 above. Click the right arrow on the command bar to run the program.
- 7) The Choose file to read dialog box appears. Use the down arrow button of the Look in: task bar to select the data file (agu1baseline.txt) to be analyzed.
- 8) After a few seconds, the heart rate IIBI and the ECG plots of the Correct.vi appears. Move the yellow cursor inside the HR IIBI plot to the end of the HR IIBI signal then click the MOVE button to see any missed or false R wave detection. Use the blue cursor inside the ECG correction plot to manually remove or correct the false R wave detection indicated by the white bar under each ECG R-wave. Click the round green Done button when done.
- 9) The Choose HR IIBI file to write dialog box appears. Enter the HR IIBI ASCII file name (agu1baselineHR.asc) in the file name field then click the save button.
- 10) The Choose BP IIBI file to write dialog box appears. Enter the BP IIBI ASCII file name (agu1baselineBP.asc) in the file name field then click the save button.
- 11) The panel partial coherence HR-BP-RESP.vi appears. Move all the red cursors (Cur 0) to 0.04 Hz positions and all the blue cursors (cur 1) to position 0.15 Hz of the

coherence and partial coherence plots. Click the right arrow to calculate the weighted values in the LF range. Once the LabVIEW program stops, print the coherence and partial coherence panels with the associated LF weighted values for records.

12) Move all the red cursors (Cur 0) to 0.15 Hz positions and all the blue cursors (cur 1) to position 0.40 Hz of the coherence and partial coherence plots. Click the right arrow to calculate the weighted values in the HF range. Once the LabVIEW program stops, print the coherence and partial coherence panels with the associated HF weighted values for records.

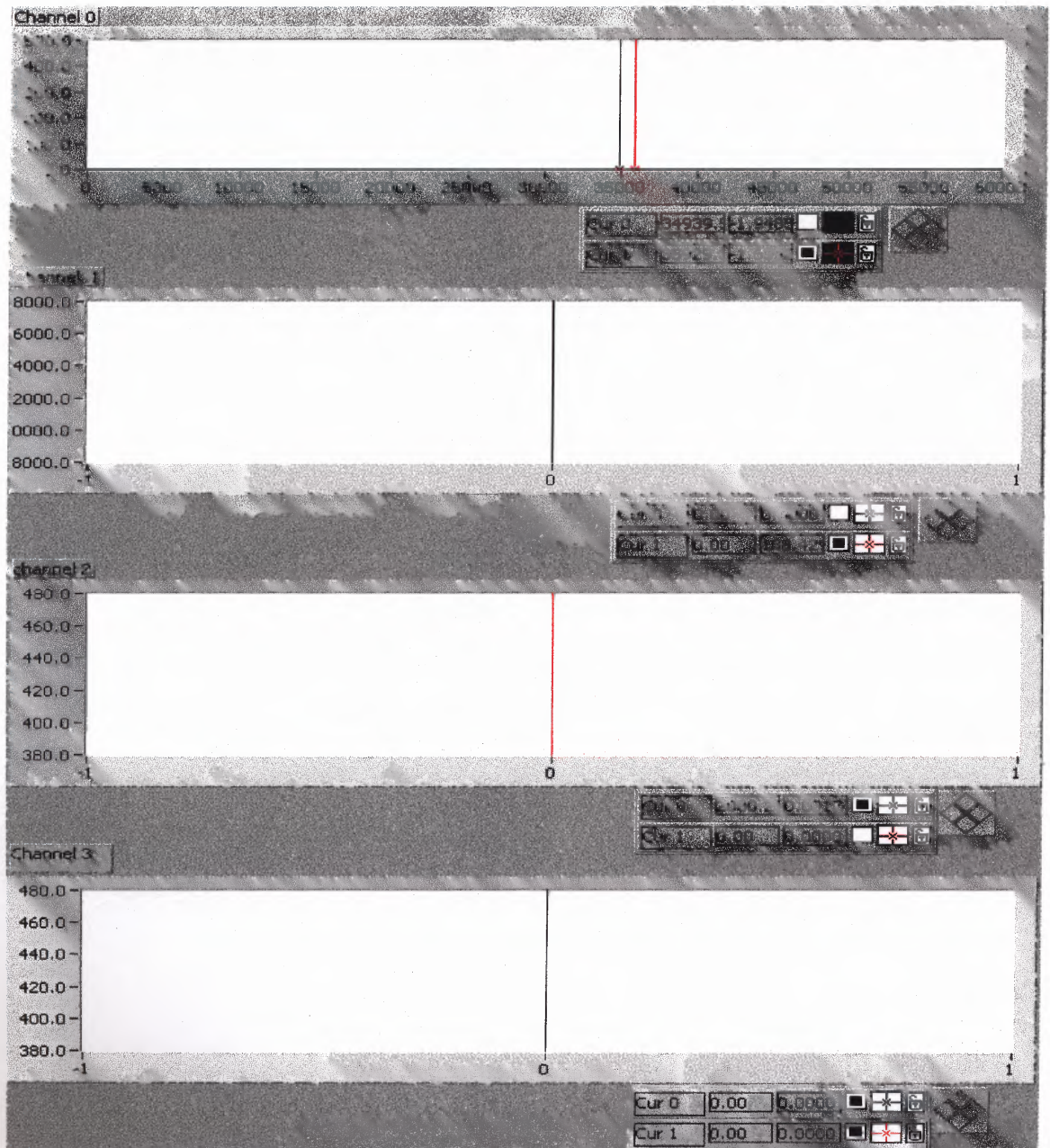
B.1.1 4dsp.vi

Below is the listing of the 4dsp.vi LabVIEW program. This program shows what signal is acquired on what channel in the data file

4dsp.vi
Connector Pane



Front Panel



B.1.2 Partial Coherence Between HR, BP & RESP

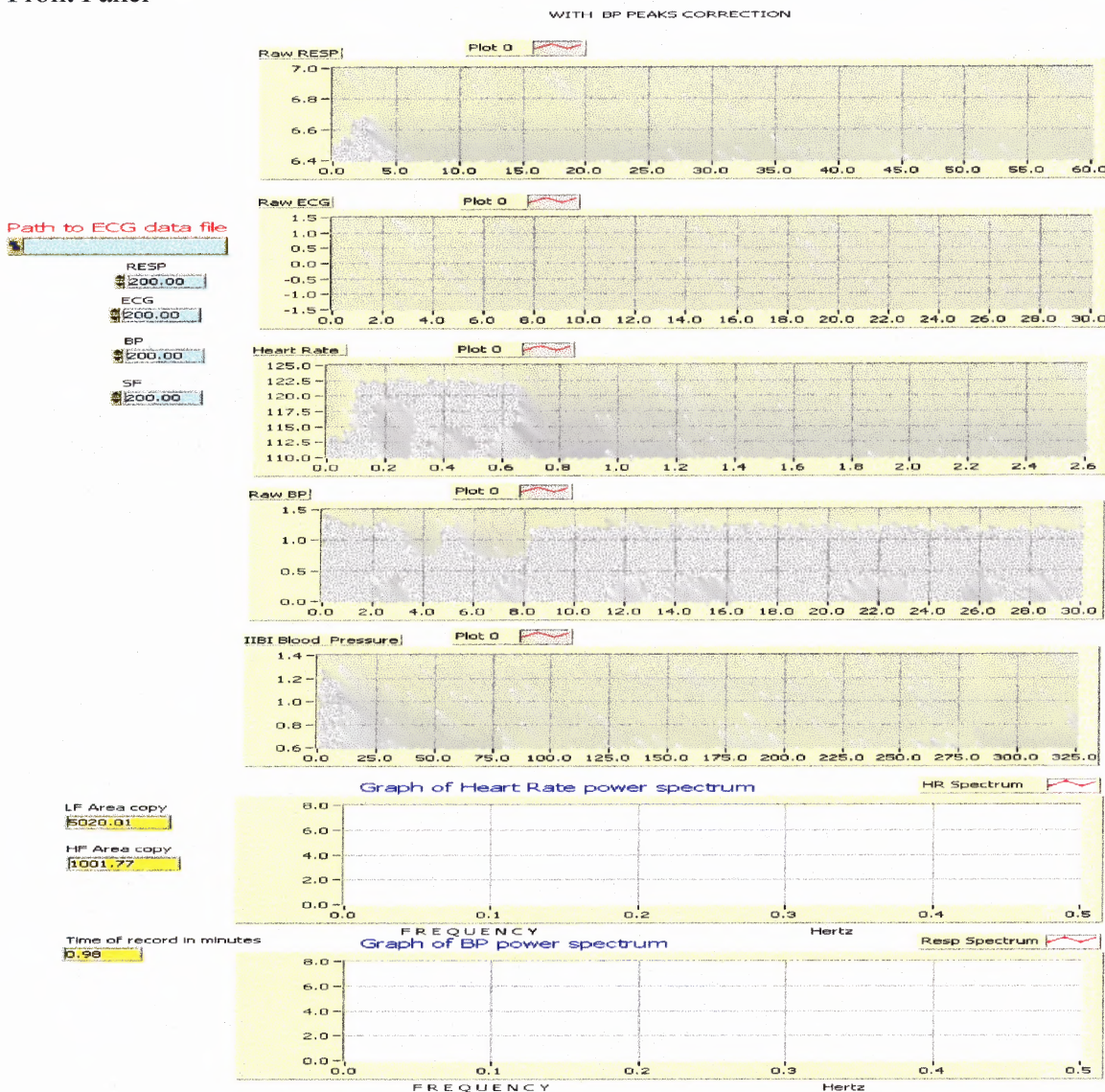
Below is the listing of the partial coherence between HR, BP & RESP LabVIEW program. This program displays the plots of coherence and partial coherence and the weighted values in both the LF and HF of the data file:

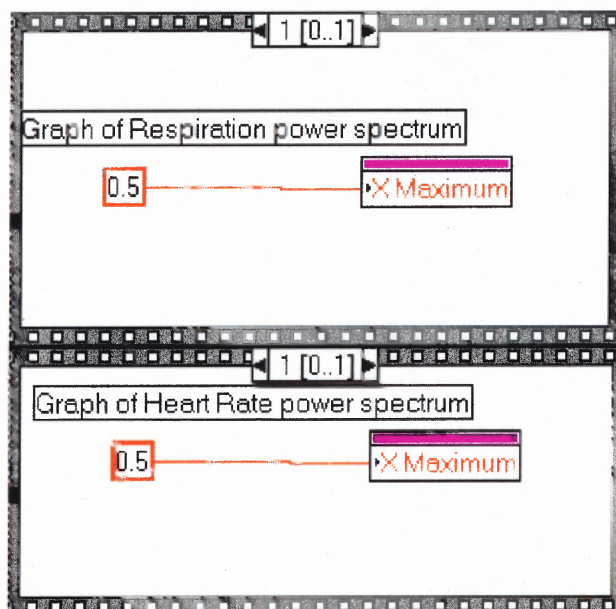
partial coherence betwn HR, BP & RESP

Connector Pane



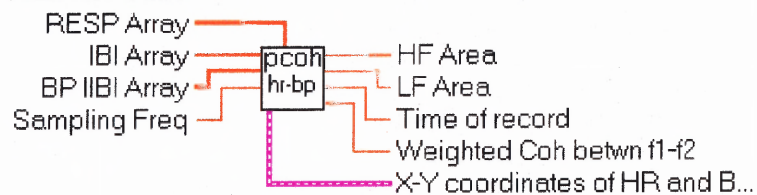
Front Panel



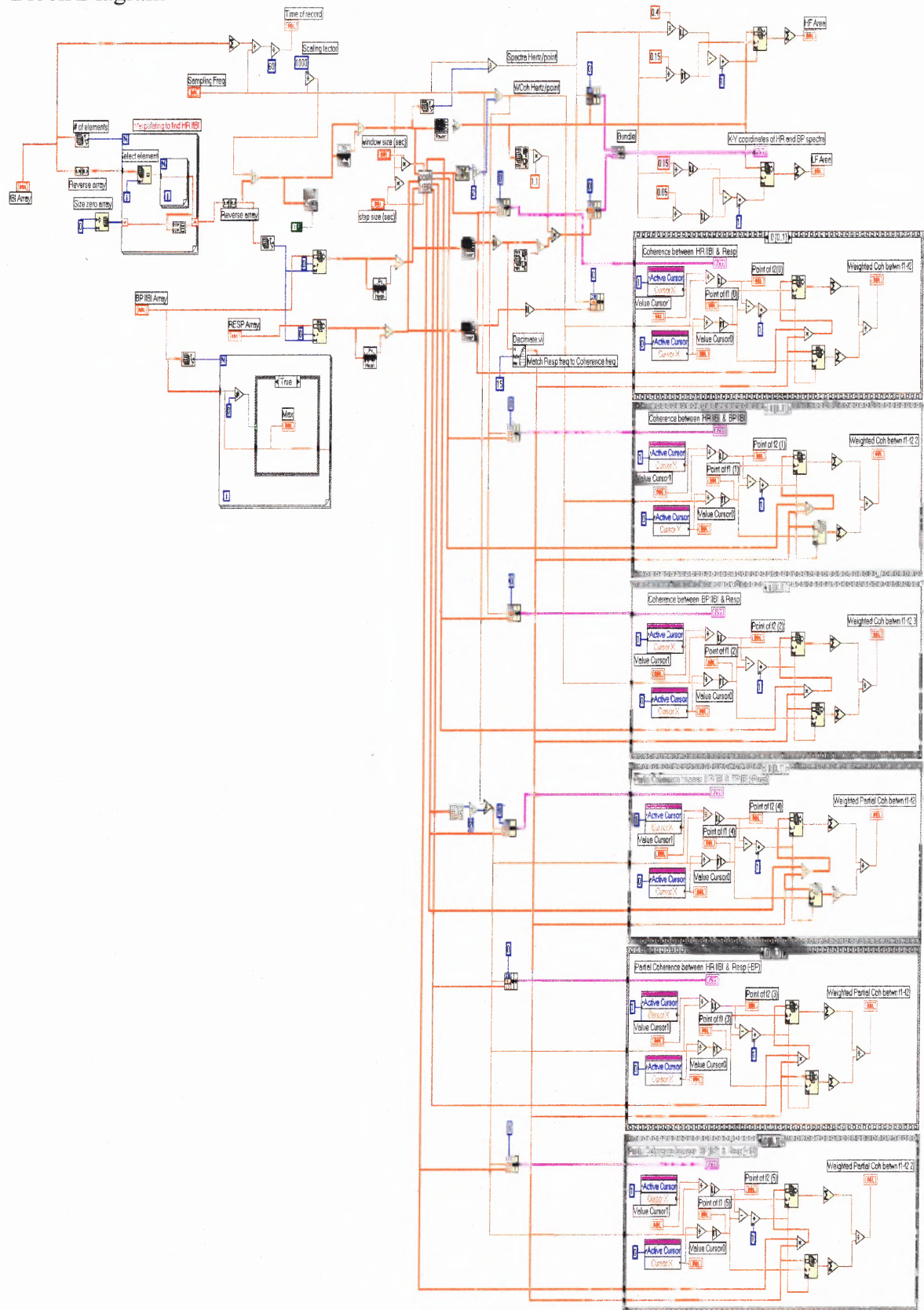


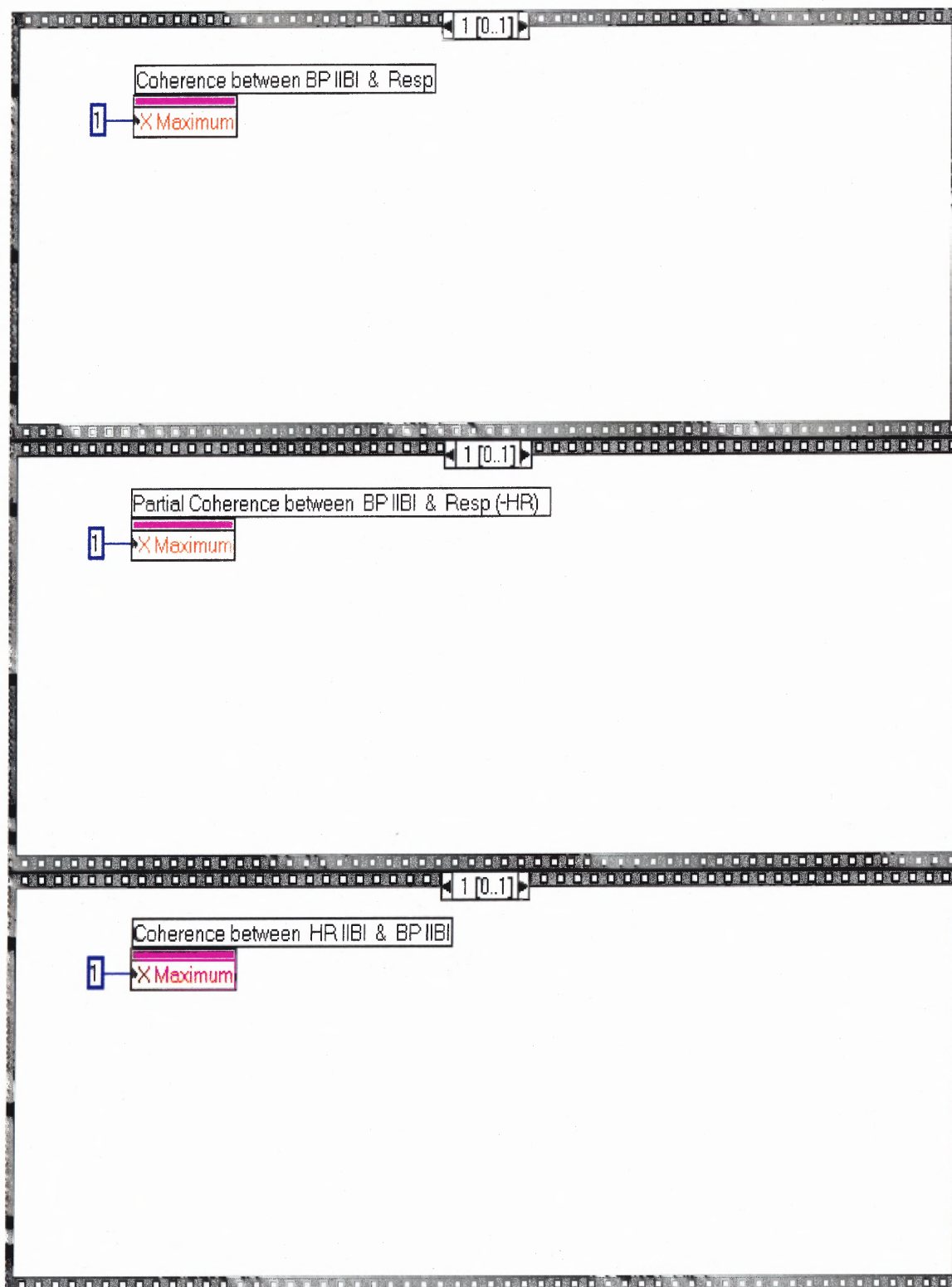
Panel of the “partial coherence HR - BP-RESP.vi” sub VI.

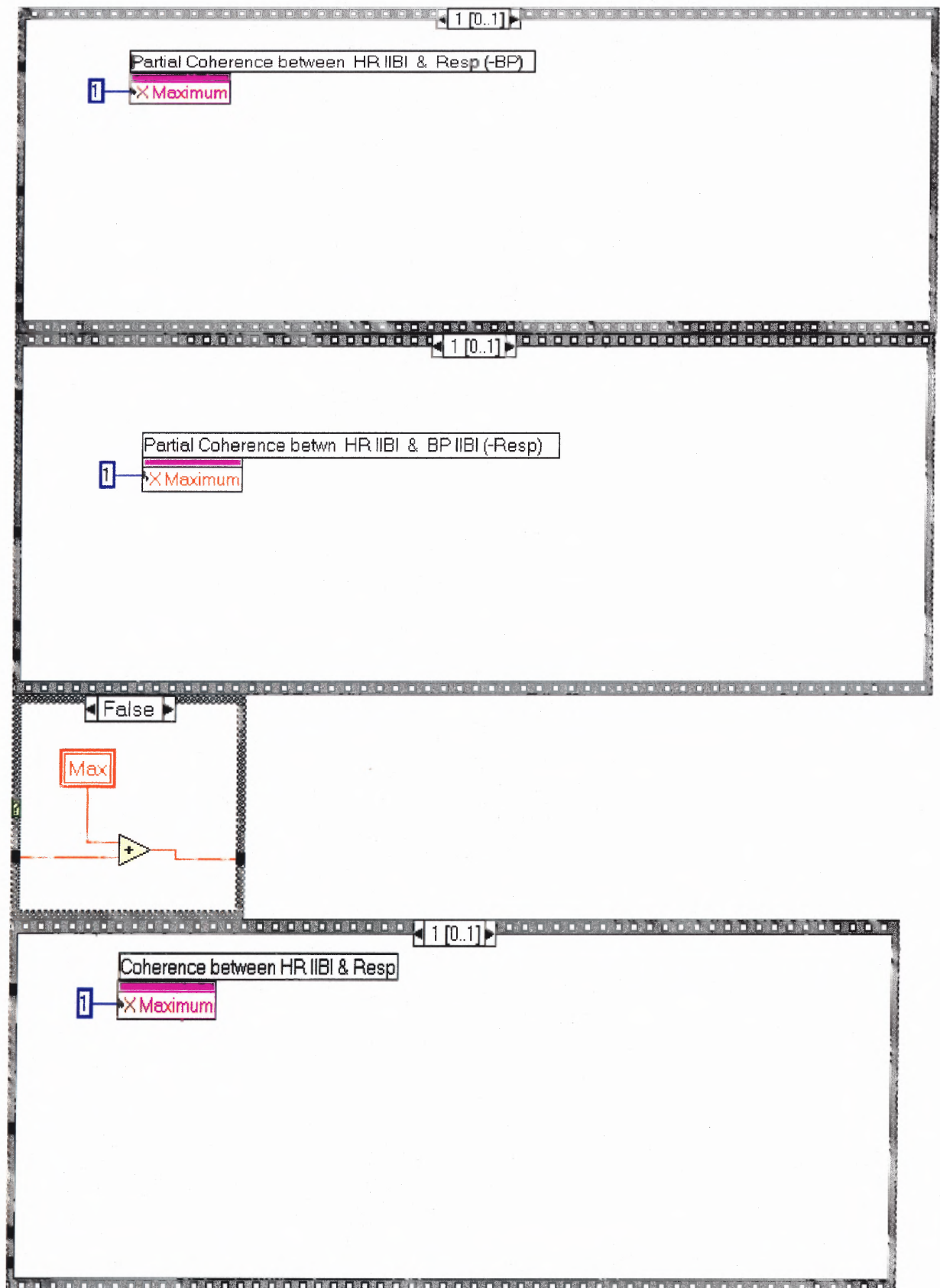
Connector Pane



Block Diagram







B.2 MATLAB Programs

This section provides the listing of different MATLAB programs used for analysis in this dissertation.

B.2.1 Test Signal of Three Sinusoids at 0.3, 0.1 and 0.5 Hz

This MATLAB program generates a test signal of three sinusoids with frequencies of 0.3, 0.1 and 0.5 Hz and saves the output signal in an ASCII file called signal_3.asc.

```
% signal.m
%
% This is the source code for creating three different signals which each signal
% is made of three sine wave with frequencies of 0.2, 0.5 and 1.0 Hertz. The
% sampling frequency for the all signals is 200 samples per second.
% Each signal is located as a one column of matrix sig_tes. The length of FFT is
% 2048 points.
% The plots of power spectrum are zoomed in. The last two lines of the instructions
% is used to save the figures in Metafile format and then is imported to Microsoft
% word (ver. 6.0a).
%
t=0:0.005:29.99;
signal_3=[sin(2*pi*0.3*t)zeros(1,1000)sin(2*pi*0.1*t)zeros(1,1000) sin(2*pi*0.5*t)];
ref=length(signal_3);
Pyy=abs(fft(signal_3,4096));
F=(200*(0:63)/4096);                                %sampling rate 200 sps
T=(ref/200)/(ref-1)*(0:ref-1);
figure(1);
plot(T,signal_3,'r');xlabel('Time(second)');ylabel('Amplitude');
pause
figure(2);
plot(F,Pyy(1:64),'r');xlabel('Frequency(Hertz)');ylabel('Power Density');
save signal_3.asc signal_3 -ascii;
```

B.2.2 Time – Frequency Analysis and Activity Plot Program

This program is a MATLAB m-file. Upon starting MATLAB, type **whitebg** for a white graphic background.

1. The data needed is the interpolated inter-beat interval ASCII file. In LabVIEW, after you have created the heart rate or blood pressure IIBI file, you must make sure it is an ASCII file with channel data in column format with the extension (*filename.asc*). In order to run the MATLAB program, type:

tfrs

2. A “select your distribution” graphical user interface will pop up. Use the mouse to click on the desired time-frequency distribution for analysis.

Short Time Fourier Transform

Wigner

Smoothed Wigner

Choi-Williams

Born Jordan Cohen (RID)

Rihaczek Margeneau

3. The program will ask you to enter the filename without extension. Type in the filename then hit return.

Agu1hrbp (of the Agu1hrbp.asc file)

4. Enter the channel number you want to analyze.

1 (or 2, 3, 4...)

5. Enter the sampling rate of the data.

200 (or the appropriate sampling rate)

6. The program will run and output the appropriate time-frequency plots and the activity plots (LF, HF and LF/HF: non-normalized and normalized) of the channel that was analyzed using the selected time-frequency distribution.

This program provides the STFT and the bilinear time-frequency analysis (Wigner, Smoothed Wigner, Choi-William, Born-Jordan-Cohen and Rihaczek-Margenau) with 3D power spectra versus time and frequency, contour plots and activity plots using the selected time-frequency distribution as outputs.

```
% This program is a modified version of the original work of Adib Mansour (1994)
% by Rindala Saliba (1996)
% Modified by Douglas Newandee 7/14/2001 for better 3D Graphs and to work with
% MATLAB 6.0 and later.
%

clear
clc
choose=menu('SELECT YOUR DISTRIBUTION', 'Short Time Fourier Transform',...
    'Wigner','Smoothed Wigner',...
    'Choi_Williams',...
    'Born_Jordan_Cohen (RID)','Rihaczek_Margenau');
clc
disp("")
disp([blanks(30) 'WELLCOME TO'])
disp([blanks(21) 'TIME FREQUENCY DISTRIBUTION'])
disp([blanks(33) 'WORLD'])
disp("")
disp("")
SIGNAL=input('Please enter name of datafile with no extension --> ','s');
filename=[SIGNAL,'.asc'];
eval(['load ' filename]);
original_rawdata=eval(SIGNAL);clear SIGNAL;
Question_1=input('Which column do you want to analyze? [1 2 3] --> ','s');
if    Question_1=='1'
    rawdata=original_rawdata(1,:);
elseif    Question_1=='2'
    rawdata=original_rawdata(2,:);
elseif    Question_1=='3'
    rawdata=original_rawdata(3,:);
end
end
Signa=rawdata;
%
Lwin=input('Please enter the length of analysis window --> ');
ffflen=input('Please enter the length of FFT analysis --> ');
skip=input('Please enter the number of the skip points --> ');
sample=input('Please enter the sample rate of the data --> ');
Question_2=input('Do you want to detrend the input signal? [y/n] --> ','s');
```

```

if Question_2=='y'
    order=input('Please enter the order of the lowpass filter --> ');
    freq=input('Please enter the cutoff frequency for LPF --> ');
    nfreq=freq/sample;
    [poles,zero]=butter(order,nfreq);
    dtrend=filtfilt(poles,zero,rawdata);
    Result_Signa=rawdata-dtrend;
    Signa=Result_Signa;
else
end
Question_3=input('Do you want to calculate Instantaneous Frequency? [y/n] --> ','s');
Question_4=input('Do you want to calculate Median Frequency? [y/n] --> ','s');
if Question_4=='y'
    LF=input('Please enter the low frequency? [Hz] --> ');
    HF=input('Please enter the High frequency? [Hz] --> ');
else
end
Question_6=input('Do you want to extract certain Frequency range? [y/n] --> ','s');
if Question_6=='y';
    LFC=input('Please enter the low frequency range in index --> ');
    HFC=input('Please enter the high frequency range in index --> ');
else
end
hlf=(Lwin+1)/2-1;
I=2*hlf+Lwin/2;
signal=hilbert([zeros(1,2*hlf),Signa,zeros(1,2*hlf)]);
signal_conjugate=conj(signal);
%
%      (Smoothed WVD using a rectangular window of odd length)
%
if choose==3
    P=input('Please enter the length of smoothing region --> ');
    distribution=['smoothed WVD'];
    G=(1/(2*P-1))*ones(hlf+1,hlf+1);
    G(:,hlf+1)=zeros(hlf+1,1);
    %
    %      (Choi-Williams)
    %
elseif choose==4
    distribution=['Choi_Williams'];
    Sigma=1;
    G=zeros(hlf+1,hlf+1);
    G(1,1)=1.0;
    for j=1:hlf;
        for i=0:hlf, G(i+1,j+1)=exp((-1)*Sigma*i*i)/(4*j*j));
        end
end

```

```

G(:,j+1)=G(:,j+1)/(2*sum(G(:,j+1))- G(1,j+1));
end
%
%           (Short Time Fourier Transform)
%
elseif choose==1
distribution=['Short Time Fourier Transform'];
G=(1/(2*hlf-1))*fliplr(triu(ones(hlf+1,hlf+1),0));
%
%           (Born-Jordan-Cohen)
%
elseif choose==5
distribution=['Born_Jordan_Cohen'];
G=fliplr(flipud(triu(ones(hlf+1,hlf+1),0)));
for i=0:hlf, G(i+1,:)=(1/(1+i))*G(i+1,:);
end
%
%           (Rihaczek-Margenau)
%
elseif choose==6
distribution=['Rihaczek_Margenau'];
G=ones(hlf+1,hlf+1);
G=0.5*diag(diag(G));
G(1,1)=1;
end
%
%           (Computation of TFDs)
%
Timeslice=floor((length(signal)-4*hlf-(Lwin/2))/skip);
kernel=zeros(fflen,Timeslice);
TFDs=zeros(Lwin,Timeslice);
if Timeslice<=0
disp(' ')
disp('---> The size of data file is less than the length of FFT');
disp('---> Therefore the process will be terminate now. ');
disp('---> Please reduce the length of FFT and try again. ');
break;
end
h = waitbar(0,'Please wait while it is processing...');
if choose<6
for n=0:skip:skip*(Timeslice-1);
for m=0:hlf,
kernel(m+1,(n/skip)+1)=(G(1,m+1)*signal(I+m+n)*signal_conjugate(I-m+n))...
+sum(G(2:hlf+1,m+1)).*(signal(I+1+m+n:I+hlf+m+n).*signal_conjugate(I+1-m+n:I+hlf-
m+n))...
+signal(I-1+m+n:-1:I-hlf+m+n).*signal_conjugate(I-1-m+n:-1:I-hlf-m+n));

```

```

end
waitbar(n/(length(signal)-4*hlf-1))
end
kernel(ffflen-hlf+1:ffflen,:)=flipud(conj(kernel(2:hlf+1,:)));
TFDs=2/ffflen*abs(fft(kernel,ffflen));
close(h)
else
distribution=['Wigner'];
for n=0:skip:skip*(Timeslice-1);
V1=(signal(I+n:I+hlf+n).*signal_conjugate(I+n:-1:I-hlf+n));
kernel(1:hlf+1,(n/skip)+1)=(V1+(sqrt(-1)*V1))';
kernel(ffflen-
hlf+1:ffflen,(n/skip)+1)=flipud((conj(V1(2:hlf+1))+[imag(V1(2:hlf+1))+(sqrt(-
1)*real(V1(2:hlf+1)))])');
waitbar(n/(length(signal)-4*hlf-1))
end
TFDs=2/ffflen*abs(fft(flipud(kernel)));
close(h)
end
% (Algorithm to calculate instantaneous frequency)
%
if Question_3=='y';
[r,C]=size(TFDs);
for i=1:C,
W=TFDs(:,i);
Y=(1:r)';
M=W.*Y;
S=sum(M);
F=sum(W);
E(i)=S/F;
end
elseif Question_3=='n';
end
%end          % correct mismatched end (DAN)
%
% (Algorithm to extract certain frequency)
%
if Question_6=='y';
symvag=sum(TFDs(LFC,1:Timeslice));
vagal=sum(TFDs(HFC,1:Timeslice));
symtopar=symvag./vagal;
end
elseif Question_6=='n';
end
%
% (Three Dimensional Graphics)

```

```

%
T=(length(Signa)/sample)/(Timeslice)*(0:Timeslice-1);
f=(sample/(2*ffilen))*(0:ffilen-1);
c=length(Signa);
ref=(c/sample)/(c-1)*(0:c-1);
%
if Question_4=='y';
    low=1;
    while f(low)<LF
        low=low+1;
    end
low_freq=low;
    high=ffilen/2+1;
    while f(high)>HF
        high=high-1;
    end
high_freq=high;
    lo_hi=low_freq:high_freq;
    desire_median_power=sum(TFDs(lo_hi,:))/2;
    [ROW,COL]=size(TFDs);
    median_frequency=zeros(1,COL);
    for slice_power=1:COL
        col_index=low_freq;
        Median_Power=TFDs(low_freq,slice_power);
        while Median_Power < desire_median_power(slice_power)
            col_index=col_index+1;
            Median_Power=Median_Power+TFDs(col_index,slice_power);
        end
        median_frequency(slice_power)=f(col_index);
    end
end
%
%           (Algorithm to Line fit the Median frequency)
%
    feeding=polyfit(T,median_frequency,1);
    fit=polyval(feeding,T);
elseif Question_4=='n';
end
disp('Do you want to look at (a)mesh&Contour , (b)mesh')
disp([blanks(24) '(c)contour,    (d)None'])
FigType=input('-->','s');
if FigType=='a';
    figure(1);
    subplot(2,1,1), mesh(T,f,TFDs);
    xlabel('Time(sec)');
    ylabel('Frequency(hertz)');
    zlabel('Magnitude');

```

```

title(['Mesh & Contour of ',eval('filename'),' using ',eval('distribution'),' distribution']);
subplot(2,1,2), contour(T,f,TFDs);
xlabel('Time(sec)');
ylabel('Frequency(Hz)');
pause
elseif FigType=='b';
figure(1);
mesh(T,f,TFDs);
xlabel('Time(sec)');
ylabel('Frequency(Hz)');
zlabel('Magnitude');
title(['Mesh of ',eval('filename'),' using ',eval('distribution'),' distribution']);
pause
elseif FigType=='c';
figure(1);
contour(T,f,TFDs);
xlabel('Time(sec)');
ylabel('Frequency(hertz)');
title(['Contour of ',eval('filename'),' using ',eval('distribution'),' distribution']);
pause
elseif FigType=='d';
end
%           (Algorithm to calculate Median frequency)
%
%
%
if Question_4=='y';
slope=(fit(3)-fit(1))/(T(3)-T(1));
S1 = sprintf('slope is %5.2f',(fit(3)-fit(1))/(T(3)-T(1)));
S2 = sprintf('Y_intercept is %5.1f,fit(2)-slope*T(2));
figure(2);
plot(T,fit,T,median_frequency,'*');
title(['Median frequency of ',eval('filename'),' ',eval('S1'),' ',eval('S2'),' ',Hertz]);
xlabel('Time(sec)');
ylabel('Frequency(Hertz)');
else
end
pause
if Question_3=='y' & Question_2=='y';
figure(3);
subplot(3,1,1), plot(ref,rawdata);
title(['Superimpose of rawdata & detrended & IF of ',eval('filename')]);
xlabel('Time(sec)');
ylabel('Amplitude');
subplot(3,1,2),plot(ref,Signa);
xlabel('Time(sec)');
ylabel('Amplitude');

```

```

subplot(3,1,3), plot(T,E);
xlabel('Time(sec)');
ylabel('frequency');
elseif Question_3=='y' & Question_2=='n'
figure(3);
subplot(2,1,1), plot(ref,rawdata);
title(['Superimpose of rawdata of ',eval('filename')]);
xlabel('Time(sec)');
ylabel('Amplitude');
subplot(2,1,2), plot(T,E);
xlabel('Time(sec)');
ylabel('Amplitude');
elseif Question_3=='n' & Question_2=='y'
figure(3);
subplot(2,1,1), plot(ref,Signa);
title(['plot of rawdata & detrended of ',eval('filename')]);
xlabel('Time(sec)');
ylabel('Amplitude');
subplot(2,1,2), plot(ref,Signa);
xlabel('Time(sec)');
ylabel('Amplitude');
elseif Question_3=='n' & Question_2=='n'
figure(3);
plot(ref,Signa);
title(['plot of rawdata of ',eval('filename')]);
xlabel('Time(sec)');
ylabel('Amplitude');
end
pause
%
%
if Question_6=='y';
figure(4);
subplot(3,1,1), plot(T,symvag);
title(['Mixture of Sym&Parasym & Parasym range & Ratio of Lowfreq to HighFreq']);
xlabel('Time(sec)');
ylabel('Amplitude');
subplot(3,1,2), plot(T,vagal);
xlabel('Time(sec)');
ylabel('Amplitude');
subplot(3,1,3), plot(T,symtopar);
xlabel('Time(sec)');
ylabel('Amplitude');
if Question_6=='n';
end
end
end

```


B.2.3 Program to Generate Activity Plots Using Wigner Distribution

This program is a MATLAB m-file. Upon starting MATLAB, type **whitebg** for a white graphic background.

1. The data needed is the interpolated inter-beat interval ASCII file. In LabVIEW, after you have created the heart rate or blood pressure IIBI file, you must make sure it is an ASCII file with channel data in column format with the extension (*filename.asc*). In order to load it into MATLAB. Type:

load Agu1hrbp.asc; Note: Agu109hrbp.asc is the *filename*.

If you now type **whos**, the file should show up as the variable Agu1hrbp.

2. Run the program:

symparl(data,'graphtitle')

Here, data is Agu1hrbp, and graphtitle is the title you choose. It must, however, be in single quotes as shown.

3. The program will ask for frequency index ranges for the calculation of the area under the high and low frequency peaks:

For the low frequency (LF) range:

.05-.15 Hz use 1:4 (rest, pace 12 & 18, exercise, recovery)

.05-.10 Hz use 1:3 (pace 8)

For the high frequency (HF) range:

.15-.4 Hz use 4:10 (rest, pace 12 & 18)

.10-.4 Hz use 3:10 (pace 8)

.15-.8 Hz use 4:20 (exercise and recovery)

4. The program creates five output graphs. If you want to print them you can do so manually.
5. On three graphs you will see a cross hair. Place it where you want your graph title to go and click the left mouse button.

B.2.3.1 Some Important Equations This section explains some of the terms and their relations in the various MATLAB programs:

#skip * #time slices < (or =) #data points in the file

LP Butterworth filter used: Cutoff frequency: 0.03 Hz

LF Range: 0.05-0.15 Hz

HF Range: 0.15-0.4 Hz

FFT: 512 points

#skip: 25 pt

1st time slice: at 256 pt

2nd time slice: at 256 + 25 = 281 pt

3rd time slice: at 281 + 25 = 306 pt

$\#time\ slices = \frac{\#data\ points - FFTsize}{skip}$ i.e. Number of spectra calculated.

$actual\ time\ of\ each\ time\ slice = \frac{\frac{FFT}{2} + (time\ slice * skip\ size)}{sampling\ rate}$

Example:

$time\ in\ sec\ of\ 3rd\ time\ slice = \frac{\frac{512}{2} + (3 * 25)}{20} = 16.55\ sec$

B.2.3.2 Frequency to Indices Conversions

The equation for converting the frequency ranges to the corresponding indices used in the analysis program is shown below:

$$Freq \text{ Resolution} = \frac{\text{sampling freq}}{\text{FFT size}} = \frac{20\text{samples / sec}}{512\text{samples}} = 0.039$$

Freq (Hz)	Index	Freq (Hz)	Index	Freq (Hz)	Index
0.039	1	0.351	9	0.663	17
0.078	2	0.390	10	0.702	18
0.117	3	0.429	11	0.741	19
0.156	4	0.468	12	0.780	20
0.195	5	0.507	13	0.819	21
0.234	6	0.546	14	0.858	22
0.273	7	0.585	15	0.897	23
0.312	8	0.624	16	0.936	24

Frequency

Indices

LF Range:	0.04-0.10 Hz	1:3
	0.04-0.15 Hz	1:4
HF Range:	0.15-0.4 Hz	4:10
	0.15-0.8 Hz	4:20

B.2.3.3 MATLAB Time-Frequency Analysis Matrix

Row represents Frequency

Column represents Time

B.2.3.4 Program to Generate SympathoVagal Activity Plots Using Wigner

Distribution This .m MATLAB program calculates the vagal tone and sympatho-vagal ratio. It is an implementation of time-frequency analysis using the Wigner distribution.

The MATLAB code for the program is given below:

```
function sympar1(rawdata,top)
% SYMPAR1(iibi,gtitle)
%
% iibi is the interpolated interbeat interval calculated
% by pslwsu, either in Matlab or in S-plus. Gtitle is the
% title of the output graphs.

% Written by Sanjay Fernando.
%
% last revision: 7/16/01 by Douglas Newandee (MATLAB 6.)
%

rawdata=rawdata(:);
order=5;
freq=0.03;
sample=20;
nfreq=freq/sample;
dtrendata=rawdata;
[row,col]=size(dtrendata);
I=1:row;
I=I(:);
A=(I/sample)/60;

% This part is for testing Janse Kaiser Wigner calculation
% algorithm with no window
%
fs=1000;
m=512; % The size of the fft we will be computing.
skip=25; % Number of points we skip to get the next segment.
p=60; % The number of freq vals we will be plotting
k=fix((row-m)/skip); % the number of spectra we compute
w=ones(size(1:m)); % window specification. Can be changed.
w=w(:);
x=hilbert(dtrendata); % Forms the analytic function of x
L=m/2;
l=-(L-1):(L-1);
n=L;
```

```

Z=zeros([p,k]);
for i=1:k
    g=x(n+1).*conj(x(n-1));
    g(2*L)=0;
    y=w.*g; % Apply window to g or kernel.

    Y=2/m*abs(fft(y,m)); % evidently because it's analytic
                        % we only need 2/N
    Z(:,i)=Y(1:p);
    n=n+skip;
end

LFC=1:4;
symvag=sum(Z(LFC,1:k));
HFC=4:20;
vagat=sum(Z(HFC,1:k));
symtopar=symvag./vagat;

%
% This section is for determining the instantaneous frequency
% from the Wigner distribution.
%

[r,c]=size(Z); %Determines the size of the matrix created by wgjka4.m.
for i=1:c; %Repetition based on number of columns.
    W=Z(:,i); %W is assigned the values of the column.
    Y=(1:r)'; %Y represents the frequencies.
    M=W.*Y;
    S=sum(M);
    F=sum(W); %Sum of the Wigner Distribution values.
    E(i)=S/F;
end

% Plotting commands

J=[12.8+(1:k)*1.25]/60;

subplot(211);
plot(A,dtrendata);
title('IBI detrended');
xlabel('time');
ylabel('amplitude');

subplot(212);
plot(J,E);
xlabel('time');

```

```
ylabel('frequency');
title('Instantaneous frequency');
```

```
faxis=(1:p)*(.0391/2);
figure
```

```
mesh(J,faxis,Z);
xlabel('time');
ylabel('frequency');
title(top);
```

```
figure
contour(J,faxis,Z);
gtext(top);
xlabel('time');
ylabel('frequency');
title('Contour plot of WD');
```

```
figure
```

```
subplot(3,1,1);
plot(J,symvag);
gtext(top);
title(' Mixture of Sympathetic and Parasympathetic');
xlabel('time');
ylabel('amplitude');
```

```
subplot(3,1,2);
plot(J,vagal);
title('Parasympathetic range');
xlabel('time');
ylabel('amplitude');
```

```
%figure
subplot(3 1 3)
plot(J,symtopar);
%gtext(top);
title('Ratio of Low Frequency to High Frequency')
xlabel('time');
ylabel('amplitude');
```

B.2.4 Wavelet Analysis and Activity Plot Program

This program is a MATLAB m-file. Upon starting MATLAB, type **whitebg** for a white graphic background.

1. The data needed is the interpolated inter-beat interval ASCII file. In LabVIEW, after you have created the heart rate or blood pressure IIBI file, you must make sure it is an ASCII file with channel data in column format with the extension (*filename.asc*). In order to run the MATLAB program, type:

d_wvlet

2. The program will ask you to enter the filename without extension. Type in the filename then hit return.

Agu1hrbp (of the Agu1hrbp.asc file)

3. Enter the channel number you want to analyze.

1 (or 2, 3, 4...)

4. Enter the sampling rate of the data.

200 (or the appropriate sampling rate)

5. Enter the window size in seconds.

1

6. Enter the fft size:

256

Make sure **fftsize** \geq **sampling rate** * **window size**. Otherwise, 3D plots will be badly scaled. Choose fft to be 128, 256, 512, 1024, 2048 or any other number in power of 2.

7. Enter name of the wavelet used:

morl (Morlet:**morl**, Meyer:**meyr**, Daubechies 4:**dB4**,...)

The program will run and output the 9 appropriate time-frequency and activity plots of the channel that was analyzed.

The MATLAB program given below calculates the wavelet coefficients and plots them in 3D as power intensity versus time and frequency as well as the regular and normalized activity plots.

```
% d_wvlet.m
%
% Matlab Wavelet Toolbox 2.0.
% Modified by D. Newandee
% 7-13-2001: using time - freq spectrogram and change to run with MATLAB 6.0
% 10-23-2001: add calculation of normalized sympathovagal ratio using chosen
% wavelet.
%
% This program will accept any wavelet from the Matlab Wavelet Toolbox 2.0 by
% entering the wavelet name in ' ' for the 'wave' variable below.
%
clear all;
close all;

SIGNAL=input('Please enter name of datafile with no extension --> ','s');
filename=[SIGNAL,'.asc'];
eval(['load ' filename]);
original_rawdata=eval(SIGNAL);clear SIGNAL;
Question_1=input('Which channel do you want to analyze? [1=O2, 2=BP, 3=resp,
4=ECG] --> ','s');
if      Question_1=='1'
    rawdata=original_rawdata(1,:);
elseif Question_1=='2'
    rawdata=original_rawdata(2,:);
elseif Question_1=='3'
    rawdata=original_rawdata(3,:);
elseif Question_1=='4'
    rawdata=original_rawdata(4,:);
end

sf=input('Please enter the sampling rate of the data --> ');
T=input('Please enter the window size in seconds --> ');
nfft=input('Please enter the fft size --> '); % must be larger than window size and in ^2
wave = input('Please enter name of wavelet used --> ','s');
```

```

x = decimate(rawdata,10);    % decimate data array
N = length(x);              % number of samples

%*sf = 1000;                % sampling frequency
%*N = 500;                  % number of samples
%%T = 1/400;                % window size in seconds (1/400 = 0.025 sec)
ws = T*sf;                  % window size in samples
%*nfft = 256;               % fft size in spectrogram command. Must be larger than
                             % window size in samples
%*wave = 'mexh';            % the wavelet to use (see wavelets table in Matlab Wavelet
Tool Box v 2.0
%

t = ( (1:(N)) ) * (1/sf);    % times
f = ( (0:(N-1))/N ) * sf;    % frequencies
index = 1:N;

% first construct the time domain and frequency domain plots
fx = abs(fft(x));

% spectrum1D.m
% function [Pyy,f]=rspec(x,Fs)
    fftsize=length(x);

% put alternative fft method here
    x=x-mean(x);
    fftx=fft(x,fftsize);
    Pyy=fftx.*conj(fftx)/fftsize;
%    f=sf*(0:(fftsize/2-1))/fftsize;
    f=sf*(0:(fftsize-1))/fftsize;
    clear fftx

    p=Pyy;

figure;
subplot(2,1,1)
    plot(t,x);
%    axis([0 20 -2 5]);
    grid on;
    xlabel('Time (sec)');
    ylabel('Amplitude');
    title(['Raw data in time domain of ',eval('filename')]);

subplot(2,1,2);
% plot(f(400:800),p(400:800)/max(p),'r');
    plot(f(1:200),p(1:200)/max(p),'r');

```

```

axis([0 1 0 2]);
grid on;
xlabel('Frequency (Hz)');
ylabel('Power');
title(['Power Spectrum of ',eval('filename')]);

%subplot(3,1,3);
% plot(f(index)/10,fx(index));
% grid on;
% axis([0 2 -2 5]);
% xlabel('frequency');
% title('frequency domain');

%*orient landscape;
print -dps wvleta.eps

% construct a spectrogram with window size, ws

[B,frequencies,times] = specgram(x, nfft, sf, ws);

% plot the spectrogram
figure;
imagesc(times, frequencies, abs(B));
colormap('hot');
colorbar('vert');axis('xy');
axis([0 100 0 2]);
xlabel('Time (sec)');
ylabel('Frequency (Hz)');
% title(['Spectrogram with T = ' num2str(1000*T) ' ms']);
title(['Spectrogram of ',eval('filename'),' using ',eval('wave'),' wavelet']);
%*orient landscape;
print -dps wvletb.eps

% make a 3D plot for better viewing
figure;
mesh(times, frequencies, abs(B));
xlabel('Time (sec)');
ylabel('Frequency (Hz)');
% title(['3D Spectrogram with T = ' num2str(10000*T) ' ms']);
title(['3D Spectrogram of ',eval('filename'),' using ',eval('wave'),' wavelet']);
% view(-60,30);
axis([0 100 0 2 0 50]);
%*orient landscape;
print -dps wvletc.eps;

```

```

% now work out the scales at which to compute the CWT
% There is a connection between scale and frequency as follows

factor = 5/(2*pi);
%freq = [100:100:4000]; % range of interested frequency
freq = [0.01:0.01:2.0]; % HRV: 0.01 - 2 Hz
scale = factor * sf ./ freq;

% make sure the string wave is set before executing the m-file

% compute the CWT plotting at the same time
figure;
coef=cwt(x, scale, wave, 'plot');
% title('scalogram - Scale vs. Time');
title(['Scalogram - Scale vs. Time of ',eval('filename'),' using ',eval('wave'),' wavelet']);
%* orient landscape;
print -dps wvletd.eps;

%
% Extract LF and HF
%
[row,col]=size(rawdata');
I=1:row;
I=I(:);
A=(I/sf)/60; % Time axis in minutes

m=512; % The size of the fft we will be computing.
skip=25; % Number of points we skip to get the next segment.
k=fix((row-m)/skip); % the number of spectra we compute

TFDs=abs(coef);
[r,C]=size(TFDs);
for i=1:C,
W=TFDs(:,i);
Y=(1:r)';
M=W.*Y;
S=sum(M);
F=sum(W);
E(i)=S/F;
end

%LFC = input('Please enter the low frequency range in index numbers. ');
LFC=1:4;
symvag=sum(TFDs(LFC,1:k));
%HFC=input('Please enter the high frequency range in index numbers. ');
HFC=4:20;

```

```

vagal=sum(TFDs(HFC,1:k));
symtopar=symvag./vagal;

% Normalize

n_symvag=symvag./(symvag+vagal);
n_vagal=vagal./(symvag+vagal);
n_symtopar=n_symvag./n_vagal;

% Plotting commands

%J=[12.8+(1:k)*1.25]/60;
J=(length(x)/sf)/(k)*(0:k-1);

% Make a "spectrogram" type plot
figure;
    imagesc(t, freq, coef);
    colormap('hsv');
    colorbar('vert');
    axis('xy');           % flip the vertical axis over
    xlabel('Time (sec)');
    ylabel('Frequency (Hz)');
% title('Scalogram - Frequency vs. Time');
    title(['Scalogram - Frequency vs. Time of ',eval('filename'),' using ',eval('wave'),'
wavelet']);
%*   orient landscape;
    print -dps wvlete.eps;

% make a 3D plot for better viewing, rotate by 45 degrees
figure;
    subplot(2,1,1), mesh(t, freq, abs(coef));
%*   [az,el]=view;
%*   view(az+45,el);
%*   view(az,el);
%   axis([0 300 0 0.5 0 3]);
%   view([55,15]);
%   grid on;
    colormap('jet');
    colorbar('vert');
    brighten(0.5);
    shading interp;

    xlabel('Time (sec)');
    ylabel('Frequency (Hz)');
    title(['3D scalogram of ',eval('filename'),' using ',eval('wave'),' wavelet']);

```

```

%* orient landscape;
%* print -dps wwletf.eps;

subplot(2,1,2), contour(t, freq, abs(coef),20);
axis([0 100 0 2]);
grid on;
xlabel('Time (sec)');
ylabel('Frequency (Hz)');
title(['Contour of ',eval('filename'),' using ',eval('wave'),' wavelet']);

% print -dps wwletf.eps;

figure;
subplot(2,1,1);
%plot(A,x);
plot(t,x);
title(['Detrended IIBI Plot of ',eval('filename'),' using ',eval('wave'),' wavelet']);
xlabel('Time (sec)');
ylabel('Amplitude');

subplot(2,1,2);
plot(t,E);
%plot(A,E);
axis([0 50 0 2]);
xlabel('Time (sec)');
ylabel('Frequency (Hz)');
title(['Instantaneous frequency Plot of ',eval('filename')]);

figure;
subplot(3,1,1);
plot(J,symvag);
%plot(A,symvag);
%gtext(top);
title(['Symp. and Parasymp Mixture (LF) Plot of ',eval('filename'),' using ',eval('wave'),' wavelet']);
%xlabel('time (sec)');
ylabel('Amplitude');

subplot(3,1,2);
plot(J,vagal);
%plot(A,vagal);
title('Parasympathetic range (HF)');
%xlabel('time (sec)');
ylabel('Amplitude');

subplot(3,1,3)

```

```

plot(J,symtopar);
%plot(A,symtopar);
%gtext(top);
title('Ratio of LF to HF')
xlabel('Time (sec)');
ylabel('Amplitude');

%order=input('Please enter the order of the lowpass filter. ');
%freq=input('Please enter the cutoff frequency for LPF. ');
%sample=input('Please enter the sample rate of the data. ');
%order=12;
%freq=0.03;
%nfreq=freq/sf;
%[poles,zeros]=butter(order,nfreq);
%dtnd_nsymvag=filtfilt(poles,zeros,n_symvag);
%dtnd_nvagal=filtfilt(poles,zeros,n_vagal);
%dtnd_nsymtopar=filtfilt(poles,zeros,n_symtopar);

figure
subplot(3,1,1);
plot(J,n_symvag);
%plot(A,n_symvag);
%gtext(top);
title(['Normalized Symp and Parasymp Mixture (NLH) Plot of ',eval('filename'),' using ',eval('wave'),' wavelet']);
%xlabel('time (sec)');
ylabel('Amplitude');

subplot(3,1,2);
plot(J,n_vagal);
%plot(A,n_vagal);
title('Normalized Parasympathetic range (NHF)');
%xlabel('time (sec)');
ylabel('Amplitude');

%figure
subplot(3,1,3)
plot(J,n_symtopar);
%plot(A,symtopar);
%gtext(top);
title('Ratio of NLF to NHF')
xlabel('Time (sec)');
ylabel('Amplitude');

```


B.2.5 System Identification Procedure

Make sure that there is an “ident” MATLAB toolbox (Version 4.0 or later) exist in the toolbox directory of MATLAB. The procedure described here is essentially the same as demo #2 in iddemo. It shows an example of a typical session with the System Identification Toolbox. First, invoke MATLAB and follow along.

1. Data have been collected from a COPD or a normal subject during one of the experimental session. Sixty thousand data points (5 minutes) were collected. The sampling interval is 5 ms (0.005 sec, 200sps). The data were loaded into MATLAB in ASCII form and are now stored as the vectors hr_2 (Heart Rate: output) and rp_2 (Respiration: input) in the file agu1.asc. First load the data:

```
load agu1.asc;
```

2. This example selects the first 25,000 data points for building a model. For convenience, the input-output vectors are merged into a matrix:

```
z2 = [ hr2 (1:25000) rp2 (1:25000)];
```

Take a look at the data,

```
idplot(z2)
```

The toolbox makes frequent use of default arguments. Default values are used when trailing arguments are omitted. In the case above, by default, all data points are graphed and the sampling interval is one time unit.

3. One can select the values between sample numbers 10,000 and 20,000 for a close-up, and at the same time obtain correct time scales, with

```
idplot(z2,10000:20000,0.005)
```

4. Remove the constant levels and make the data zero mean with

z2 = dtrend(z2);

5. Now, fit to the data a model of the form:

$$y(t) + a_1 y(t - T) + a_2 y(t - 2T) = b_1 u(t - 3T) + b_2 u(t - 4T) \quad (\text{B.1})$$

where T is the sampling interval (here 0.005 seconds). This model, known as an ARX model, tries to explain or compute the value of the output at time t , given previous values of y and u .

The best values of the coefficients a_1 , a_2 , b_1 and b_2 can be computed with

th = arx(z2,[10 10 3]);

6. The numbers in the second argument tell arx to find a model (B.1) with ten a -parameters, ten b -parameters, and three delays. The result is stored in the matrix th in a somewhat coded form. To specify the actual sampling interval, enter

th = sett(th,0.005);

7. There are several ways to display and illustrate the computed model. With

present(th);

the coefficient values of (B.1) and their estimated standard deviations are presented on the screen.

8. Next, one might ask how to evaluate how well the model fits the data. A simple test is to run a simulation whereby real input data is fed into the model, and compare the simulated output with the actual measured output. For this, select a portion of the data that was not used to build the model, for example, from sample 25,001 to 50,000:

rp = dtrend(rp₂(25001:50000));

hr = dtrend(hr₂(25001:50000));

```
ysim = idsim( rp , th );
```

```
plot([ hr (40000:50000) ysim(40000:50000)])
```

Note that the function `compare` does this sequence of commands more efficiently.

One can see that the model is quite capable of describing the system, even for data that were not used in calculating the fit.

9. To compute and graph the poles and zeros of the ARX model, use

```
zpth = th2zp(th);
```

```
zpplot(zp th);
```

10. If one wants to know the frequency response, one can compute the frequency function of the model and present it as a Bode plot by entering

```
gth = th2ff(th);
```

```
bodeplot(gth);
```

11. Compare this transfer function with a transfer function obtained from a nonparametric, spectral analysis method. Such an estimate is obtained directly from the data

```
gs = spa(z2);
```

```
gs = sett(gs,0.005);
```

The sampling interval, 0.005, is set by the second command in order to obtain correct frequency scales. The function `spa` also allows you to select window sizes, frequency ranges, etc. All these values have been given as default values.

12. One can then compare the estimate of the transfer function obtained by spectral analysis versus the one obtained from the model (B.1) with

```
bodeplot([gs gth]);
```

Make sure the agreement is quite good. Else rerun the

13. Finally, plot the step response of the model. The model comes with an estimate of its own uncertainty. Ten different step responses are computed and graphed. They correspond to "possible" models, drawn from the distribution of the true system (according to our model):

```
step=ones(30,1);
```

```
idsimsd(step,th);
```

Spectral Analysis

14. The function `spa` performs spectral analysis according to the procedure in (3.35)-(3.37) of [42].

```
[G,PHIV] = spa(z);
```

15. Here `z` contains the output-input data as above. `G` and `PHIV` are matrices that contain the estimated frequency function G_N and the estimated disturbance spectrum Φ_v in (3.37). They are coded into a special format, the `freqfunc` format, which allows you to plot them using the function `bodeplot` or `ffplot`:

```
[G,PHIV] = spa(z);
```

```
bodeplot(G);
```

```
bodeplot(PHIV);
```

`bodeplot` gives logarithmic amplitude and frequency scales (in rad/sec) and linear phase scale, while `ffplot` gives linear frequency scales (in Hz). The details of the `freqfunc` format are given in [42] and by typing:

```
help freqfunc;
```

16. To obtain correct frequency scales you can operate with the command `sett` on `G` or give the sampling interval as an optional argument to `spa`. By omitting the argument `PHIV`, only the transfer function estimate `G` is computed:

`G =spa(z);`

B.2.6 Principal Components Analysis

Make sure that there is a MATLAB “Stats” toolbox (Version 3.0 or later) exist in the toolbox directory of MATLAB. The procedure described here is essentially the same as the principal component analysis tutorial of the Multivariate statistics section of [68]. It shows an example of a typical PCA session with the Statistics Toolbox. A new data set has been created from the actual physiological data of the respiration, heart rate and blood pressure signals as well as the coherence and partial coherence in the LF and HF regions for both COPD and normal subjects. The data set is saved as an excel file (cpcohdata.xls) with columns as names of the subjects and 15 HRV parameters. The 55 rows show the values of the 15 HRV parameters for all 47 COPD and 8 normal subjects. The 47 COPD subjects are numbered as rows 2-48. Rows 49-56 show the data for the normal subjects. The 15 different HRV parameters of the normal and COPD subjects in the data file are:

'rsp'	respiration (rate)
'HR'	heart rate
'BP'	blood pressure
'LF_coh_HR_rsp'	LF coherence between heart rate and respiration
'LF_coh_HR_BP'	LF coherence between heart rate and blood pressure
'LF_coh_BP_rsp'	LF coherence between blood pressure and respiration
'HF_coh_HR_rsp'	HF coherence between heart rate and respiration
'HF_coh_HR_BP'	HF coherence between heart rate and blood pressure
'HF_coh_BP_rsp'	HF coherence between blood pressure and respiration
'LF_pcoh_HR_rsp'	LF partial coherence between heart rate and respiration
'LF_pcoh_HR_BP'	LF partial coherence between heart rate and blood pressure
'LF_pcoh_BP_rsp'	LF partial coherence between blood pressure and respiration
'HF_coh_HR_rsp'	HF partial coherence between heart rate and respiration
'HF_coh_HR_BP'	HF partial coherence between heart rate and blood pressure
'HF_coh_BP_rsp'	HF partial coherence between blood pressure and respiration

1. Invoke MATLAB. Let's start by clearing all figures and work area and load the data in cpcohdata.xls.

```
>> close all
```

```
>> clear all
```

```
>> [cpdata, categories] = xlsread('cpcohdata.xls');
```

```
>> whos
```

Name	Size	Bytes	Class
categories	2x15	1962	cell array
names	55x3	330	char array
cpdata	55x15	3720	double array

The whos command generates a table of information about all the variables in the workspace.

The cpcoh data set (cpcohdata.xls file) contains 3 variables:

- categories, a string matrix containing the names of the HRV parameters.
- names, a string matrix containing the names of the COPD and normal subjects.
- cpdata, the data matrix with 55 rows and 15 columns.

2. Let's look at the value of the categories variable.

```
>> categories
```

```
categories =
```

```
Columns 1 through 6
```

```
'rsp' 'HR' 'BP' 'LF_coh_' 'LF_coh_' 'LF_coh_'
[] [] [] 'HR_rsp' 'HR_BP' 'BP_rsp'
```

```
Columns 7 through 11
```

```
'HF_coh_' 'HF_coh_' 'HF_coh_' 'LF_pcoh_' 'LF_pcoh_'
'HR_rsp' 'HR_BP' 'BP_rsp' 'HR_rsp' 'HR_BP'
```


Columns 12 through 15

```
'LF_pcoh_' 'HF_pcoh_' 'HF_pcoh_' 'HF_pcog_'
'BP_rsp'   'HR_rsp'   'HR_BP'   'BP_rsp'
```

3. To get a quick impression of the ratings data, make a box plot.

```
>> boxplot(cpdata,0,'+',0)
```

```
>> set(gca,'YTicklabel',categories)
```

These commands generate the plot below. Note that there is substantially more variability in the ratings of the arts and housing than in the ratings of crime and climate.

Ordinarily one might also graph pairs of the original variables, but there are too many two-variable plots. Perhaps principal components analysis can reduce the number of variables we need to consider.

Sometimes it makes sense to compute principal components for raw data. This is appropriate when all the variables are in the same units. Standardizing the data is reasonable when the variables are in different units or when the variance of the different columns is substantial (as in this case).

4. One can standardize the data by dividing each column by its standard deviation.

```
>> stdr = std(cpdata);
```

```
>> sr = cpdata./repmat(stdr,55,1);
```

5. Now it is ready to find the principal components.

```
>> [pcs,newdata,variances,t2] = princomp(sr);
```

The following sections explain the four outputs from princomp:

- “The Principal Components (First Output)”
- “The Component Scores (Second Output)”

- “The Component Variances (Third Output)”
- “Hotelling’s T2 (Fourth Output)”

The Principal Components (First Output)

The first output of the princomp function, pcs, contains the 15 principal components.

These are the linear combinations of the original variables that generate the new variables.

6. Let’s look at the first three principal component vectors.

```
>> p3=pcs(:,1:3)
```

```
p3 =
```

```
0.2167 -0.1183 -0.1847
0.2066 -0.1977 -0.4588
0.2000 -0.2014 -0.4580
-0.2819 -0.3377 0.1507
-0.3001 0.1087 -0.3137
-0.2786 -0.3063 -0.1575
-0.2915 -0.0762 0.2091
-0.2585 0.3470 0.0879
-0.2663 0.3242 -0.1213
-0.3025 -0.3570 0.0794
-0.2793 0.1323 -0.3511
-0.2737 -0.2694 -0.2520
-0.2049 -0.3636 0.2074
-0.2168 0.2623 -0.0036
-0.2592 0.1920 -0.3122
```

```
>>
```

The largest weights in the first column (first principal component) are the first and second elements, corresponding to the variables respiration and heart rate. To show the orthogonality of the principal components, note that premultiplying them by their transpose yields the identity matrix.

```
>> I = p3'*p3
```

```

I =
1.0000    -0.0000   -0.0000
-0.0000    1.0000   -0.0000
-0.0000   -0.0000    1.0000

```

The Component Scores (Second Output)

The second output, `newdata`, is the data in the new coordinate system defined by the principal components. This output is the same size as the input data matrix.

7. A plot of the first two columns of `newdata` shows the ratings data projected onto the first two principal components.

```

>> plot(newdata(:,1),newdata(:,2),'+')
>> xlabel('1st Principal Component');
>> ylabel('2nd Principal Component');

```

8. The function `gname` is useful for graphically identifying a few points in a plot like this. You can call `gname` with a string matrix containing as many case labels as points in the plot. The string matrix `names` works for labeling points with the subject names.

```

>> gname(names)

```

Move your cursor over the plot and click once near each point at the top right. As you click on each point, MATLAB labels it with the proper row from the `names` string matrix. When you are finished labeling points, press the Return key.

The labeled subjects are the normal subjects in data set. Perhaps one should consider them as a completely separate group. If `gname` is called without arguments, it labels each point with its row number.

9. One can create an index variable containing the row numbers of all the chosen normal subjects.

```
>> normal = [48 49 50 51 52 53 54 55];
```

```
>> names(normal,:)
```

```
ans =
```

```
ba  
ja  
rajf  
rajm  
ka  
ma  
ro  
so
```

10. To remove these rows from the ratings matrix, type the following.

```
>> rsubset = cpdata;
```

```
>> nsubset = names;
```

```
>> nsubset(normal,:) = [ ];
```

```
>> rsubset(normal,:) = [ ];
```

```
>> size(rsubset)
```

```
ans =
```

```
47 15
```

11. To practice, repeat the analysis using the variable `rsubset` as the new data matrix and `nsubset` as the string matrix of labels.

The Component Variances (Third Output)

12. The third output, `variances`, is a vector containing the variance explained by the corresponding column of `newdata`.

```
>> variances
```

```
variances =
    3.4083
    1.2140
    1.1415
    0.9209
    0.7533
    0.6306
    0.4930
    0.3180
    0.1204
```

13. One can easily calculate the percent of the total variability explained by each principal component.

```
>> percent_explained = 100*variances/sum(variances)
```

```
percent_explained =
```

```
    37.8699
    13.4886
    12.6831
    10.2324
     8.3698
     7.0062
     5.4783
     3.5338
     1.3378
```

14. A “Scree” plot is a pareto plot of the percent variability explained by each principal component.

```
>> pareto(percent_explained)
```

```
>> xlabel('Principal Component')
```

```
>> ylabel('Variance Explained (%)')
```

We can see that the first three principal components explain roughly two thirds of the total variability in the standardized ratings.

Hotelling's T2 (Fourth Output)

15. The last output of the `princomp` function, `t2`, is Hotelling's T2, a statistical measure of the multivariate distance of each observation from the center of the data set. This is an analytical way to find the most extreme points in the data.

```
>> [st2, index] = sort(t2);    % Sort in ascending order.

>> st2 = flipud(st2);        % Values in descending order.

>> index = flipud(index);    % Indices in descending order.

>> extreme = index(1)

    extreme =

         10

>> names(extreme,:)

    ans =

    ecc
```

It is not surprising that the ratings for COPD subject 'ecc' is the furthest from the average COPD group.

B.2.7 Cluster Analysis Program

This program is a MATLAB m-file. Upon starting MATLAB, type **whitebg** for a white graphic background.

1. The data needed is the data set formed from 15 HRV parameters as the results of PCA on real COPD/Normal data and cross-spectral analysis. The data set is saved as an ASCII file. In order to load it into MATLAB. Type:

load Agu1.asc; Note: Agu1 is the *filename*.

If you now type **whos**, the file should show up as the variable Agu1.

2. Run the program using the general format:

[RITrue,RISelf,EstIndex]=DoClustering(Algorithm,Data,k,TrueID,Repetitions)

[algo, self, 2]=DoClustering(kmeans, Agu1,5,,2)

Here, data is Agu1, k=5 clusters and run 2 repetitions.

3. The program will run and output a plot with five separate clusters as asked in the above command.

The MATLAB program below performs the cluster analysis on the data set created using the principal components obtained from the PCA on the 12 different HRV parameters and actual heart rate, blood pressure and breathing (respiration) rate.

```
function [RITrue,RISelf,EstIndex]=DoClustering(Algorithm,Data,k,TrueID,Repetitions)
% DOCLUSTERING Performs cluster analysis of specified data using specified
% algorithm.
%
% [RITrue,RISelf,Index]=DOCLUSTERING(Algorithm,Data,k,TrueID,Repetitions)
% where Algorithm is the name of the clustering algorithm (string),
%
% Data is 2-d matrix, with variables as columns and records as rows,
%
% k is number of clusters to search for,
%
% TrueID is a vector of class labels, one for each row in "Data", ([]->not known)
% and Repetitions is the number of times to repeat the algorithm (default 1).
% RITrue is the (adjusted) Rand Index comparing the solution to the true labels
% (where known). RISelf is the (adjusted) Rand Index between pairs of solutions
% (when Repetitions > 1).
% Index is the estimated labels of each record.
%
% AlgorithmList=DOCLUSTERING with no parameters returns list of all
% the algorithms available
```

% Copyright (C) David Corney 2000 D.Corney@cs.ucl.ac.uk

%If no inputs, then return list of all algorithms used (arbitrary order).

if nargin == 0

```
    RITrue={'kmeans','EM_spherical','EM_elliptical', ...
           'hier_centroid','hier_complete','hier_single', ...
           'fuzzy','random'};
```

```
    return
```

end

if nargin < 3

```
    error('DOCLUSTERING requires at least 3 arguments');
```

```
    help(mfilename)
```

```
    return
```

end

if nargin < 4, TrueID=[]; end %no known class labels

if nargin < 5, Repetitions = 1;end %only do it once

if nargin < 6, options = 0;

```

end

[R,C]=size(Data);
if length(TrueID)>0 & length(TrueID)~=R
    error('DOCLUSTERING number of labels does not match number of records');
    return
end

if k == 1                                %Only want one cluster? Well, ...OK
    RITrue=0;RISelf=0;
    EstIndex=ones(R,1);
    return
end

%Hierarchical clustering - calculate distance/dissimilarity matrix
if strcmp(Algorithm,'hier',4) == 1
    if Repetitions > 1, warning('Only performing one hierarchical clustering execution');end

%Hier. is deterministic; no point in repeating it
    Repetitions = 1;

%Next line does fast distance calculations as given by Peter Acklam, Oslo,
%www.math.uio.no/~jacklam
    distance=sqrt(sum(abs(repmat(permute(Data, [1 3 2]), [1 R 1]) -
    repmat(permute(Data, [3 1 2]), [R 1 1])).^2,3));
    distance=distance+diag(ones(1,R). *Inf);
end

%Do the clustering
for i =1:Repetitions
    InitCentres = ChooseInitialCentres(Data,k);           %randomly choose starting point
                                                         %(where needed)

    switch Algorithm
    case 'kmeans'
        EstIndex(i,:) = dcKMeans(Data,k,InitCentres)';
    case 'EM_spherical'
        [mix, index,likelihood]=dcEMGMM(Data, k, 'spherical', 1);
        EstIndex(i,:)=index';
    case 'EM_elliptical'
        [mix, index,likelihood]=dcEMGMM(Data, k, 'full', 1);
        EstIndex(i,:)=index';
    case {'hier_complete'}
        cluster = dcAgg(distance, 'complete', k);
        for j = 1:k
            EstIndex(i,cluster{j})=j;
        end
    end
end

```

```

case {'hier_single'}
    cluster= dcAgg(distance, 'single', k);
    for j = 1:k
        EstIndex(i,cluster{j})=j;
    end
case {'hier_centroid'}
    cluster = dcAgg(distance, 'centroid', k);
    for j = 1:k
        EstIndex(i,cluster{j})=j;
    end
case 'fuzzy'
    m=1.5;
    EstIndex(i,:) = dcFuzzy(Data,k,m,InitCentres);
case 'random'
    EstIndex(i,:) = floor(rand(1,R)*k+1);           %randomly assign labels
                                                    %otherwise
    error(sprintf('DOCLUSTERING - unsupported algorithm "%s"',Algorithm))
end                                                    %of switch/case

%return adjusted Rand index (accuracy) if true labels are given
if length(TrueID)>0
    RITrue(i)=RandIndex(EstIndex(i,:), TrueID);
else
    RITrue(i)=-1;
end

end %of repetitions loop

%Calculate adjusted Rand index between each pair of solutions found
if Repetitions > 1
    l=0;
    for i=1:Repetitions-1
        for j=i+1:Repetitions
            l=l+1;
            RISelf(l)=RandIndex(EstIndex(i,:)',EstIndex(j,:)');
        end
    end
else
    RISelf=0;
end
end

```

B.2.8 Cross-correlation Program

The program below calculates the correlation indices for selecting the best time-frequency representation.

```
function xy = corrcoef(x,y)
%CORRCOEF Correlation coefficients.
% CORRCOEF(X) is a matrix of correlation coefficients formed
% from array X whose each row is an observation, and each
% column is a variable.
% CORRCOEF(X,Y), where X and Y are column vectors is the same as
% CORRCOEF([X Y]).
%
% If C is the covariance matrix,  $C = \text{COV}(X)$ , then CORRCOEF(X) is
% the matrix whose (i,j)'th element is
%
%  $C(i,j)/\text{SQRT}(C(i,i)*C(j,j))$ .
%
% See also COV, STD.

% J. Little 5-5-86
% Revised 6-9-88 LS 2-13-95 BJ
% Copyright 1984-2001 The MathWorks, Inc.
% $Revision: 5.8 $ $Date: 2001/04/15 12:01:28 $

switch nargin
case 1
    c = cov(x);
case 2
    c = cov(x,y);
otherwise
    error('Not enough input arguments.');
```

end

```

d = diag(c);
xy = c./sqrt(d*d');
```

APPENDIX C

CROSS-SPECTRAL ANALYSIS

Equations C.1-C.5 are the equations to calculate the partial coherence function between to signals with the effect of the third signal removed. Equations C.6-C.20 show the partial coherence functions for combinations of HR, BP and respiration signals.

C.1 General Partial Coherence Equation

$$\gamma_{2y1}^2(f) = \frac{|G_{2y1}(f)|^2}{G_{221}(f)G_{yy1}(f)} \quad (C.1)$$

where

$$G_{2y1}(f) = G_{2y}(f) - \frac{G_{21}(f)}{G_{11}(f)} G_{1y}(f) \quad (C.2)$$

$$G_{221}(f) = G_{22}(f) - \frac{G_{21}(f)}{G_{11}(f)} G_{12}(f) \quad (C.3)$$

$$G_{yy1}(f) = (1 - \gamma_{1y}^2) G_{yy}(f) \quad (C.4)$$

$$\gamma_{1y}^2(f) = \frac{|G_{1y}(f)|^2}{G_{11}(f)G_{yy}(f)} \quad (C.5)$$

C.2 Partial coherence of HR and BP (extract Resp)

$$\gamma_{HBR}^2(f) = \frac{|G_{HBR}(f)|^2}{G_{HHR}(f)G_{BBR}(f)} \quad (C.6)$$

where

$$G_{HBR}(f) = G_{HB}(f) - \frac{G_{HR}(f)}{G_{RR}(f)} G_{RB}(f) \quad (C.7)$$

$$G_{HHR}(f) = G_{HH}(f) - \frac{G_{HR}(f)}{G_{RR}(f)} G_{RH}(f) \quad (C.8)$$

$$G_{BBR}(f) = (1 - \gamma_{RB}^2) G_{BB}(f) \quad (C.9)$$

$$\gamma_{RB}^2(f) = \frac{|G_{RB}(f)|^2}{G_{RR}(f)G_{BB}(f)} \quad (C.10)$$

Note:

H: Heart Rate IIBI signal

B: Blood Pressure IIBI signal

R: Respiration signal

C.3 Partial coherence of HR and Resp (extract BP)

$$\gamma_{HRB}^2(f) = \frac{|G_{HRB}(f)|^2}{G_{HHB}(f)G_{RRB}(f)} \quad (C.11)$$

where

$$G_{HRB}(f) = G_{HR}(f) - \frac{G_{HB}(f)}{G_{BB}(f)} G_{BR}(f) \quad (C.12)$$

$$G_{HHB}(f) = G_{HH}(f) - \frac{G_{HB}(f)}{G_{BB}(f)} G_{BH}(f) \quad (C.13)$$

$$G_{RRB}(f) = (1 - \gamma_{BR}^2) G_{RR}(f) \quad (C.14)$$

$$\gamma_{BR}^2(f) = \frac{|G_{BR}(f)|^2}{G_{BB}(f)G_{RR}(f)} \quad (C.15)$$

Note:

H: Heart Rate IIBI signal

B: Blood Pressure IIBI signal

R: Respiration signal

C.4 Partial coherence of BP and Resp (extract HR)

$$\gamma_{BRH}^2(f) = \frac{|G_{BRH}(f)|^2}{G_{BBH}(f)G_{RRH}(f)} \quad (C.16)$$

where

$$G_{BRH}(f) = G_{BR}(f) - \frac{G_{BH}(f)}{G_{HH}(f)} G_{HR}(f) \quad (C.17)$$

$$G_{BBH}(f) = G_{BB}(f) - \frac{G_{BH}(f)}{G_{HH}(f)} G_{HB}(f) \quad (C.18)$$

$$G_{RRH}(f) = (1 - \gamma_{HR}^2) G_{RR}(f) \quad (C.19)$$

$$\gamma_{HR}^2(f) = \frac{|G_{HR}(f)|^2}{G_{HH}(f)G_{RR}(f)} \quad (C.20)$$

Note:

H: Heart Rate IIBI signal

B: Blood Pressure IIBI signal

R: Respiration signal

REFERENCES

- [1] Berntson, G., J. Cacioppo, and K. Quigley. Respiratory sinus arrhythmia: autonomic origins, physiological mechanisms, and psychophysiological implications. *Psychophysiology*, 30:183-196, 1993.
- [2] Sleight, P., B. Casadei. Relationships Between heart rate, respiration and blood pressure variabilities. In: Malik M . Camm A J (eds); *Heart rate Variability*. Armonk. NY Futura Publishing Company, Inc. 1995.
- [3] Pagani M, Lucini D, Pizzinelli P, Sergi M, Bosisio E, Mela GS, Malliani A., "Effects of aging and of chronic obstructive pulmonary disease on RR interval variability." *J Auton Nerv Syst* 59(3), (Jul 1996): 125-32
- [4] Guyton, A. C. *Human Physiology and Mechanisms of Disease*. W.B. Saunders Company, Philadelphia, 1987.
- [5] Vander, A. J., J. H. Herman, and D. S. Luciano. *Human Physiology*. New York: McGraw-Hill Publishing Company, sixth edition, 1994.
- [6] Fox, S. *Human Physiology*. Wm. C. Brown Publishers, Dubuque, Iowa, fourth edition, 1993.
- [7] Higgins, M. W., et al. Incidence, Prevalence, and mortality. *Clinical epidemiology of COPD* 1990. Marcel Dekker Publishers. New York, NY. 23-43.
- [8] Kamath, M. D., and E. L. Fallen, "Power spectral analysis of heart rate variability: A noninvasive signature of cardiac autonomic function," *Crit. Rev. in Biomed. Eng.*, vol. 21, no. 3, pp. 245-311, 1993.
- [9] Hodgkin, J. E. Prognosis in chronic obstructive pulmonary disease. *Clinics Chest Med.* 1990; II, 555-69.
- [10] www.uoregon.edu/~bradw/371blackboard/Lab/VO2max.html, 1/20/2002.
- [11] Akselrod, S., D. Gordon, J. Madwed, N. Snidman, D. Shannon, and R. Cohen. Hemodynamic regulation: investigation by spectral analysis. *AJP*, 249:H867-H875, 1985.
- [12] Madwed, J., P. Albrecht, R. Mark, and R. Cohen. Low frequency oscillations in arterial pressure and heart rate: a simple computer model. *American Journal of Physiology*, 256(25): H1573-1579, 1989.

- [13] Madwed, J., and R. Cohen. Heart rate response to hemorrhage induced 0.05-hz oscillations in arterial pressure in conscious dogs. *American Journal of Physiology*, 260(29): H1248-H1253, 1991.
- [14] Lipsitz, L., J. Mietus, G. Moody, and A. Goldberger. Spectral characteristics of heart rate variability before and during postural tilt: relations to aging and risk of syncope. *Circulation*, 81:1803-1810, 1990.
- [15] Malliani, A., M. Pagani, F. Lombardi, and S. Cerutti. Cardiovascular neural regulation explored in the frequency domain. *Circulation*, 84:482-492, 1991.
- [16] Sleight, P., M. La Rovere, A. Mortara, G. Pinna, R. Maestri, S. Leuzzi, M. Bianchini, L. Tavazzi, and L. Bernard. Physiology and pathophysiology of heart rate and blood pressure variability in humans: is power spectral analysis largely an index of baroreflex gain? *Clinical Science*, 88:103-109, 1995.
- [17] Higgins, M. W., et al. Incidence, Prevalence, and mortality. *Clinical epidemiology of COPD* 1990. Marcel Dekker Publishers. New York, NY. 23-43.
- [18] Qian, S., and D. Chen, "Joint Time-Frequency Analysis: Methods and Applications". Prentice Hall, Inc., 1996
- [19] Lipsitz, L., J. Mietus, G. Moody, and A. Goldberger. Spectral characteristics of heart rate variability before and during postural tilt: relations to aging and risk of syncope. *Circulation*, 81:1803-1810, 1990.
- [20] Qian, S., "Short Time Fourier Transform and Gabor Expansion". National Instrument, Inc. slides presentation, 1997.
- [21] Amin, M., L. Cohen and W. J. Williams, "Methods and Applications for Time-Frequency Analysis" *Conference Notes*, University of Michigan, 1993.
- [22] Cohen, L., "Time-Frequency Distributions – A Review," *Proceedings of the IEEE*, vol. 77, no.7, July 1989.
- [23] Ziemer, R. E., and W. H. Tranter. *Principles of Communications*. Houghton Mifflin Company, third edition, 19-119, 1990.
- [24] Hall, P., Kerkyacharian, G. & Picard, D., "Block threshold rules for curve estimation using kernel and wavelet methods," *Ann. Statist.*, 26, 922-942, 1998.
- [25] Bloomfield, P; "Fourier Analysis of Time Series: An Introduction". Wiley, New York, 1976.
- [26] Jenkins, GM; Watts, DG; "Spectral analysis and its applications". Holden-Day, 1968.

- [27] Jones, D.L. and T.W. Parks, "A Resolution Comparison of Several Time-Frequency Representations," *IEEE Transactions on Signal Processing*, vol. 40, no.2, February 1992.
- [28] Boashash, B. *Time-Frequency Signal Analysis Methods and Applications*, Wiley Halsted Press, 1992.
- [29] Berger, R. D., P. Saul, and R. Cohen, "Transfer Function Analysis of Autonomic Regulation I. Canine Atrial Rate Response," *Am. J. Physiol.* 256 (*Heart Circ. Physiol.* 25): H143-144, 1989.
- [30] Baraniuk, R.G. and D.L. Jones, "A Signal Dependent Time-Frequency Representation: Optimal Kernel Design," *IEEE Trans. Signal Proc.*, 41:3543-3549, December 1993
- [31] Bertinieri G. Dirienzo, Cavallazzi A, et al. "Evaluation of baroreceptor reflex by blood pressure monitoring in unanesthetized cats". *Am J Physio.* 1988; 254 (*Heart Circ Physiol* 23) H377-H383.
- [32] Loughlin. P., J. Pitton, and L.E. Atlas, "Bilinear Time-Frequency Representations: New Insights and Properties," *IEEE Trans. Signal Proc.*, 41:750-767, 1993.
- [33] Sang Shin, S. J., W.N. Tapp, S.S. Reisman, and B.H. Natelson, "Assessment of autonomic regulation of heart rate variability by the method of complex demodulation," *IEEE Trans. on Biomed Eng.*, vol. 36, no. 2, pp. 274-282, 1989.
- [34] Statistics Tool Box User's Guide, Version 3. *The Math Works, Inc.*, 2000.
- [35] Bracewell, R., "*The Fourier Transform and Its Applications*," McGraw-Hill, New York, 1965.
- [36] Cohen, L., "*Time-Frequency Analysis*," Prentice Hall, Inc. 1995
- [37] Mallat, S., "*A Wavelet Tour of Signal Processing*," 2nd Edition, Academic Press, 1999.
- [38] Krauss, T. P., L. Shure, J. N Little, *Signal Processing Toolbox Users Guide*, The MathWorks, pp 1-72 - 1-73, June 1994.
- [39] Classen, T. A. C. M., and W.F.G. Mecklenbrauker. "The Wigner Distribution-a Tool for Time-Frequency Signal Analysis", *Philips J. Res.* 35, Part I, 217-250; Part II. 276-300; Part III, 372-389, 1980.
- [40] Qian, S., and D. Chen, "*Joint Time-Frequency Analysis: Methods and Applications*". Prentice Hall, Inc., 1996

- [41] Mallat, S. G., "A Theory for Multiresolution Signal Decomposition: The Wavelet Representation," MS-CIS-87-22, GRASP Lab. 102, Univ. of Pennsylvania, May 1987.
- [42] Gabor, D., "Theory of Communication," *J. of the IEEE*, vol. 29, pp. 429-457.
- [43] Faye, G. and G.F. Boudreaux-Bartels, "Mix Time-Frequency Signal Transformations," *The Transforms and Application Handbook*, 2nd ed., A.D. Poularikas, Editor-in-Chief, CRC Press LLC, 2000.
- [44] Berger, R. D., P. Saul, J. Albrecht, and S. Stein. Respiratory effects on arterial pressure: a novel signal analysis approach. *Proceedings IEEE EMBS*, 10:533-534, 1988.
- [45] Adib, M., "Implementation of time-frequency distribution software and its use to study biological signals," NJIT MS. Thesis, January 1995.
- [46] Ward, J.H., "Hierarchical Grouping to Optimize an Objective Function," *Journal of the American Statistical Association*, 58:236-244, 1963.
- [47] Efromovich, S., "Quasi-Linear wavelet estimation," *J. Am. Statist. Ass.*, 94, 189-204, 1999.
- [48] Vetterli, M., "Wavelets and Filter Banks for Discrete-Time Signal Processing," To appear in *Wavelets and Their Applications*, R. Coifman et al. ed., Jones and Barlett 1991.
- [49] Berntwon, G. G., J.T. Cacioppo, and K.S. Quigley, "Respiratory sinus arrhythmia: Autonomic origins, physiological mechanisms, and psychophysiological implications," *Psychophysiology*, vol. 30, pp. 183-196, 1993.
- [50] Bendat, J.S. and A.G. Piersol. *Random Data: Analysis and Measurement Procedures*. John Wiley & Sons, Inc., 1971.
- [51] Porges, R., "Signals and Systems: Continuous and Discrete," 2nd ed., McMillan Publishing Company, New York, 1989.
- [52] Hartigan, J.A., "Clustering Algorithms," Wiley, New York, 1975
- [53] Ljung, L. *System Identification Toolbox User's Guide*, Version 4. The Math Works, Inc., 1997.
- [54] Jo, J.A., "Model Based Assessment of Autonomic Control in Obstructive Sleep Apnea Syndrome (OSAS) During Sleep," USC, PhD Dissertation, 1999.

- [55] Haar, A., "Zur theorie der orthoganalen funktionensysteme," *Math. Annal.*, 69, 331-371, 1910
- [56] Hotelling, H., "Analysis of a Complex of Statistical variables into Principal Components," *Journal of Educational Psychiatry*, 24:417-441, 1933.
- [57] http://fonsg3.let.uva.nl/praat/manual/Principal_component_analysis.html, 11/2001
- [58] Taylor, A., "Recognizing Biological Sounds Using Machine Learning," URL. http://www.cse.unsw.edu.au/~andrewt/papers/warbler_ai95/wabler_ai95.html, 11/2001.
- [59] www.statsoft.com/textbook/stmulasca.html, 11/2001
- [60] www.statsoft.com/textbook/stcoran.html, 11/2001
- [61] Brillinger, DR, "Identification of point process systems". *Ann Probability* 3: 909–929, 1975.
- [62] Rosenberg, JR; Amjad, AM; Breeze, P; Brillinger, DR; Halliday, DM, "The Fourier approach to the identification of functional coupling between neuronal spike trains". *Prog Biophys molec Biol*, 53: 1–31, 1989.
- [63] Wiener, N., "Generalized harmonic analysis". *Acta Math*, 55: 117–258, 1930.
- [64] Halliday DM; Rosenberg JR; Amjad AM; Breeze P; Conway BA; Farmer SF; "A framework for the analysis of mixed time series/point process data – Theory and application to the study of physiological tremor, single motor unit discharges and electromyograms". *Prog Biophys molec Biol*, 64: 237–278, 1995.
- [65] Bloomfield, P; "*Fourier Analysis of Time Series: An Introduction*". Wiley, New York, 1976.
- [66] Brillinger, DR; "*Time Series – Data Analysis and Theory*", 2nd ed., Holden Day, San Francisco, 1981.
- [67] Jenkins, GM; Watts, DG; "*Spectral analysis and its applications*". Holden-Day, 1968.
- [68] Hlawatsch, F., and G.F. Boudreaux-Bartels, "Linear and Quadratic Time-Frequency Signal Representations," *IEEE Signal Processing Magazine*, pp. 21-67, April 1992.
- [69] Saliba, R., "Bilinear Time-Frequency Representations of Heart Rate Variability and Respiration During Stress," *NJIT, PhD Dissertation*, January 1997.

- [70] Tazebay, M.V., R.T. Saliba and S.S. Reisman, "Adaptive Time-frequency Analysis of Autonomic Nervous System," *Proceedings of the 17th IEEE Annual International Conference of the Engineering in Medicine and Biology Society*, Montreal, Canada, 1995.